Hyphenation of capillary isotachophoresis and capillary electrophoresis-mass spectrometry for online preconcentration and separation of amino acids

Dissertation

der Mathematisch-Naturwissenschaftlichen Fakultät
der Eberhard Karls Universität Tübingen
zur Erlangung des Grades eines
Doktors der Naturwissenschaften
(Dr. rer. nat.)

vorgelegt von
Tanja Melzer
aus Wiesbaden

Tübingen
2020

Gedruckt mit Genehmigung der Mathematisch-Naturwissenschaftlichen Fakultät der Eberhard Karls Universität Tübingen.

Tag der mündlichen Qualifikation:	15.02.2021
Stellvertretender Dekan:	Prof. Dr. József Fortágh
1. Berichterstatter:	Prof. Dr. Carolin Huhn
2. Berichterstatter:	Prof. Dr. Günter Gauglitz

„Ich kann nur hoffen, dass es irgendwie noch als Kunst durchgeht.”

Knorkator - Ich bin der Boss

Danksagung

Bereits in der ersten Woche meines Chemiestudiums wurde mir gesagt, Chemiestudium bedeute vor allem, die persönliche Frustrationstoleranz zu erhöhen. Eine Aussage, die für mich sowohl Studium als auch die Arbeiten für diese Dissertation treffend beschreibt - und ich bin dankbar für jede frustrierende Minute, denn im Gegenzug ist die chemische Analytik so fesselnd und vielseitig und bietet unbezahlbare Erfolgsmomente. Mit dieser Arbeit findet nun zumindest mein Studium im weiteren Sinne ein Ende - das Lernen wird hoffentlich weitergehen. In diesem Sinne möchte ich all den Menschen danken, die mich auf diesem langen Weg begleitet haben und mir die Erstellung dieser Arbeit ermöglicht haben.

Zuallererst möchte ich meiner Doktormutter, Prof. Carolin Huhn, danken. Vielen Dank, dass Du mir dieses spannende, vielseitige Thema anvertraut hast. Ich danke Dir auch für viele fachliche Diskussionen, Deinen hilfreichen Input, wenn ich in einer Sackgasse feststeckte, und für Deine uneingeschränkte Unterstützung und Dein Verständnis in den vergangenen Jahren.

Ich möchte auch Ihnen, Prof. Günter Gauglitz, herzlich dafür danken, dass Sie sich bereit erklärt haben, zweiter Betreuer und auch zweiter Berichterstatter für diese Arbeit zu sein. Ebenso gilt mein Dank Prof. Reinhold Fink und Prof. Michael Lämmerhofer, die sich bereit erklärt haben, als Prüfer an der Disputationsprüfung teilzunehmen.

Ich hatte das Glück, diese Arbeit in einem unfassbar tollen Arbeitskreis anfertigen zu können. Vielen Dank für viele gute Diskussionen, Gespräche, gemeinsame Tagungen, Weinlesen, Mittagspausen, etc. Ich werde diese Zeiten vermissen. Vielen Dank an Dr. Daniel Sydes für die Weitergabe Deines Wissens zum 2D Setup. Ich möchte auch Dr. Pablo Kler herzlich danken (muchas gracias!) für wertvollen Input zum 2D Setup, als auch für die hilfreichen Diskussionen und Erklärungen zu komplexen theoretischen Grundlagen. Benjamin Rudisch, vielen Dank für Dein Elektronikwissen, Deine Programmierfähigkeiten, die Bastelunterstützung und Dein offenes Ohr an so vielen Tagen - ohne Dich wäre ich stellenweise aufgeschmissen gewesen. Danke an Hannes Graf für das Bauen und Optimieren der Leitfähigkeitsdetektoren. Außerdem danke ich Benedikt Wimmer, Michel Banet und Dr. Martin Meixner für diverse Kaffeepausen und gute Gespräche, sowohl fachlich als auch privat. Sarah Knoll, Dr. Jorina Wicht und Tobias Rösch - Danke, dass auch ihr immer ein offenes Ohr hattet und so tolle Bürokollegen wart. Vielen Dank außerdem auch an Dr. Martin Pattky, Dr. Sonja Metternich und Imke Stamme für die gemeinsame Zeit. Ebenso möchte ich natürlich dem gesamten Arbeitskreis Gauglitz für die gute Zusammenarbeit und die gemeinsame Zeit danken.

Mein Dank gilt auch den Studierenden, die mich im Rahmen ihrer Modulpraktika oder Abschlussarbeiten bei dieser Arbeit unterstützt haben: Pascal Rath, Yazhen Yang und Alexandra Haake.

Einen besonderen Dank möchte ich an dieser Stelle an Dr. Monika Bach und Dr. Wilhelm E. Kincses aussprechen, die mir in meiner Anfangszeit an der CFH sehr viele Freiräume für die Fertigstellung dieser Arbeit eingeräumt haben. Herzlichen Dank für Ihre Unterstützung!

Ich möchte meinen Eltern, Eva und Horst, danken - dafür, dass ihr mich immer unterstützt habt, mental und auch finanziell, obwohl ich schon lange aus dem Haus war. Ich konnte mich jederzeit auf euch verlassen und auf euer Verständnis und eure Motivation zählen. Außerdem ganz herzlichen Dank an meinen Bruder Philipp: Du warst wohl immer mein größter Fan und stolzer auf mich und meine Leistungen, als ich es selbst je sein könnte.

Last but not least: Vielen, vielen Dank, Christoph und Robine, für alles, was ihr für mich getan habt und noch immer für mich tut.

Erklärung nach § 6 Abs. 2 der PromO der Mathematisch-Naturwissenschaftlichen Fakultät

Chapter 2: Challenges and applications of isotachophoresis coupled to mass spectrometry and capillary electrophoresis-mass spectrometry

Literature research and writing was done completely by me. Carolin Huhn aided with valuable input and the correction of the manuscript. Benedikt Wimmer conducted CE-MS measurements of glyphosate from soil extracts depicted in this chapter (Figure 2.2). This introductory chapter was published slightly shortened and modified as a review article in Electrophoresis, June 2020, Volume 41, Issue 12, pp. 1045-1059 [1].

Chapter 3: Analysis of amino acids by two-dimensional hyphenation of isotachophoresis with capillary electrophoresis-mass spectrometry for online preconcentration and separation

The idea to hyphenate ITP with CE-MS via a microfluidic interface came from Carolin Huhn as major focus of this work. Proof of principle measurements with the capillary coupling setup had already been accomplished within our work group. The vial holder for this setup was designed by Pablo Kler and the external high voltage source connected to this vial holder was developed and built by Peter Zipfl and Daniel Lutz from CalvaSens GmbH in Aalen. The equipment used was the same as in Kler et al. [2] with improvements on the chip design by Sydes et al. [3], aided by Benjamin Rudisch. CDC detectors used in the single capillary setup were constructed by Hannes Graf within the scope of his Master thesis [4]. Benjamin Rudisch constructed the electronics to control the external pressure unit and designed the external vial holder with my input for the pressure adapter for the vial's lid, which was built by the University's workshop. This improvised vial lid enabled external pressure application.

I designed the study regarding new electrolyte systems and conducted the CE-MS, ITP-MS and ITP/CE-MS measurements. ITP-MS measurements were partly conducted by student workers, Pascal Rath and Yazhen Yang, under my supervision. Data evaluation and visualization, as well as literature search and writing were completely done by me. Carolin Huhn corrected the manuscript.

Chapter 4: Influence of different organic solvents in hydroorganic background electrolytes on electroosmotic and electrophoretic mobilities

The idea to investigate the influences of isopropanol on the electroosmotic flow and effective electrophoretic mobilities of amino acids came up during discussions with Pablo

Kler and Carolin Huhn about the CE-MS method employed in the 2D setups. I designed the study. CE-C^4D measurements were carried out by me and by Alexandra Haake within the scope of her Bachelor thesis [5] under my supervision. I accomplished data evaluation and visualization. Literature search was conducted by me with valuable input concerning physicochemical characteristics by Carolin Huhn. Writing of this chapter was done completely by me and Carolin Huhn corrected the manuscript.

Chapter 5: Comparison of different proteolytic enzymes for peptide analysis via capillary electrophoresis-mass spectrometry

Carolin Huhn had the idea to investigate the applicability of Glu-C, Lys-C and Lys-N as alternative to trypsin for CE-MS based peptide analyses. I conducted all experimental work for this chapter, as well as data evaluation and visualization, literature research and writing. Carolin Huhn corrected the manuscript.

Table of contents

Abstract

The hyphenation of isotachophoresis with capillary electrophoresis-mass spectrometry (ITP/CE-MS) is considered to improve the detection limits in CE-MS analyses which are often insufficient due to the low sample injection volumes. Although the combination of transient isotachophoresis with CE-MS is commonly applied, the two-dimensional ITP/CE-MS hyphenation is still scarcely used. In this work, two different 2D ITP/CE-MS setups based on a combination of a custom-made microfluidic glass chip interface with commercial capillaries are presented.

Hydroorganic electrolyte systems with high MS-compatibility and tolerance for aqueous samples were developed for the simultaneous preconcentration of the proteinogenic amino acids as cations within one isotachophoretic zone. New electrolyte systems included imidazole as leading ion and H^+ as terminating ion, while either trimethylpyruvic acid or difluoroacetic acid were applied as counterions to obtain sufficiently low pH values. In direct ITP-MS analyses, detection limits in the low micromolar range were obtained. Up to 30 % of the capillary could be filled with sample at concentrations below 1 µmol/L.

For CE-MS, a hydroorganic (isopropanol/water) acetic acid background electrolyte was optimized for both, high MS-compatibility and compatibility with the ITP electrolytes in 2D hyphenations. Sufficient separation efficiency and resolution for qualitative determinations of all analytes were obtained with detection limits in the micromolar range. The influence of hydroorganic BGEs on the electroosmotic flow and effective electrophoretic mobilities of the analytes was investigated in BGEs containing 10-30 % isopropanol, dimethyl sulfoxide or acetonitrile or 10-50 % methanol. No changes in selectivity were observed and results indicate that solvent parameters such as e.g. relative permittivity and relative viscosity are not sufficient to describe and predict CE separations.

The new electrolyte systems were applied in a capillary coupling ITP/CE-MS setup, using a home-made vial-handler with an external high voltage source for second dimension. Sample transfer proved difficult due to a lack of an intermediate detector. In a single capillary ITP/CE-MS setup, a side capillary was introduced for counterflow generation. With this setup, the choice of electrolytes becomes independent from the sheath liquid, which was used for counterflow generation in other publications. This work shows the applicability of L-S-L, T-S-T and BGE-S-BGE modes in a single capillary setup for the first time. Counterflow conditions and capillary lengths were optimized for optimal sample transfer to obtain best separation conditions.

Digests of bovine serum albumin with trypsin, Lys-C, Lys-N or Glu-C following the same protocol were analyzed with CE-MS. The expectation that proteases other than trypsin are better suited for subsequent CE-MS analyses of peptides was not fulfilled as Lys-C provided similar results as trypsin, although it was expected to result in higher peptide charges as it only cleaves the protein at lysine sites. Results obtained for digests with Lys-N and Glu-C were inferior to trypsin.

Zusammenfassung

Die Kopplung der Isotachophorese mit Kapillarelektrophorese-Massenspektrometrie (ITP/CE-MS) bietet eine Möglichkeit zur Verbesserung der Nachweisgrenzen bei CE-MS Analysen, die aufgrund des geringen Injektionsvolumens häufig unzureichend sind. Obgleich die Kombination von transienter Isotachophorese mit CE-MS häufig angewendet wird, wird die zweidimensionale ITP/CE-MS-Kopplung noch kaum verwendet. In dieser Arbeit werden zwei verschiedene 2D-ITP/CE-MS-Setups vorgestellt, die auf der Kombination eines maßgeschneiderten mikrofluidischen Glaschip-Interfaces mit kommerziellen Kapillaren basieren.

Für die simultane Aufkonzentration der proteinogenen Aminosäuren als Kationen innerhalb einer isotachophoretischen Zone wurden hydroorganische Elektrolytsysteme mit hoher MS-Kompatibilität und Toleranz für wässrige Proben entwickelt. Imidazol wurde als Leition verwendet und H^+ diente als Folgeion, während entweder Trimethylbrenztraubensäure oder Difluoressigsäure als Gegenionen genutzt wurden, um ausreichend niedrige pH-Werte zu erhalten. Mittels direkter ITP-MS-Kopplung wurden mit diesen Elektrolytsystemen Nachweisgrenzen im niedrigen mikromolaren Bereich erhalten. Bis zu 30 % der Kapillare konnten mit Proben in Konzentrationen unter 1 µmol/L beladen werden.

Für CE-MS wurde ein hydroorganischer (Isopropanol/Wasser) Essigsäure-Hintergrundelektrolyt sowohl für eine hohe MS-Kompatibilität als auch für die Kompatibilität mit den ITP-Elektrolyten in der 2D-Kopplung optimiert. Trennungen in diesem BGE boten eine ausreichende Trenneffizienz und Auflösung für die qualitative Bestimmung aller Analyte. Nachweisgrenzen lagen im mikromolaren Bereich. Der Einfluss hydroorganischer BGEs auf den elektroosmotischen Fluss und die effektive elektrophoretische Mobilität der Analyte wurde in BGEs untersucht, die 10-30 % Isopropanol, Dimethylsulfoxid oder Acetonitril oder 10-50 % Methanol enthielten. Die Ergebnisse zeigten keine Änderungen der Trennselektivität. Lösungsmittelparameter wie z.B. die relative Permittivität und die relative Viskosität reichten nicht aus, um die Einflüsse auf elektroosmotischen Fluss und effektive elektrophoretische Mobilitäten verlässlich vorherzusagen.

Die neu entwickelten Elektrolyte wurden in einem Kapillar-Kopplungs-ITP/CE-MS-Setup mit mikrofluidischem Glaschip-Interface unter Verwendung eines eigens angefertigten Vialhandlers mit externer Hochspannungsquelle als zweitem CE-Gerät verwendet. Mangels Detektionsmöglichkeit an der Schnittstelle der beiden Dimensionen erwies sich der Probentransfer als schwierig. In einem Einkapillar-ITP/CE-MS-Setup wurde über ein T-Stück aus geätztem Glas eine Seitenkapillare ergänzt, die der Erzeugung des

Rückflusses zum Rücktransport des ITP Stacks diente. Mit diesem Aufbau ist die Wahl der Elektrolyte unabhängig von der Zusammensetzung des Sheath Liquids, welches in anderen Publikationen zur Rückflussgeneration verwendet wurde. In dieser Arbeit konnte erstmals ein Aufbau für 2D-Trennungen etabliert werden, mit dem alle drei möglichen Modi, nämlich L-S-L, T-S-T und BGE-S-BGE, genutzt werden konnten. Die Rückflussbedingungen und Kapillarlängen wurden optimiert, um einen vollständigen Probentransfer und dadurch bestmögliche Trennbedingungen in der zweiten Dimension zu erhalten.

Enzymatische Verdaue von Rinderserumalbumin mit Trypsin, Lys-C, Lys-N oder Glu-C nach dem gleichen Protokoll wurden mit CE-MS analysiert. Entgegen der Erwartung, dass andere Proteasen als Trypsin für nachfolgende CE-MS-Analysen von Peptiden besser geeignet sind, lieferte Lys-C ähnliche Ergebnisse wie Trypsin, obwohl keine Spaltung an Arginin stattfand, weshalb höhere Ladungen an den generierten Peptiden erwartet wurden. Die Ergebnisse für Verdaue mit Lys-N und Glu-C waren tryptischen Verdauen unterlegen.

1. Introduction

Capillary-based electromigrative separation techniques are gaining increasing interest to tackle actual analytical tasks which are difficult or impossible to solve with chromatographic techniques. Especially capillary electrophoresis, providing separation based on hydrodynamic radius and charge of analytes, is on the rise for the analysis of pharmaceuticals and environmentally relevant compounds, which are difficult to be monitored by common reversed-phase high performance liquid chromatography due to their high polarity and/or ionic nature. The combination of capillary electrophoresis with mass spectrometry offers new analytical possibilities. This combination is applied for investigations ranging from small ionic molecules to proteomics and metabolomics. The low consumption of solvents, chemicals and sample and the minimal sample preparation required in many cases are the most commonly mentioned advantages of this separation technique [6]. Nevertheless, due to the small sample volumes injected, mostly only a few nanoliters, the concentration detection limits of capillary electrophoresis with mass spectrometric detection are often insufficient for trace analysis. Therefore, offline sample enrichment techniques such as solid phase extraction have to be applied, increasing workload and time. Online approaches to increase capillary loadability and/or enrich analytes are commonly employed as well, e.g. sample stacking or transient isotachophoresis [7].

Isotachophoresis is another method of the family of electromigrative separation techniques. Analytes are separated according to their electrophoretic mobility in consecutive analyte zones between a leading and a terminating electrolyte. The concentration of each analyte zone depends on its preceding zone, thus, enrichment of analytes is possible during separation. Due to this enrichment, the capillary loadability of isotachophoresis is generally higher than in capillary electrophoresis. While the combination of transient isotachophoresis with capillary electrophoresis is commonly applied, two-dimensional coupling of isotachophoresis and capillary electrophoresis is rarely conducted. This work focuses on this two-dimensional hyphenation of isotachophoresis and capillary electrophoresis to improve the sample loadability and optimize the separation methods for highest preconcentration and separation of amino acids with subsequent mass spectrometric detection. Using a hybrid setup consisting of a microfluidic glass interface with capillaries, different instrumental setups, hyphenation modes and electrolytes are compared.

For preconcentration of all proteinogenic amino acids in one isotachophoretic zone, organic solvents are required in the electrolytes. To achieve best sample transfer and optimal conditions for the transition from isotachophoresis to capillary electrophoresis in

the second dimension, an organic modifier is required in the background electrolyte for capillary electrophoresis as well. As the physicochemical parameters of organic solvents are known to affect electromigration of solutes [8-11], the influence of organic solvents in the background electrolyte of capillary electrophoresis separations on the electroosmotic flow and analyte electrophoretic mobilities is investigated.

An interesting application of the hyphenation of isotachophoresis and capillary electrophoresis-mass spectrometry is the analysis of enzymatic protein digests. The most commonly applied enzyme for protein digestion is trypsin, which is considered the “gold standard” [12] for chromatographic separations, as it generates peptides of similar mass and charge. However, the separation mechanism of capillary electrophoresis strongly differs from chromatographic separations and alternative proteases might be better suited for electromigrative separations than trypsin. Thus, capillary electrophoresis-mass spectrometry analyses of bovine serum albumin digested with different endoproteases as alternatives to trypsin are examined to enhance resolution in capillary electrophoresis-based protein analysis.

2. Challenges and applications of isotachophoresis coupled to mass spectrometry and capillary electrophoresis-mass spectrometry

This introductory chapter was published slightly shortened and modified as a review article in Electrophoresis, June 2020, Volume 41, Issue 12, pp. 1045-1059 [1].

2.1. Abstract

Electrophoretic separations are of growing interest to tackle a wide field of complex analytical challenges. Nevertheless, capillary electrophoresis, as the most commonly used electromigrative separation technique, still suffers from insufficient detection limits due to low capillary loadabilities. Isotachophoresis, a special form of capillary electrophoresis, is of growing interest as preconcentration method for capillary electrophoresis and is also interesting to be applied as an independent analytical method. While mass spectrometric detection is common for capillary electrophoresis, the combination of isotachophoresis with mass spectrometry is still a niche technique. In this chapter, we want to give an overview on isotachophoretic effects in capillary electrophoresis-mass spectrometry and isotachophoresis-mass spectrometry methods, as well as coupling techniques of isotachophoresis with capillary electrophoresis-mass spectrometry. The challenges and possibilities associated with mass spectrometric detection in isotachophoresis and its coupling to capillary electrophoresis are critically discussed.

2.2. Introduction

Capillary isotachophoresis (ITP), as a special form of capillary electrophoresis (CE), has first been described at the beginning of the 20th century [13]. Although still rather a niche technique, there is quite a number of publications on ITP, including several biannual reviews published by the group of Petr Boček [14-23]. Already in 1983, Everaerts et al. [24] reviewed new directions in isotachophoresis coming up at that time. Due to its concentrating power, interest in ITP is increasing as a possibility to overcome the difficulty with poor loadability and, thus, insufficient detection limits in capillary-based electromigrative separation methods. ITP can also be used to remove matrix components, which are either not included in the mobility window spanned by leading and terminating electrolyte or are not transferred to the second dimension in 2D applications.

Mass spectrometry (MS) is increasingly applied for liquid and gas phase separation techniques and gains rising impact also in electromigrative separations, as recently shown in reviews on CE-MS by Pantůčková et al. [25] and Stolz et al. [26]. It provides (exact) mass information and enables structural/molecular characterization by

fragmentation. In addition, detection limits are greatly enhanced compared to photometric detection. Online ITP-MS and ITP coupled to capillary electrophoresis-mass spectrometry (ITP/CE-MS) are rarely used, as they have special requirements on instrumentation and electrolytes as will be pointed out in this chapter. In contrast, transient ITP (tITP) preconcentration steps prior to CE-MS are often applied.

In this chapter, we want to discuss several aspects of the combination of ITP and MS, basics of ITP can be found in books dedicated to ITP [27-28] and in the reviews summarized in Table A1 in the appendix. First, we look at ITP phenomena in CE-MS, which are mostly unwanted and hardly recognized. They occur because the outlet vial is replaced by the electrospray ionization (ESI) needle, very often with a sheath liquid (SL), which has a different composition to the background electrolyte (BGE). In CE-MS applications, ITP boundaries may form and migrate inversely from the MS to the CE inlet, often impairing the separation. We then focus on the special features of the direct coupling of ITP-MS, and discuss transient ITP/CE-MS applications. Finally, the resulting peculiarities of ITP column-coupled to CE-MS in 2D applications are highlighted. Tables with details on reviews and studies cited are presented in the appendix (Table A1, Table A2, Table A3 and Table A4).

2.3. Principle of isotachophoretic separations

In ITP, a discontinuous buffer system is applied for preconcentration and electromigrative separation of analytes. In principle, analytes are introduced between a leading electrolyte (LE) and a terminating electrolyte (TE) and are arranged in zones between a leading ion and a terminating ion in the order of their effective electrophoretic mobilities. Then, migration takes place at constant velocity [28]: in contrast to capillary electrophoresis, all analytes migrate with the velocity of the leading ion which remains stable when a constant current is applied. A scheme of the principle of the process and the distribution of the potential and the electric field strength during the steady state of the isotachophoretic separation is given in Figure 2.1. Furthermore, ITP exhibits a concentration effect which can be described by the Kohlrausch regulating function, the “beharrliche Funktion”: the concentration of an analyte zone depends on the concentration of the preceding zone. Therefore, by adjusting the concentration of the leading ion, analytes can either be concentrated or diluted during the separation process [27]. This phenomenon necessitates quantification of signal zones via their length or their volume. Quantification is thus independent of the signal intensity. Mostly, non-selective conductivity detection, such as capacitively-coupled contactless conductivity detection (C^4D), is applied for ITP separations.

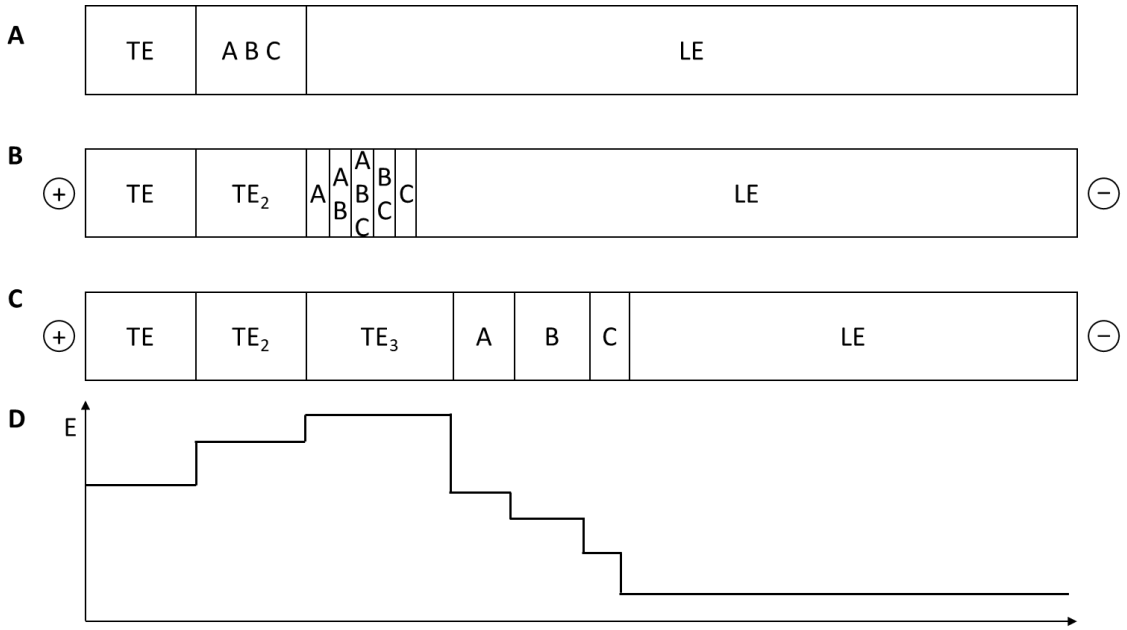

Figure 2.1: Principle of ITP separation of three analytes A, B and C with electrophoretic mobilities $\mu_C > \mu_B > \mu_A$. (A) The initial conditions in the capillary where a sample plug is introduced between leading electrolyte LE and terminating electrolyte TE. (B) Voltage application starts the isotachophoretic process, analytes separate into zones according to their mobility and their concentrations adapt to the preceding zone, as well as the concentration of TE at the boundary, indicated as TE_2. (C) Steady state in separation: all analytes migrate with the same velocity as the LE in completely separated zones, by TE zones TE_3 and TE_2 with adapted concentrations according to the Kohlrausch regulating function. (D) Distribution of electric field strength E in the capillary under steady state conditions in C.

2.4. ITP phenomena in CE-MS

More often than possibly expected, conditions of transient ITP are also present in CE-MS analysis for two reasons: 1) a transient ITP may evolve due to the sample composition with ionic macrocomponents present as well-known from CE-UV or CE-conductivity methods. 2) ITP conditions may evolve in CE-MS due to the fact that the outlet vial is replaced by the MS and (most often) a sheath liquid with a different composition than the BGE is used. An example for transient ITP phenomena from our work is given in Figure 2.2, showing the mass traces of phosphate and glyphosate from anionic CE-MS analysis of glyphosate in environmental soil extracts. Glyphosate was desorbed and extracted from soil samples with potassium hydroxide and disodium phosphate. Phosphate acted as transient LE in a sample-induced ITP during the measurements, while formate from the BGE was the transient TE. In Figure 2.2A the phosphate concentration in the sample was low enough to allow the ITP stack to dissolve and to detect glyphosate as CE signal. As shown in in Figure 2.2B, the high phosphate concentration leads to stable ITP conditions until detection, visible from the narrow glyphosate signal directly attached to the broad phosphate signal. Problems with

quantification due to quenching effects are likely if no isotope-labeled internal standard is used. In anionic CE-MS, tITP phenomena are likely since acetic acid (HAc) and formic acid (FA) BGEs are often used, with acetate and formate functioning as transient TE (see Figure 2.2). For cationic ITP, ammonia may be a transient LE and H^+ may act as transient TE. H^+ can be used as a transient TE despite its high absolute electrophoretic mobility when buffered electrolytes are used. Its frontal migration is then controlled by the buffering counterion, as a reaction to e.g. neutral HAc occurs at the boundary ([27], pages 30-32). Sample-induced transient ITP can be advantageous to improve detection limits as will be discussed in Section 2.6.2 but can also negatively affect the CE separation as shown in Figure 2.2B, where the ITP stack did not dissolve.

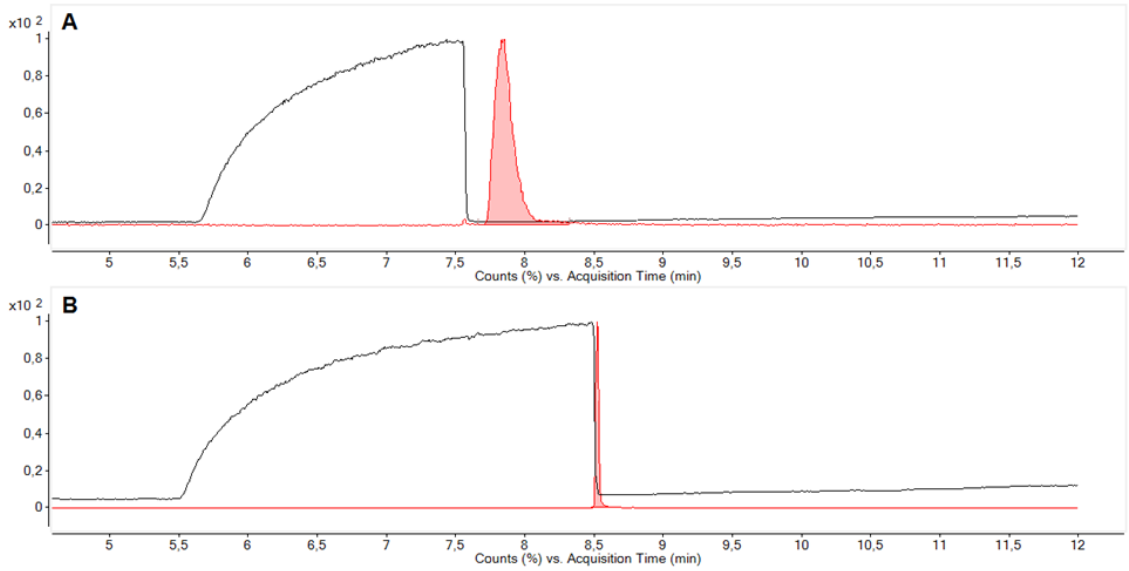

Figure 2.2: Mass traces of phosphate (black) and glyphosate (red) in anionic CE-MS analysis of environmental soil extracts showing a sample-induced tITP. Samples were extracted with potassium hydroxide and disodium phosphate ((A) c = 50 mmol/L, (B) c = 100 mmol/L), then acidified with sulfuric acid to pH 3. BGE: 175 mmol/L FA, adjusted to pH 2.8 by addition of ammonium.

This effect was observed e.g. by Jooß et al. [29] who obtained unwanted isotachophoresis in their column-coupling CE/CE-MS setup. A relatively large fraction of the BGE was cotransferred with the analyte into the second dimension, where its coion functioned as a leading ion. Clearly, the protein of interest was focused in a sharp zone in an ITP stack.

The second ITP phenomenon is rarely addressed: whereas the inlet vial in CE-MS measurements contains BGE, the “outlet vial” contains SL, which may induce unwanted ITP phenomena with a great potential to disturb or at least change separations. As described by Foret et al. [30], the formation of an ITP step migrating from the MS interface to the capillary inlet is possible: the authors described that - depending on the

composition of BGE and SL - the ITP boundary can be sharp or diffuse (see Figure 2.3). A sharp boundary is present if the mobility of the BGE counterion is higher than that of the counterions in the SL. In contrast, if the mobility is lower, a diffuse boundary will form. In either case, changes in pH occur and affect separation efficiency and selectivity. Exemplarily, standard proteins were applied as model analytes in cationic CE-MS measurements applying a 20 mmol/L *ε*-aminocaproic acid BGE with phosphoric acid as counterion (pH 4.4) and 50 % (v/v) methanol in water with 1 % HAc as SL [30]. The higher mobility of phosphoric acid than HAc at the given pH caused an inverse ITP from the MS to the inlet, which induced a reversal of the migration order of two proteins in comparison to the same measurements without inverse ITP (i.e. with HAc as BGE counterion). Nevertheless, due to the inverse ITP, phosphoric acid could be used as counterion despite being non-MS-compatible as it was replaced by HAc from the SL [30]. This means, that it is difficult to fully control the pH of the BGE over the course of one measurement. Generally, having the same counterion in the SL as in the BGE helps to reduce this phenomenon, however, concentration and, consequently, slight pH changes will (always) occur.

In counterelectroosmotic separations (e.g. for cationic peptide analysis with a cationic coating and reversed polarity), an inverse ITP may evolve with a high mobility BGE ion such as ammonia serving as LE and an ion from the SL (e.g. H^+) serving as TE. The ITP boundary migrates inversely to the electroosmotic flow (EOF) but in the same direction as the analytes. This phenomenon can be even more problematic than the “normal” inverse ITP, as the analytes may be taken up by the ITP stack, preventing any further separation and - depending on the relative velocities of ITP and EOF - also detection.

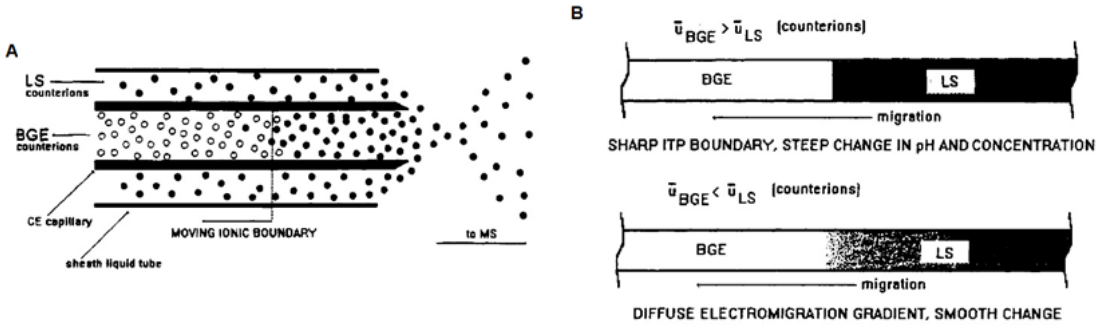

Figure 2.3: Influence of sheath liquid ions on the BGE. (A) depicts how SL (here abbreviated as LS) counterions (filled dots) penetrate the BGE (empty dots). (B) illustrates the generation of either a sharp boundary, if the mobility of BGE counterions is higher than that of the SL counterions (upper picture), or a diffuse boundary, if the mobility of the SL counterions is higher than that of the BGE counterions (lower picture). Reprinted with permission from [30]. Copyright (1994) American Chemical Society.

In Figure 2.4, the inverse cationic ITP process in the capillary during CE-MS analysis is visualized for anionic CE-MS analyses of the anions glyphosate and its metabolite aminomethylphosphonic acid on a neutrally coated capillary with suppressed EOF at reverse polarity [31]. To aid electrospray generation, a small pressure was applied during the measurements (30 mbar). A conductivity detector was mounted in front of the MS interface to observe the conductivity changes during the CE separation. The BGE consisted of ammonium formate (compare Figure 2.2). The CE counterion ammonium acted as leading ion. The SL was made of 50 % (v/v) isopropanol in water with 0.01 % FA, delivering H^+ as TE to the capillary to maintain charge balancing.

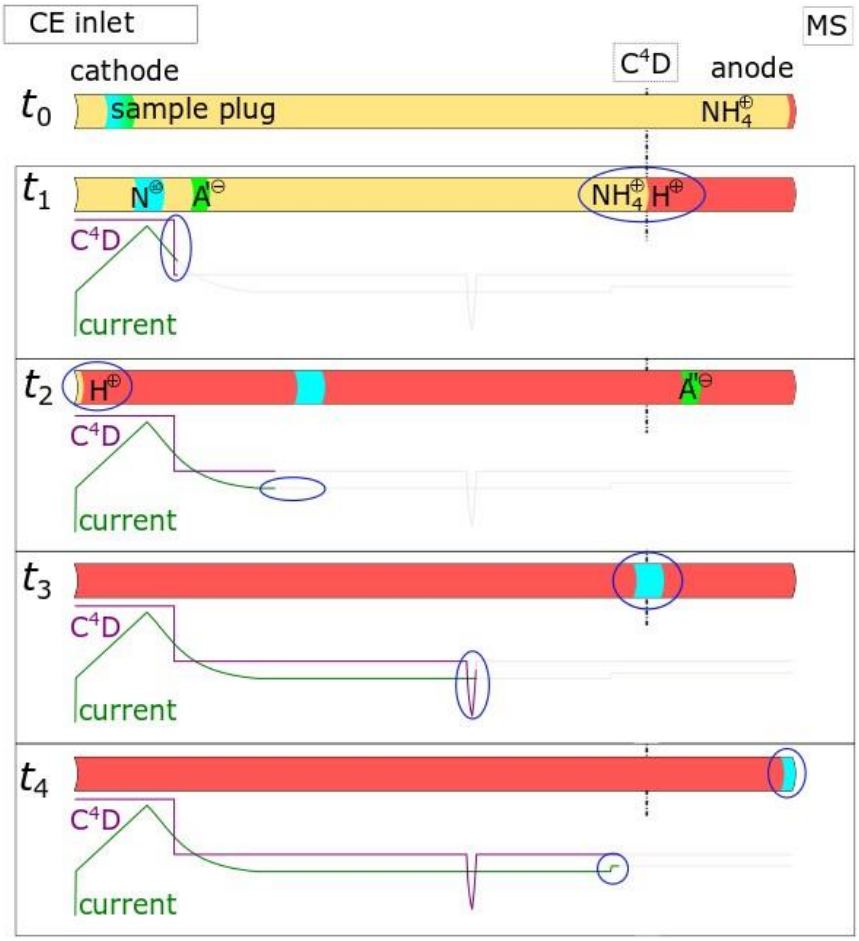

Figure 2.4: Schematic depiction and experimental results of an inverse ITP occurring in the capillary based on anionic CE-MS analyses of glyphosate and aminomethylphosphonic acid (not visible in C^4D) at different time points t_0-t_4 during the separation on a neutrally coated capillary. The traces of current (green) and C^4D (purple) are shown. Separation at -30 kV and 30 mbar. The C^4D was placed in front of the SL interface of the mass spectrometer (51.7 cm effective length, 13.3 cm distance to capillary outlet; total length 65 cm). Same BGE as in Figure 2.2. Ammonia counterions (yellow) are dynamically replaced by H^+ counterions (red). For further explanations, see text. Reprinted from [31] with permission from the author. Image annotations were translated.

At the beginning (t_0 in Figure 2.4), a sample plug was introduced at the cathodic end of the capillary filled with BGE. As soon as voltage was applied (t_1), the analytes started migrating towards the anodic end of the capillary. The applied pressure accelerated the movement of the analytes and induced a slow transport of the neutral sample plug towards the MS. At the same time, NH_4^+ ions migrated towards the cathode at the CE inlet, followed by H^+ from the SL. As the electrophoretic mobility of NH_4^+ is higher than that of H^+ in a buffered system, a sharp boundary formed visible as a typical ITP step by conductivity detection. The current decreased with increasing length of the H^+ zone in the capillary and stabilized as soon as all NH_4^+ ions left the capillary (t_2). At t_3, the neutral sample plug passed the conductivity detector. The current slightly increased when this plug left the capillary (t_4). In this example, the pH of the CE separation changed during the separation process.

With common CE-MS electrolytes relatively high pressure would be required to prevent the entrance of counterions from the SL and thus the inverse ITP. This would reduce separation efficiency and resolution due to parabolic flow and reduced separation time. Alternatively, addition of the transient leading ion to the SL is considered helpful although ITP conditions may persist even with leading ion in the TE (see Section s 2.5.1 and 2.5.4, and [32-34]). Clearly, disturbances due to changes in pH and/or conductivity and an inverse ITP of like charge have to be considered when optimizing a BGE for a CE-MS separation.

2.5. Direct coupling of ITP-MS

2.5.1. Restricted buffer selection

Direct coupling of ITP with mass spectrometric detection has rarely been applied, although introductory publications are already about 30 years old [35-36]. The explanation is simple: the number of MS-compatible electrolytes in electromigration techniques is very limited, which is e.g. shown in reviews by Pantůčková et al. [25] and Stolz et al. [26]. FA, HAc and ammonium are predominantly applied as BGE. Accordingly, the number of fully MS-compatible leading/terminating ions and especially counterions for ITP-MS coupling is very limited. The counterion in ITP is present in all analyte zones and, thus, can lead to quenching effects in the ion source and fouling when working with MS detection. Furthermore, the counterion has to be delivered by the SL which acts as outlet vial in ITP-MS. It may strongly impair ionization efficiency, except when counter-EOF ITP separations with a high EOF towards the MS are conducted [30]. This limitation complicates the creation of suitable and optimized mobility windows between leading and terminating ion. Nevertheless, there are possibilities to overcome

these difficulties, as was shown by the Boček group in publications on electrolyte tuning strategies for ITP-MS [32, 34, 37-38]. Using only a few small organic acids and varying their combination and concentration in LE and TE in different operational modes of ITP, they demonstrated several possibilities to shift (and narrow) the mobility window towards the mobility of the analytes of interest. This strategy enabled an impressive selectivity tuning, promising for targeted ITP-MS coupling approaches. A closer look on these methods will be given in Section 2.5.4.

Malá and Gebauer [39] discussed electrolyte systems for anionic ITP of weak acids, which requires a medium to alkaline pH range. As common volatile acids have rather low pK_a values (up to 5) they are fully deprotonated and have high effective electrophoretic mobilities and cannot serve as terminating ions. Thus, the slowest possible terminating ion in aqueous anionic electrolytes was chosen, which is OH^-, when using a weak base as counterion [30-31, 39]. As counterions, the weak bases ammonium, triethylamine and ethanolamine were tested to separate pharmaceutical acids (best conditions: LE: 10 mmol/L HAc with 10 mmol/L triethylamine; TE: 10 mmol/L triethylamine with 2-6 mmol/L HAc). In contrast to measurements with ammonia, with triethylamine it was possible to stack all analytes. With ethanolamine, problems with carbonate entering the electrolyte due to diffusion of CO_2 were observed at the high pH of the chosen LE of 7.77.

In a second study on ITP-MS at medium to high pH, this time on cationic ITP, Malá and Gebauer [40] used HAc and FA as counterions and triethanolamine, ammediol, ethanolamine, tripropylamine, and triethylamine as leading and termination ions for the separation of beta-blockers. The selectivity was tuned via the stacking window optimizable by a variation of the concentration of HAc and the choice of the leading and termination ions. The broadest mobility window was reached using triethylamine and triethanolamine as LE and TE constituents.

2.5.2. Special considerations for EOF and anionic ITP applications

For cationic ITP-MS, direct coupling is well possible as both the analytes and the electroosmotic flow migrate towards the MS. For small proteins, a DB-17-coated capillary was used to reduce adsorption to the capillary wall [35]. Interestingly, most studies on anion analysis by ITP-MS used reverse separation polarities with -20 or -25 kV or low currents with a low EOF [32, 37-38, 41-43] (see also Table A2 in the appendix). Using MS detection in anionic ITP-MS, care has to be taken, when the EOF is directed towards the CE inlet. In most studies presented so far, the EOF was rather low at the relatively low pH chosen and counteracted by suction effects of the ESI source (see Table A2). Obviously, neither SL nor air were sucked into the capillary. However, there are also studies using a reversed anionic ITP-MS (also called EOF-driven ITP [39]), where

reverse separation polarity was applied and the ITP stack migrates to the capillary inlet [39, 44]. A high EOF transports ITP zones towards the MS. Accordingly, the bare fused silica capillary is filled with TE before the sample is injected. This approach requires an LE coion with an electrophoretic mobility smaller than the electroosmotic mobility, which narrows the ITP mobility window for fast analytes.

Smith et al. [35] and Malá and Gebauer [39] pointed out that, besides reduction of adsorption, coated capillaries are advantageous for ITP-MS since EOF velocities depend on the local pH and electrolyte composition. At conditions of strong local EOF discontinuities, mixing of zones may occur at band boundaries, which become more diffuse [35]. Also, a nonlinear dependence of peak height on sample volume under alkaline conditions may result [39].

2.5.3. Aspects of quantification

As the concentration of an analyte zone depends on the concentration of the preceding zone and, thus, finally on the leading ion concentration, a higher absolute amount of analyte in the sample will not increase the signal intensity in MS, UV or conductivity detection. Two ITP modes can be distinguished depending on the concentration of the analyte: peak mode and plateau mode [28, 45-46]. Plateau mode refers to the commonly known ITP step profiles with analyte concentrations large enough to have distinct zones resolved by the detection system used. The zone length provides quantitative information. In contrast, at low analyte concentration, no plateau evolves, instead, the ITP zone appears as a peak in the isotachopherogram [28, 45-46]. In this case, detection may become challenging or even impossible depending on the spatial and temporal resolution of the detector. For quantification, it is necessary to discriminate peak and plateau mode: as long as the concentration of the analyte is too low to reach a migration in the plateau mode ITP, peak area is preferably used for quantification. Care has to be taken to find a suitable TE as tailing of ITP boundaries may appear and impair quantification, if the TE composition and pH are not well optimized. Especially for the low concentration range, mass spectrometric detection is advantageous as comigrating substances can be discriminated, which would not be possible with e.g. photometric detection. In plateau mode ITP, the zone length provides the quantitative information, which is largely independent of the signal intensity given by the detection system itself. In contrast, in peak mode ITP, the sensitivity of the detector is relevant for the limit of detection, especially when it comes to trace analysis. In this regard, mass spectrometry offers superior detection limits, spatial and temporal resolution compared to conductivity and UV detection. While quantification in ITP with UV or conductivity detection is almost

always conducted in plateau mode, quantification in ITP-MS is mainly conducted in peak mode and comparable to CE-MS.

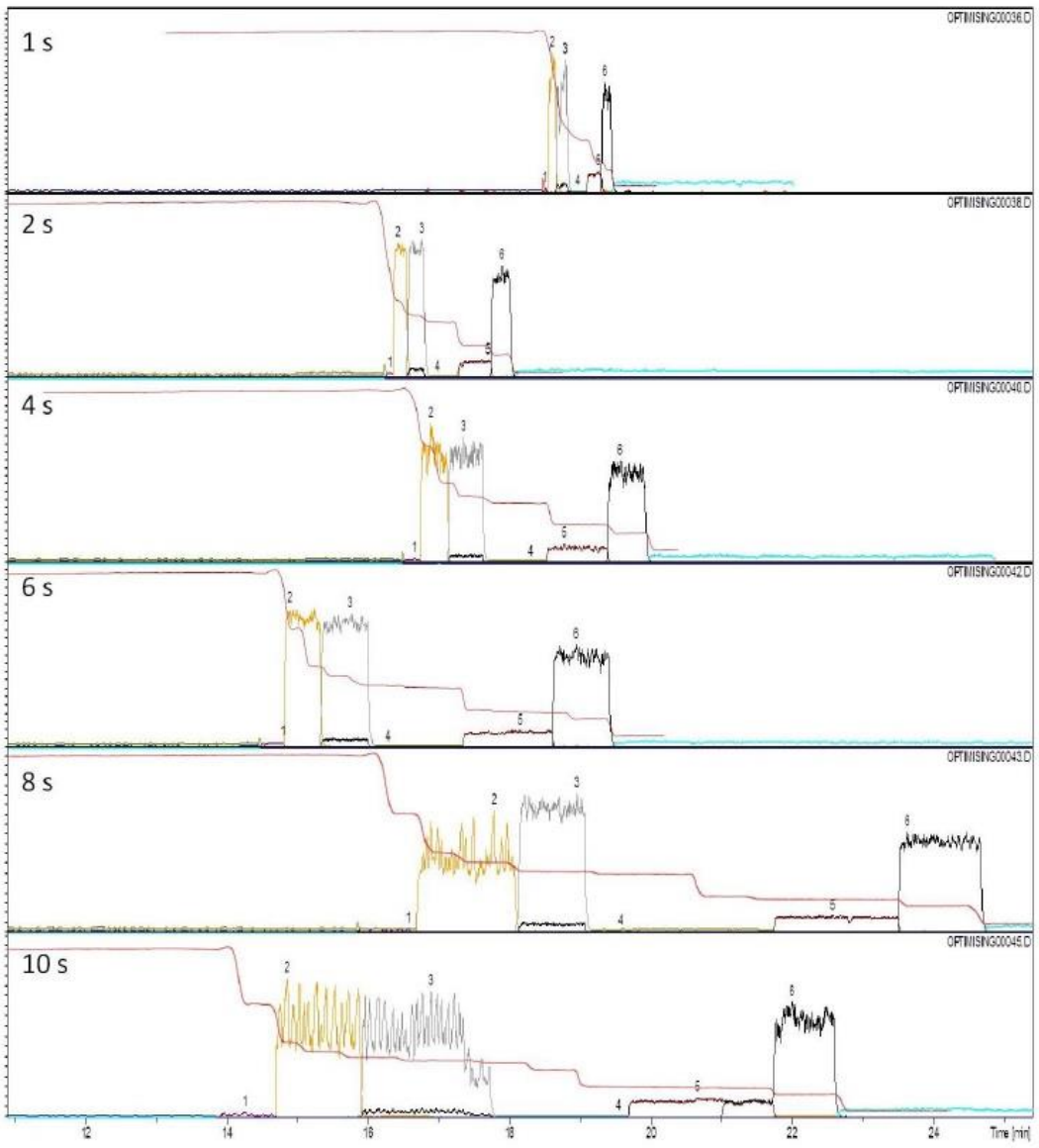

Figure 2.5: Anionic ITP-MS analysis with parallel conductivity detection of a mixture of oxalic acid (1), salicylic acid (2), citric acid (3), glycolic acid (4), succinic acid (5) and shikimic acid (6). LE: 10 mmol/L HCl with 300 mmol/L β-alanine, pH 3.1, TE: 100 mmol/L hexanoic acid. The injection time of the analyte mixture was varied between 1 s and 10 s. The extracted ion isotachopherogram of each analyte (labeled with the respective number) and corresponding trace of conductivity detection (red line) are shown. Reprinted from [47] with permission from the author.

However, ITP-MS conducted in plateau mode offers new possibilities of quantification, not yet fully exploited. Figure 2.5 clearly shows advantages of MS compared to conductivity detection with regard to spatial resolution at low analyte amounts injected [47]. Conductivity detection was not able to resolve the signals of the analytes when

small volumes are injected, as visible for injections of 1 s or 2 s in Figure 2.5. The first four analytes migrated in narrow zones (1 s injection, 18.5-19.0 min) and were not distinguishable by conductivity detection but by MS due to the additional mass information and superior spatial resolution. Only at higher analyte loads, discrimination becomes possible with conductivity detection. Furthermore, transient mixed zones resulting from insufficient ITP separation after high volume injection (compare 10 s injection, 21.0-21.8 min showing a transient mixed zone of succinic acid (zone 5, 19.7-21.8 min) and shikimic acid (zone 6, 21.0-22.7 min)) are clearly distinguishable in MS detection, but cannot be identified by conductivity detection and may be misinterpreted as a distinct zone of a matrix component.

The differences in intensities in the mass traces of analytes result from differing ionization efficiencies, while the length of each plateau contains the quantitative information [47]. This means that in plateau mode ITP, signal “intensity” depends on the ionization efficiency of the analyte, but is not decisive for quantification. Thus, even an analyte with very poor ionization efficiency and detection limits in CE-MS may be quantified in ITP-MS as long as a (weak) signal is detected and the plateau-mode is reached. In conclusion, ITP-MS probably offers new methods of quantification at low concentrations independent of the ionization efficiency. Ideally, isotope-labeled internal reference standards are used to generate quantitative data. In this case, ITP can also be used in cases, where macrocomponents in the sample would impair CE-MS measurements. Then, quenching effects in the ion source do not affect quantification as long as signals of analytes and internal standard are visible and experience the same signal impairment.

2.5.4. Applications of ITP-MS

Only few publications address ITP-MS. This is due to the restricted selection of MS-compatible leading, terminating and counterions and the rather low selectivity of ITP, as described above. Nevertheless, ITP has been used to prepare samples for offline mass spectrometric analysis, e.g. to investigate hydrogenation products of aromatic quaternary ammonium ions for relative quantification as presented by Kenndler and Haidl [48] or for sample fractionation of human urine samples applying two-dimensional ITP with discrete spacers to narrow the mobility window for the selective analysis of buserelin with subsequent tandem mass spectrometry (MS/MS) analysis [49].

Only few studies used ITP-MS in a direct coupling for a broad range of analytes. A summary of these articles with experimental details and comments can be found in the appendix, Table A2. The first publication of online ITP-MS dates back to 1989 when Udseth et al. [36] presented the first ITP-MS hyphenation for the analysis of quaternary phosphonium and ammonium salts, dopamine, epinephrine, lysine and arginine.

Detection limits in the picomolar range were reached when using injections of up to 10 µL. In the same year, Smith et al. [35, 50] published methods with ITP coupled to a SL-supported ESI-MS to analyze peptides and small proteins. After these preliminary studies, it took nearly 20 years until publications on this technique came up again, now aiming to optimize the mobility window and, thus, selectivity of ITP with MS-compatible electrolyte systems. Early publications on anionic ITP using reverse polarity were published by Zhao et al. for the analysis of nucelotides [42] and the characterization of enzymatic peroxidation [43], both at low pH but with an electrolyte system not well MS-compatible (LE: 7 mmol/L HCl, 13 mmol/L β-alanine (pH 3.9) and TE: 10 mmol/L caproic acid (pH 3.4)).

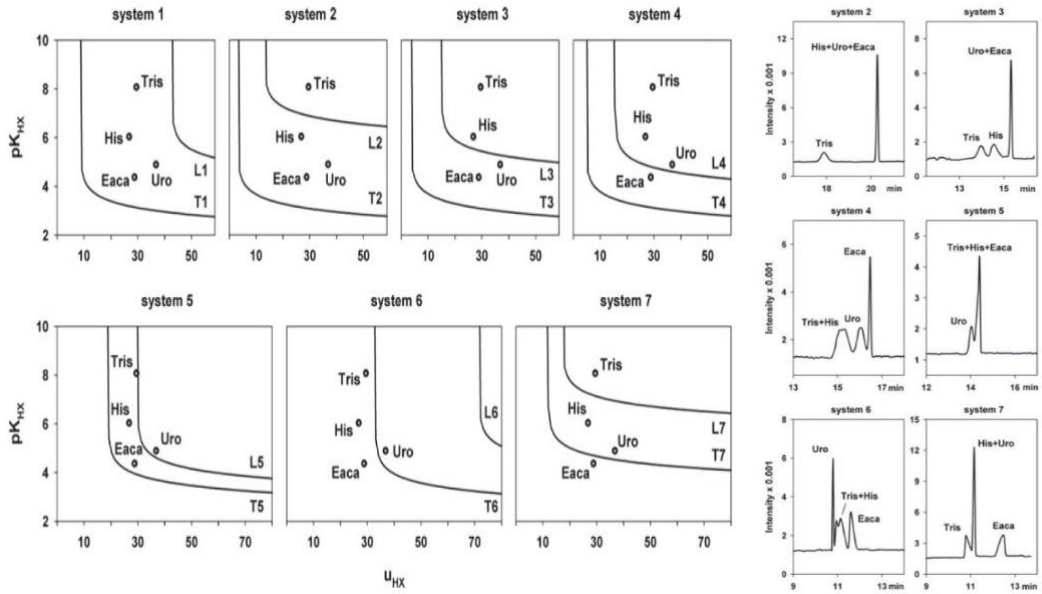

Figure 2.6: Calculated mobility windows in electrolyte systems with ammonium as leading ion and H^+ from HAc as terminating ion. The systems differ in the concentrations of ammonium and HAc in both LE and TE. The area between the lines in the plots of pK_a values against mobilities (pK_{HX}-u_{HX}) defines the mobility window of the moving boundary ITP system, the dots mark the properties of the four analytes tris(hydroxymethyl)aminomethane (Tris), histidine (His), hexamethylene tetramine (Uro) and ε-aminocaproic acid (Eaca). The panels on the right are ITP-MS mass traces from single ion monitoring of the analyte mixtures in the respective electrolyte systems. System 1: LE 10 mmol/L NH_4^+ + 20 mmol/L HAc, TE 1 mmol/L NH_4^+ + 23.54 mmol/L HAc. System 2: LE 10 mmol/L NH_4^+ + 10 mmol/L HAc, TE 2 mmol/L NH_4^+ + 13.15 mmol/L HAc. System 3: LE 10 mmol/L NH_4^+ + 12 mmol/L HAc, TE 2 mmol/L NH_4^+ + 15.15 mmol/L HAc. System 4: LE 10 mmol/L NH_4^+ + 20 mmol/L HAc, TE 2.5 mmol/L NH_4^+ + 22.95 mmol/L HAc. System 5: LE 4 mmol/L NH_4^+ + 28 mmol/L HAc, TE 2.05 mmol/L NH_4^+ + 28.77 mmol/L HAc. System 6: LE 4 mmol/L NH_4^+ + 20 mmol/L HAc, TE 0.2 mmol/L NH_4^+ + 21.50 mmol/L HAc. System 7: LE 0.8 mmol/L NH_4^+ + 0.8 mmol/L HAc, TE 0.5 mmol/L NH_4^+ + 0.92 mmol/L HAc. Reprinted from [34] with permission from John Wiley & Sons.

The Boček group investigated several methods for electrolyte tuning to optimize the mobility window in ITP-MS by varying electrolytes made of FA, lactic acid, propionic acid

and HAc to selectively analyze diclofenac, ibuprofen, salicylic acid, benzoic acid and *p*-hydroxybenzoic acid as model analytes [32, 37-38]. They showed that different modes can be used such as free acid ITP, where no counterion is added to the electrolytes [37], moving boundary ITP with two different coions in both electrolytes [32], spacer techniques to separate analytes in the ITP stack from each other [38] and even presented a system which develops two independent ITP systems with different velocities in the same capillary [38]. In case of free acid ITP, they reported ITP-MS quantification limits in the picomolar range for diclofenac and ibuprofen in drinking and river water using FA as LE and propionic acid as TE [37]. The mobility window was successfully narrowed towards individual anionic analytes by adjusting the electrolyte concentrations of LE and TE, but it was also shown that increasing the selectivity becomes challenging when analyte mobilities are very similar [37]. The same method was combined with offline solid phase extraction (SPE) to further improve detection and quantification limits to the low picomolar range [41]. Malá and Gebauer [39] used anionic ITP-MS at pH 7.77 for the analysis of sulfonamides in drinking and river water with a limit of quantification of about 0.7 nmol/L using OH^- as termination ion with LE and TE composed of HAc and triethylamine as electrolytes. Similarly, de Lassichère et al. [44] used a system of LE: 80 mmol/L HAc with 200 mmol/L ammonium hydroxide, pH 9.55 and TE: 0.175 % ammonium hydroxide (OH^- as termination ion) for the quantification of amyloid beta peptides in cerebrospinal fluid in an inverse ITP at high EOF and normal polarity. The limit of detection was 0.04 nmol/L and allowed to discriminate patients suffering from Alzheimer's disease from controls. Concentrations in the nanomolar range of beta-blockers with pK_a values between 9 and 10 were determined in extracts of dried blood spots in cationic peak mode ITP, which could directly be injected [40] (LE: 10 mmol/L triethylamine and 6 mmol/L HAc at pH 10.6 and TE: 10 mmol/L triethanolamine and 10 mmol/L HAc).

Similar experiments were conducted for various cationic analytes in orange juice [34]. Ammonium (as acetate salt) was employed as LE and H^+ from HAc served as terminating ion. The mobility window and selectivity in moving boundary ITP were modified by addition of leading ion to the terminating electrolyte at low concentration. Thus, two coions were present in both LE and TE, namely ammonium and H^+. The changes in the mobility window resulting from this tuning method are visible in Figure 2.6. The plots show the dependence of the pK_a of the acid pK_{HX} on the mobility u_{HX} for different LEs and TEs. The mobility window is enframed by these two lines and only analytes with parameters within this area will be preconcentrated. Clearly, it is possible to shift the mobility window of this electrolyte system in order to include or exclude distinct analytes

(compare Figure 2.6) for optimal selectivity. Detection limits were determined to be in the higher picomolar range [34]. Based on the same strategy, cationic ITP-MS separation of pesticide metabolites in drinking and river water revealed comparable detection limits [33]. The presented methodologies and techniques are suitable to optimize mobility windows and enhance selectivity towards targeted analytes in MS-compatible electrolytes. Nevertheless, widening the mobility window, e.g. for screening techniques, is not possible. Instead, the strategy presented will inherently narrow the mobility window compared to classic ITP systems consisting of one coion and one counterion in each electrolyte.

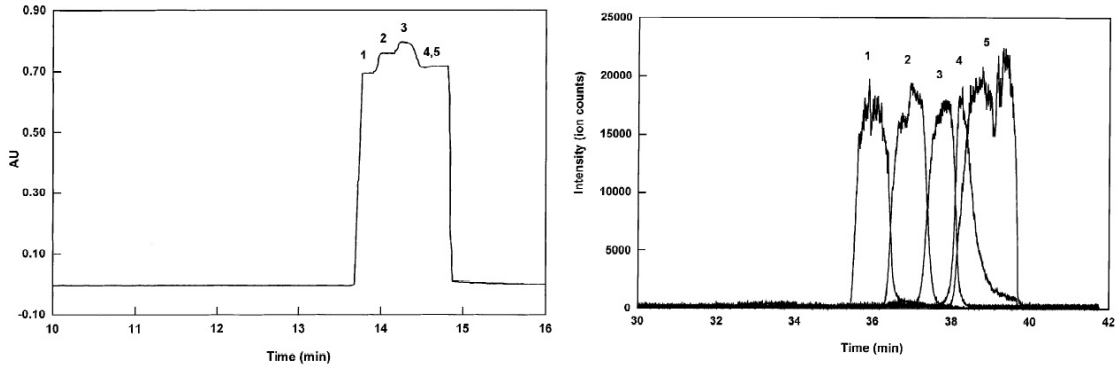

Figure 2.7: Isotachopherograms of separation of human angiotensins by ITP-UV (left) and ITP-MS (right). LE 10 mmol/L ammonium acetate, TE 10 mmol/L HAc, 20 cm sample plug of angiotensins (30 µmol/L). Reprinted from [51] with permission from Elsevier.

ITP-MS coupling was used for the cationic analysis of human angiotensin peptides using ammonium acetate and acetic acid as LE and TE [51]. A comparison of ITP-UV and ITP-MS traces under similar conditions (Figure 2.7) reveals that in the UV trace, analytes 4 and 5 cannot be distinguished. The extracted ion isotachopherograms of ITP-MS analysis show a mixed zone consisting of two incompletely separated analytes. A method with similar electrolytes for the analysis of human angiotensins was applied by Kler et al. [52] for comparison with ITP/CE-MS. Kler et al. [2] also developed a nonaqueous ITP-MS (NAITP) method for all proteinogenic amino acids in electrolytes containing dimethyl sulfoxide (DMSO) to overcome the Eigen-Zundel-Eigen effect and strongly reduce the mobility of the terminating H^+. This enabled the cationic stacking of all proteinogenic amino acids including the weak bases aspartic acid and glutamic acid in a single run with imidazole as leading ion (Figure 2.8). Originally, taurine was intended as terminating ion, but the mass spectrum clarified that H^+ was the true terminating ion, an information which would not have been accessible with conductivity detection. Here, peak mode ITP was present with the stack of amino acids being too narrow to be

resolved by conductivity detection. In contrast, the extracted ion isotachopherograms clearly identified all amino acids (Figure 2.8).

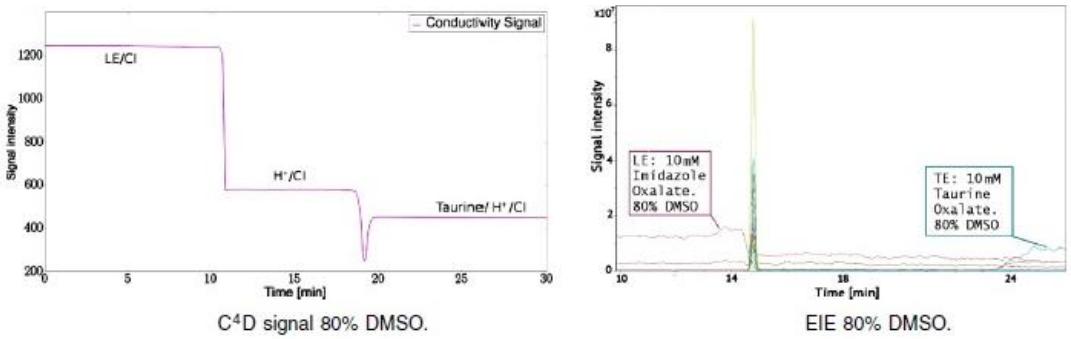

Figure 2.8: C^4D trace and extracted ion isotachopherogram of all proteinogenic amino acids in ITP-C^4D-MS with 80 % (v/v) DMSO in leading and terminating electrolyte. Imidazole was employed as leading ion, H^+ served as terminating ion migrating before taurine. Oxalic acid was used for pH adjustment and as counterion. Clearly, all amino acids were stacked in a narrow zone (= peak mode) too short to be resolved by C^4D detection but visible in the MS signal. Reprinted from [2] with permission from Springer Nature.

In a hydrodynamically closed large bore capillary ITP/ITP-MS system, cationic vitamins, tryptic peptides and thiamine were determined in undiluted whole blood samples with detection limits in the higher picomolar range using ammonium acetate and HAc as LE and TE [53]. A fused silica capillary connected the instrument elution block with the ESI-MS and a syringe pump delivered the SL, which further transported the zones to the MS by pressure. The preseparation column of the ITP/ITP instrument was used to successfully remove matrix macrocomponents.

Mass spectrometry has also been coupled to free-flow isotachophoresis for the anionic determination of Alexa Fluor 448, citric acid, fluorescein and glycolic acid as model analytes by Park et al. [54] using formic acid as LE and propionic acid as TE. In this setup, it was necessary to delay the detection in order to account for the necessary ESI flow rates as a makeup flow had to be used. Only after 2 min the composition of the free-flow isotachophoresis effluent and makeup flow mixture was stable over time. Changing the flow rate ratio at the inlet flows on either side of the device allowed scanning the ITP window from LE to TE.

Vio et al. [55] coupled ITP to inductively-coupled plasma-mass spectrometry (ICP-MS) to analyze lanthanides using 2-hydroxy-2-methylbutyric acid with acetic acid as LE and acetic acid as TE. For the measurement of lanthanide standards, they applied a hybrid micro device consisting of a chip injection compartment and a capillary. Isotope ratio fractionation was possible in ITP-ICP-MS: the isotopes of a distinct lanthanide migrated in the same zone and could be differentiated by ICP-MS. It was shown that a mass dependent migration time drift of the isotopes occurred within the lanthanide's ITP

zone [55]. In another approach, the group employed a capillary coupling setup consisting of an injection and a separation capillary for the determination of lanthanides in reconstituted nuclear fuel samples using the same electrolyte system [56]. The injection capillary had a larger inner diameter and allowed injecting lower concentrated samples due to a higher loadability leading to a preconcentration factor of 100. It was stressed that mass dependent migration time drifts of isotopes of one element within ITP plateaus make ITP-ICP-MS an interesting technique for isotope ratio fractionation [56].

2.6. Hyphenation of ITP to CE-MS

2.6.1. Modes and reviews

CE-MS has many advantages such as low consumption of chemicals and a very high separation efficiency [57], but its major drawback is its poor concentration detection limit, due to limited loadability (typically nanoliters). The coupling of ITP with CE-MS can overcome these disadvantages by employing the intrinsic concentration capability and higher loadability of ITP. Most often tITP is applied as an online preconcentration method. Coupling of ITP and CE-MS in two-dimensional approaches (ITP/CE-MS) is less commonly applied but it combines the advantages of both techniques and has a higher preconcentration ability than tITP/CE-MS.

Several reviews discussed the combination of ITP and CE with various detection techniques (see also Table A1): tITP/CE is often included in reviews on online sample preconcentration for small ions from high conductivity matrices [7, 58]. The Foret group [59] reviewed multidimensional liquid phase separation techniques for mass spectrometry, including a theoretical discussion on orthogonality and peak capacity. An overview on column coupling strategies in electromigrative separations and coupling of electromigrative and chromatographic separation methods was given by Kler et al. [60]. Reviews on multidimensional capillary electrophoresis describing comprehensive and heart-cut two-dimensional separations, different interfaces for coupling and microfluidic techniques, as well as three-dimensional capillary electrophoresis were published by Grochocki et al. [61-62]. An overview on miniaturized ITP including ITP/CE and tITP/CE, demonstrating the trend towards miniaturization also for electromigrative separation techniques, was published by Chen et al. [63].

We here focus on the online combination of tITP and ITP with CE-MS to discuss the opportunities, drawbacks and specialties resulting from the hyphenation of these techniques.

2.6.2. Transient ITP in CE-MS

For tITP in CE and CE-MS analyses, a suitable leading and/or terminating ion in the sample or in a solution injected before/after the sample plug induces transient ITP conditions. The BGE coion may serve as LE or TE ion. In many cases, a leading or terminating ion is added to the sample to generate and control tITP but also sample-induced tITP may be present with fast ionic matrix macrocomponents such as chloride and sodium or potassium in biofluids, see also Figure 2.2. Detailed theoretical discussions on conditions needed for tITP sample self-stacking were given by Gebauer et al. [64-65]. In the following, selected publications on tITP/CE-MS are discussed. Details of experimental conditions and validation parameters are presented in Table A3 in the appendix.

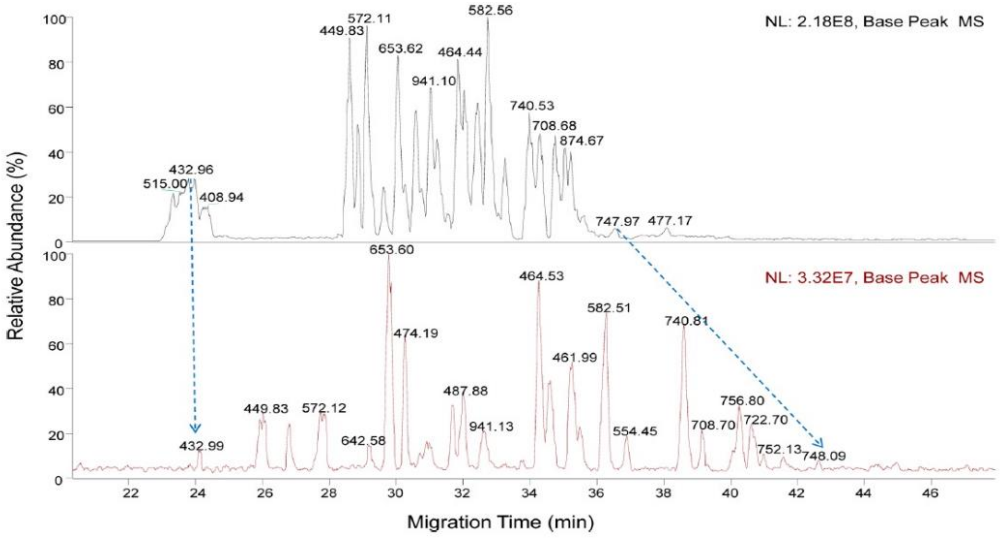

Figure 2.9: Base peak electropherograms of bovine serum albumin tryptic digest analysis with sheathless tITP/CE-MS. Two different sample volumes were injected: 198.8 nL (upper trace) and 28.4 nL (lower trace). The higher injection volume decreases the available separation path in the capillary. Resolution is further diminished due to tITP. Sample diluted in LE. LE: ammonium acetate, BGE: 0.1 mol/L acetic acid in 10 % (v/v) methanol in water. Reprinted with permission from [66]. Copyright (2016) American Chemical Society.

tITP/CE-MS evokes sharper peaks than in CE-MS alone and can already improve detection limits but the conditions have to be chosen carefully: on the one hand, tITP offers a higher loadability as diffusion effects present at higher injection volumes in CE are counteracted by the preconcentration process during tITP. On the other hand, higher injection volumes decrease the remaining separation distance for CE separation, affecting detection times, separation efficiency and resolution. With classical detection methods such as UV or conductivity detection, a lower peak capacity may hinder peak identification. With MS detection, the additional selectivity given by MS can overcome

these challenges but it must be kept in mind that comigrating analytes can evoke quenching effects impairing quantitative precision and, in case of MS/MS analysis, reduce fragmentation times. An example of effects from increased injection volumes is visible in Figure 2.9, showing tITP/CE-MS analysis of tryptic digests of bovine serum albumin at injection volumes of 28.4 nL and 198.8 nL (factor 7).

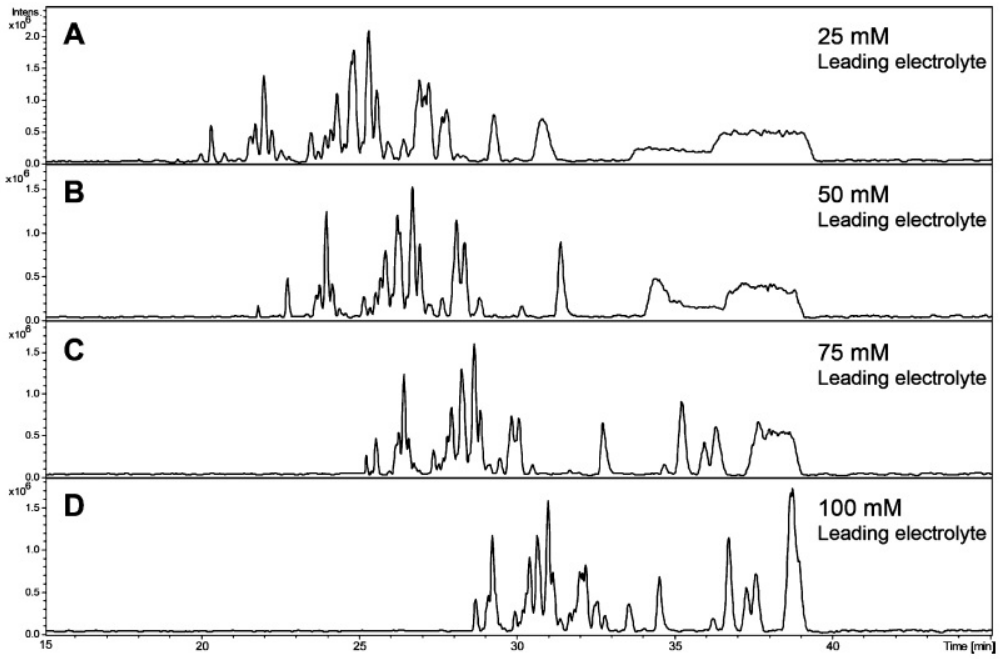

Figure 2.10: Influence of leading electrolyte concentration in tITP/CE-MS on the detection times and migration time window. Base peak electropherograms of tITP/CE-MS analyses of 2.5 ng of a tryptic milk digest separated in a neutrally coated capillary, sample loading filling 37 % of the capillary, sample dissolved in LE. LE: ammonium acetate, BGE: 10 % (v/v) acetic acid. Reprinted with permission from [67]. Copyright (2012) American Chemical Society.

As visible in Figure 2.10, the influence of concentration of transient LE or TE has to be optimized for preconcentration as the amount of LE or TE injected defines the migration time analytes spend stacked isotachophoretically. As described in Section 2.4, a full ITP-MS may persist up to the detection point, instead of CE-MS (compare Figure 2.2B). Increasing the LE concentration results in a smaller migration window (spanned between first and last analyte signal) with lowered peak capacity but also longer analysis times (as shown in Figure 2.10), which may at least partially be compensated by MS detection. However, the longer the migration in the ITP mode, the stronger is the positive influence on preconcentration and separation efficiency as visible in Figure 2.10. In this example, especially the peak shape of signals of low mobility analytes profited from the higher LE concentration as tITP compensated for the broad injection plug.

The majority of tITP/CE-MS methods published so far focused on preconcentration and separation of peptides and proteins [29, 68]. Early studies were published e.g. by Thompson et al. [69] with detection limits for proteins in the submicromolar range being 100-fold lower than in CE-MS without tITP (LE: ammonium acetate, TE: HAc, BGE: aminohexanoic acid), or by Foret et al. [70] who could increase the injected volume of protein samples 30-fold, adding HAc as transient TE in a triethylamine BGE. In this study, tITP did not significantly increase measurement times but delivered a focused protein stack as a perfect starting condition for CE to achieve detection limits in the nanomolar range. In a recent study by Stock et al. [71], tITP/CE-MS was applied to monitor molecular processes of a recombinant allergen under thermal stress, using ammonium as transient leading ion and FA as BGE. Due to the low pH of the BGE, the separation took place at close to zero EOF. By tITP, the injection volume could be increased by a factor of 5 and the preconcentration allowed the detection of low abundant species [71]. Peptide hormones were analyzed by tITP/CE-MS in different approaches: Gysler et al. [72] reached 700 fmol absolute detection limits for human interleukin-6 and nine different degradation products. Ammonium acetate was employed as BGE and samples were dissolved in HAc which acted as TE (H^+ as transient TE ion). Peptide hormones in rat hypothalamus tissue were examined in an HAc BGE with ammonium acetate as transient LE by Xia et al. [73] in a submicromolar range with a sensitivity enhancement by a factor of 230 due to tITP. Opioid peptides in human plasma were determined by combining online SPE with tITP/CE-MS by Medina-Casanellas et al. [74], gaining an improvement in the detection limit by a factor up to 5000 in comparison to CE-MS. Ammonia and H^+ were used as LE and TE in an HAc/FA BGE with ammonia for pH adjustment. Detection limits were reduced to 0.01 µg/L by the tITP step in comparison to CE-MS (0.05 mg/L) and SPE-CE-MS (0.1 µg/L).

tITP/CE-MS is widely used for the analysis of tryptically digested proteins. Phosphopeptides from tryptically digested dry bovine milk powder were analyzed with tITP/CE-MS at very low flow rates for ESI-MS (below 15 nL/min) [67]. The concentration of ammonium in the sample serving as transient leading ion was optimized (see Figure 2.10). Peptides from a tryptic digest of ovalbumin present at a ratio of 1 to 500 000 compared to tryptic peptides of cytochrome c could be identified by MS/MS with a detection limit of 0.1 nmol/L [75] due to the increased loadability by tITP. Larsson et al. [76] examined tryptic peptides of cytochrome c, melagatran, substance P and calcitonin gene-related peptides in rat brain tissue by tITP/CE-MS using a single quadrupole mass spectrometer both qualitatively and quantitatively, achieving detection limits in the low

nanomolar range. A microfluidic setup combining online tryptic digestion with subsequent tITP/CE-MS analysis was introduced by Gao et al. [77].

Several methods combining tITP/CE with a sheathless interface for MS have been published. As no SL is present, a moderate to high EOF is necessary to provide sufficient volume flow for the ESI. Thus, there is no necessity to assure counterions to be present in the SL. For example, the investigation of online solid phase microextraction (SPME) with CE-MS, including an intermediate tITP step induced by the SPME elution buffer resulted in improved signal-to-noise ratios for tryptic peptides from *Pyrococcus furiosus* in comparison to CE-MS and nano-liquid chromatography-MS [78]. Busnel et al. [79] found detection limit improvements by factors between 10 and 86 due to tITP for tryptic peptides from bovine serum albumin and *Escherichia coli*. Detection limits were in the low nanomolar range but a decreased peak capacity was observed, too. Quantification limits below 50 pmol/L were obtained for peptides by tITP/CE-MS with a sheathless electrospray interface and single reaction monitoring mass spectrometry by Wang et al. [80]. Using ammonium acetate as LE and an HAc BGE with 10 % (v/v) methanol added, quantification limits were approximately 30 times lower than in analyses without tITP. Subsequently, the group employed the same setup and electrolyte system for tITP/CE-MS analysis of peptides in a tryptic bovine serum albumin digest, obtaining a linear range over four orders of magnitude with high reproducibility and picomolar quantification limits [81]. Subnanomolar quantification limits were estimated for kemptide in a similar setup by Guo et al. [66]. In a short communication, Heemskerk et al. [82] presented a tryptic digest of immunoglobulin G in human plasma with picomolar detection limits, 40-fold improved sensitivity and a possibility for glycosylation profiling by sheathless tITP/CE-MS. Impressive results were published by Gahoual et al. [83-84] who employed tITP/CE with sheathless MS/MS for peptide sequencing of monoclonal antibodies. They were able to determine the amino acid sequence from a tryptic digest of trastuzumab, reaching 100 % sequence coverage from a single injection together with the identification of post-translational modifications.

Other analytes than peptides have been analyzed by tITP/CE-MS as well: metabolites in human urine were detectable in a subnanomolar to nanomolar range due to sensitivity improvement by up to two orders of magnitude using tITP. An increased number of metabolite features was observed [85], showing the applicability of sheathless CE-MS interfaces also for metabolomics. Oligosaccharides in *Pseudomonas aeruginosa* were investigated as model analytes by a SL-supported tITP/CE-MS method to be used for the structural characterization of lipopolysaccharides. A 10- to 50-fold sensitivity improvement was achieved by tITP and up to 50 % of the capillary could be filled with

analyte [86]. In this setup, anionic analysis was carried out under reversed polarity on uncoated capillaries, causing an EOF towards the inlet. Thus, a small pressure had to be applied to prevent analyte loss and intake of air into the capillary from the ion source. Triethylamine formate was applied as BGE, serving as transient LE, and 2-(N-morpholino)ethanesulfonic acid was used as transient TE. Samples were dissolved in BGE. Due to the counter-EOF separation conditions, the TE could be kept at the capillary inlet for several minutes to prolong the ITP process while only a small amount of 2-(N-morpholino)ethanesulfonic acid, not well compatible with ESI, entered the MS [86]. Lagarrigue et al. [87] examined anionic alkylmethylphosphonic acids in aqueous extracts of soil samples and diluted rat urine in an ammonium acetate BGE containing 35 % methanol with glycine as transient TE. The TE solution contained the same amount of methanol and was injected prior to the sample at counter-EOF conditions. Anionic separation was then conducted at normal polarity on uncoated capillaries, and analytes were transported to the SL-supported MS interface by the EOF. The group obtained 40-fold sensitivity improvement by tITP [87].

2.6.3. Two-dimensional ITP/CE-MS

2.6.3.1. Ideas and strategies

For 2D ITP/CE-MS three different electrolytes are employed (see also Table A4 in the appendix for an overview on all articles considered here): LE and TE for ITP and BGE for CE. In many cases, either LE or TE are used as BGE in the second dimension, the modes are called L-S-L (S for sample) and T-S-T [88-90]. A schematic representation of both L-S-L and T-S-T mode for cationic separations is given in Figure 2.11. If the BGE is different from both LE and TE, the mode is called BGE-S-BGE (Figure 2.11) [88-90]. As the electromigration behavior in ITP versus CE is different, the coupling can be regarded as two-dimensional [91].

In general, a cotransfer of some LE and TE with the sample to the second dimension will occur, which may impair MS detection when components are not MS-compatible. The second dimension always starts with a tITP, which has to be resolved for CE-MS analysis. This may fail when too much LE or TE are cotransferred, see e.g. [51]. The amount of cotransferred LE or TE determines the duration of the tITP and may significantly affect the CE separation as described in Sections 2.4 and 2.6.2, and by the Boček group [91]. The electrolyte combination chosen determines analysis time and dispersion effects in the second dimension [89].

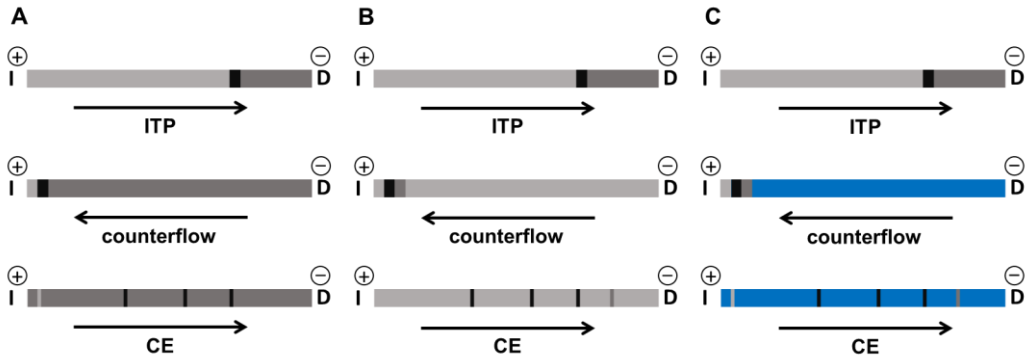

Figure 2.11: Schematic depiction of (A) L-S-L, (B) T-S-T and (C) BGE-S-BGE modes in an exemplary cationic ITP/CE single capillary setup with counterflow. I: injection, D: detection, dark gray: leading electrolyte, light grey: terminating electrolyte, blue: background electrolyte, black: sample/analytes. In (A) LE is used as BGE in the second dimension, in (B) TE is used as BGE, in (C) LE, TE and BGE are three different electrolytes.

For capillary coupling ITP/CE-MS, coatings were often applied (see Table A4 in the appendix) to better control the migration times and, thus, transfer steps. The commercial instrumentation consists of capillaries made of polytetrafluoroethylene [92-95], sometimes (methyl-)hydroxyethyl cellulose was added to further suppress the EOF [94-95]. For ITP/CE-MS analysis of peptides, proteins and oligonucelotides, adsorbed neutral coatings were applied to fully suppress the EOF and reduce sorption phenomena [51-52, 70, 96-98]. In rare cases, dynamic coatings were applied [99-100]. Peterson et al. [51] reported higher separation efficiencies and the possibility to use shorter capillaries to reduce analysis times. Kler et al. [52] demonstrated that EOF differences in separation columns and interface may lead to band broadening due to mixing effects at the channel intersections.

For online ITP/CE-MS hyphenation, single capillary approaches, in which ITP and CE take place in the same capillary, and capillary coupling setups are possible, which use different interfaces to combine ITP and CE capillaries as summarized in a review by Kler et al. [60] focusing on technical aspects. Chip-based multidimensional separations were reviewed by Tia and Herr [101]. In both modes but especially the latter, intermediate detection is important for an appropriate sample transfer. The sample transfer can either be a single or multiple heart-cut or a front-/end-cutting strategy in T-S-T and L-S-L systems.

2.6.3.2. Two-dimensional single capillary ITP/CE-MS

A complete ITP process is present in two-dimensional approaches with a change of at least one electrolyte in the second dimension [102], which is also possible using a single capillary: a counterflow is used to keep the ITP stack at the capillary inlet or to push the

focused ITP zones back towards the inlet after completion of the ITP enrichment process. Band broadening due to counterflow is counteracted by the self-sharpening effect of ITP. Major advantages compared to tITP/CE are: 1) higher loadability (up to 67 % of the capillary), as the separation distance in the second dimension is not reduced, 2) sensitivity enhancement factors of up to 200, and 3) the possibility for matrix removal [96, 98-100, 103-104]. So far, only L-S-L and T-S-T systems have been applied using the current profile to estimate the position of the analyte stack.

To our knowledge, the combination of single capillary ITP/CE with mass spectrometric detection has been published only twice. Lamoree et al. [105] investigated clenobuterol and analogues and β-antagonists in calf urine with impressive detection limits in the subnanomolar range. The counterflow was induced and stopped by leveling the inlet vial. The SL, acting as outlet, had a similar composition as the BGE. Van der Vlis et al. [106] analyzed various pharmaceuticals with an online combination of liquid-liquid electroextraction with single capillary ITP/CE-MS. The sample plug was kept at the capillary inlet during electroextraction and ITP by a pressure-induced counterflow, though the authors did not state the instrumental details of pressure generation. A 200-fold sensitivity enhancement compared to CE-MS was obtained with nanomolar detection limits. Nevertheless, the applicability of ITP/CE-MS in a single capillary setup is limited to L-S-L systems as the SL used for the counterflow also serves as LE and BGE. This strongly minimizes the number of suitable electrolytes and can often be disadvantageous for ionization efficiency. In the publications, this issue was not discussed.

2.6.3.3. Two-dimensional capillary coupling ITP/CE-MS

Basic considerations: capillary coupling ITP/CE-MS generally involves separations, which take place in distinct capillaries which are coupled via a suitable interface [60]. It allows to fully exploit the advantages of both separation mechanisms such as 1) a higher capillary loadability based on 2) an increased flexibility in capillary dimensions (diameter and length), 3) formation of narrow zones for an optimal analyte transfer to the second dimension, 4) the possibility for an efficient matrix removal by cutting techniques including heart-cutting, and 5) a greater flexibility in electrolyte combinations. Depending on the interface chosen, it is easier to employ BGE-S-BGE compared to single capillary modes, so that non-MS-compatible electrolytes can be used in the ITP dimension offering a greater flexibility for leading and terminating ion selection and, thus, selectivity tuning.

There are several examples of capillary coupling ITP/CE without MS detection. Foret et al. [70] applied this hyphenation for the analysis of 10 µL protein samples with

intermediate conductivity and final UV detection gaining a concentration factor of 2000. Piešťanský et al. [95] used a commercial ITP/ITP instrument for capillary coupling ITP/CE analysis of varenicline in urine and obtained detection and quantification limits in the low µg/L range with UV detection with a better selectivity than CE-UV. An impressive example for ITP/CE with multiple front-cuts was given by Bowerbank and Lee [97]: a CE capillary was inserted into a wide bore ITP capillary. Applying intermediate UV detection of angiotensin model analytes and an L-S-L system, a periodic counterflow allowed to transfer fractions of the ITP sample stack after ITP refocusing, while the CE separation was conducted. 20- to 50- fold improved concentration detection limits for proteins were achieved by Ölvecká et al. [107] using a poly(methylmethacrylate) chip in a hydrodynamically closed ITP/CE with conductivity detection.

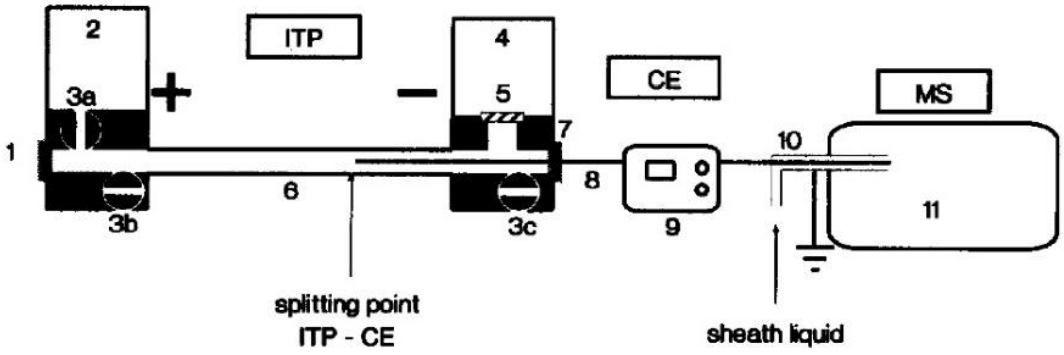

Figure 2.12: Online ITP/CE-MS coupling as applied by Reinhoud et al. [108]. (1) Injection silicone-rubber septum, (2) terminating buffer vial connected to positive voltage, (3a-c) valves for ITP capillary flushing, (4) grounded leading buffer vial (potential raised to +2 kV during injection), (5) membrane to hydrodynamically close ITP capillary, (6) 150 x 0.32 mm i.d. ITP capillary, (7) septum for insertion of CE capillary into ITP capillary, (8) 700 x 0.075 mm i.d. or 700 x 0.04 mm CE capillary, (9) UV absorbance detector, (10) sheath liquid assisted sprayer needle, (11) electrospray MS. Reprinted from [108] with permission from Elsevier.

Only seven publications addressed the challenges of capillary coupling ITP/CE-MS. These include a suitable interface accepting high voltages with intermediate detection ideally at the bifurcation point and preventing adsorption of analytes or electrolytes. Furthermore, a very low dead volume is preferred to minimize sample loss, carryover and band broadening [60]. A hydrodynamic and electrokinetic decoupling of both separation dimensions is favorable for highest flexibility in electrolyte combinations [52]. Electric decoupling of the two dimensions facilitates MS detection since the ESI needle has a fixed voltage and the capillary to the MS is (hydrodynamically) open. Whereas the first aspect may be critical with regard to analyte and electrolyte migration upon voltage switching, the latter may complicate the filling of the two dimensions with appropriate electrolytes. Optimized sample transfer (electrokinetically or hydrodynamically) with

minimal cotransfer of ITP electrolytes prevents large amounts of non-MS-compatible buffer components to enter the MS and, thus, gives more freedom in the choice of electrolytes. In addition, the risk of persisting ITP conditions in the second dimension is reduced [29].

Already in the early 90s Reinhoud et al. [108] presented the analysis of anthracyclines in an L-S-L system with the CE capillary inserted into the hydrodynamically closed ITP capillary via a septum. The sample stack was transferred electrokinetically to the second dimension. Voltages between the dimensions were not decoupled. For analyte transfer, the cathode potential was increased in favor of the CE capillary. A schematic depiction of this setup is given in Figure 2.12.

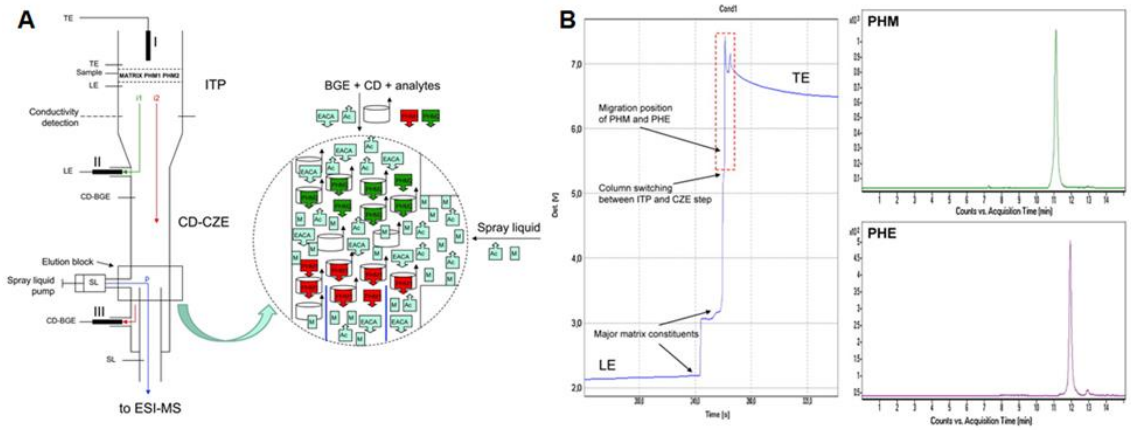

Figure 2.13: (A) ITP/chiral CE-MS setup used by Piešťanský et al. in several publications [92-94]. The upper part depicts the ITP column with TE vial and LE vial. i1 marks the driving current during the ITP step. The sample is transferred to the second dimension filled with BGE (cyclodextrins as chiral selector), i2 marks the driving current during the second dimension separation. The separated analytes are pumped through a capillary from the elution block to the ESI-MS instrument with SL (p). The close-up shows the arrangement of electrolyte and SL components. Reprinted from [94] with permission from John Wiley & Sons. (B) ITP/CE-MS analysis of pheniramine (PHM) and phenylephrine (PHE) spiked to human urine using heart-cutting. Conductivity isotachopherogram of the first dimension and extracted ion electropherograms of CE-MS. Reprinted from [93] with permission from Elsevier.

Angiotensin peptides were investigated in an L-S-L ITP/CE-MS system using a quartz tee as bifurcation point [51]. The focusing/separation voltage was applied continuously and multiple front-cuts were made using LE counterflow between fractions (applied from the bifurcation point) to push back remaining analyte zones, which were then refocused upon ITP. The group observed an unsatisfactory transition of the last two analyte zones from tITP stacking to CE separation mechanism which they assumed to be based on the cotransfer of TE to the second dimension and the short separation distance in the CE capillary, showing that careful analyte transfer to the second dimension is crucial, as well

as an adequate separation distance i.e. capillary length in the CE-MS dimension. Nevertheless, detection limits were improved by at least two orders of magnitude [51].

Piešťanský et al. [92-94] analyzed small molecules in human urine using a commercial modular capillary electrophoresis analyzer with bifurcation block for ITP/CE-MS with electrokinetic and hydrodynamic decoupling from the MS (see scheme in Figure 2.13A). SL was used to pump analytes and electrolytes from the elution block to the MS via a separate capillary, so that MS detection was from a hydrodynamic flow, not from CE. Band broadening and loss of resolution or even analytes are possible.

With this setup, the SL composition is independent of the applied electrolytes and can be optimized for highest ionization efficiency. Major urine matrix components were successfully eliminated from the separation process [92] and even chiral CE-MS was achieved [94]. The group stressed the excellent sensitivity of their method compared to ITP/ITP due to higher MS-compatibility of the BGE. Detection and quantification limits were in the low to medium ng/L range for pharmaceuticals [92-94]. Exemplarily, Figure 2.13B shows the ITP/CE-MS analysis of pheniramine and phenylephrine with heart-cutting. The analyte zone is too narrow to be visible by conductivity detection but delivers perfect starting conditions for the second dimension CE-MS separation, resulting in low peak widths as visible in the extracted ion electropherograms [93].

Kler et al. [52] discussed requirements for the interface comparing results with a polyether ether ketone T-junction interface vs. a microfluidic glass chip interface for capillary coupling ITP/CE-MS analysis of human angiotensin peptides in an L-S-L system. The hybrid approach with the glass interface (see Figure 2.14B, top pictures) connected to standard capillaries showed superior separation efficiencies due to lower dead volumes in the interface. All proteinogenic amino acids were analyzed by NAITP/CE-MS (see Figure 2.14C, right) using this glass chip interface. To our knowledge, this is the only publication on ITP/CE-MS coupling applying a BGE-S-BGE mode. Independent electric circuits for both dimensions were established (Figure 2.14A), which were connected via a bifurcation [2]. This setup allowed the application of non-MS-compatible electrolytes in the ITP dimension as only small amounts of LE and TE were transferred to the second dimension. Hydrodynamic closure of the dimensions to avoid suction effects from the ion source, however, is still a challenge and under further investigation. An improved version of the microfluidic glass chip with close to zero dead volume was introduced by Sydes et al. [3] (Figure 2.14B, bottom pictures).

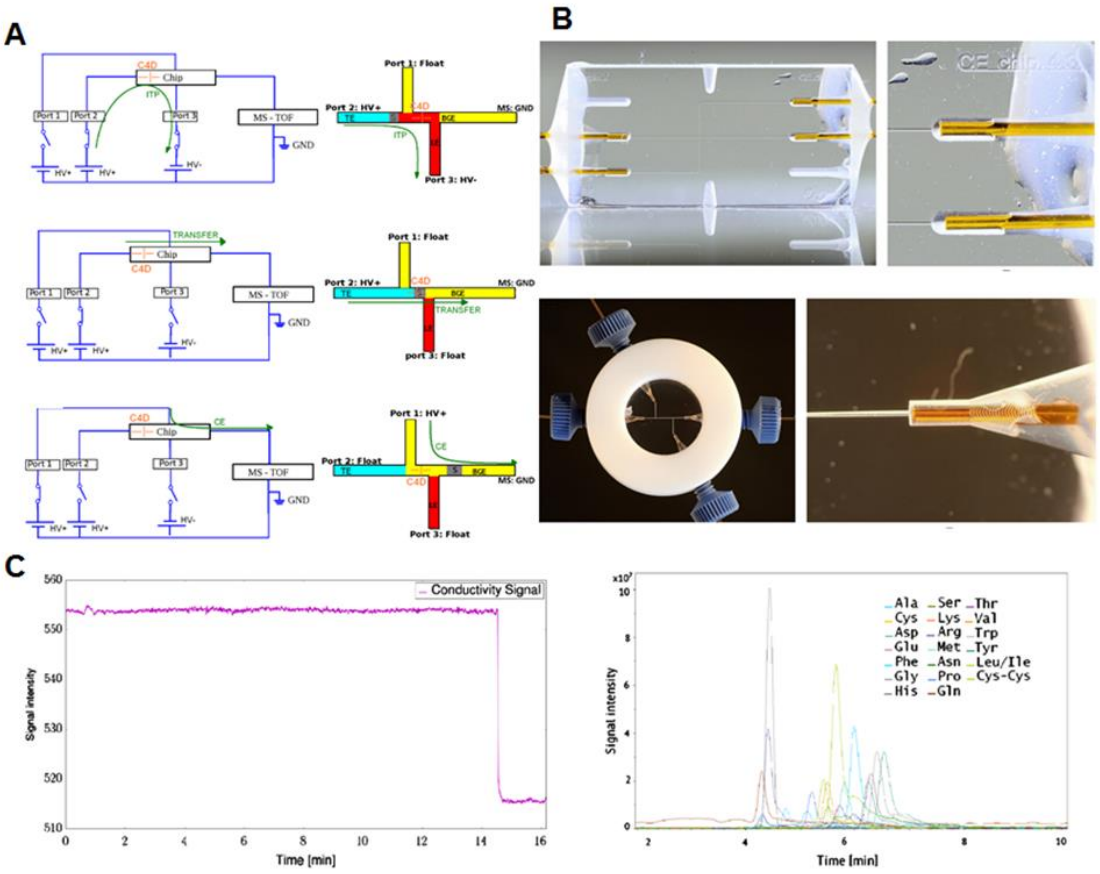

Figure 2.14: (A) Operational scheme of NAITP/CE-MS of all proteinogenic amino acids. Top: NAITP, middle: sample transfer, bottom: CE-MS. Reprinted from [2] with permission from Springer Nature. (B) Microfluidic glass chip interfaces for capillary coupling ITP/CE-MS. Top: cross-shaped microfluidic glass chip as applied by Kler et al. [2, 52] and details of capillary fittings. Bottom: close to zero dead volume microfluidic glass chip interface and details of capillary fitting. Reprinted from [3] with permission from John Wiley & Sons. (C) ITP/CE-MS analysis of proteinogenic amino acids. Left: conductivity isotachopherogram of the first dimension, right: the combined extracted ion electropherograms of the second dimension. Reprinted from [2] with permission from Springer Nature.

2.7. Conclusion

ITP-MS is still a niche technique in separation science. The main challenge is the low number of MS-compatible electrolytes which are suitable for isotachophoretic stacking of analytes. Nevertheless, it has proven to be a powerful method with only a small number of different MS-compatible substances and clever electrolyte tuning. Detection limits in the low picomolar range were achieved and the mobility window was successfully narrowed for targeted analyses.

Due to the higher loadability and its preconcentration power, the combination of ITP with CE-MS is very promising and has been conducted in different ways. The most prominent combination is the introduction of a tITP step to CE-MS analysis. Commonly, loadability can be increased 30-fold, and sensitivity enhancement factors of 200 were reached. In combination with solid phase extraction, detection limits could even be enhanced by a

factor of 5000 while removing matrix components. Detection limits of tITP/CE-MS in the subnanomolar range are possible.

The actual two-dimensional coupling of ITP with CE-MS can either be conducted in a single capillary comparable to tITP/CE-MS or in capillary coupling approaches. The former has rarely been applied with MS detection as the needed counterflow generation can be challenging with MS but 200-fold sensitivity enhancement and subnanomolar detection limits have been reported. Capillary coupling approaches use a variety of different interfaces, ranging from bifurcation blocks of commercial ITP/ITP instruments to polymeric or microfluidic glass interfaces. In this strategy, each separation dimension is conducted in its own capillary, thus, specific advantages of ITP and CE are exploited as far as possible: higher capillary inner diameters in the first dimension improve the loadability and high concentration factors can be achieved. Very narrow zones can be injected into the second dimension for CE separation, optimized for best separation efficiency. It has been shown that injection volumes up to 10 µL were possible, leading to a 2000-fold sensitivity improvement. Approaches of capillary coupling ITP/CE-MS revealed subnanomolar detection limits and enabled removal of major matrix components. Thus, these approaches are very promising for future applications. However, further technical improvements are still necessary.

The combinations of ITP with MS and especially ITP/CE-MS are very promising, which indicates that electromigrative separation techniques can well serve as complementary separation techniques to common chromatographic methods. This combination will probably overcome the CE-inherent obstacle of insufficient concentration detection limits due to limited loadability.

3. Analysis of amino acids by two-dimensional hyphenation of isotachophoresis with capillary electrophoresis-mass spectrometry for online preconcentration and separation

3.1. Abstract

The analysis of amino acids is often achieved by capillary electrophoresis-mass spectrometry (CE-MS) as it does not demand for elaborate derivatization methods, which would be needed for detection by UV or laser-induced fluorescence, and it adds additional information on *m/z* values for analyte assignment. Nevertheless, CE-MS often suffers from poor concentration detection limits. By online hyphenation of CE with the concentration power of isotachophoresis (ITP), detection limits can be improved significantly. In this work, ITP and CE-MS methods were optimized for highest compatibility with each other and with MS detection. For ITP, hydroorganic electrolytes containing 80 % dimethyl sulfoxide with imidazole as leading ion and H^+ as terminating ion using difluoroacetic acid or trimethylpyruvic acid were most convincing. An acetic acid hydroorganic background electrolyte containing 20 % isopropanol was developed for CE-MS analysis. Two different setups for 2D ITP/CE-MS measurements with intermediate conductivity detection were introduced: first, a new straightforward single capillary setup with a microfluidic glass chip interface enabled to introduce a side capillary for counterflow generation. This helped to overcome limitations of counterflow generation and electrolyte/MS-compatibility observed for single capillary setups previously published. Amino acids were successfully preconcentrated and separated in L-S-L, T-S-T and BGE-S-BGE mode with this setup, providing a comprehensive proof of concept for this newly developed setup. Second, a capillary coupling setup using the same microfluidic glass chip interface is presented for amino acid analysis.

3.2. Introduction and motivation

3.2.1. ITP and CE-MS analyses of amino acids

Amino acids have to be analyzed in various matrices. While capillary electrophoresis (CE) analysis of amino acids is common, the number of publications on isotachophoresis (ITP) analysis of amino acids is low. The ITP separation of amino acids is mainly conducted in plateau-mode (see Chapter 2) and only distinct amino acids are analyzed at a time due to the wide range of electrophoretic mobilities which cannot be included within a single ITP mobility window in aqueous electrolyte systems. Depending on the target amino acids, they are separated either as cations or anions. UV or conductivity detection are often applied in the literature. For direct UV detection, derivatization is needed [109]. Amino acids may also be used as spacer ions in ITP of analytes such as

e.g. proteins [110]. As they can also be applied as carrier ampholytes in isoelectric focusing (IEF), Procházková et al. [111] developed a method combining carrier ampholyte-free IEF with ITP/ITP to clean up amino acids for application as carrier ampholytes. The group estimated detection limits in the nmol/L range using conductivity detection, based on the high concentration power of the method. Hirokawa et al. [112] conducted extensive computer simulations on mobilities and pK_a values of 26 amino acids (both anionic and cationic measurements) to assess the separability of these amino acids. Amino acids were also analyzed by anionic gradient elution ITP with detection limits in the nanomolar range [113-114]. In gradient-elution ITP, analytes are concentrated from a sample reservoir under variable counterflow to keep the analytes close to the capillary inlet. By this, longer concentration periods can be implemented before a reduction of the counterflow allows analyte migration towards the UV-detector. In cationic peak-mode ITP-UV with copper ions, which is complexed by histidine, detection limits in the nanomolar range were obtained as well [115]. Anionic peak-mode ITP-UV of derivatized amino acids resulted in absolute detection limits of 250 fmol for derivatized glutamic acid [116]. Most of the work on amino acid analysis with ITP was conducted to improve the separation of a few selected amino acids from each other and from matrix components. Contrary to that, Kler et al. [2] developed a comprehensive method for all 20 proteinogenic amino acids with the aim of concentrating all analytes in one mixed zone for subsequent transfer to a second dimension. With this method, using imidazole as leading ion, even aspartic acid and glutamic acid could be implemented into the mixed zone in cationic peak-mode ITP by employing electrolytes based on dimethyl sulfoxide (DMSO) as solvent. As DMSO is an aprotic solvent, the electrophoretic mobility of H^+ is reduced by suppressing the Eigen-Zundel-Eigen (EZE) flipping mechanism, which normally strongly increases the actual mobility of H^+ (as a terminating ion) in aqueous electrolytes.

Several biannual reviews on electromigrative amino acid analysis were published, started by Smith [117-118] and followed by Poinsot et al. [119-127]. Up to date, detection was mainly conducted via UV absorbance or laser-induced fluorescence (LIF), often necessitating derivatization. Direct analyses with detection by indirect UV, capacitively-coupled contactless conductivity detection (C^4D) and mass spectrometry (MS) evolved in the past years. The first direct CE-MS methods were already published in the beginning of the 90s. MS can detect underivatized amino acids and adds further selectivity and identification power. While MS is able to distinguish comigrating analytes, CE can separate isobaric compounds (such as lysine and glutamine or leucine and isoleucine), making this combination especially powerful.

The most commonly applied buffers for amino acid analysis in CE-MS are ammonium, acetate, formate and mixtures thereof [119-127] which are also the most commonly applied CE-MS buffer substances in general [25, 128]. Detection limits in the low micromolar range can be achieved in CE-MS methods covering all proteinogenic amino acids in different matrices e.g. blood plasma [129], urine [130-131] or food and beverages [130, 132]. In the last 5 years, publications reported detection limits in the nanomolar range with optimized methods, but mainly for methods developed for certain selected amino acids [125-127]. Rodrigues et al. [133] presented a method for a set of 20 amino acids with comparable detection limits due to the addition of analyte stacking techniques.

Transient isotachophoresis (tITP) as a preconcentration technique commonly used in CE measurements (compare Chapter 2) provides a simple possibility to improve detection limits. tITP was applied in CE analyses of amino acids, e.g. for the determination of L-histidine in diluted human blood plasma by Hattori and Fukushi [134]: they combined tITP with field-amplified sample stacking from electrokinetic sample injection in their CE-UV analyses using an acetic acid/ammonia background electrolyte (BGE), with ammonia acting as transient leading ion. The group obtained detection limits in the subnanomolar range [134]. Arginine, lysine, histidine and ornithine were analyzed by tITP/CE with indirect UV detection in human plasma by Okamoto et al. [135]. tITP was induced by injection of HCl after the sample stack, using sodium from the matrix as transient leading ion. Detection limits in the low nanomolar range were reached after minimal sample preparation (centrifugation and acidification) [135].

To our knowledge, the 2D hyphenation of ITP with CE for amino acid analysis was published only three times: Reinhoud et al. [100] analyzed derivatized amino acids in an automated single capillary ITP/CE-LIF setup. Up to 50 % of the capillary could be filled with sample without problems from band broadening. After ITP preconcentration, the sample was transported back towards the inlet by a counterflow, using an L-S-L mode for hyphenation. Davis et al. [136] combined gradient-elution ITP with CE-LIF either in a capillary or a microfluidic glass chip device. Six derivatized amino acids were separated as anions in an L-S-L system (compare Chapter 2), reaching detection limits in the picomolar range due to the extensive preconcentration in the first dimension combined with the high separation efficiency of the second dimension. An interface was not needed in this single capillary setup: gradient-elution ITP under variable counterflow enabled preconcentration of the analytes near to the capillary inlet. Then, the terminating electrolyte (TE) reservoir was replaced by leading electrolyte (LE) and the counterflow was stopped for CE separation [136]. Kler et al. [2] introduced a BGE-S-BGE system for

ITP/CE-MS of all proteinogenic amino acids in one separation run. In this method, derivatization was not needed and MS-compatibility was achieved by combining commercial capillaries with a custom-made microfluidic glass chip interface.

3.2.2. Two-dimensional hyphenation of ITP and CE-MS

3.2.2.1. Microfluidic interfaces

In two-dimensional hyphenations of electromigrative separation techniques, suitable interfaces have to be developed. Comprehensive reviews on interfaces and hyphenation techniques were published by Kler et al. [60] and Grochocki et al. [61-62], see also Chapter 2. The comparison of the performance of a polyetherether ketone T-junction with a microfluidic glass chip in a hybrid capillary-microfluidic setup was published by Kler et al. [52], showing the superiority of the latter due to reduced surface heterogeneity (only fused silica interfaces), reduced dead volume and improved precision concerning sample handling and transfer. This setup was then applied in the capillary coupling ITP/CE-MS for amino acid analysis [2]. Interfaces for this kind of hyphenation must provide 1) similar surface properties as the capillaries, 2) a low dead volume, 3) stability against high voltage application and 4) mechanical rigidity.

A follow-up to these microfluidic glass chips was introduced by Sydes et al. [3]: a microfluidic glass chip without the need for bonding a glass lid was produced by laser-induced etching, allowing to obtain fully circular channels in the chip (vs. semi-circular in the etched and bonded chip). Furthermore, this interfacing chip could be placed in a custom-made mounting which allowed to connect the capillaries to the chip via screws instead of gluing. Commercially available silicone was sufficient to seal the capillary-chip connections.

3.2.2.2. Single capillary 2D setup

In contrast to tITP/CE-MS, in which ITP is carried out as sample preconcentration process in the beginning of the CE-MS separation, single capillary 2D ITP/CE-MS (sc-ITP/CE-MS) approaches aim to combine a complete isotachophoretic preconcentration with a CE-MS separation, but without elaborate additional equipment which is needed in capillary coupling approaches: both ITP and CE are carried out in the same capillary (compare Chapter 2). There are two major operational modes: 1) after completion of the ITP separation, the sample stack is transported back to the capillary inlet by a counterflow before starting the second dimension CE separation or 2) the sample stack is kept close to the capillary inlet during the ITP process by a low permanent counterflow and the second dimension CE separation is started by stopping this counterflow. In both cases, the self-sharpening effect of ITP is employed to reduce

diffusional band broadening resulting from the counterflow. sc-ITP/CE-MS offers a simple hyphenation of two electromigrative methods as it can be conducted using commercial equipment. This hyphenation method was applied for several different analytes such as drugs [103-104], peptide hormones and proteins [96, 99], fluorescent small molecules [100] or oligonucleotides [98] with detection limits reaching the low nanomolar range. UV detection was employed in most cases, LIF and conductivity detection were also used. Mass spectrometry was only used in two studies on sc-ITP/CE [105-106]. The hyphenation to MS faces two problems: 1) the only source to generate the needed counterflow is the sheath liquid used in CE-ESI-MS as the outlet vial is replaced by the ion source. Thus, the sheath liquid must be identical or at least similar to the LE or TE (depending if L-S-L or T-S-T mode is chosen), often resulting in impaired ionization efficiencies of analytes. 2) This further limits the number of available substances for ITP and CE electrolytes as they need to be MS-compatible (as discussed in Chapter 2).

3.2.2.3. Capillary coupling 2D setup

Capillary coupling 2D ITP/CE-MS (cc-ITP/CE-MS) setups have the highest flexibility concerning choice of capillaries and electrolytes and, thus, improved MS-compatibility. However, a suitable interface is needed and sample transfer has to be carried out carefully to avoid sample loss. If interfaces with a common intersection (i.e. the connecting part of both dimensions for sample transfer without the need for a valve, used e.g. by Sydes et al. [3]) are applied, the switch of the voltage from the first dimension to the second dimension is sufficient for sample transfer, while in T-junctions, hydrodynamic pressure might be needed to push the sample stack to the second dimension. Intermediate detection at the common intersection or right in front of the bifurcation point is needed to determine the moment when to switch the dimensions. If intermediate detection at the common intersection is not available, the moment to switch dimensions can be estimated based on the migration velocity of the ITP or based on the determination of the column constant. With this setup, matrix removal and heart-cutting sample transfer are conducted more easily than in sc-ITP/CE-MS setups. An overview of applications using cc-ITP/CE-MS is given in Chapter 2.

3.2.2.4. Motivation and objective

The two-dimensional hyphenation of ITP with CE-MS to improve the detection limits of amino acids is investigated in this work based on previous work by Kler et al. [2]. We want to reach the highest flexibility in the choice of electrolytes concerning the ITP preconcentration and the separation of amino acids for CE-MS. Furthermore, MS-

compatibility is envisaged to be increased. DMSO-based hydroorganic ITP electrolytes for preconcentration of 19 proteinogenic amino acids and cystine are required in regard to 1) simultaneous preconcentration of all analytes in one isotachophoretic zone, using imidazole as leading ion and H^+ as terminating ion, 2) tolerance for aqueous sample plugs concerning current stability and suppression of the EZE of H^+, 3) highest possible MS-compatibility to improve amino acid analysis by direct ITP-MS coupling and ITP/CE-MS hyphenation. The electrolyte systems developed are optimized for maximum sample load and lowest detection limits. A background electrolyte for CE-MS separations with sufficient separation efficiency for all analytes and highest compatibility with both the MS detection and the ITP electrolyte systems is developed.

To investigate the influence of ITP electrolytes cotransferred to the second dimension in ITP/CE-MS hyphenations, analytes are dissolved in different ratios of TE and LE and are injected for CE-MS analysis to imitate different sample transfer and cutting techniques commonly used in ITP/CE-MS hyphenations. The separations of simulated analyte plugs from ITP can also help to understand the transition from the isotachophoretic analyte zone towards the CE separation mechanism with the electrolytes developed.

Two 2D setups are tested with a microfluidic glass chip interface to concentrate and separate all proteinogenic amino acids. The sc-ITP/CE-MS hyphenation without the need for sophisticated additional equipment and improved MS-compatibility is investigated for the applicability in amino acid analysis in L-S-L, T-S-T and BGE-S-BGE mode 2D separations. This setup is introduced as an alternative to a cc-ITP/CE-MS setup, as it is expected to be more straightforward for 2D applications and less demanding regarding sample transfer. To overcome the challenges of counterflow generation and the limited number of applicable electrolytes, the setup is modified by introducing a side capillary for counterflow application. By this, preconcentration becomes independent from the sheath liquid.

The cc-ITP/CE-MS 2D hyphenation is investigated in regard to precise sample-cutting without intermediate detection at the interface. As a hybrid of commercial and home-made/custom-made equipment, this setup is an example for a more sophisticated 2D setup with improved flexibility, MS-compatibility and probably concentration and separation efficiency. The challenges arising from the more sophisticated setup and the higher need for precise sample transfer are examined.

3.3. Materials and methods

3.3.1. Chemicals

Isopropanol (LC-MS grade) and dimethyl sulfoxide (≥ 95.5 %) were acquired from Carl Roth (Karlsruhe, Germany). Acetic acid (100 %, LC-MS grade), glycine, imidazole, L-alanine, L-arginine monohydrochloride, L-asparagine monohydrate, L-cystine, L-glutamic acid, L-glutamine, L-isoleucine, L-leucine, L-phenylalanine, L-serine, L-valine, methanol (LC-MS grade), sodium hydroxide (30 % aq.) and water (LC-MS grade) were purchased from Merck (Darmstadt, Germany). Difluoroacetic acid (≥98 %), L-lysine, L-threonine, L-tryptophan, L-tyrosine, oxalic acid (≥ 98 %) and trimethylpyruvic acid were from Sigma-Aldrich (Steinheim, Germany). DL-aspartic acid was acquired from Serva Feinbiochemica (Heidelberg, Germany). DL-methionine was from EGA-Chemie (Steinheim, Germany). Hydrochloric acid (analytical grade) was purchased from Fisher Scientific (Loughborough, UK), L-proline from Fluka (Steinheim, Germany), and L-histidine from amresco (Solon, OH, USA). Trifluoroacetic acid (≥ 99 %) was purchased from VWR BDH Prolabo chemicals (Fontenay-sous-Bois, France).

3.3.2. Buffers and working solutions

3.3.2.1. Amino acid stock solutions

Table 3.1: Composition of mixed stock solutions of amino acids AA1 and AA2 with a concentration of 1 mmol/L of each analyte. Additionally, molar masses M_R and monoisotopic masses of the protonated ion ($[M+H]^+$) of each analyte are given.

AA1	M_R in g/mol	$[M+H]^+$ in u	AA2	M_R in g/mol	$[M+H]^+$ in u
glycine	75.1	76.0	alanine	89.1	90.1
serine	105.1	106.1	proline	115.1	116.1
valine	117.1	118.1	threonine	119.1	120.1
leucine	131.2	132.1	isoleucine	131.2	132.1
aspartic acid	133.1	134.0	asparagine	132.1	133.1
lysine	146.2	147.1	glutamine	146.1	147.1
methionine	149.2	150.1	glutamic acid	147.1	148.1
phenylalanine	165.2	166.1	histidine	155.2	156.1
tyrosine	181.2	182.1	arginine	174.2	175.1
cystine	240.3	241.0	tryptophan	204.2	205.1

The proteinogenic amino acids and cystine were prepared in stock solutions of 10 mmol/L. Tyrosine and cystine were dissolved in 0.5 % (v/v) ammonia aq., tryptophan was dissolved in 40 % (v/v) methanol (MeOH) in water and phenylalanine was dissolved

in 30 % (v/v) MeOH in water. All other analytes were dissolved in water. Then, two mixed stock solutions, AA1 and AA2, see Table 3.1, with 1 mmol/L of selected analytes were prepared, separating isobaric compounds (i.e. leucine and isoleucine, lysine and glutamine). The composition of each mixed stock solution, as well as molar masses of the analytes and monoisotopic masses of the protonated analyte ions are listed in Table 3.1. Injection solutions were prepared by further dilution of the mixed stock solutions with water to the required concentration.

3.3.2.2. Electrolytes

For optimization of isotachophoretic separations of amino acids, four different nonaqueous or hydroorganic electrolyte systems were tested. All systems used imidazole as leading ion and H^+ as terminating ion (compare Chapter 2 and [27]). DMSO/water mixtures were used as solvent. Trifluoroacetic acid, oxalic acid, trimethylpyruvic acid or difluoroacetic acid were applied as counterions. The compositions of the different electrolyte systems for ITP are given in Table 3.2. For CE-MS measurements of amino acids, a hydroorganic BGE consisting of 13.2 % (v/v) acetic acid and 20 % (v/v) isopropanol in water was applied. All electrolytes were degassed by ultrasonication for 10 min before use.

Table 3.2: Compositions of the electrolyte systems applied for isotachophoretic measurements of amino acids.

Electrolyte system	Leading electrolyte	Terminating electrolyte
A	10 mmol/L imidazole	20 mmol/L TFA
	35 mmol/L TFA[1]	
	99 % (v/v) DMSO in water	99 % (v/v) DMSO in water
B	10 mmol/L imidazole	15 mmol/L OA
	25 mmol/L OA[2]	
	80 % (v/v) DMSO in water	80 % (v/v) DMSO in water
C*	10 mmol/L imidazole	15 mmol/L TMPA
	25 mmol/L TMPA[3]	
	80 % (v/v) DMSO in water	80 % (v/v) DMSO in water
D*	10 mmol/L imidazole	15 mmol/L DFA
	25 mmol/L DFA[4]	
	80 % (v/v) DMSO in water	80 % (v/v) DMSO in water

*[1] trifluoroacetic acid, [2] oxalic acid, [3] trimethylpyruvic acid, [4] difluoroacetic acid, * optimal electrolyte system for ITP-MS and ITP/CE-MS*

3.3.3. Instrumentation

All experiments were conducted using an Agilent 7100 Capillary Electrophoresis (Agilent Technologies, Waldbronn, Germany) coupled to an Agilent 6150 Quadrupole LC/MS system via a sheath liquid assisted electrospray ionization interface (Agilent Technologies, Santa Clara, CA, USA). Sheath liquid was delivered by an Agilent 1260 Infinity isocratic pump (Agilent Technologies, Waldbronn, Germany) with 1/100 flow split. For cc-ITP/CE-MS setups, a home-made multi-vial holder with the possibility of raw pressure application and a custom-made multiport high voltage source (CalvaSens, Aalen, Germany) were used. Microfluidic glass chip interfaces were manufactured by LightFab (Aachen, Germany) using selective laser-induced etching [3]. For conductivity detection, either eDAQ 225 C^4D systems with 120 C^4D headstage for capillary electrophoresis (eDAQ Incorporated, Denistone East, NSW, Australia; detection settings: 100 Hz sampling speed, signal range of 5 V, frequency 700 kHz, amplitude 80 % with headstage gain on) or home-made capacitance-to-digital-converter (CDC) detectors (sampling rate 9.1 Hz, excitation voltage of 5 V, 32 kHz square wave signal, electrode length 2 × 20 mm) with Python-based software [4] were used. Backpressure in sc-ITP/CE-MS setups was controlled using an electronic pressure controller from Parker Hannifin Corporation (Mayfield Heights, OH, USA) with home-made control electronics and Python-based software, enabling to precisely reduce raw pressure to values between 100 and 1000 mbar. The pressure controller was coupled to a home-made vial holder. Fused silica capillaries with 50 µm i.d. and 100 µm i.d. were purchased from Polymicro Technologies (Phoenix, AZ, USA).

3.3.4. Methods

3.3.4.1. Capillary preparation

Bare fused silica capillaries with 50 µm i.d. for CE-MS and 100 µm i.d. for ITP(-MS) were used: capillaries for 1D ITP-MS and CE-MS measurements were cut to a length of 50 cm. Capillary lengths for 2D setups are given in the respective sections (compare Sections 3.3.4.6 and 3.3.4.7). Prior to the first use, capillaries were flushed with methanol, 1 mol/L NaOH, 1 mol/L HCl and water at 1 bar for 10 min each. Capillary ends at the MS interface were polished to an angle of 90 ° or 45 ° (see table legends) with a home-made polishing device. Then, approx. 5 mm of the polyimide coating were thermally removed. Capillary ends, which were connected to the microfluidic glass chip interface in 2D setups, were polished to an angle of 90 ° to obtain tight connections between capillaries and channels in the chip.

3.3.4.2. ITP-MS measurements

Samples were injected hydrodynamically at 100 mbar for 1 s. To determine the capillary loadability, injection times were increased as stated. In this case, the injection time correlating with the plug length was determined by measuring the time it took for the sample front to reach the MS when pumping sample solution through the capillary at 100 mbar without voltage application. After injection, the capillary inlet was dipped twice into fresh TE to avoid carryover. Then, TE was injected at 50 mbar for 1 s. Separation voltage was ramped from 1 to 30 kV during the first 30 s, then kept stable at 30 kV during the measurement. In-between measurements, the capillary was flushed with LE at 1 bar for 5 min. The temperature inside the instrument was kept at 25 °C to maintain stable separation conditions. For determination of detection limits, the analyte mixes AA1 and AA2 (see Table 3.1) were diluted and measured in triplicate in a concentration range of 1 nmol/L to 100 µmol/L. Capillary loadability was investigated using a mixture of all analytes at a concentration of 1 µmol/L each. For blank measurements, TE was injected instead of sample.

3.3.4.3. CE-MS measurements

Samples were injected hydrodynamically at 100 mbar for 1 s. After injection, the capillary inlet was dipped twice into fresh BGE to avoid carryover. Then, BGE was injected at 50 mbar for 1 s. Separation voltage was ramped from 1 to 25 kV during the first 30 s, and then kept at 25 kV during the measurement. 20 mbar positive internal pressure were applied to aid electrospray generation. In-between measurements, the capillary was flushed with BGE at 1 bar for 5 min. The temperature inside the instrument was kept at 25 °C. The analyte mixes AA1 and AA2 (see Table 3.1) were diluted and measured in triplicate in a concentration range of 500 nmol/L to 1 mmol/L to determine limits of detection and the linear range. For blank measurements, BGE was injected instead of sample.

3.3.4.4. Simulation of transient ITP in CE-MS after heart-cutting

Arginine, methionine and aspartic acid were taken as model analytes at a concentration of 100 µmol/L each. For injection, the analyte mixture was further diluted by a factor of 10 using mixtures of LE and TE of electrolyte system B (see Table 3.2), varying the amount of TE between 0 and 100 % in steps of 10 % (v/v). Samples were injected at 100 mbar for 3 s, the capillary was dipped twice into 50 % (v/v) MeOH in water after injection to avoid carryover. A separation voltage of 15 kV was applied and the instrument was kept at 25 °C. Between runs, the capillary was flushed with BGE at 1 bar for 5 min.

3.3.4.5. Interface setup for 2D measurements

A microfluidic glass chip with flow channel diameters of 100 µm was used as interface in both the sc- and the cc-ITP/CE-MS setups. The chip was placed in a home-made mounting allowing to fix capillaries to the glass chip via screwing with finger-tight fittings. The capillary-chip connections were sealed with dried silicone, which was cut to little cubes (Figure 3.1A), then the capillary end was pinned through the silicone, inserted into the chip and screwed to the glass chip, see Figure 3.1B. In general, fixing of capillaries to the glass chip was conducted while flushing the capillaries and chip with water or BGE to avoid generation of bubbles inside the separation path.

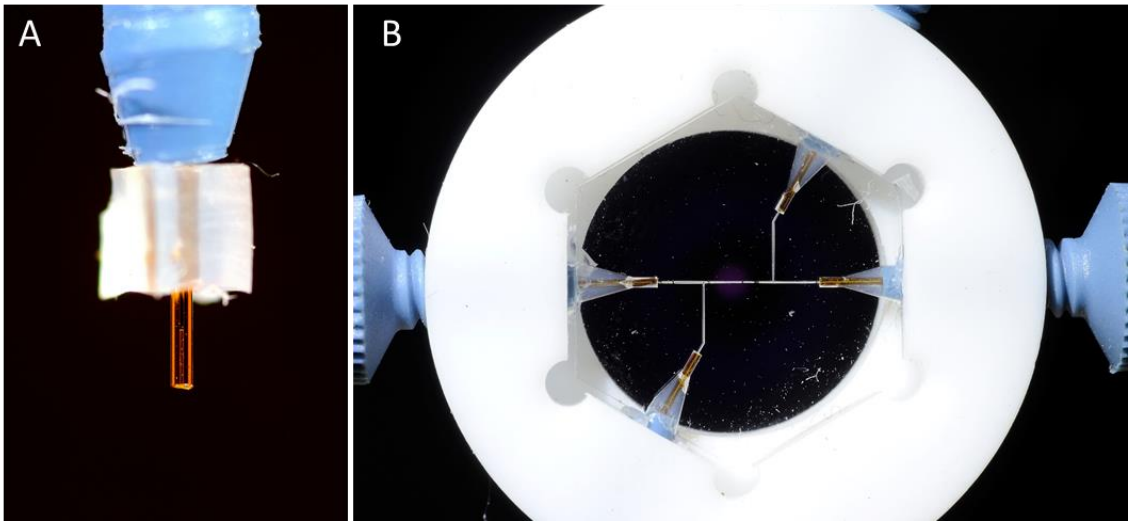

Figure 3.1: (A) Capillary end inserted into finger-tight fittings and pinned through dried silicone cube. (B) Four capillaries were screwed to the glass chip in a custom-made mounting, sealed with silicone.

3.3.4.6. Single capillary 2D ITP/CE-MS setup operation

Figure 3.2 shows a schematic depiction of the setup used for sc-ITP/CE-MS measurements. The unused flow channel of the glass chip interface was sealed with silicone. Capillary A1 had an i.d. of 100 µm and a length of 35 cm. Capillary A2 with an i.d. of 50 µm was cut to a length of 25 cm. The side capillary B, which was needed to flush the sample plug back towards the inlet after preconcentration by ITP, had an i.d. of 50 µm and was kept as short as possible with 12 cm in length. Mixtures of all amino acids at concentrations of 50 µmol/L or 100 µmol/L each were used as samples. Measurements with this setup were conducted in six consecutive steps. Between measurements, the whole system was flushed with LE at 1 bar for at least 5 min.

Step 1: All capillaries were flushed with LE of electrolyte system D (see Table 3.2).

Step 2: The side capillary B was filled with BGE by pressurizing the vial at port S until the conductivity signal of CDC3 at capillary B close to the glass chip interface (see Figure 3.2) revealed the presence of BGE.

Step 3: Sample was introduced from the CE into capillary A1 by hydrodynamic injection at 50 mbar for 5 s. The capillary inlet was dipped twice into fresh TE (electrolyte system D, see Table 3.2) to avoid carryover. Then, TE was injected at 50 mbar for 1 s.

Step 4: A separation voltage of 30 kV was applied between CE inlet and MS, while the side channel was left floating. From the migration time of the sample stack observed in the CDC detectors at the beginning of capillary A1 (CDC1) and at the front of the interface (CDC2), the time point when the sample reached the bifurcation point of separation path and side capillary B could be calculated. Based on this, the time to start the pressure-induced counterflow was determined.

Step 5: At the time determined in Step 4, i.e. shortly before the sample plug could pass the bifurcation point, a counterflow of BGE was generated by the pressure controller and applied via vial S at capillary B (see Figure 3.2) to flush the sample plug back towards the inlet. Counterflow pressure was varied between 100 mbar and 500 mbar, while the separation voltage was either switched off or kept stable at a value between 5 kV and 30 kV. The best combination for the counterflow generation was a pressure of 200 mbar and 10 kV separation voltage.

Step 6: After the sample plug reached the capillary inlet, again monitored via the CDC1 and CDC2 at capillary A1, the counterflow was stopped and separation voltage was set to 25 kV between the CE inlet and the MS to start the second dimension CE-MS measurement. The side channel was left floating.

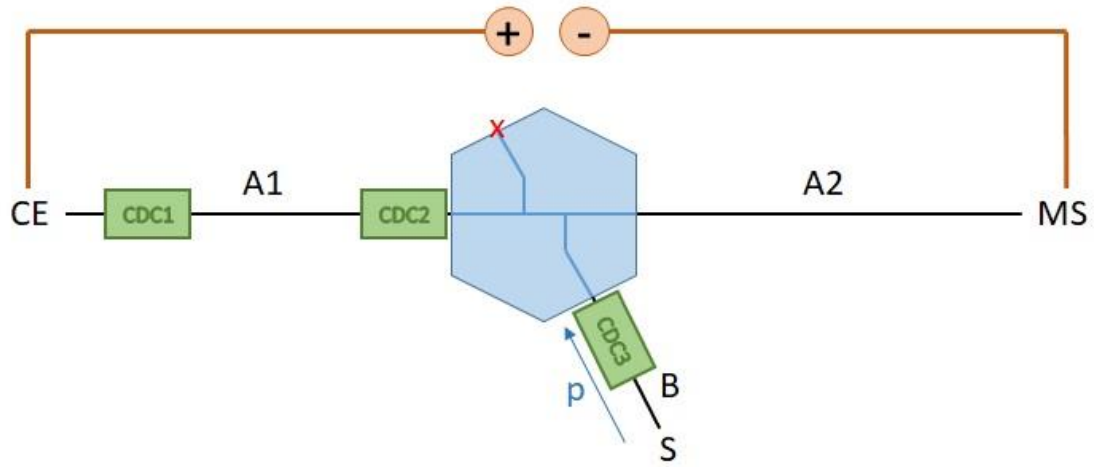

Figure 3.2: Schematic depiction of the sc-ITP/CE-MS setup. CE: inlet of the commercial CE instrument, MS: interface to the mass spectrometer, S: home-made vial housing for backpressure application regulated by an electric pressure controller, the direction of pressure application for the counterflow is marked by the blue arrow p, A1: first part of the separation capillary (100 µm i.d., ≥ 35 cm) connecting the CE to the glass chip interface, A2: second part of the separation capillary (50 µm i.d., ≤ 25 cm) connecting the glass chip interface to the MS, B: side capillary (50 µm i.d., 12 cm) connecting a BGE-filled vial in the home-made vial housing to the glass chip interface. Three CDC detectors were used: CDC1 was placed at the beginning of the separation path, CDC2 in front of the glass chip interface and CDC3 at the side capillary close to the glass chip interface. The unused flow channel of the glass chip interface was blocked with silicone, indicated by the red x.

3.3.4.7. Capillary coupling 2D ITP/CE-MS setup operation

A schematic depiction of the cc-ITP/CE-MS setup is given in Figure 3.3. Capillary A1 with 100 µm i.d. was cut to a length of 45 cm, capillaries A2, B1 and B2 had 50 µm i.d. and a length of 35 cm each. A mixture of arginine, methionine and aspartic acid with a concentration of 100 µmol/L each was used as sample. Measurements with this setup were carried out in five consecutive steps. Between single measurements, the whole system was flushed with LE for at least 10 min.

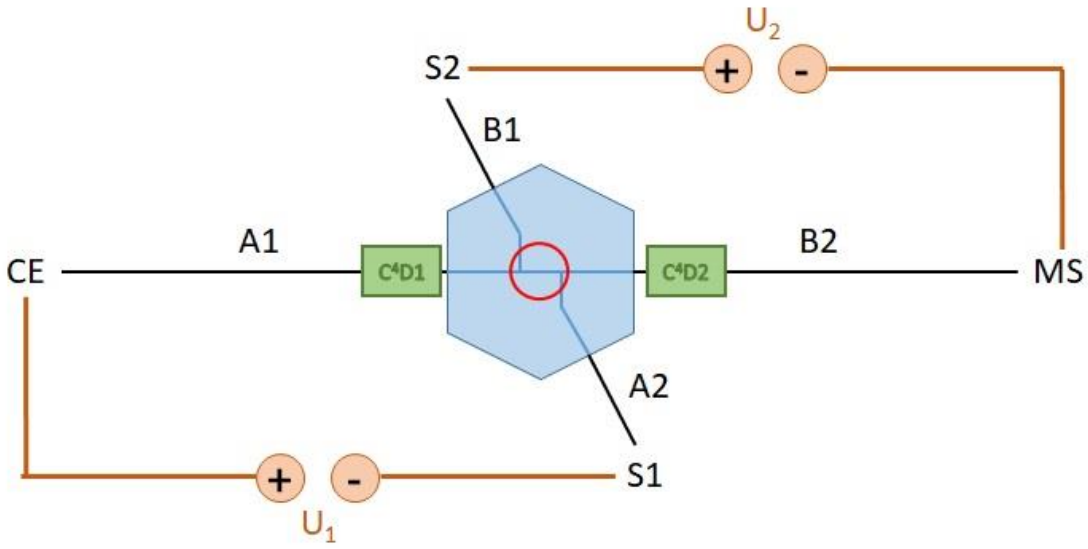

Figure 3.3: Schematic depiction of the cc-ITP/CE-MS setup. CE: inlet of the commercial CE instrument, MS: interface to the mass spectrometer, S1: first-dimension outlet to the home-made vial housing, S2: second-dimension inlet from the home-made vial housing, A1: first part of the ITP dimension capillary (100 µm i.d., 45 cm) connecting the CE to the glass chip interface, A2: second part of the ITP dimension capillary (50 µm i.d., 35 cm) connecting the glass chip interface to the home-made vial housing, B1: first part of the CE dimension capillary (50 µm i.d., 35 cm) connecting the high voltage source of the home-made vial housing to the glass chip interface, B2: second part of the CE dimension capillary (50 µm i.d., 35 cm) connecting the glass chip interface to the MS. ITP voltage (U_1) was applied from CE to S1, CE voltage (U_2) was applied from S2 to MS. Two conductivity detectors (C^4D) were used, C^4D1 placed in front and C^4D2 placed at the rear of the glass chip interface. The red circle marks the common intersection (5 mm) of both dimensions.

Step 1: All capillaries were flushed with LE of electrolyte system B from the CE inlet (see Table 3.2).

Step 2: Capillaries A1 and A2 were blocked with a vial containing silicone to flush capillaries B1 and B2 with BGE (see Section 3.3.2.2).

Step 3: The blocking vials were removed and sample was introduced into capillary A1 from the CE by hydrodynamic injection at 100 mbar for 5 s, the capillary inlet was dipped twice into fresh TE (electrolyte system B) to reduce possible cross contamination, then TE was injected hydrodynamically at 100 mbar for 1 s.

Step 4: A constant separation voltage of 30 kV (U_1 in Figure 3.3) was applied from the CE to external multiport high voltage source via S1 for ITP separation. Based on the migration time from the capillary inlet to the conductivity detector in front of the glass chip

interface, the time at which the sample plug reached the common intersection of the interface was calculated.

Step 5: When the sample plug reached the common intersection (red circle in Figure 3.3) of the glass chip interface, voltage from CE was stopped to terminate the first dimension measurement. Then, a separation voltage of 12 kV (U_2 in Figure 3.3) was applied from the external multiport high voltage source via S2 to start the CE separation towards the MS.

3.3.4.8. Mass spectrometric detection

Mass spectrometric parameters were similar in all measurements of ITP-MS, CE-MS and ITP/CE-MS. Sheath liquid consisted of 50 % (v/v) isopropanol with 0.1 % (v/v) of the respective counterion of the CE separation added. Spray chamber conditions varied for capillaries polished to an angle of 90° or 45°. For capillaries polished to an angle of 90°, electrospray settings were: sheath liquid flow rate of 5 µL/min, drying gas flow rate of 12 L/min at 250 °C, nebulizer pressure of 5 psig (which was lowered to 1 psig during flushing between measurements and sample injection to avoid suction effects). For capillaries polished to an angle of 45°, electrospray settings were: sheath liquid flow rate of 4 µL/min, drying gas flow rate of 4 L/min at 250 °C, nebulizer pressure of 4 psig (lowered to 1 psig during flushing and sample injection). In both cases, the fragmentor voltage was set to 100 V and the capillary voltage was 4000 V. Protonated molecular ions were generated at positive polarity and measured in single ion monitoring mode for analytes and imidazole.

3.3.4.9. Data acquisition and processing

All mass spectrometric data were acquired with Agilent OpenLab CDS ChemStation Rev. C.01.05 (Agilent Technologies, Santa Clara, CA, USA), transformed to *.xlsx* format using OpenChrom (Lablicate, Hamburg, Germany) and processed with Origin 2020 (OriginLab Corporation, Northampton, MA, USA). For determination of migration times, peak intensities and peak areas, the peak analysis tool was applied. CE-MS data were processed using the following settings: constant median baseline, automated search for positive peaks by local maxima and peak filtering by height (80 %) and automated peak integration from baseline. Due to the less stable baseline in ITP-MS measurements, ITP-MS data were processed using the following settings: baseline from 1st and 2nd derivation (zeroes), 20 baseline points with a threshold of 0.5, smoothing window of 2 and polynomial order of smoothing of 1, automated search for positive peaks by local maxima, peak filtering by height (80 %) and automated integration from baseline.

3.4. Results and discussion

3.4.1. 1D-Isotachophoresis-mass spectrometry

3.4.1.1. Choice of the counterion for ITP-MS electrolyte systems

For the isotachophoretic separation of all proteinogenic amino acids as cations, electrolyte systems with sufficiently low pH to protonate all analytes are needed. However, the cationic effective electrophoretic mobilities of the acidic amino acids aspartic acid and glutamic acid are generally low and in an electrolyte system using H^+ as terminating ion, the effective electrophoretic mobility of H^+ is high due to the EZE in aqueous buffer systems. Thus, the acidic amino acids migrate slower than H^+ and are not included in the isotachophoretic mobility window. Instead, they migrate zone electrophoretically in the TE. To overcome the EZE, Kler et al. [2] developed nonaqueous and hydroorganic electrolyte systems to include all proteinogenic amino acids in the isotachophoretic stacking process. Imidazole was used as leading ion and H^+ as terminating ion. Trifluoroacetic acid (TFA) or oxalic acid (OA) served as counterions to adjust the pH to a sufficiently low value. DMSO and DMSO/water mixtures were used as solvents, as DMSO is an aprotic solvent and diminishes the electrophoretic mobility of H^+ by inhibiting the EZE (compare Chapter 4).

In this work, the electrolyte systems of Kler et al. [2] were further optimized for ITP and for higher MS-compatibility. Although both systems (see Table 3.2, electrolyte systems A and B) enabled the simultaneous isotachophoretic stacking of all proteinogenic amino acids, they exhibited some major drawbacks. Electrolyte system A, with TFA as counterion, was very sensitive to water, both in the electrolytes (even in low amounts) and in aqueous samples. Electrolytes with TFA demanded 99 % (v/v) DMSO as solvent and our experiments with this electrolyte system showed that the tolerance for water in samples was very low, preventing large volume injections of aqueous samples. Furthermore, TFA seemed to have a negative effect on the ionization efficiency, probably due to ion suppression. Electrolyte system B with OA as counterion, on the other hand, tolerated higher amounts of water in the sample. The electrolytes were dissolved in 80 % (v/v) DMSO and large volume injection of aqueous samples was less problematic than with electrolyte system A. Nevertheless, in our experiments, electrolyte system B exhibited the major drawback of OA impairing MS detection due to ion suppression and especially too low volatility. Already after a few ITP-MS measurements with this electrolyte system, OA started crystallizing in the ion source, causing massive sample carryovers. As this could severely contaminate the ion source and mass spectrometer

already at low sample throughput, this electrolyte system was not considered for further ITP-MS measurements.

Since electrolyte systems A and B were found to have critical disadvantages for ITP-MS measurements, new counterions were tested using the following criteria: 1) pK_a values close to TFA (pK_a 0.60) or at least OA (pK_a 1.27) to guarantee a sufficiently low pH in the LE and TE, 2) MS-compatibility, 3) sufficient water tolerance of the new electrolyte system to allow measurements of aqueous samples and 4) solubility in 80 % (v/v) DMSO. Two substances fulfilled all four requirements: trimethylpyruvic acid (TMPA) and difluoroacetic acid (DFA) with pK_a values of 1.47 and 1.00, respectively (data from PeakMaster 5.3 Complex database [137]). Both substances could be applied at the same concentrations as OA (compare Table 3.2, electrolyte systems C and D) and both new electrolyte systems enabled isotachophoretic measurements of all proteinogenic amino acids as cations. Therefore, these electrolyte systems were used for subsequent ITP-MS investigations and sc-ITP/CE-MS (see Section 3.4.3).

3.4.1.2. Determination of detection limits in ITP-MS

Detection limits (LODs) for the proteinogenic amino acids in peak-mode isotachophoresis using electrolyte systems C and D were determined using mixed amino acid standards AA1 and AA2 (compare Table 3.1). Aqueous standards in a concentration range between 1 nmol/L and 100 µmol/L for each analyte were measured in triplicate and TE was injected under similar conditions for blank measurements. Calculations of detection limits and the relative standard deviations (RSDs) according to DIN 32645:2008-11 [138] used the peak area integrated from extracted ion isotachopherograms. Results are given in Table 3.3 for electrolyte system C and D.

Amino acid detection limits were between 1.7 and 54.4 µmol/L measured with electrolyte system C and between 1.1 and 69.1 µmol/L with electrolyte system D. In case of electrolyte system D, not all amino acids were visible in the isotachopherograms, probably due to ion suppression effects in combination with instable electrospray conditions. Furthermore, the detection limits determined were rather high compared to the expected preconcentration power of ITP and the sensitivity of the MS detection. One of the major reasons for these high detection limits is the difficulty of obtaining clean blank measurements: amino acids are ubiquitous substances and the ITP mechanism causes concentration of even the slightest trace amounts, thus, the isotachopherograms of blank measurements always showed small analyte signals. Carry-over prevention was attempted by flushing the capillaries between measurements and washing the capillary inlet after injection. Nevertheless, cross contamination must be considered a possible cause for unsuccessful blank measurements. Quantitative precision was low with RSDs

ranging from 2.1 % to 66.3 % and 1.3 % to 84.3 % for electrolyte systems C and D, respectively.

Table 3.3: LODs and RSDs of peak areas of amino acids with electrolyte system C (i.e. TMPA as counterion) and D (i.e. DFA as counterion), see Table 3.2, in peak-mode ITP-MS according to DIN 32645:2008-11 [138]. Samples were measured in triplicate, LODs and quantitative precision were calculated based on the peak area of the extracted ion isotachopherogram. The capillary end at the MS interface was polished to an angle of 90° or 45°.

	electrolyte system C capillary end 90°		**electrolyte system D capillary end 90°**		**electrolyte system D capillary end 45°**	
AA1	**LOD in µmol/L**	**RSD in %**	**LOD in µmol/L**	**RSD in %**	**LOD in µmol/L**	**RSD in %**
glycine	11.3	10.6	14.0	17.1	4.2	5.1
serine	18.5	17.2	3.4	4.2	4.4	5.3
valine	3.7	2.8	1.1	1.3	1.4	1.7
leucine	4.6	5.7	3.9	4.8	3.2	3.9
aspartic acid	3.3	4.0	51.3	62.6	4.2	5.1
lysine	13.1	15.9	69.1	84.3	2.9	3.6
methionine	3.6	4.4	9.0	11.0	5.1	6.2
phenylalanine	1.8	2.2	13.2	16.1	2.5	3.0
tyrosine	22.7	17.2	19.5	22.4	11.2	12.8
cystine	1.7	2.1	n.a.	n.a.	4.4	5.4
AA2						
alanine	33.4	40.7	8.4	10.3	4.7	5.7
proline	2.9	3.5	2.3	2.8	1.3	1.6
threonine	5.8	7.1	1.3	1.6	2.1	2.5
isoleucine	4.3	5.2	2.3	2.8	1.2	1.5
asparagine	3.2	3.9	6.7	8.2	2.6	3.2
glutamine	54.4	66.3	25.0	28.7	4.8	5.8
glutamic acid	11.5	10.7	n.a.	n.a.	2.3	2.8
histidine	8.0	8.4	13.5	6.6	4.0	4.9
arginine	53.4	65.1	n.a.	n.a.	3.7	4.5
tryptophan	3.6	4.4	n.a.	n.a.	2.3	2.8

The low precision is due to two factors: 1) the limited compatibility of DMSO with MS detection due to its rather low volatility and 2) the fact that all amino acids of a mixed standard migrated in a narrow isotachophoretic stack. The latter could result in strong ion suppression effects as all analytes reach the ion source at the same time.

Considering the quantitative precision, both electrolyte systems are similarly suited for ITP-MS measurements of amino acids.

As visible from Table 3.3, polishing the capillary end to an angle of 45° improved electrospray stability in the spray chamber as well as the concentration detection limits of the ITP-MS, now ranging from 1.2 to 11.2 µmol/L using electrolyte system D. The quantitative precision was improved to RSD values between 1.5 % and 12.8 %. Unfortunately, the measurements with capillaries polished to 45° using electrolyte system C with TMPA as counterion (Table 3.2) were not yet successful. However, the results indicate an influence of the electrospray stability on peak area and, thus, quantitative precision and detection limits.

The results obtained here give an impression on the concentrating ability of ITP-MS but also show that the hyphenation to CE-MS is mandatory to fully exploit the preconcentration power of ITP as analytes are separated from DMSO and from each other in the second dimension. The ITP-MS results clearly demonstrated that all amino acids are effectively preconcentrated and included in the mobility window of the new electrolyte systems C and D

3.4.1.3. Sample loadability

One of the main advantages of ITP compared to CE is the high possible sample load while keeping sharp zones in peak-mode ITP at low analyte concentrations. To determine the maximum capillary volume which could be filled with sample while still gaining sharp peaks and, thus, a small ITP stack for transfer to the second dimension, the injection time was gradually increased. A sample containing all amino acids at a concentration of 1 µmol/L each was used. Plug lengths between 1 cm and 20 cm were tested using injection times of 4 s to 80 s at 100 mbar with electrolyte system C and of 5 s to 100 s at 100 mbar for electrolyte system D. The differences in injection times for the two electrolyte systems are probably a result of slightly different viscosities due to different counterions.

As shown in Figure 3.4A for electrolyte system C (compare Table 3.2), all amino acids are still stacked in one sharp isotachophoretic zone (Figure 3.4A) at an injection plug of 15 cm length, which corresponds to 30 % of the capillary length and an injection volume of 1.2 µL. Injections of sample plugs of 16 cm or higher with a concentration of 1 µmol/L resulted in a broad isotachophoretic mixed zone with some analytes starting to destack, as visible in Figure 3.4B for an injection plug length of 20 cm.

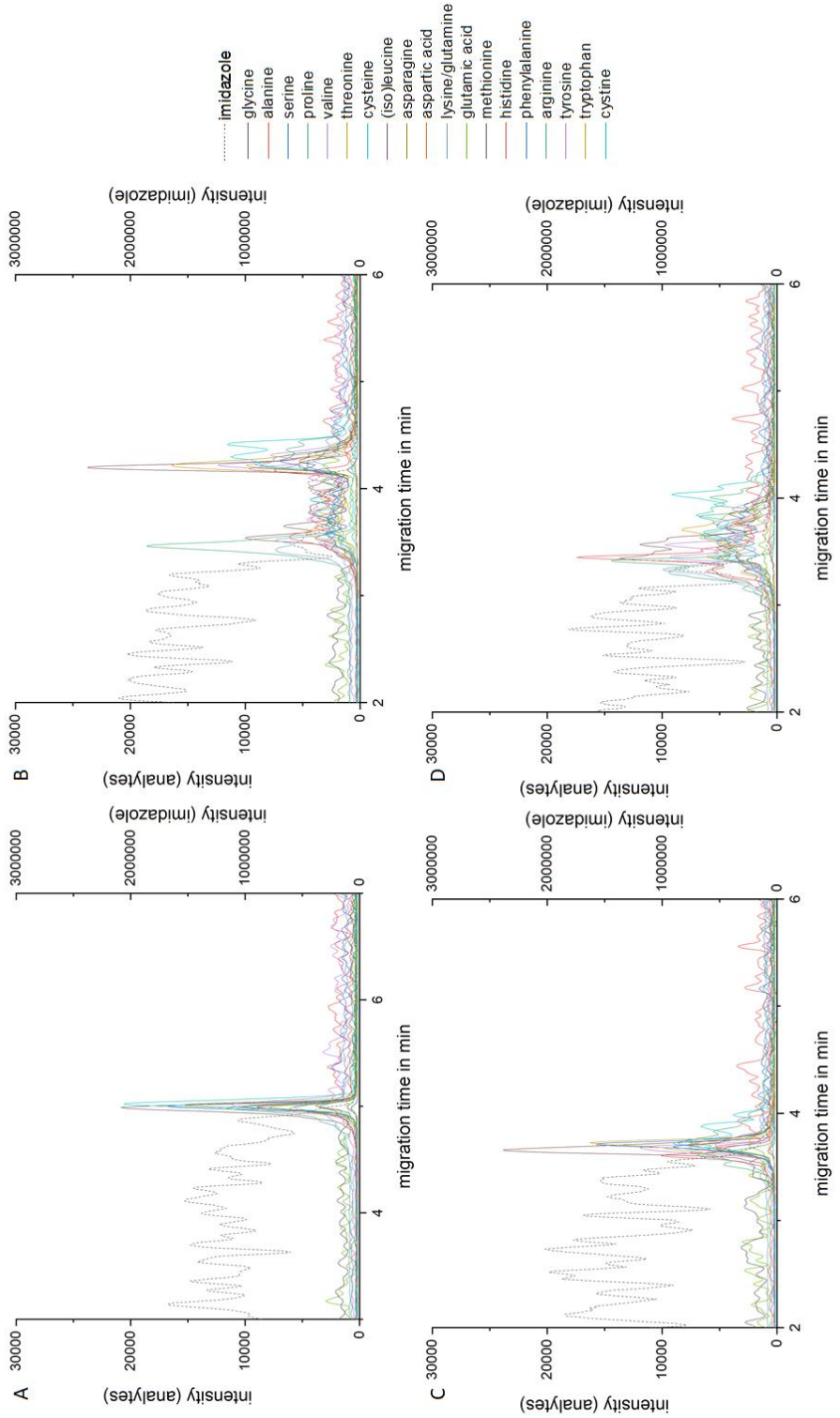

Figure 3.4: Extracted ion isotachopherograms of 1 µmol/L amino acid mixture with electrolyte systems C (panels A, B) and D (panels C, D). The dashed line with corresponding right y-axis displays the extracted ion isotachopherogram of the leading ion imidazole. A 50 cm bare fused silica capillary with 100 µm i.d. and 30 kV separation voltage were used. Hydrodynamic injections at 100 mbar were adjusted to injections times resulting in sample plugs of 15 cm (30 % of the capillary length, panels A, C) and 20 cm (40 % of capillary length, panels B, D). The corresponding injection times for panels A, B, C and D were 60 s, 80 s, 75 s and 100 s.

The results obtained for sample plugs of 15 cm and 20 cm sample plug length in electrolyte system D are displayed in Figure 3.4C and D. With this electrolyte system, the amino acid zone begins to broaden already at injection sample plug length of approximately 15 cm, corresponding to a hydrodynamic injection of 75 s at 100 mbar. Comparable to electrolyte system C, approx. 30 % of the capillary volume could be filled with sample, enabling an injection volume of approx. 1.2 µL. Higher injection volumes evoked a plateau-mode ITP which is disadvantageous for precise sample transfer in 2D applications. For later application in two-dimensional setups with a microfluidic glass chip interface, a sharp stack of amino acids is preferred as it simplifies the complete sample transfer to the second dimension. Thus, the maximum capillary loadability for the purposes in this work was determined to be 30 % of the capillary volume in both electrolyte systems C and D for amino acid concentrations below 1 µmol/L in the sample.

3.4.2. Capillary electrophoresis-mass spectrometry

3.4.2.1. Choice of background electrolyte and detection limits

The cationic separation of proteinogenic amino acids in CE-MS including the acidic amino acids aspartic acid and glutamic acid requires a sufficiently low pH (i.e. below the pI of aspartic acid of 2.85) in the BGE to ensure protonation of all analytes. Coufal et al. [139] used a 2.3 mol/L acetic acid BGE, containing hydroxyethylcellulose as dynamic coating, for the analysis of twenty underivatized proteinogenic amino acids with conductivity detection, which provided excellent separation and migration time reproducibility and good peak symmetry. To adapt this BGE for MS-compatibility, hydroxyethylcellulose had to be eliminated which resulted in slightly poorer resolution and separation efficiency. Thus, a free acid BGE [37] using 2.3 mol/L acetic acid (pH 2.2) was employed for the separation of the proteinogenic amino acids.

In order to enhance the compatibility of the two dimensions with regard to the differences in the hydrodynamic viscosities of the electrolytes (approx. 3 mPa·s in 80 % (v/v) DMSO in water vs. 1 mPa·s in water [8]), the BGE was further modified by using of 20 % (v/v) isopropanol (iPrOH) in water as solvent. By this, the differences in viscosities were reduced by half. The influence of hydroorganic BGEs on the separation of amino acids was investigated in this work as well (see Chapter 4).

The CE method developed in this work well separated the isobaric pairs, leucine/isoleucine and lysine/glutamine, to reach reliable identification of all analytes, see Figure 3.5. The isobaric pair of leucine/isoleucine could be separated with a resolution of 0.8 (based on migration times and full width at half maximum), which was sufficient for qualitative determinations. Most likely, at low analyte concentrations, this

resolution would be sufficient for quantitative analysis. Nevertheless, for highest precision in this study, the amino acids were split into two groups to separate the isobaric pairs (see Table 3.1).

Table 3.4: LODs and RSDs of peak areas of amino acids with 2.3 mol/L acetic acid BGE in CE-MS according to DIN 32645:2008-11 [138]. Samples were measured in triplicate, LODs and quantitative precision were calculated based on the peak area of the extracted ion isotachopherogram. The capillary end at the MS interface was polished to an angle of 45°.

AA1	LOD in µmol/L	RSD in %	AA2	LOD in µmol/L	RSD in %
glycine	15.4	1.6	alanine	9.6	0.8
serine	48.9	4.3	proline	1.4	0.1
valine	31.0	3.1	threonine	6.1	0.4
leucine	31.7	3.2	isoleucine	7.4	0.7
aspartic acid	5.9	0.6	asparagine	6.7	0.6
lysine	39.4	4.4	glutamine	10.3	1.0
methionine	17.3	1.8	glutamic acid	13.2	1.3
phenylalanine	18.7	1.9	histidine	23.7	2.4
tyrosine	84.3	5.8	arginine	21.8	2.2
cystine	92.7	6.3	tryptophan	48.0	3.3

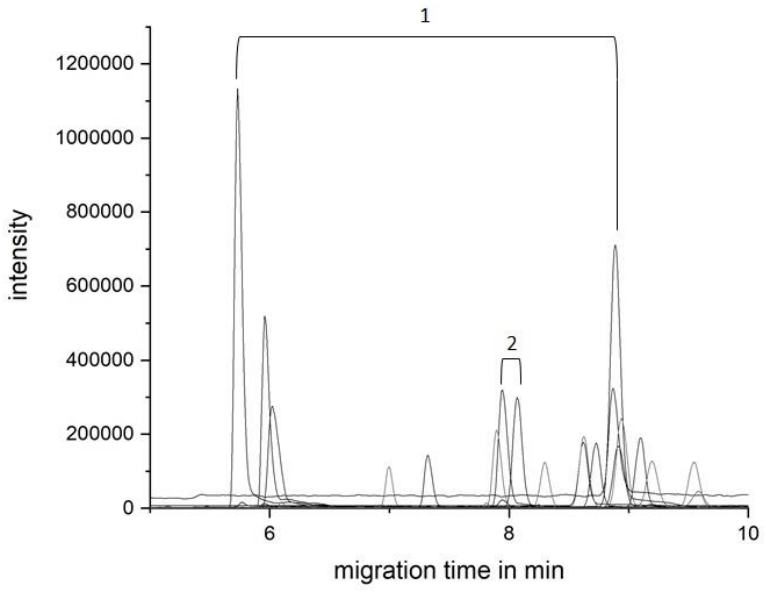

Figure 3.5: Extracted ion electropherograms of CE-MS measurement of amino acids with the isobaric pairs lysine/glutamine (1) and leucine/isoleucine (2) indicated. Separation was conducted in a 50 cm capillary with 50 µm i.d. Hydrodynamic injection at 100 mbar for 1 s of mixed sample (1 mmol/L), 25 kV separation voltage was applied with 20 mbar internal pressure during the separation. 2.3 mol/L acetic acid in 20 % (v/v) iPrOH was employed as BGE.

Detection limits for the proteinogenic amino acids in CE-MS were determined using the mixed amino acid standards given in Table 3.1. Standards in a concentration range between 500 nmol/L and 1 mmol/L for each analyte were measured in triplicate and BGE was injected under the same conditions for blank measurements. Concentration detection limits of the amino acids were between 1.4 and 92.7 µmol/L. The relative standard deviations of peak areas were below 6.5 % (see Table 3.4).

3.4.2.2. Transient ITP conditions in second dimension CE-MS

As already explained in Chapter 2, the transfer of sample from the first to the second dimension in 2D ITP/CE-MS separations leads to conditions of a tITP at the beginning of the second dimension. Depending on the cutting technique and the cutting precision, the amount of LE and TE cotransferred to the second dimension varies. Especially the amount of leading ion, which is imidazole in all ITP electrolyte systems used in this work, was expected to influence the tITP in the beginning of the second dimension separation in BGE-S-BGE and T-S-T modes, as the terminating ion H^+ is present as coion in the BGE and facilitates the transition of the TE zone. If the tITP does not dissolve quickly, resolution between amino acids is reduced, which is critical especially for the peak pair leucine/isoleucine (resolution 0.8).

To investigate the behavior of the sample plug in BGE-S-BGE mode, the sample plug transferred together with adjacent LE and TE was simulated by injection of analytes dissolved in the ITP electrolyte system B (compare Table 3.2) for CE-MS analysis. Arginine, methionine and aspartic acid were chosen as model analytes as they cover the whole range of pI values of the proteinogenic amino acids. The analytes were dissolved in BGE for reference. Simulations started with analytes dissolved in TE, then, LE was added gradually to finally reach 100 % LE. In detail, the amount of LE was increased by steps of 10 % (v/v) so that the simulation covered the whole range of LE/TE ratios and possible CE starting conditions after sample transfer. The different ratios of LE/TE in the sample plug were intended to simulate different heart-cut sample transfer precisions. The cotransfer of high amounts of LE was expected to be critical for CE-MS measurements, as it transferred the highest amount of the leading ion imidazole in the sample plug. At too high imidazole concentrations, we expect that the tITP conditions prevail over a longer migration path. For CE-MS analyses, 2.3 mol/L acetic acid in 20 % (v/v) iPrOH was used. Samples were injected hydrodynamically at 100 mbar for 3 s. Based on the data from Section 3.4.1.3, the sample plug in this simulation was longer than 5 mm, which is the length of the common intersection of the microfluidic glass chip interface used in our 2D setups. Nevertheless, due to the preconcentration process, ITP stacks are expected to be shorter than 5 mm.

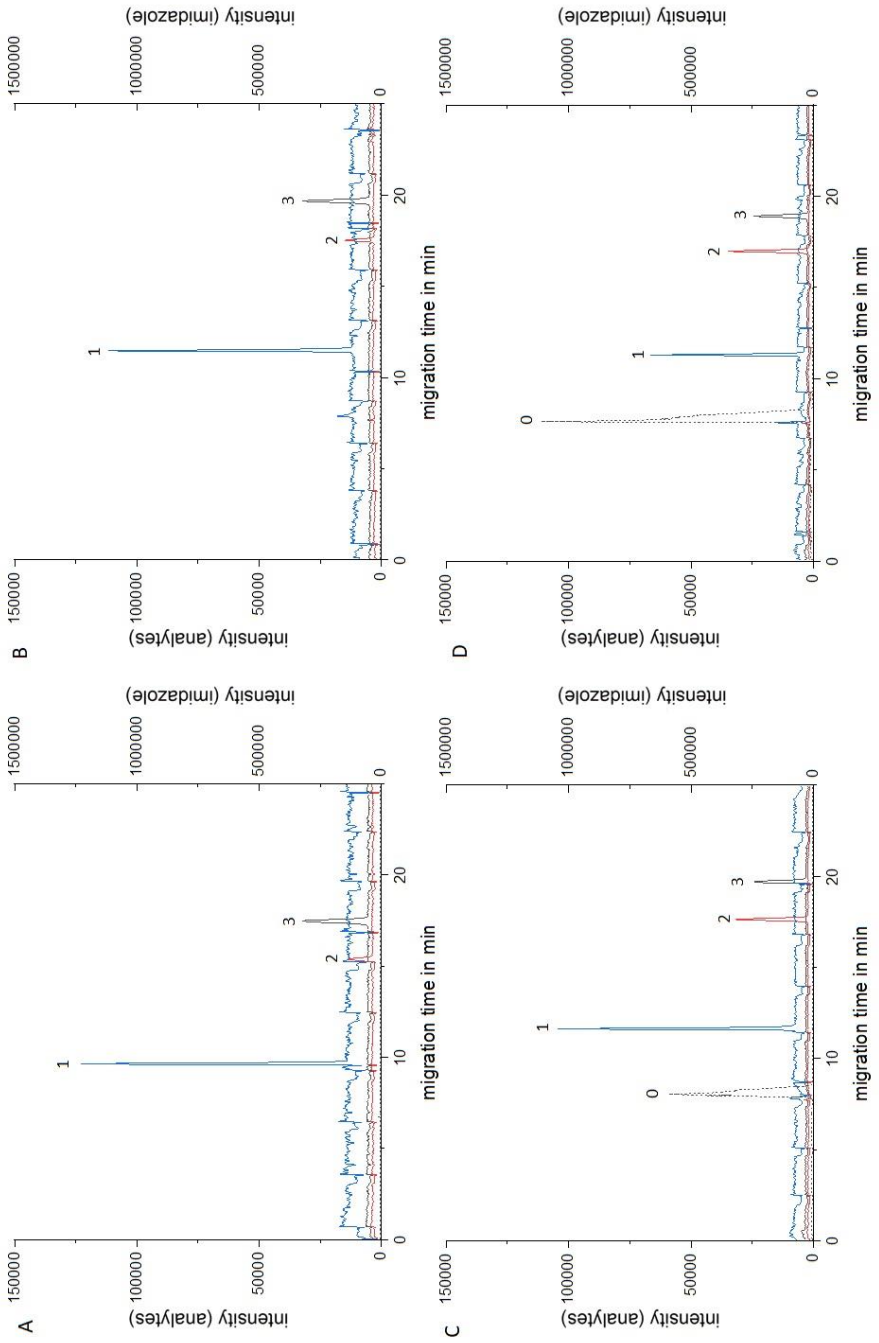

Figure 3.6: Extracted ion electropherograms of arginine (1), methionine (2) and aspartic acid (3) at a concentration of 100 µmol/L each. Analytes dissolved in (A) BGE, (B) 100 % TE, (C) 50 % (v/v) LE and 50 % (v/v) TE, and (D) 100 % LE. LE and TE of electrolyte system B were used, see Table 3.2. BGE: 2.3 mol/L acetic acid in 20 % (v/v) iPrOH, 50 cm bare fused silica capillary with 50 µm i.d., hydrodynamic injection at 100 mbar for 3 s, separation voltage of 15 kV. The right y-axis and dashed line correspond to the extracted ion electropherogram of imidazole (0). Figure 3.6A shows the extracted ion electropherograms of the analytes dissolved in BGE used as reference. This corresponds to the CE-MS analysis of the model analytes without preconcentration effects from tITP. The analytes were clearly separated with high separation efficiency with base widths between 0.3 and 0.5 min. The separation window for the model analytes was approx. 8 min.

In all experiments, all analytes were well separated and signals were recognized as sharp peaks with comparable base peak widths as obtained for the signals of the analytes dissolved in BGE. In cases with LE in the sample plug, the imidazole signal was well separated from the amino acid signals, indicating that the tITP stack was completely dissolved in all experiments. The migration time window spanned between arginine and aspartic acid decreased slightly with increasing LE content in the sample.

Figure 3.6B shows the extracted ion electropherograms of the model analytes dissolved in 100 % TE. The migration times increased by approx. 2 min for each analyte, caused by the retardation induced by tITP. The results for the simulation of 50 % (v/v) TE and 50 % (v/v) LE in a transferred plug are shown in Figure 3.6C. The increased signal intensity of methionine observed in this measurement could be a result of fast destacking of the ITP conditions, reducing the diffusion effects on methionine [89].

As visible from the extracted ion electropherograms in Figure 3.6D, showing the analysis of analytes in 100 % LE, the base widths of the peaks were between 0.2 and 0.4 min, i.e. slightly reduced in comparison to the previous measurements. The migration time window was approx. 7.5 min, which was only a minor reduction in comparison to the previous experiments. This indicated that even the transfer of a high amount of the leading ion imidazole would not affect the separation of the analytes in the second dimension in a 2D setup.

It has to be stressed that the sample plug was injected as a mixture of TE and/or LE and the analytes, thus, the sample plug composition was different from that which would enter the second dimension in a 2D measurement, also with regard to the concentration of the adapted TE. In 2D setups, the sample plug would already be an isotachophoretic stack, i.e. leading ion followed by analytes followed by terminating ion. We can assume a faster dissolution of this transferred ITP stack, so from the results obtained with these simulation measurements, it is expected that the cutting precision with our electrolytes is robust against LE and TE cotransfer. The separation of the model analytes was comparable in all setups and the increasing amount of imidazole in the sample plug did not negatively affect the separation of the amino acids.

3.4.3. Instrumental strategy for 2D ITP/CE-MS setups

Both setups in this work, the sc-ITP/CE-MS and cc-ITP/CE-MS setup, used a microfluidic T-configuration glass chip interface as developed by Sydes et al. [3]. Figure 3.7 shows a newer generation of this interface which was optimized for higher mechanical rigidity. Flow channels were completely circular and had an inner diameter of 100 µm.

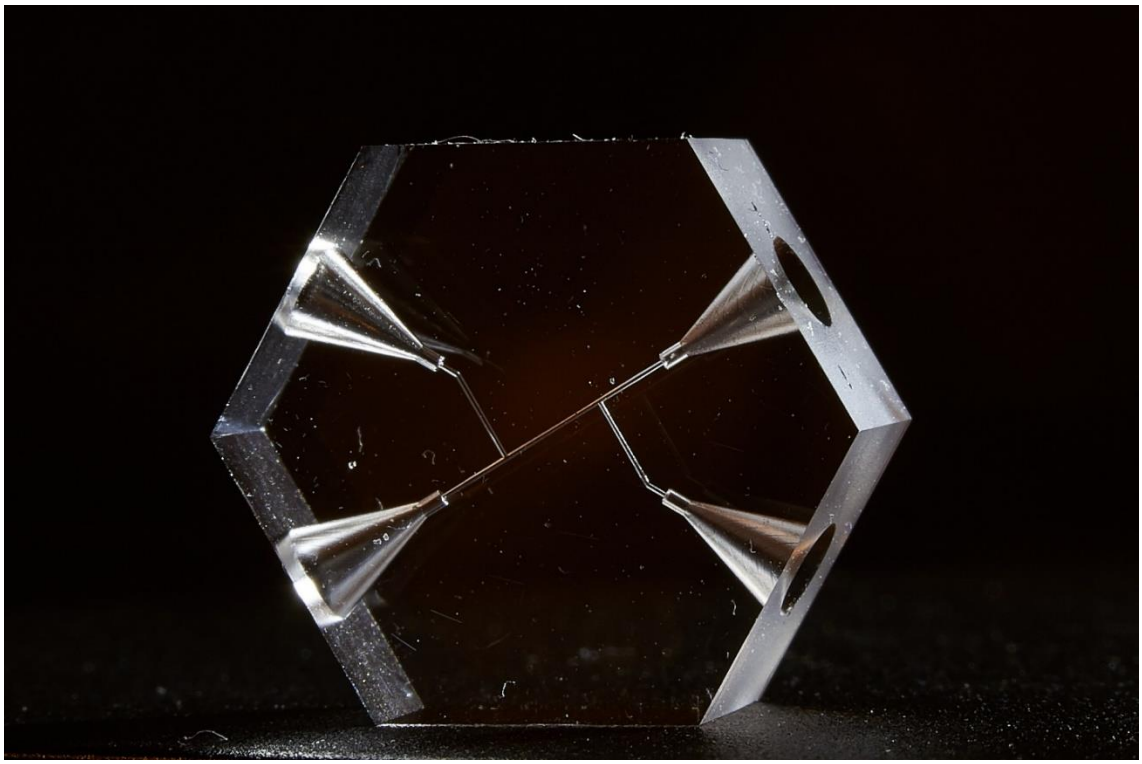

Figure 3.7: Microfluidic glass chip interface produced by laser-induced etching with flow channels of an inner diameter of 100 µm. The flow channels were connected by a common intersection of 5 mm length.

The chip was held in place by a custom-made mounting, allowing to fasten capillaries with finger-tight fittings. The capillary-chip connection was sealed with dried commercial silicone, as shown in Section 3.3.4.5. Up to at least 2 bar were applicable for flushing steps without leaking.

In our sc-ITP/CE-MS setup, the straight flow channels in the chip were used to connect the capillary from the CE with the capillary inserted to the MS. One side channel of the interface was sealed completely, and a side capillary was connected to the second side channel. The side capillary was inserted into a vial in a home-made vial holder, allowing the application of precise pressures between 100 and 1000 mbar via an external pressure controller. Thus, the counterflow generation was decoupled from the sheath liquid and the composition of the counterflow solution could freely be chosen. Both separation dimensions took place in the same capillary: the ITP separation ran between the inlet and the bifurcation point, whereas the CE separation ran from the inlet to the MS. Three home-made capacitance-to-digital-converter (CDC) detectors were used for intermediate detection in this setup: CDC1 was placed close to the capillary inlet inside the commercial CE, CDC2 was placed directly in front of the interface and CDC3 was placed close to the interface at the side capillary. The setup is shown in Figure 3.8 and schematically depicted in Figure 3.2.

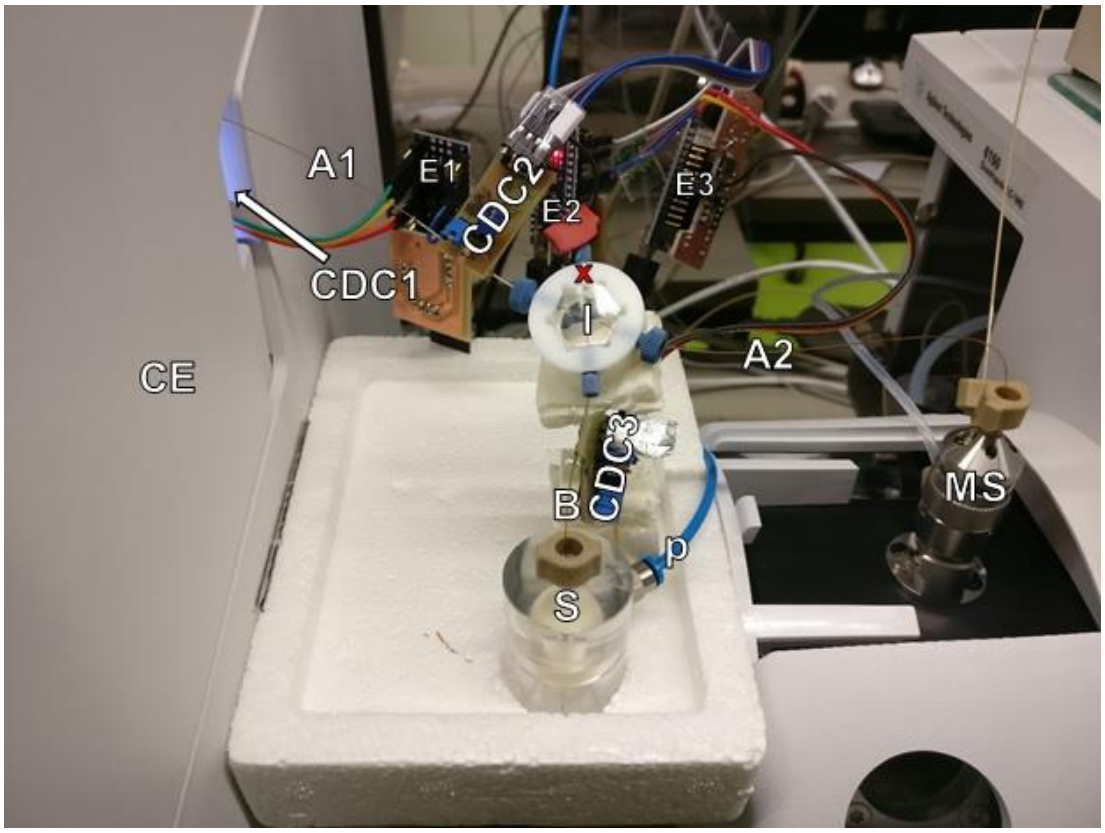

Figure 3.8: sc-ITP/CE-MS setup used in this work. The microfluidic glass chip interface (I) mounted with CDCs placed on capillary A1 close to the inlet inside of the CE (CDC1) and in front of the interface (CDC2), and on the side capillary B (CDC3). A commercial CE instrument and an MS instrument with ESI source were used. The side capillary B was fixed in a home-made vial holder (S) connected to an external pressure control unit (not visible) via a pressure hose (p), allowing to apply a counterflow. E1, E2 and E3 are the electronics to control the CDCs. The red x marks the unused chip channel sealed with silicone (compare Figure 3.2).

This setup increased the flexibility in counterflow generation due to the side capillary with the external pressure controller. Furthermore, only one high-voltage source was needed, i.e. voltage was applied via the commercial CE, and the whole process of ITP preconcentration, counterflow and subsequent CE-MS separation could be operated under application of high voltage. The time point for sample transfer was calculated based on the signal recognized by the CDCs, as will be explained in the following Section 3.4.4.1.

In the cc-ITP/CE-MS setup used in this work, a home-made multi-vial handler with an external high voltage source formed the outlet for the ITP dimension and the inlet for the CE dimension. Practically, this provided a second small, custom-made CE instrument, as in the cc-ITP/CE-MS setup both dimensions needed individual electric circuits. Two C^4Ds were used for intermediate detection: C^4D1 was placed in front of the interface and C^4D2 was placed behind the interface (see also Figure 3.3 for a schematic picture). With the interface used, both dimensions were not hydrodynamically decoupled. Thus, if flushing of a single dimension was needed, the capillaries of the other dimension had to

be blocked as described in Section 3.3.4.7. The straight flow channel in the interface (see Figure 3.7) was used to connect both dimensions. The common intersection of all four channels in the chip was used for sample transfer. Thus, the sample plug length to be transferred was determined by the length of the common intersection (5 mm).

3.4.4. Single capillary 2D ITP/CE-MS

3.4.4.1. Intermediate detection and transition to second dimension

In an sc-ITP/CE-MS setup, proteinogenic amino acids should be simultaneously concentrated by ITP and subsequently separated by CE-MS in one measurement. A schematic depiction of the setup is given in Figure 3.2. A microfluidic glass chip was used as interface to introduce a side capillary for application of a counterflow after the ITP process was finished. The first dimension ITP takes place in capillary A1 and before the sample stack reaches the bifurcation point in the interface, the sample plug is flushed back towards the inlet by the counterflow. Then, the inlet vial is exchanged for the BGE and the sample stack is separated under CE conditions, using capillaries A1 and A2 as separation path.

The timing to switch from ITP measurement to counterflow to CE-MS analysis is crucial in this setup to avoid the loss of sample both at the bifurcation point during ITP before and at the capillary inlet during counterflow. Furthermore, it is important to keep the LE plug in front of the sample stack as short as possible (except in L-S-L systems) to enable complete dissolution of the tITP upon detection in CE-MS, although the influence of higher amounts of LE was generally expected to be rather low from the results described in Section 3.3.4.4.

In this work, we used three home-made CDC detectors in the setup: CDC1 close to the inlet of capillary A1, CDC2 right in front of the microfluidic glass chip interface and CDC3 was placed close to the interface on the side capillary (compare Figure 3.2 and Figure 3.8). The latter detector was used to control filling of the side capillary with BGE in order to reduce the amount of cotransferred LE during counterflow, which was induced from the side capillary B (compare Step 2 in Section 3.3.4.6).

The ideal moment to stop the ITP measurement and induce the counterflow to transport the sample plug back towards the capillary inlet was approximated from the migration time of the TE recorded in CDC2. The velocity of the ITP v_{ITP} was determined via Equation (3.1)

$$v_{\mathrm{ITP}} = \frac{L_{\mathrm{eff,CDC2}}}{t_{\mathrm{TE,CDC2}}} \qquad (3.1)$$

with the effective capillary length from inlet to CDC2 $L_{\mathrm{eff,CDC2}}$ and the migration time of the TE to CDC2 $t_{\mathrm{TE,CDC2}}$. From this velocity, the migration time of the sample stack to reach

the bifurcation point, i.e. the time to start the counterflow $t_{startCF}$, was estimated taking the remaining path length to the bifurcation point into account. To avoid sample loss at the bifurcation point, the sample was only allowed to migrate another 2 cm, which will be assigned to as L_{rem}.

$$t_{\mathrm{startCF}} = \frac{L_{\mathrm{rem}}}{v_{\mathrm{ITP}}} + t_{\mathrm{TE,CDC2}} \qquad (3.2)$$

At $t_{startCF}$, a counterflow was applied from the side capillary B with high voltage still applied to stabilize the ITP stack. By application of a counterflow, the sample stack was not only transported back towards the inlet but, simultaneously, all capillaries were filled with BGE to prepare the capillaries for the second dimension CE-MS measurement.

To determine the moment to stop the counterflow, t_{stopCF}, the BGE signal of both CDC1 and CDC2 leading to $t_{CF,CDC1}$ and $t_{CF,CDC2}$, were considered. Furthermore, as CDC1 could not be placed directly at the capillary inlet (due to technical restrictions it was placed at an effective length of 13.5 cm), the sample plug was allowed to be transported back for another approx. 10 cm ($L_{CF,rem}$). The time needed to transport the sample along $L_{CF,rem}$ was calculated as $t_{CF,rem}$.

$$t_{\mathrm{CF,rem}} = \frac{t_{\mathrm{CF,CDC1}} - t_{\mathrm{CF,CDC2}}}{L_{\mathrm{eff,CDC2}} - L_{\mathrm{eff,CDC1}}} \cdot l_{\mathrm{CF,rem}} \qquad (3.3)$$

The counterflow was stopped at the time point t_{stopCF} which was the sum of the observed $t_{CF,CDC1}$ and the calculated $t_{CF,rem}$.

$$t_{\mathrm{stopCF}} = t_{\mathrm{CF,CDC1}} + t_{\mathrm{CF,rem}} \qquad (3.4)$$

Equation (3.4) was used to define the moment to stop the counterflow and start the CE-MS measurement. Figure 3.9 exemplarily shows the conductivity traces of CDC1 and CDC2 during an sc-ITP/CE-MS measurement conducted in BGE-S-BGE mode together with the timing of ITP, counterflow application and CE-MS (see Section 3.3.4.6). The different electrolytes, i.e. LE and TE of electrolyte system D (see Table 3.2) for ITP and 2.3 mol/L acetic acid in 20 % (v/v) iPrOH as BGE, exhibited different intensities in the CDC detectors. Capillaries were filled with LE at the beginning of the measurement, voltage was applied and the ITP stack migrated towards the MS, passing CDC1 first and CDC2 second.

The adapted TE reached CDC1 at 7.4 min (445 s) before it reached CDC2 at 16.5 min (990 s), visible as step-like drop in the signal. The first vertical line marks the moment of counterflow application $t_{startCF}$, calculated based on Equations (3.1) and (3.2).

$$v_{\mathrm{ITP}} = \frac{L_{\mathrm{eff,CDC2}}}{t_{\mathrm{TE,CDC2}}} = \frac{32\ \mathrm{cm}}{990\ \mathrm{s}} = 0.03\ {}^{\mathrm{cm}}/_{\mathrm{s}}$$

$$t_{\mathrm{startCF}} = \frac{L_{\mathrm{rem}}}{v_{\mathrm{ITP}}} + t_{\mathrm{TE,CDC2}} = \frac{2\ \mathrm{cm}}{0.03\ {}^{\mathrm{cm}}/_{\mathrm{s}}} + 990\ \mathrm{s} = 1052\ \mathrm{s}$$

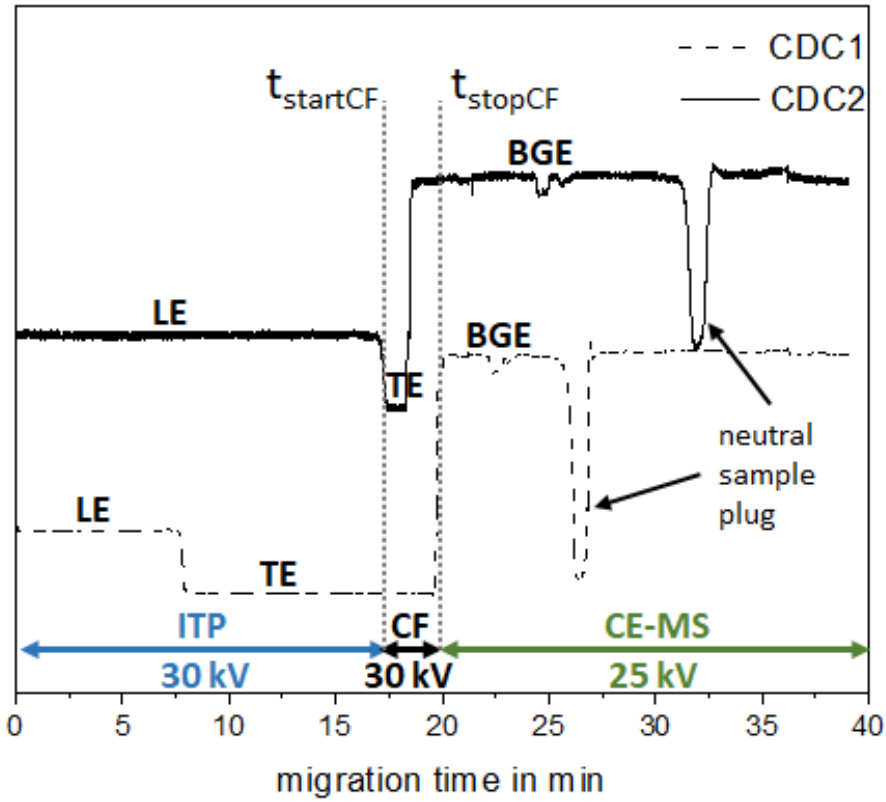

Figure 3.9: Conductivity traces of an sc-ITP/CE-MS measurement of amino acids in BGE-S-BGE mode: electrolyte system D for ITP, BGE: 2.3 mol/L acetic acid in 20 % (v/v) iPrOH for CE-MS. Hydrodynamic injection of 50 µmol/L aqueous mixture of all proteinogenic amino acids at 50 mbar for 5 s, 30 kV ITP separation voltage, 500 mbar counterflow (CF) under application of 30 kV; 25 kV CE-MS separation voltage. The steps of the process are marked along the migration time axis with vertical lines indicating the switching events and double arrows indicating time spans from ITP (blue double arrow) to counterflow $t_{startCF}$ (black double arrow) to CE-MS t_{stopCF} (green double arrow). CDC1 was placed close to the capillary inlet (13.5 cm effective length), CDC2 was placed close to the microfluidic glass chip interface (32 cm effective length). For a schematic depiction of the setup, see Figure 3.2.

The counterflow was started after 17.4 min as visible in Figure 3.9. After 10 s of counterflow, the conductivity of the BGE was recognized in CDC2. The BGE reached CDC1 after 97 s of counterflow. The remaining counterflow time was calculated to be 48 s based on Equation (3.3).

$$t_{\mathrm{CF,rem}} = \frac{t_{\mathrm{CF,CDC1}} - t_{\mathrm{CF,CDC2}}}{L_{\mathrm{eff,CDC2}} - L_{\mathrm{eff,CDC1}}} \cdot L_{\mathrm{CF,rem}} = \frac{97\ \mathrm{s} - 10\ \mathrm{s}}{32\ \mathrm{cm} - 13.5\ \mathrm{cm}} \cdot 10\ \mathrm{cm} = 48\ \mathrm{s}$$

The second vertical line in Figure 3.9 marks the moment, when the counterflow was stopped, t_{stopCF}, and the second dimension CE-MS measurement was started. The counterflow was stopped after 2.4 min, calculated via Equation (3.4), starting the CE-MS separation after 19.9 min of total analysis time, as visible in Figure 3.9.

$$t_{\mathrm{stopCF}} = t_{\mathrm{CF,CDC1}} + t_{\mathrm{CF,rem}} = 97\ \mathrm{s} + 48\ \mathrm{s} = 145\ \mathrm{s} = 2.4\ \mathrm{min}$$

During the counterflow, the LE signal in front of the sample stack should be visible as a step-like signal between the TE and the BGE signal, if the cutting was imprecise. In Figure 3.9, it was almost invisible, which was a good indication of a precise process, i.e. the LE plug in front of the sample was sufficiently short. Neutral sample plug components such as water and DMSO were visible as a dip in the BGE signal at 26 min in CDC1 and 32 min in CDC2 (Figure 3.9). They were transported through the capillaries by the remaining EOF and the suction induced from the electrospray in the ion source. As the migration times in ITP can vary due to e.g. contaminations or changes in sample composition, all calculations to determine the ideal moment for voltage switching between both dimensions had to be conducted for every single measurement directly during the analysis. In future, changes of signal intensities may be recognized automatically to generate trigger signals after automated calculations based on migration times. This enables sc-ITP/CE-MS separations without manual interaction for sample transfer. Thus, improved sample transfer precision is expected by eliminating human error.

The approximations and calculations shown for sc-ITP/CE-MS in BGE-S-BGE mode were also applicable for L-S-L and T-S-T modes. In L-S-L, the recognition of TE signals in the CDCs was most relevant for optimized sample transfer timing and best separation efficiency in CE-MS. In addition to conductivity changes, the current was monitored throughout the measurement when working under constant voltage conditions. During ITP measurements, the current steadily decreased due to the increasing amount of TE in the capillary. Thus, during counterflow, the current increased again when the TE was removed from the capillary. Consequently, the current profile could be taken as a second indication when the sample plug reached the capillary inlet. In the literature, this approach was used to set the end of the counterflow application when 90 % of starting current was reached [104]. In T-S-T mode, the current observation was not possible as the current remained low when TE was used for counterflow generation and as BGE. Conductivity changes between adapted and non-adapted TE were too low to be recognized by the CDC detectors. Instead, the signal of the LE plug which remained in front of the sample during counterflow was taken into account to determine t_{stopCF}.

In each operational mode, the counterflow had to be timed carefully to avoid sample loss by flushing the sample stack out of capillary at the inlet while removing the TE as far as possible. In all measurements, TE was not observed to considerably affect the second dimension separation, as expected from the results in Section 3.3.4.4.

3.4.4.2. Capillary lengths and filling

In the setup used for BGE-S-BGE mode, all separation capillaries were first filled with LE. The side capillary for counterflow application was then filled with BGE (until a change of the conductivity was visible in CDC3) to ensure a short length of the LE plug before counterflow application. The ratio of the capillary lengths of A2 to A1 (compare Figure 3.2 and Figure 3.8) defined the amount of BGE present in A2 after loading BGE during the counterflow application. If the ratio was too small, some LE would still remain in capillary A2, the second part of the CE-MS migration path, after the counterflow was stopped. This could negatively affect the second dimension CE-MS measurement. The different inner diameters of the capillaries used had to be taken into account as well, as both capillaries were flushed from the side capillary B (see Figure 3.2). In the experimental setup used here, the optimal length of the capillary A2 with 50 µm i.d. was approx. 72 % of capillary A1 with 100 µm i.d., e.g. capillary lengths of 35 cm for A1 and 25 cm for A2. The optimum ratio was determined by measurements with gradually increasing lengths of capillary A1.

An example of an electropherogram recorded when the ratio was insufficient (i.e. A2 was too long) is given in Figure 3.10A. The extracted ion electropherograms of proteinogenic amino acids from an sc-ITP/CE-MS separation in the BGE-S-BGE mode are presented. Capillary A1 had a length of 33 cm and capillary A2 had a length of 25 cm, i.e. capillary A2 had a length of 76 % of capillary A1. The imidazole signal (dashed line) in the first 2 min of the separation, as well as the disturbing signals recorded during the first 5 min indicate that capillary A2 was too long to be completely flushed with BGE by counterflow application. Nevertheless, separation of amino acids was achieved and negative effects were only minor (compare Section 3.3.4.4 on tITP simulations). Possibly, the suction effect of the MS was large enough to remove a fraction of the LE during the CE-MS separation. Remaining LE in A2, however, can evoke current fluctuations and influence the separation in CE-MS after dissolution of the ITP stack. Migration times higher by a factor of approx. 2-2.5 were observed (see Figure 3.10A) compared to analyses with optimized capillary lengths (Figure 3.10B). Thus, in L-S-L and BGE-S-BGE mode, optimized capillary lengths enable faster analyses.

3.4.4.3. Comparison of operational modes: L-S-L, T-S-T and BGE-S-BGE

The choice of the optimal operational mode in sc-ITP/CE-MS measurements is based on several considerations: L-S-L and T-S-T are seemingly easier to apply, as only two instead of three electrolytes are needed. The ITP electrolyte systems used in our work were not optimized for MS detection but for the simultaneous isotachophoretic stacking of all proteinogenic amino acids. Due to the high amount of DMSO, the high viscosity of

the electrolytes resulted in total separation times of approx. 18 minutes per measurement in L-S-L and T-S-T modes.

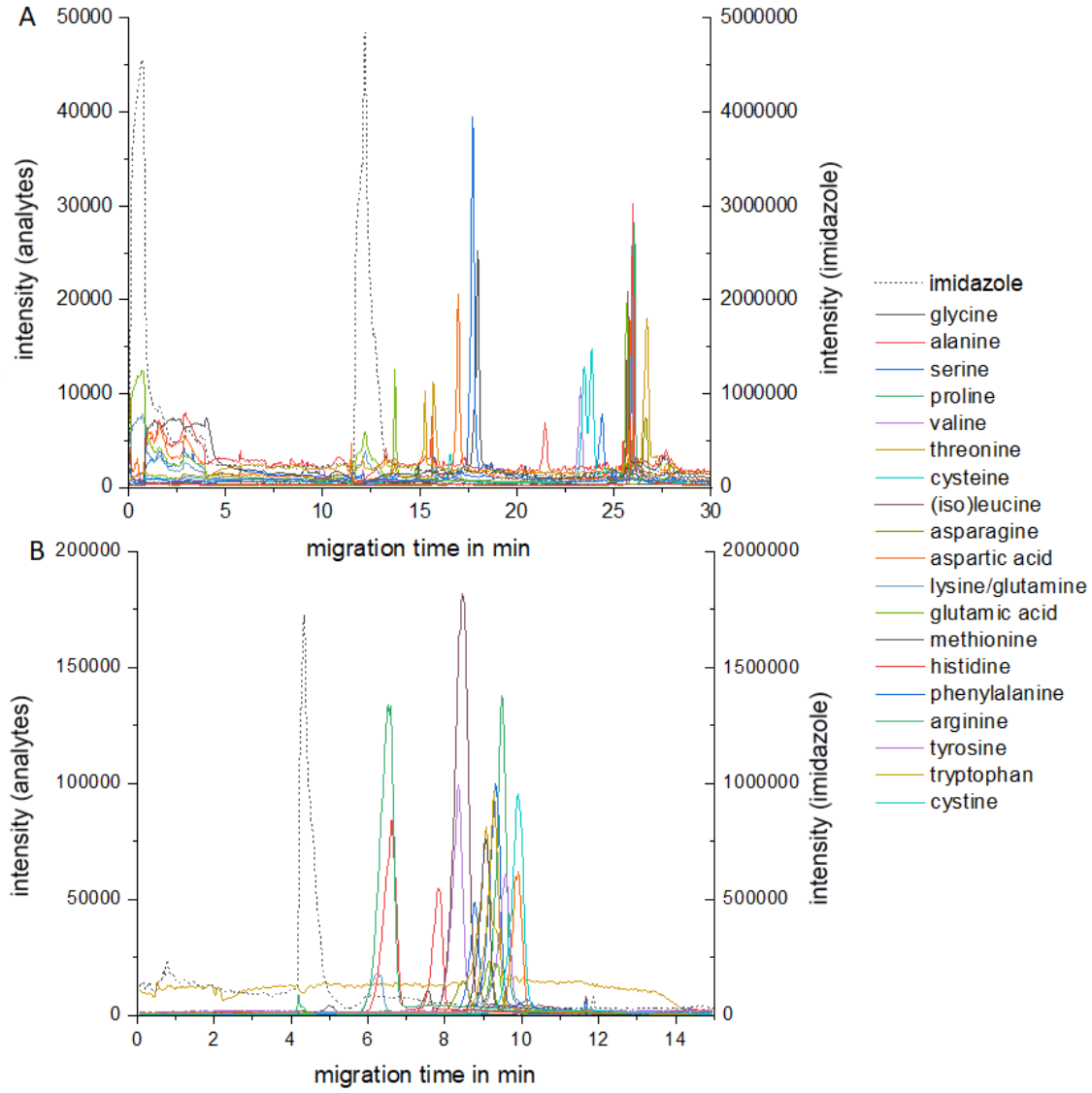

Figure 3.10: (A) Example of an electropherogram obtained with insufficient capillary length ratio (capillary A1 33 cm with 100 µm i.d., capillary A2 25 cm with 50 µm i.d.) and (B) with optimized capillary length ratio (A1 35 cm with 100 µm i.d., A2 25 cm with 50 µm i.d.) Extracted ion electropherograms of proteinogenic amino acids ((A) 100 µmol/L, (B) 500 µmol/L) in BGE-S-BGE mode sc-ITP/CE-MS, electrolyte system D for ITP, 2.3 mol/L acetic acid in 20 % (v/v) iPrOH as BGE, hydrodynamic injection 50 mbar for 5 s, 30 kV ITP separation voltage, 500 mbar counterflow under application of 30 kV, 25 kV CE-MS separation voltage. The right y-axis and dashed signal line correspond to the extracted ion electropherogram of the leading ion imidazole which was cotransferred with the sample plug.

The L-S-L mode, using LE as BGE for the second dimension, showed that the precision of cutting was not critical, as the tITP at the beginning of the CE-MS separations dissolved quickly. The current course was used as another indicator (besides conductivity detection) for the time point when the sample plug reached the inlet of capillary A1 during the counterflow application. However, as visible from Figure 3.11A,

the separation window obtained in this mode for the proteinogenic amino acids was approx. 4 min. In addition, the high amount of imidazole in the LE probably led to major ion suppression in the ion source. Imidazole is present in the ion source throughout the whole separation, as is visible from its strong signal with constant intensity (dashed line in Figure 3.11A). The signal intensity obtained for analytes was lower than in other modes (see Figure 3.10B and Figure 3.11B) although the samples had the same concentrations. Furthermore, this mode did not offer optimal conditions for MS (concerning both ionization efficiency and instrument maintenance) as imidazole is not well MS-compatible. Nevertheless, very sharp peaks with small base widths were obtained when operating sc-ITP/CE-MS in L-S-L mode, indicating that the ITP stack prevailed during the application of counterflow.

Figure 3.11B shows the extracted ion electropherograms of the proteinogenic amino acids from sc-ITP/CE-MS analysis operated in T-S-T mode. In this mode, proper cutting seemed to be crucial as the amount of imidazole was too high and the tITP conditions at the beginning of the CE-MS measurement did not dissolve quickly enough. This resulted in a very high separation efficiency but very low resolution; the separation of the amino acids was incomplete. The separation window was only approx. 2 min.

To improve the MS-compatibility and optimize the separation of the amino acids in the second dimension, a BGE-S-BGE mode was used for sc-ITP/CE-MS measurements. Electrolyte system D (see Table 3.2) was used for ITP and a BGE optimized for CE-MS (see Section 3.3.2.2) was applied in the second dimension CE-MS separation. Operation in BGE-S-BGE mode resulted in shorter separation times in the second dimension (approx. 11 min, see Figure 3.10B) than in the two other modes. The migration window of the amino acids was comparable to the L-S-L mode (approx. 4 min). Signal intensities were clearly higher than in the L-S-L mode and were also slightly improved for distinct analytes compared to the T-S-T mode.

However, these first experiments in BGE-S-BGE mode did not result in increased signal intensities compared to 1D CE-MS measurements, probably due to insufficient separation efficiency. Measurements in this mode resulted in very broad signals, i.e. peaks with a high base width of up to 1 min for several analytes. It is possible, that due to application of 30 kV and filling the capillaries with BGE, the ITP stack started to dissolve already during the counterflow. The self-sharpening effects were no longer present and the analytes experienced effects from hydrodynamic diffusion and the parabolic flow profile induced by the strong counterflow. Consequently, a broad and diffuse sample stack could have reached the capillary inlet without preconcentration

effects at the start of the second dimension CE-MS. Further optimization of the counterflow conditions is discussed in the following section.

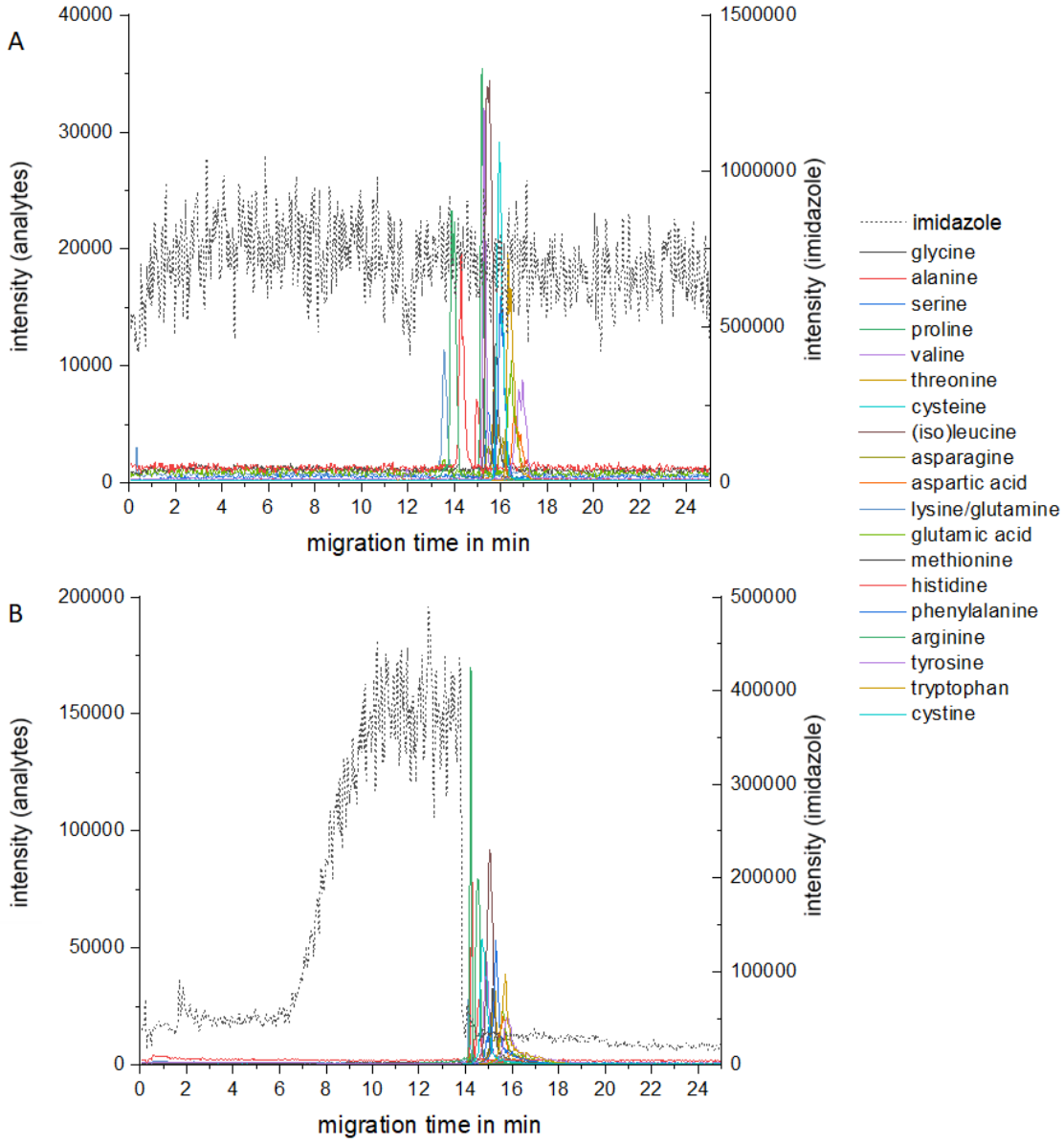

Figure 3.11: Extracted ion electropherograms from sc-ITP/CE-MS analysis of proteinogenic amino acids (500 µmol/L) in (A) L-S-L mode and (B) T-S-T mode. Capillary A1 35 cm length with 100 µm i.d., capillary A2 25 cm length with 50 µm i.d. Electrolyte system D for ITP, 2.3 mol/L acetic acid in 20 % (v/v) iPrOH as BGE, hydrodynamic injection 50 mbar for 5 s, 30 kV ITP separation voltage, 500 mbar counterflow under application of 30 kV, 25 kV CE-MS separation voltage. The right y-axis and dashed signal line correspond to the extracted ion electropherogram of the leading ion imidazole.

3.4.4.4. Optimization of applied pressure and voltage during counterflow application

As the insufficient peak shapes and peak base widths in BGE-S-BGE mode sc-ITP/CE-MS separations were expected to result from the counterflow conditions,

counterflow pressure was optimized. Figure 3.12 shows an example for the small peak base widths which can be obtained by an induced tITP phenomenon in CE-MS. LE was injected before and TE after the sample plug to induce tITP conditions at the beginning of the CE-MS separation. Sharp peaks were obtained in a separation window of 15 min. The analytes were clearly separated from imidazole. The long total analysis time of 30 min resulted from the development of tITP which had to be dissolved before the migration of the analytes in CE started and from the long migration path through capillaries A1 and A2. The measurement was taken as a reference to judge the optimization of the counterflow conditions.

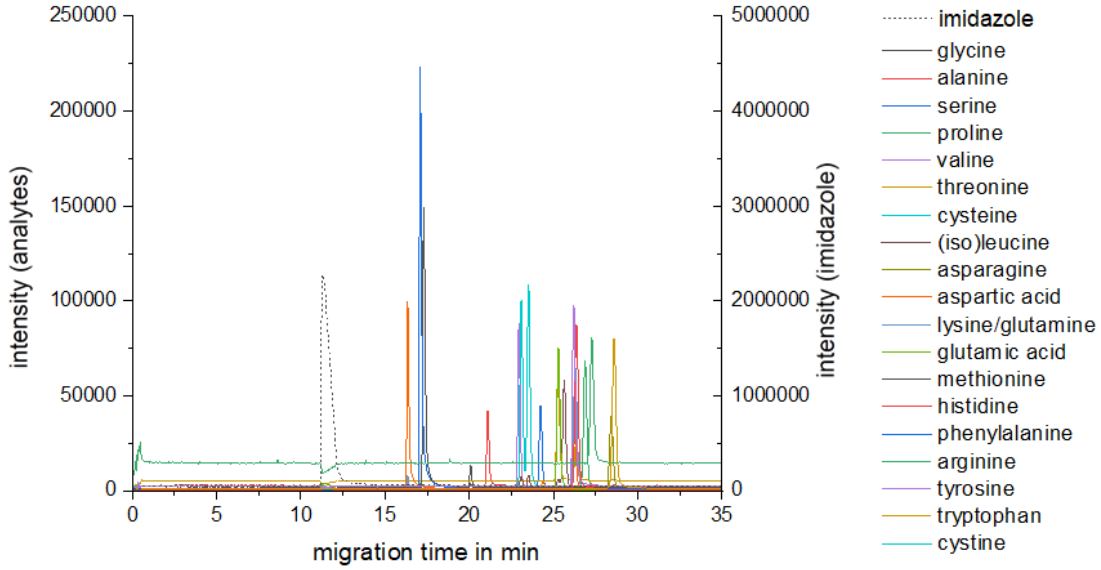

Figure 3.12: Extracted ion electropherograms from tITP/CE-MS analysis of proteinogenic amino acids (100 µmol/L) using the sc-ITP/CE-MS setup. Capillary A1 35 cm with 100 µm i.d., capillary A2 25 cm with 50 µm i.d. Hydrodynamic injection of LE (electrolyte system D), then sample, then TE (electrolyte system D), then BGE (2.3 mol/L acetic acid in 20 % (v/v) iPrOH), each at 50 mbar for 5 s, to create tITP conditions at the beginning of the separation. 25 kV CE-MS separation voltage. The right y-axis and dashed line correspond to the extracted ion electropherogram of the leading ion imidazole.

The optimization was conducted by first reducing the pressure applied during the counterflow in steps of 100 mbar to reduce hydrodynamic diffusion effects from the pressure. The counterflow pressure was reduced to 200 mbar. At lower pressures, the counterflow time became overproportionally long or was even too low to push the ITP stack back towards the inlet as it still migrated due to the voltage applied during counterflow.

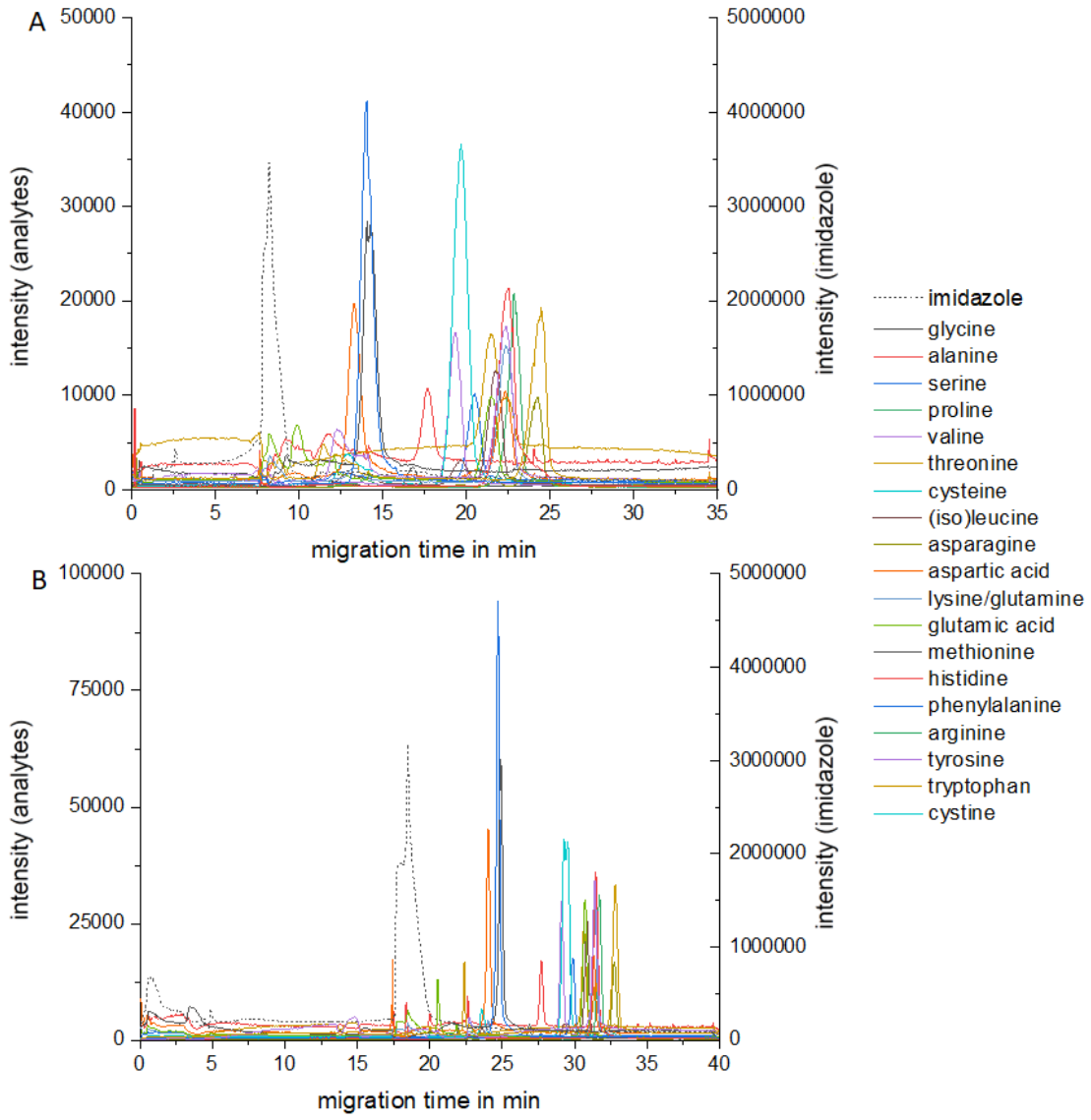

Figure 3.13: Extracted ion electropherograms of proteinogenic amino acids (100 µmol/L) from sc-ITP/CE-MS analysis in BGE-S-BGE mode with (A) 30 kV and (B) 10 kV applied during 200 mbar counterflow. Capillary A1 35 cm with 100 µm i.d., capillary A2 25 cm with 50 µm i.d. Hydrodynamic injection at 50 mbar for 5 s. Electrolyte system D for ITP, BGE: 2.3 mol/L acetic acid in 20 % (v/v) iPrOH. 30 kV ITP separation voltage, 25 kV CE-MS separation voltage. The right y-axis and dashed line correspond to the extracted ion electropherogram of the leading ion imidazole.

Figure 3.13A shows the extracted ion electropherograms obtained for amino acids from sc-ITP/CE-MS in BGE-S-BGE mode with a counterflow of 200 mbar under application of 30 kV. The separation window of the amino acids was clearly improved (compared to Figure 3.10B with 500 mbar counterflow) but the peak shape was not yet adequate. We hypothesized that the ITP stack already began to dissolve during the counterflow due to the application of the same high voltage as applied for the ITP measurement and too few leading and terminating ions in front of and behind the analyte stack, respectively. Counterflow conditions without parallel application of voltage did not improve the results,

thus, the voltage applied during counterflow was reduced in steps of 5 kV. The optimum voltage to be applied during the counterflow was 10 kV. At this voltage, good peak shapes were obtained in CE-MS analysis with a separation window of approx. 12 min for the amino acids (see Figure 3.13B), as well as increased signal intensities. At lower voltages, the signal widths increased again, probably as the voltage was too low to effectively stabilize the ITP conditions against the counterflow. With the optimized separation conditions of 200 mbar counterflow and 10 kV separation voltage, signal intensities were increased by a factor of approx. 1.5-2 in comparison to 1D CE-MS measurements at the same sample concentration.

3.4.4.5. Large volume injection

The main idea of 2D ITP/CE-MS separations is the combination of the high capillary loadability of ITP to preconcentrate analytes into a sharp stack with the high resolution and separation efficiency of CE-MS. To make use of the higher loadability of ITP/CE-MS, a large volume injection into the sc-ITP/CE-MS setup was tested by injecting a plug with a length of approx. 10 cm of an amino acid mixture with a concentration of 100 µmol/L each which is approx. 29 % of the ITP separation path in capillary A1 and approx. 17 % of the total separation path length (capillaries A1 + A2). The injection volume was approx. 0.8 µL.

The large volume injection shortened the separation path length of the ITP separation by approx. 1/3 and it is possible, that a precise cutting failed due to the changes in migration times and migration behavior. The extracted ion electropherogram of the leading ion imidazole (dashed line in Figure 3.14) was visible from the beginning of the separation with an elevated signal intensity in front of and behind the analyte stack, while imidazole was only present in front of the analytes in measurements with lower capillary load (compare e.g. Figure 3.13). It seemed as if the counterflow application was insufficient to completely remove LE from capillary A2 because the sample plug was broader and could not be transported as close to the inlet as in the previous measurements under normal injection conditions. This probably led to the insufficient separation of the amino acids due to the undissolved ITP conditions during the second dimension measurement. Another possible explanation for the insufficient separation is capillary overloading: the results presented in Section 3.4.1.3 showed that 30 % of the capillary could be filled with sample at a concentration of 1 µmol/L. For large volume injection experiments, concentrations of 100 µmol/L of sample were used to fill 17 % of the capillary, i.e. an injection of a clearly higher absolute amount of amino acids. Capillary overloading could have led to transient mixed zones and the development of plateau-mode ITP and, thus, disturb the CE-MS separation in the second dimension.

For better results, the ratio of capillary lengths of A2 to A1 has to be adapted for large volume injection applications. For this, especially the length of A1 has to be increased to provide a prolonged separation pathway for the first dimension ITP. The dependence of large volume injections on the analyte concentrations remains to be elucidated. Further experiments are needed to take advantage of the full power of the sc-ITP/CE-MS setup, but the results presented in this work already demonstrate that this setup helps to remarkably improve concentration detection limits while using a relatively simple setup compared to capillary coupling two-dimensional methods.

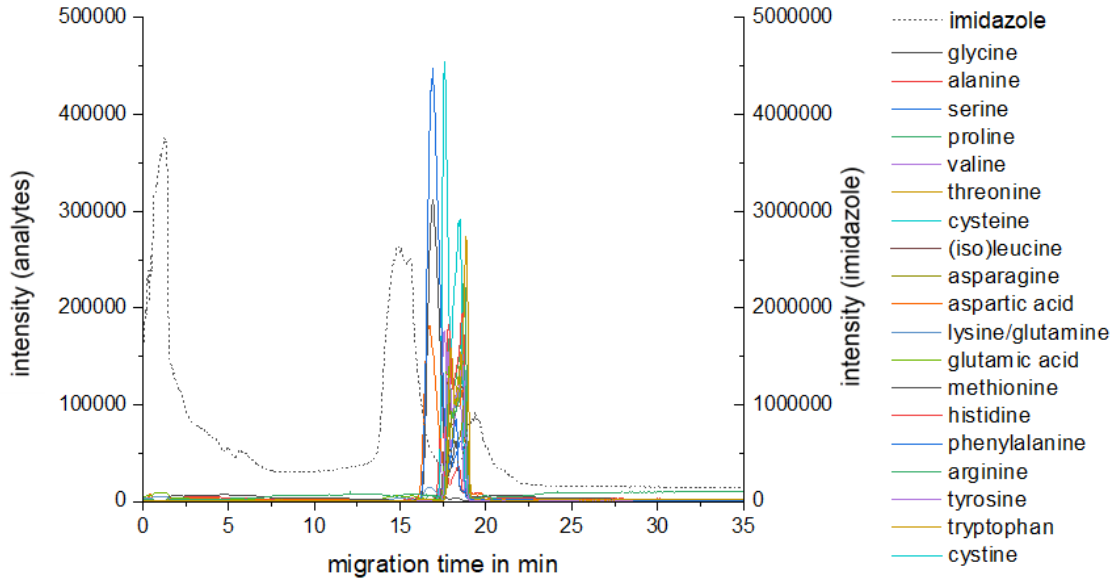

Figure 3.14: Extracted ion electropherograms of proteinogenic amino acids (100 µmol/L) from sc-ITP/CE-MS analysis in BGE-S-BGE mode. Capillary A1 35 cm with 100 µm i.d., capillary A2 25 cm with 50 µm i.d. Hydrodynamic large volume injection at 1000 mbar for 32 s, corresponding to a sample plug length of approx. 10 cm. Electrolyte system D for ITP, BGE 2.3 mol/L acetic acid in 20 % (v/v) iPrOH for CE-MS. 30 kV ITP separation voltage, 200 mbar counterflow under application of 10 kV, 25 kV CE-MS separation voltage. The right y-axis and dashed line correspond to the extracted ion electropherogram of the leading ion imidazole.

3.4.5. Capillary coupling 2D ITP/CE-MS

3.4.5.1. Sample transfer and voltage switching

In contrast to the sc-ITP/CE-MS setup, each separation dimension is conducted in a separate capillary in the capillary coupling mode of two-dimensional ITP/CE-MS. In this work, the two dimensions were coupled via the common intersection of the microfluidic glass chip interface (red circle in Figure 3.3). The sample was introduced from the commercial CE instrument into capillary A1, then voltage was applied from the CE instrument to outlet S1 to start the ITP process, i.e. the current should run through capillaries A1 and A2 (see stepwise description in Section 3.3.4.7 for reference). As soon as the analytes reach the common intersection, voltage application between the

CE inlet and the outlet S1 was stopped and then applied between inlet S2 and the MS (see Figure 3.3). By this, the current ran through capillaries B1 and B2 for CE-MS separation of the analytes using the volume of the common intersection as sample plug. For cc-ITP/CE-MS, the position of the analyte stack in the first dimension was determined using conductivity detectors placed in front of the glass chip interface on capillary A1 (C^4D1) and at the rear end of the interface (C^4D2) on capillary B2 (see Figure 3.3). As no detection directly at the common intersection was available during this work, we had to operate the system based on calculations and estimations. Equation (3.2) was used to determine the time point for voltage switching and analyte transfer. The analyte transfer is critical in cc-ITP/CE-MS as analytes are easily lost: 1) if the voltage is switched too early, the analytes will not have reached the common intersection, yet. 2) If the voltage is switched too late, the analytes may have left the common intersection already. In this work, the sample transfer was never successful when the analyte position was predicted via Equation (3.2). Differences in sample composition or impurities in the electrolytes may have influenced the ITP velocity. Even the use of freshly prepared electrolytes and sample in every run did not result in reproducible migration times. These factors added up to strong differences in the velocity of the ITP system when operating ITP under constant voltage instead of constant current conditions, as the latter was not available with the equipment employed in this work.

3.4.5.2. Determination of the column constant

In cc-ITP/CE-MS setups, the timing of the sample transfer is crucial for reliable results. If detection at the bifurcation point or common intersection of the interface is not possible, the sample transfer time must be determined via calculations. One approach tested here is the determination of the column constant C_{col} of the first dimension capillary, which describes the ratio of the migration path from injection to detection (in front of the interface) to the migration path from detection to the bifurcation point. Based on this ratio, the time point for sample transfer can be calculated.

This calculation is based on the migration time of the LE-TE boundary of the ITP recorded with the conductivity detectors in front of (C^4D1) and behind (C^4D2) the interface, following Equation (3.5)

$$C_{\mathrm{col}} = \frac{t_{\mathrm{I}\rightarrow\mathrm{C^4D1}}}{t_{\mathrm{C^4D1}\rightarrow\mathrm{B}}} \qquad (3.5)$$

with the migration time from injection to the detector in front of the chip $t_{I\rightarrow C^4D1}$ and the migration time from this detector to the bifurcation point (i.e. the end of the common intersection) $t_{C^4D1\rightarrow B}$. While $t_{I\rightarrow C^4D1}$ was directly accessible from the measurements, $t_{C^4D\rightarrow B}$ had to be determined indirectly in two steps.

$$t_{C^4D1\rightarrow B} = t_{C^4D1\rightarrow C^4D2} - t_{B\rightarrow C^4D2} \quad (3.6)$$

Based on Equation (3.6), the migration time from C^4D1 to C^4D2 (see Figure 3.3) was determined by running the ITP through the glass chip interface until it reached the second conductivity detector. Thus, $t_{C^4D1\rightarrow C^4D2}$ was directly accessible from the same measurements conducted to determine $t_{I\rightarrow C^4D1}$. In a second step, capillary A2 was filled with LE by flushing the complete system with LE. Then, this capillary was blocked using a silicone-filled vial and the remaining capillaries were filled with TE. The ITP process started from the bifurcation point when voltage was applied and $t_{B\rightarrow C^4D2}$ could be determined. Finally, $t_{C^4D1\rightarrow B}$ was calculated using Equation (3.6) and with this value, C_{col} was calculated (Equation (3.5)). All migration times needed to determine C_{col} were determined in triplicate, using electrolyte system B (compare Table 3.2) and without sample injection. The results of the distinct measurements, the average values and relative standard deviations are summarized in Table 3.5.

Table 3.5: Migration times determined from blank ITP measurements with electrolyte system B (Table 3.2) through the microfluidic glass chip interface for determination of the column constant. Hydrodynamic injection of TE at 100 mbar for 5 s. For further explanation, see text.

	t_{m1} in min	t_{m2} in min	t_{m3} in min	$t_{ø}$ in min	RSD in %
$t_{I\rightarrow D1}$	40.77	40.71	40.26	40.58	0.69
$t_{D1\rightarrow D2}$	4.93	4.99	4.79	4.90	2.09
$t_{B\text{-}D2}$	2.05	1.88	1.80	1.91	6.68

From the data in Table 3.5, using Equations (3.5) and (3.6), a value of C_{col} = 13.56 was calculated for the given setup with electrolyte system B. It is important to mention that this column constant is only applicable for this specific setup. If capillary dimensions are changed, C_{col} has to be determined again. Based on C_{col}, the time when the sample reaches the common intersection in the setup was calculated using Equation (3.7).

$$t_{C^4D1\rightarrow B} = \frac{t_{I\rightarrow C^4D1}}{C_{col}} \quad (3.7)$$

Nevertheless, even after determination of C_{col} and the calculation of $t_{C^4D1\rightarrow B}$, no signals for the amino acids were observed in cc-ITP/CE-MS, indicating that the sample transfer to the second dimension remained unsuccessful using C_{col}. Several aspects may serve for explanation: first, the precision of the migration times used to calculate C_{col} may have been too low. As the common intersection is very small, slight deviations from the actual value could have led to incorrect values of $t_{C^4D1\rightarrow B}$ so that the voltage was switched too early or too late, resulting in the loss of the analytes. Especially the determination of $t_{B\rightarrow C^4D2}$ was difficult due to the setup: capillary A2 was blocked with a silicone-filled vial to flush the remaining system with TE. If the flow through capillary A1 was not fully

suppressed, e.g. by improper sealing, some TE may have already entered this capillary, resulting in wrong values for $t_{B \rightarrow C^4D2}$. Furthermore, the conditions for the determination of C_{col} were not completely comparable to the conditions in the capillaries during the cc-ITP/CE-MS measurements: as capillary B2, which was connected with the MS, could not be blocked, the whole system was filled with LE first, then capillaries A1 and A2 were blocked to flush capillaries B1 and B2 with BGE. Thus, the common intersection was already filled with BGE during the ITP measurement in the first dimension. Future work may employ on-chip conductivity detection to enable precise cutting events.

3.5. Conclusive discussion and outlook

3.5.1. Electrolyte optimization

Two new ITP electrolyte systems were developed for the simultaneous preconcentration of amino acids in one isotachophoretic zone based on electrolyte systems introduced by Kler et al. [2]. DFA or TMPA were applied as counterions, enabling to obtain a sufficiently low pH to preconcentrate all analytes as cations while strongly improving the MS-compatibility of the electrolyte systems in contrast to the previous electrolyte system with OA as counterion. Furthermore, up to 30 % of the capillaries could be filled with aqueous sample without current breakdowns and disturbances, which were observed when using TFA as counterion. ITP-MS detection limits under optimized conditions were in the low to medium micromolar range with electrolyte system D, i.e. with DFA as counterion, although the migration of all analytes in one isotachophoretic zone induced ion suppression. Thus, the LODs determined did not reach detection limits in the nanomolar to subnanomolar range reported in the literature for ITP separations of selected amino acids, e.g. by gradient elution ITP-UV [114] of derivatized aspartic acid and glutamic acid or by ITP-MS of histidine [34]. Both electrolyte systems were considered equally suitable for ITP-MS and ITP/CE-MS applications. Electrolyte system D with DFA as counterion was employed for sc-ITP/CE-MS measurements.

An acetic acid BGE for the separation of all analytes in CE-MS was developed based on a BGE introduced by Coufal et al. [139]: the dynamic coating was omitted to reach MS-compatibility and 20 % (v/v) iPrOH in water was used as solvent. The addition of iPrOH was envisaged to improve the compatibility with the viscosity of the hydroorganic electrolyte systems used in the ITP dimension in two-dimensional measurements. Care was taken that the isobaric pairs glutamine/lysine and leucine/isoleucine were sufficiently resolved. While lysine and glutamine were perfectly separated, the critical pair of leucine/isoleucine was separated with a resolution of 0.8. The separation of these isomers in CE is difficult to achieve: Klampfl and Ahrer [132] showed that the resolution

can be improved by increasing the electrolyte concentration. In several approaches with formic acid BGEs at concentrations up to 1 mol/L, isoleucine and leucine were not baseline separated [129-131, 133]. In contrast, Coufal et al. [139] reached a high resolution for these isomers. In their study, the migration time window spanned between first and last migrating amino acid was approx. 20 min. On the contrary, the migration time window was strongly reduced (approx. 5 min, compare Figure 3.5) in our work due to the removal of the dynamic coating from Coufal's BGE. Additionally, suction effects of the electrospray ionization probably induced a hydrodynamic flow in the capillary towards the MS, increasing flow velocity and, thus, reducing the separation efficiencies and migration time window. In CE-C^4D test measurements with the same BGE, we observed migration time windows of approx. 10 min for the amino acids. However, our results were considered sufficient for qualitative purposes but the analytes were split into two groups for highest precision in quantitative measurements during the evaluation of performance parameters. Concentration detection limits were in the low to medium micromolar range. For most amino acids, the stacking process in ITP-MS slightly improves the detection limits when similar amounts of sample are injected. The detection limits determined for CE-MS were higher than the values of CE-MS methods in the literature which were in the submicromolar to low micromolar range in several approaches [130-131, 133]. To further improve detection limits, further optimization of the BGE but also the sheath liquid should be envisaged to improve separation efficiency and resolution, reduce quenching effects and enhance ionization efficiency. The application of a capillary coating should be considered as an alternative approach to enhance the resolution of the analytes.

3.5.2. Challenges and benefits of the newly introduced 2D ITP/CE-MS setups

A new sc-ITP/CE-MS setup with intermediate conductivity detection was developed: by introducing a microfluidic glass chip interface and a side capillary, challenges of counterflow generation and the limited electrolyte/MS-compatibility were overcome. In literature, counterflow generation in sc-ITP/CE-MS was mainly induced by height difference (e.g. [99, 105]) or by applying pressure (e.g. [96, 103-104, 106, 140]). Thus, either the electrolyte in the outlet vial or the sheath liquid (in case of ITP/CE-MS) was used as source for the counterflow and mainly L-S-L modes were applied. Bergman et al. [99] introduced a side channel via a T-piece to apply LE counterflow by lifting a syringe connected to the side channel for CE-UV.

Our new setup offers new possibilities compared to the sc-ITP/CE-MS setups presented in literature: 1) the sheath liquid can be chosen independently of the separation electrolytes, thus, it can be optimized for ITP mobility windows, MS-compatibility and minimal influence on analyte ionization efficiency. 2) The BGE-S-BGE mode is applicable

in this setup, as the counterflow can be used to fill the capillaries with a BGE independent of the ITP electrolytes and the sheath liquid. Thus, all electrolytes (LE, TE, BGE) can be optimized independently for each dimension to obtain the best possible concentration effects and separations as well as highest MS-compatibility. The addition of the interface with the side capillary with pressurization only requires a small instrumental expenditure. It is more easily applicable than cc-ITP/CE-MS approaches.

The sc-ITP/CE-MS setup was optimized with regard to capillary lengths and counterflow conditions and successfully applied to preconcentrate and separate amino acids in L-S-L, T-S-T and BGE-S-BGE mode, providing a comprehensive proof of principle for this setup. To our knowledge, this is the first application of BGE-S-BGE mode in a sc-ITP/CE-MS hyphenation.

This new two-dimensional setup in combination with the employed electrolytes still suffers some ‘teething problems’. The repeatability of the method was rather low, especially if the setup was changed due to blocked or broken capillaries or had to be disassembled and reassembled again. It was difficult to obtain stable currents under high voltage application. This was mainly due to the capillary-glass chip connections which had to be absolutely free of air bubbles and properly sealed. Current stability during the CE-MS dimension separation was a major problem. Several measurements could not be conducted completely as the current rapidly decreased to zero. It is hypothesized, that this was induced by contamination of the microfluidic interface with silicone from the sealing at the capillary-glass chip interfaces which was observed by microscopy of the flow channels. Silicone is susceptible to corrosion catalyzed by acetic acid, which was used as BGE in the second dimension. Although the interface was cleaned with glacial acetic acid and ultrasonication whenever current problems arose, the contamination of the microfluidic channels could not be removed completely. In future applications, other sealing materials than silicone are envisaged.

Further work needs to be conducted concerning large volume injections and further optimization of capillary lengths for longer injection plugs. In contrast to the T-junction used by Bergman et al. [99], the microfluidic glass chip interface used to introduce the side capillary can be equipped with intermediate detection directly at the bifurcation point, which is envisaged in the future and is expected to improve the sample transfer precision. Intermediate detection close to the bifurcation point will be useful for process automation to improve feasibility and reproducibility.

A cc-ITP/CE-MS setup was introduced as a more sophisticated but, in principle, more powerful alternative to the sc-ITP/CE-MS setup. A home-made multi-vial holder with an external high voltage source was employed to provide a second electric circuit for the

second dimension CE-MS separation. Both dimensions were independent of each other in regard to voltage application. Separation dimensions were switched by stopping voltage application to the first dimension and starting voltage application to the second dimension. The microfluidic glass chip interface was used as common intersection to connect both dimensions hydrodynamically.

Compared to sc-ITP/CE-MS, some limitations of this setup remained at the end of this thesis: 1) the equipment needs a second high-voltage source and vial holder. 2) The capillary lengths of the side capillaries (A2 and B1 in our setup, see Figure 3.3) are rather long. A further instrumental optimization should allow to use shorter capillaries for capillaries A1 and B2 to enable higher field strength and reduced separation times. 3) The order of filling the capillaries with LE/TE and BGE is determined by the setup as the capillary inserted to the MS cannot be blocked, and, 4) due to this, the common intersection is filled with BGE during the ITP measurement which could possibly disturb or at least influence the ITP process. 5) The precision of the timing of the sample transfer has to be further improved, which is best accomplished by an intermediate detection directly in the interface.

The cc-ITP/CE-MS setup as introduced in this work seems very promising, when precision of the sample transfer timing is improved. We expect that with this setup, the increased freedom of choosing capillaries and electrolyte systems will be at least comparable if not superior to the sc-ITP/CE-MS setup. In principle, it should be possible to transfer the ITP stack from the first dimension to the second with a higher precision and a lower amount of LE and TE being cotransferred. Heart-cutting techniques are facilitated by the common intersection. This could also result in improved MS-compatibility. Work on on-chip conductivity detection is currently conducted, which will improve the precision of the sample transfer to the second dimension. If intermediate detection at the common intersection is available, the combination of commercial instruments with home-made and custom-made equipment offers high flexibility and we expect promising results with the improved intermediate detection techniques.

4. Influence of different organic solvents in hydroorganic background electrolytes on electroosmotic and electrophoretic mobilities

4.1. Abstract

Nonaqueous capillary electrophoresis has gained an increasing interest during the past decades and is used increasingly to target analytical challenges difficult to tackle with aqueous capillary electrophoresis (CE). The physicochemical background of CE separations in nonaqueous background electrolytes (BGE) has been discussed. In contrast, similar discussions are largely missing for hydroorganic BGEs with the transition from aqueous to nonaqueous electrolytes, despite the fact that many CE applications include organic solvents to improve separation selectivity, resolution or solubility of analytes. The understanding of the progression of different physicochemical parameters upon increasing the content of organic solvents is still in an early stage. In this work, hydroorganic BGEs containing low amounts (up to 50 %) of protic (methanol, isopropanol) and aprotic solvents (acetonitrile, dimethyl sulfoxide) with a wide range of permittivities were applied to investigate the progression of the electroosmotic flow (EOF) and the effective electrophoretic mobilities of all proteinogenic amino acids. We discuss the dependence of the EOF and effective electrophoretic mobilities on the BGE composition with regard to changes of the relative permittivity, hydrodynamic viscosity, autoprotolysis and hydrogen bonding ability in these hydroorganic mixtures.

4.2. Introduction

4.2.1. Hydroorganic background electrolytes – the transition from aqueous to nonaqueous capillary electrophoresis: basic considerations

Nonaqueous capillary electrophoresis (NACE) has gained increasing interest as there are strong differences in selectivity compared to aqueous capillary electrophoresis (CE) [141]. Several reviews on NACE have been published (see e.g. [142-146]) showing the versatility of nonaqueous background electrolytes to extend the application of capillary electrophoretic separation methods. Nevertheless, organic solvents must fulfill certain criteria to be applicable for CE [28, 146]: solvents must be non-inflammable and liquid at room temperature, have a low reactivity, low vapor pressure and ideally low intrinsic conductivity due to limited autoprotolysis. Electrolytes and analytes must be present as solvated ions or at least charged ion pairs (or in equilibrium between these species) in the given solvent. Furthermore, the background electrolyte (BGE) solvent has to be compatible with the detection method chosen, limiting e.g. the application of certain solvents in UV detection. Organic BGEs are applied for several reasons such as improved solubility of analytes, higher separation selectivity and efficiency for certain

analytes. These improvements are based on changes in analyte mobilities, the induction of different separation mechanisms, faster analysis due to the possibility of applying higher voltages (lower current and Joule heating), better compatibility with mass spectrometric detection, as well as reduced sorption of analytes to bare fused silica capillary surfaces [142].

Low amounts of water are generally accepted in NACE [147], but the term refers to BGE compositions without intentional addition of water [148]. Nevertheless, even small amounts of water in organic BGEs can have considerable impacts on parameters which influence the electroosmotic flow (EOF) and analyte electrophoretic mobilities and, thus, the separation selectivity and efficiency, as will be discussed in the following section. Using mixtures of organic solvents and water to create hydroorganic BGEs is a possibility to overcome some of the obstacles present when using nonaqueous BGEs, as some effects on e.g. pK_a or EOF are far less pronounced [149] and reliable pH determination is simplified [142]. Publications on the basics of hydroorganic CE (HOCE) separations are rare. The synergy of different solvent parameters (e.g. viscosity and relative permittivity) is difficult to understand, the prediction of migration behaviors in HOCE is not possible today. Some research was conducted to understand changes of the EOF in hydroorganic BGEs, see e.g. [8, 150-151], on analyte mobilities and separation efficiencies (e.g. [149, 152-155] in CE, [9-11] in ITP). In this study, further understanding of the underlying effects is gained by comparing the effects of four solvents, protic methanol (MeOH) and isopropanol (iPrOH), and aprotic acetonitrile (ACN) and dimethyl sulfoxide (DMSO), the latter largely differing in their relative permittivity and other parameters.

4.2.2. Motivation: the choice of organic solvents and analytes for the investigation of hydroorganic background electrolytes

In this work, the dependence of cationic effective electrophoretic mobilities of amino acids and EOF on the solvent composition of the BGE is investigated in hydroorganic BGEs with MeOH, ACN, iPrOH and DMSO. Acetic acid (HAc) is used as electrolyte in the BGEs. MeOH, ACN and mixtures thereof are the most commonly applied organic solvents in CE due to their acceptable relative permittivity, low viscosity and good UV transparency (compare Table 4.1) [142, 146-147]. Electrophoretic mobilities and pK_a values of different analytes as well as the EOF were already determined in BGEs of MeOH, ACN, mixtures of both (e.g. [156-163]) and also in hydroorganic BGEs containing MeOH and ACN [8, 149, 155]. DMSO is less commonly applied for NACE due to its high viscosity, low UV transparency and limited compatibility with mass spectrometry (MS). Basic characteristics of DMSO/water mixtures were studied including the ionization of

weak acids [164], density and viscosity [165], solvation and ion association [166], autoprotolysis [167], dielectric properties [168] and the influence on EOF and zeta-potential [8]. Kler et al. [2] used DMSO as solvent for nonaqueous ITP to reduce the mobility of the proton functioning as termination ion by disturbing the Eigen-Zundel-Eigen mechanism (EZE), see Chapter 3. DMSO is an aprotic solvent but in contrary to ACN, it has a high relative permittivity and is able to act as proton acceptor for hydrogen bond formation. iPrOH is rarely applied in NACE and only few investigations on iPrOH/water mixtures were conducted (e.g. [8, 167, 169-170]). This solvent was chosen as a protic solvent with a high viscosity but a low relative permittivity.

The set of proteinogenic amino acids was chosen as set of model analytes as a wide range of pI and pK_a values is covered. Furthermore, the amino acids have a wide spectrum of basic to acidic properties as well as polarity, including polar and nonpolar analytes. Cystine is included as it is the oxidation product of cysteine and may be produced in DMSO. The data obtained for the EOF and effective electrophoretic mobilities in hydroorganic BGEs in this work is used to approach deeper understanding of the influences of several interacting parameters (given in Table 4.1) in HOCE. These different parameters will be discussed in the following sections with regard to changes in EOF and effective electrophoretic mobilities.

4.3. Theoretical background

4.3.1. Solvent parameters influencing electroosmotic flow and electrophoretic mobility

The EOF in CE depends on the relative permittivity ε of the BGE solvent, the zeta-potential ζ of the capillary wall, the solvent's dynamic viscosity η and the capillary radius r [171] and can be described by Equation (4.1).

$$\mu_{\mathrm{EOF}} = \frac{\varepsilon \cdot \zeta}{4 \cdot \pi \cdot \eta \cdot r} \qquad (4.1)$$

The zeta-potential depends on the BGE composition, e.g. the ionic strength. Its magnitude is not directly accessible. Therefore, the EOF can be calculated from experimental data using Equation (4.2).

$$\mu_{\mathrm{EOF}} = \frac{L_{\mathrm{cap}} \cdot L_{\mathrm{eff}}}{U \cdot t_{\mathrm{EOF}}} \qquad (4.2)$$

In this equation, only parameters directly accessible from the electropherogram, here the migration time of the EOF marker t_{EOF}, and experimental parameters, i.e. the total capillary length L_{cap}, the effective capillary length L_{eff}, the applied voltage U are taken into

account. This equation is applicable only under certain conditions such as constant voltage, constant buffer compositions and very diluted samples.

The electrophoretic mobility of analytes depends, simply speaking, on the hydrodynamic radius of an ion and its charge. The velocity of an ion v_e is a result of the electrophoretic mobility μ of the ion and the applied electric field strength E, with μ being the proportionality constant.

$$v_e = \mu \cdot E \tag{4.3}$$

The measured mobility μ_{mes} can be calculated from the migration time t_m of an analyte obtained from the electropherogram by Equation (4.4), similar to the calculation of μ_{EOF}.

$$\mu_{mes} = \frac{L_{cap} \cdot L_{eff}}{U \cdot t_m} \tag{4.4}$$

The measured mobility is the sum of μ_{EOF} and the effective electrophoretic mobility μ_{eff} of an analyte (see Equation (4.5)). As the EOF can vary based on the BGE or be influenced by impurities and, thus, is able to mask the mobility of an analyte in the electric field, μ_{EOF} is subtracted from μ_{mes} to obtain the effective mobility μ_{eff} of an analyte [171].

$$\mu_{eff} = \mu_{mes} - \mu_{EOF} \tag{4.5}$$

$$\mu_{eff} = \frac{L_{cap} \cdot L_{eff} \cdot (t_{EOF} - t_m)}{U \cdot t_m \cdot t_{EOF}} \tag{4.6}$$

The effective electrophoretic mobility can be used to analyze the influence of organic solvents in the BGE on the migration of analytes in an electric field independent of μ_{EOF}. Several solvent parameters influence the EOF and electrophoretic mobilities of electrolytes and analytes: 1) relative permittivity, 2) viscosity and density, 3) its autoprotolysis constant, ergo its basicity/acidity, and 4) the ability to form hydrogen bonds [172]. Table 4.1 lists these parameters for the solvents used in this study. As the parameters and properties interact, it is difficult to determine the role of a single parameter in electrophoretic separations. In hydroorganic solvent mixtures, this becomes even more complicated because the changes of the parameters are not necessarily linear throughout the transition from aqueous through hydroorganic to organic solvents.

The relative permittivity ε, also referred to as dielectric constant, influences solubility and ion pairing processes. Generally, it is assumed that in solvents with $\varepsilon < 30$ ion pairing is favored [28]. At high relative permittivities, only solvated ions will be present in solution. As visible from Table 4.1, the relative permittivities of MeOH and ACN are very close to this value and ε of iPrOH lies well below. In solvents with lower relative permittivity, ion pairing and ion association of both analytes and electrolytes are possible or even

favored. Then, higher field strengths can be applied due to less Joule heating. However, electrophoretic mobilities and EOF will be decreased [28].

Table 4.1: Relative permittivity ε, dynamic viscosity η, dipole moment and autoprotolysis constant of the solvents used in this study, i.e. water, MeOH, iPrOH, ACN and DMSO at 25 °C [173-174].

solvent	hydrogen bonding	ε	η in mPa·s	ε/η	dipole moment in Debye	autoprotolysis constant
Water	amphiprotic	78.4	0.89	88	1.9	14.0
MeOH	amphiprotic	32.7	0.55	59	2.9	16.9
iPrOH	amphiprotic	19.9	2.04	10	1.7	21.1
ACN	aprotic protophobic	35.9	0.34	106	3.9	32.2
DMSO	aprotic protophilic	46.5	1.99	23	4.1	31.8

The viscosity η of a solvent gives an idea on the hydrodynamic friction an ion encounters during its electromigration through a solvent. It also influences the solvation radius. Higher solvent viscosities are associated with reduced electrophoretic mobilities and EOF because of the higher friction, which is expected e.g. for DMSO and iPrOH (compare Table 4.1). In hydroorganic mixtures, the viscosity does not change linearly with changes in the solvent ratios due to density differences and differences in partial molar volumes. The ratio of relative permittivity and viscosity ε/η can be applied as an estimation for separation speed as both electrophoretic mobilities and EOF are considered proportional to this ratio [146].

The autoprotolysis constant describes the ability of a solvent to self-dissociate. Autoprotolysis influences protonation equilibria of analytes and can induce changes in their pK_a values based on changes in ion stabilization mechanisms. A small autoprotolysis constant refers to a higher autoprotolysis of the solvent and, thus, greater acidity/basicity. The acidity and basicity of a solvent govern the solvation and association processes. Solvents undergoing autoprotolysis produce lyonium ions (anions) and lyate ions (cations) and are called amphiprotic solvents (e.g. water, MeOH, iPrOH). Solvents with a high autoprotolysis constant, which are unable to undergo autoprotolysis, are referred to as aprotic solvents (e.g. ACN, DMSO). Autoprotolysis influences the conductivity of a solvent as it influences the number of charge carriers in solution and, therefore, the EOF is affected as well. Thus, a lower current and low Joule heating are expected in solvents with high autoprotolysis constants, which helps to improve separation efficiency.

Amphiprotic solvents are generally capable to form hydrogen bonds, which is one of the main analyte-solvent interaction mechanisms including proton donation/acceptance [156]. Hydrogen bonds in amphiprotic solvents evoke a strong solvation of ions and, thus, prevent or at least diminish ionic interaction between analyte ions and electrolyte ions. Subsequently, in solvents with low permittivity but the ability to form hydrogen bonds such as iPrOH (as visible in Table 4.1), ion pairing will be suppressed [175-176]. In aprotic solvents, the ability to form hydrogen bonds is generally reduced or non-existent. DMSO can act as proton acceptor to form hydrogen bonds (protophilic aprotic solvent), while in ACN hydrogen bonding does not occur (protophobic aprotic solvent) [172, 177]. Then, it is predominantly the dipole moment which determines the arrangement of solvent molecules around positively and negatively charged ions [28] with ion-dipole interactions as the main analyte-solute interactions. In this case, ion association or ion pair formation tend to be more pronounced if the solvent's relative permittivity is low (e.g. ACN but not DMSO, Table 4.1).

To summarize, autoprotolysis, hydrogen bonding and dipole moment influence the arrangement of solvent molecules around analyte and electrolyte ions. Solvation shells in organic solvents are generally smaller than in water, inducing a higher selectivity for small structural differences in CE separations, as was shown e.g. by Posch et al. [178]. Nevertheless, the changes in ion solvation change the electrophoretic mobilities, as these parameters influence the stabilization of cations and anions and, thus, the extent of ion pairing.

Elevated conductivities are often present in protic solvents. Especially in water with its strong hydrogen bonds and a three-dimensional structure, an extraordinarily high limiting mobility of H^+ and OH^- is caused by a special transport mechanism (i.e. EZE) with flipping H-bonds instead of a pure electromigration of solvated H^+ (and OH^-). This effect is strongly reduced in organic solvents (e.g. ACN, DMSO) and hydroorganic mixtures but is present in amphiprotic solvents (e.g. MeOH), though to a lesser extent than in water [142].

With regard to the EOF, the influence of the relative permittivity and the viscosity on the electroosmotic mobility is obvious from Equation (4.1): a higher relative permittivity will increase the EOF, while a higher viscosity decreases the EOF. The ratio ε/η is considered proportional to the EOF and, therefore, often taken into account to estimate the EOF [146-147]. Nevertheless, the other parameters described above for their influence on solute mobilities also affect the EOF, as they change the zeta-potential. In CE separations, mainly fused silica capillaries are applied. Thus, the capillary walls consist of silanol groups, which remain protonated only at low pH values. Under medium

to high pH conditions, the silanol groups are deprotonated, resulting in a negatively charged capillary surface. The zeta-potential is the electric potential between the BGE and the stationary fluid layer (Stern layer) which is attached to the negative capillary surface for charge balancing. The solvation and charge of both, the anionic silanol groups and the cations from the BGE present in the Stern layer are influenced by the addition of organic solvents to an aqueous BGE, similarly to dissolved analyte ions as described above, with strong changes in the zeta-potential possible. A better stabilization of the surface charge and ions in the attached fluid layer will lead to an increase of the zeta-potential and, thus, to an increased EOF as can be deduced from Equation (4.1). Upon addition of organic solvents, the zeta-potential mostly decreases as a result of a potential drop within the attached fluid layer and/or a reduction of the negative surface charge [8]. Therefore, the EOF is expected to be reduced in most hydroorganic BGEs as will be discussed in Section 4.6 for the solvents used in this study.

4.3.2. pH, pKa and ionic strength in hydroorganic background electrolytes

One of the most important parameters for separation selectivity in CE separations is the pH of the BGE [148]. The thermodynamic pH, which describes the theoretical activity of protons in the given solvent based on theoretical pK_a values [176], is difficult to be determined in nonaqueous BGEs. Thus, the determination is often circumvented [173] and the pH remains unknown with some disadvantages with regard to a full understanding of the separation conditions. Nevertheless, there are several methods to measure the pH in BGEs for NACE, which were described by Kenndler [147]. One commonly applied method is the determination of the apparent pH (also denoted as pH*), i.e. the pH measured in nonaqueous media with electrodes calibrated in common all-aqueous setups. Due to the uncertainty of the liquid-junction potential based on the transfer from aqueous to nonaqueous media, the apparent pH is not related to the actual activity of protons [142, 148, 176]. However, it is a useful tool to approximate relative acidities of different nonaqueous and hydroorganic BGEs. A correction factor for the liquid-junction potential can be used to calculate the pH from the apparent pH determined experimentally but the available data is still very limited [148]. In hydroorganic BGEs, at least at low percentages of the organic solvent, not determining the pH is less problematic than in nonaqueous BGEs, in which the acidity of solutes decreases drastically [173]. Furthermore, the apparent pH measured with an all-aqueous setup is supposedly closer to the actual proton activity as it has been shown that small amounts of water in organic solvents exhibit stronger changes of pK_a values than small amounts of organic solvent added to water [142, 148].

The changes of the pH value for a specific acid-base combination upon addition if organic solvents are based on changes of pK_a values in different solvents. The basicity of a solvent influences the stabilization of ions and is connected to the autoprotolysis of the solvent as described in the previous section. Most organic solvents exhibit a lower basicity than water (e.g. MeOH basicity is slightly lower, ACN is much less basic, compare autoprotolysis constants in Table 4.1). The destabilization of ions based on a lower basicity leads to changes of pK_a values [147, 156]. Bosch et al. [179] measured increasing pK_a values for neutral and anionic acids in hydroorganic buffers with increasing ACN contents which corroborates findings in several other publications on pK_a shifts in MeOH/water and ACN/water mixtures, e.g. [149, 155]. For basic analytes, pK_a shifts for the cation acid seem to be less pronounced [142, 156]. Espinosa et al. [180] even observed a decrease of pK_a values of bases with increasing ACN contents in hydroorganic buffers. This difference can be explained by the differences in ion stabilization: while water has a strong ability to stabilize both anions and cations, the anion stabilization in MeOH is only medium, low in DMSO and very low in ACN [173], thus, pK_a values of anionic acids are strongly affected. The ability to stabilize cations remains very high in pure MeOH and DMSO, but is low in pure ACN [173]. In CE separations, the changes of pK_a values directly affect electrophoretic mobilities and can even induce changes in the migration order, as observed by Cantu et al. [156] in NACE separations. However, ion pairing has to be considered as well. Changes of pK_a values in NACE can also deliberately be exploited for separations, e.g. for cationic separation of analytes in organic media which would otherwise not be ionized under purely aqueous conditions [147].

In both HOCE and NACE, pK_a shifts affect not only analytes and substances used as electrolytes, but also the capillary surface of uncoated fused silica capillaries as the silanol groups are weak neutral acids with pK_a values around 5 to 6 in aqueous media [142]. Schwer and Kenndler [8] showed that the pK_a value of the silanol groups increases upon addition of organic solvent and, thus, the zeta-potential decreases, inducing a reduction of the EOF. Nevertheless, as some organic solvents favor cation stabilization, the charge of the capillary surface could become positive and a reversed EOF is induced, which was observed e.g. in BGEs of pure MeOH and DMSO without supporting electrolytes [157].

The degree of ionization of all substances in hydroorganic BGEs influences the ionic strength, which is a parameter influencing resolution, sorption to the capillary wall, separation efficiency, stacking effects and migration times in CE [158]. The ionic strength may be reduced due to ion association and ion pair formation which are pronounced

especially in ACN and sometimes in DMSO [181]. These processes neutralize the charge of the ions and reduce analyte and electrolyte mobilities and, thus, conductivities in CE separations. In NACE with ACN electrolytes, increased ionic strength even promotes interaction with counterions to form ion pairs and, if the pK_a of analytes is several units above the pH of the BGE, the analyte migration is largely based on heteroconjugation [176], which is the conjugation of different species e.g. a cation acid with the anion of the electrolyte.

HAc, which is used as electrolyte in this study, is a weak electrolyte which does not dissociate completely even in purely aqueous media [142]. It is sometimes classified as an amphiprotic protogenic solvent [172]. Being a neutral acid, its pK_a strongly shifts upon addition of organic solvents [164, 179]. The pK_a value of HAc, which is 4.8 in water, was determined to be 7.9 in 95 % MeOH, 9.7 in pure MeOH, 11.3 in pure iPrOH, 22.3 in pure ACN and 12.6 in pure DMSO [28, 173, 182]. Its degree of dissociation was shown to be reduced e.g. in MeOH/water mixtures [183] and DMSO/water mixtures [164]. Furthermore, HAc can undergo dimerization through hydrogen bond formation in pure nonpolar solvents as ACN, in addition to homoconjugation or heteroconjugation with analyte ions [175]. Even the formation of triple ions is possible in media with low relative permittivities. Dimerization of HAc was also observed in aqueous media at high HAc concentrations [175] and, thus, could also possibly occur in HOCE. Nevertheless, in hydroorganic mixtures of ACN/water, homoconjugation of acetate with HAc is compromised due to the pronounced hydrogen bond donor ability of water [142]. Overall, it can be expected that the ionic strength in hydroorganic HAc BGEs will decrease with increasing organic solvent contents.

4.4. Materials and methods

4.4.1. Chemicals

Dimethyl sulfoxide (≥ 95.5 %), acetonitrile (LC-MS grade), and isopropanol (LC-MS grade) were obtained from Carl Roth (Karlsruhe, Germany). Glacial acetic acid, sodium hydroxide (30 % aq.), methanol (LC-MS grade), L-alanine, L-arginine monohydrochloride, L-asparagine monohydrate, L-cysteine, L-cystine, L-glutamic acid, L-glutamine, glycine, L-isoleucine, L-leucine, L-phenylalanine, L-serine and L-valine were purchased from Merck (Darmstadt, Germany). Ammonia (25 % aq.), L-lysine, L-threonine, L-tryptophan and L-tyrosine were acquired from Sigma-Aldrich (Steinheim, Germany). L-histidine was obtained from Amresco (Solon, OH, USA) and L-proline from Fluka (Steinheim, Germany). DL-aspartic acid was purchased from Serva Feinbiochemica (Heidelberg, Germany). DL-methionine was obtained from EGA-Chemie

(Steinheim, Germany). Hydrochloric acid (analytic grade) was from Fisher Scientific (Loughborough, UK). Ultrapure water was generated via a PureLab Classic water purification system from ELGA LabWater (High Wycombe, UK).

4.4.2. Buffers and working solutions

4.4.2.1. Sample solutions

All proteinogenic amino acids and cystine were prepared in stock solutions of 10 mmol/L. Tyrosine and cystine were dissolved in 0.5 % (v/v) ammonia aq., tryptophan was dissolved in 40 % (v/v) MeOH in water and phenylalanine was dissolved in 30 % (v/v) MeOH in water. All other analytes were dissolved in water. Working solutions were prepared by further dilution with water to a final concentration of 1 mmol/L.

4.4.2.2. Background electrolytes

Hydroorganic BGEs consisted of acetic acid in organic solvent/water (v/v) mixtures. Each BGE contained 13.2 % (v/v of final volume) glacial acetic acid, corresponding to a concentration of 2.3 mol/L in water. The organic solvent was added at different percentages of the final volume by substitution of the respective volume of water (compare Table A5 in the appendix). Effects of non-ideal behavior in partial molar volumes were neglected. DMSO, iPrOH, and ACN were added at percentages of 10 % (v/v), 20 % (v/v) and 30 % (v/v), MeOH in addition at 40 % (v/v) and 50 % (v/v). A completely aqueous BGE was prepared for reference measurements. All BGEs were degassed by ultrasonication for 10 min.

4.4.3. Instrumentation

Measurements were conducted using a Prince 560 capillary electrophoresis system from Prince Technologies (Emmen, The Netherlands). For capacitively-coupled contactless conductivity detection (C^4D), an eDAQ 225 C^4D system with 120 C^4D headstage for capillary electrophoresis from eDAQ Incorporated (Denistone East, NSW, Australia) was applied. Settings for conductivity detection were: 100 Hz sampling speed, signal range of 5 V, frequency 700 kHz, amplitude 80 % with headstage gain on. Fused silica capillaries with 50 µm i.d. were purchased from Polymicro Technologies (Phoenix, AZ, USA).

4.4.4. Methods

4.4.4.1. Capillary preparation

Capillaries were cut to a length of 50 cm (in case of BGEs with 30 % ACN and 50 % MeOH 49.5 cm). The exact position of the flexible C^4D headstage varied slightly. Thus, the effective lengths were measured to be between 33.5 cm and 34.5 cm from the inlet

as stated in the respective figure legends. Before use, all capillaries were flushed with MeOH, 1 mol/L NaOH, 1 mol/L HCl and water at 1 bar for 10 min each, then with BGE at 1 bar for 30 min.

4.4.4.2. Separation of amino acids

Samples were injected hydrodynamically at 100 mbar for 3 s. A separation voltage of 30 kV was applied and the temperature in the instrument was maintained at 25 °C to guarantee similar separation conditions for all measurements. Measurements were stopped after the EOF signal, visible as difference in conductivity between BGE and aqueous sample plug, reached the conductivity detector. Thus, measurement times varied between 10 and 30 min depending on the BGE applied. After each run, the separation capillary was flushed with BGE at 1 bar for 5 min. All 22 analytes were measured separately in triplicate. Blank measurements for current determination were conducted under the same separation conditions without injection.

4.5. Results

4.5.1. Determination of electric current and electroosmotic flow

The influence of organic solvents in the BGE on the electroosmotic flow was investigated with two amphiprotic solvents (MeOH, iPrOH) and two aprotic solvents (ACN, DMSO) added at different percentages (see Section 4.4.2.2). Whenever percentages are stated in the following sections, they refer to percentages by volume.

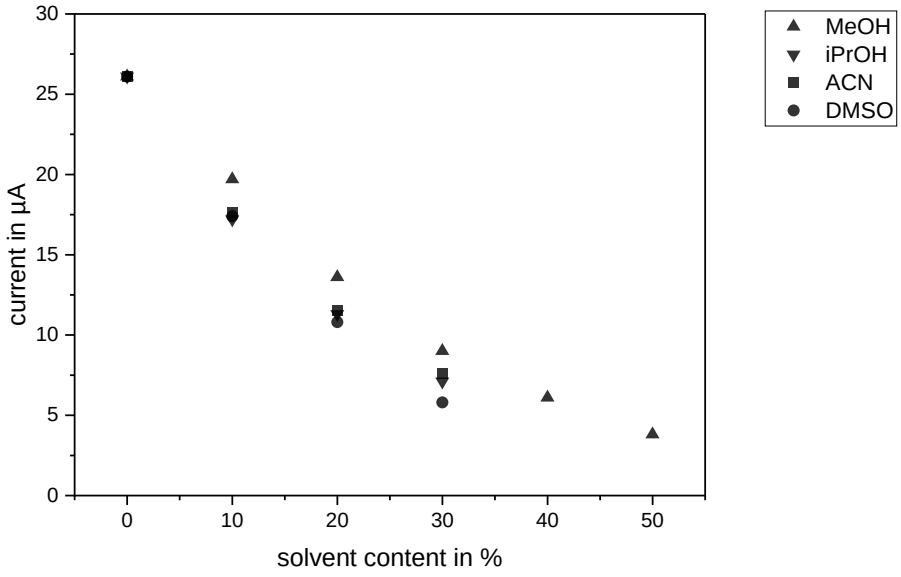

Figure 4.1: Influence of organic solvent content on the electric current measured at a separation voltage of 30 kV. The progression throughout increasing organic solvent contents (percentage in v/v) is shown starting from completely aqueous buffer. Separation conditions: 13.2 % (v/v) glacial acetic acid with varying organic solvent contents according to x-axis as BGE, blank measurements without injection, bare fused silica capillaries. Capillary length during measurements with aqueous BGE: L_{cap} = 50 cm, L_{eff} = 34.4 cm. For capillary lengths of measurements in hydroorganic BGEs, compare Figure 4.3.

To avoid capillary breakage and run failures due to e.g. bubble formation, the minimum current limit was set to 4 µA. This limited the applicability of higher percentages of the organic solvents to 30 %, except for MeOH, where up to 50 % could be used. The dependence of the electric current on the content of each solvent is shown in Figure 4.1. The current remained stable throughout the measurements and was determined in blank measurements to avoid disturbances from the sample plug.

Figure 4.1 shows a decrease of current with increasing amounts of organic solvent in the BGE. This dependence was similar for all four solvents applied in this study. MeOH exhibited the highest currents, allowing an amount of up to 50 % MeOH in the BGE. The current observed in iPrOH and ACN containing BGEs was comparable, the current in DMSO containing BGEs was slightly lower than the former.

The mobility of the EOF for all BGEs was determined from experimental CE data using Equation (4.2) as an average of all measurements with one BGE, i.e. 22 analytes measured separately in triplicate. Thus, the number of measurements taken into account for each EOF determination was n = 66. Calculated values of μ_{EOF} for all BGEs are depicted in Figure 4.2.

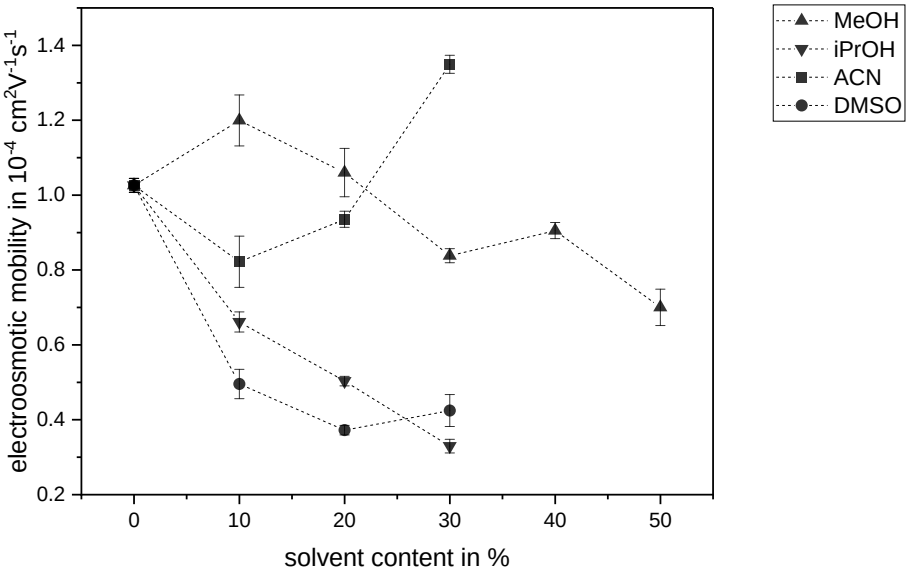

Figure 4.2: μ_{EOF} plotted against organic solvent content of MeOH, iPrOH, ACN or DMSO in BGE, percentage is given in v/v. The standard deviations are indicated as error bars (n = 66) for each data point. Separation conditions: 13.2 % (v/v) glacial acetic acid with varying organic solvent contents according to x-axis as BGE, hydrodynamic injection of 1 mmol/L samples at 100 mbar for 3 s, 30 kV separation voltage, C^4D detection, bare fused silica capillaries. Capillary length during measurements with aqueous BGE: L_{cap} = 50 cm, L_{eff} = 34.4 cm. For capillary lengths of measurements in hydroorganic BGEs, compare Figure 4.3.

The course of the EOF is different for all four solvents we used in our studies. In hydroorganic BGEs with MeOH, an increase of the EOF was observed when going from aqueous BGE to BGE containing 10 % MeOH. With further increase of the MeOH content in the BGE, the EOF showed a steady decrease. The EOF in BGEs with iPrOH

showed a steady, strong decrease with increasing iPrOH content. In BGEs with ACN as organic solvent, the EOF progression was observed to be reversed to the values obtained in BGEs with MeOH: in BGEs containing 10 % ACN, the determined EOF was lower than in aqueous BGE, but increased with further increase of the ACN content. When switching from aqueous BGE to the BGE with 10 % DMSO, a strong decrease of the EOF was observed. The EOF remained stable upon further increase of the DMSO content.

Mostly, the precision for μ_{EOF} was below 7 %, often below 5 %. However, in some cases, higher RSD values up to 10 % were observed. In some cases, μ_{EOF} shifted throughout the measurement series (due to t_{EOF} shifts of up to 5 min, e.g. in BGEs with 30 % DMSO), in other cases μ_{EOF} showed comparatively strong variations, but without a distinct trend (due to t_{EOF} variations of up to 4 min, e.g. in BGEs with 50 % MeOH). The variations do not seem to correlate with the solvent properties given in Table 1. It is assumed that longer conditioning can reduce the fluctuations of μ_{EOF} and improve RSD values by reducing hysteresis effects. Effects from ion depletion or pH changes in the BGE can be excluded as major source of variation as the inlet and outlet vial contained 3 mL of BGE each and BGE was renewed every 22 measurements. The 22nd measurement with old BGE and the 23rd measurement with fresh BGE did not exhibit a difference in t_{EOF}. We tested, if the sample composition caused changes in the EOF, as tyrosine and cystine solutions contained ammonia to dissolve the analytes. No influences of the sample composition on the EOF were observed.

4.5.2. Determination of electrophoretic mobilities of amino acids

To investigate the influence of partially organic BGEs on the effective electrophoretic mobilities of amino acids, all proteinogenic amino acids and cystine (the oxidation product of cysteine) were measured in the different BGEs in triplicate. Values for μ_{eff} were calculated using Equation (4.6). To simplify the interpretation of the results, the 22 analytes were categorized into four groups: basic analytes (lysine, arginine and histidine), acidic analytes (glutamic acid and aspartic acid), nonpolar analytes (alanine, valine, methionine, leucine, isoleucine, proline, tryptophan and phenylalanine) and polar analytes (tyrosine, threonine, glutamine, glycine, serine, asparagine, cysteine and cystine). As all analytes of one category showed similar trends during the measurements, one analyte of each group is chosen to show the dependence of μ_{eff} on the BGE composition exemplarily. To cover the wide pI range of the amino acids, the amino acid with the highest and lowest pI, arginine (Arg, pI 10.76) and aspartic acid (Asp, pI 2.85), are chosen to represent the basic and acidic amino acids, respectively. Phenylalanine

(Phe) represents the nonpolar analytes and serine (Ser) is chosen as a representative polar amino acid, both having a medium pI in the amino acid range (Phe 5.84, Ser 5.68). The dependence of the effective electrophoretic mobilities of the MeOH content in the BGE is shown in Figure 4.3A. A decrease of μ_{eff} with increasing MeOH content was observed for all analytes. For basic analytes, which have a higher effective electrophoretic mobility in cationic separations, the decrease of μ_{eff} was most pronounced, followed by the decrease of μ_{eff} of polar analytes, while the decrease μ_{eff} of nonpolar and acidic analytes was less pronounced. The effective electrophoretic mobilities in BGE containing 50 % MeOH were reduced by 44 % for Arg, 27 % for Ser, 19 % for Phe and 17 % for Asp compared to the μ_{eff} values determined in a purely aqueous BGE. The values for μ_{eff} seemed to remain almost constant for MeOH contents of 40-50 % MeOH in the BGE and did not decrease further with further increase of MeOH content. For polar, nonpolar and acidic analytes, even a slight increase of μ_{eff} from 40 % to 50 % MeOH content was observed.

In BGEs containing iPrOH, the effective electrophoretic mobilities decreased strongly and steadily with increasing iPrOH content, as is shown in Figure 4.3B. The differences in the changes of μ_{eff} between the differently categorized analytes were not as pronounced as in MeOH containing BGEs. μ_{eff} of basic and polar analytes seemed to be slightly more affected than μ_{eff} of nonpolar and acidic analytes. In comparison to the values obtained from measurements in aqueous BGE, μ_{eff} values in BGEs with 30 % iPrOH were reduced by about 53 % for all analytes.

The course of μ_{eff} for chosen analytes in BGEs with increasing contents of ACN is depicted in Figure 4.3C. Upon increasing the content of aprotic ACN in the BGE, the effective electrophoretic mobilities of basic and polar analytes were observed to be reduced, although far less pronounced than upon increasing MeOH contents. The μ_{eff} values obtained in BGEs with 30 % ACN were reduced by 17 % for Arg and 8 % for Ser compared to the μ_{eff} values from measurements in aqueous BGE. For nonpolar and acidic analytes, the effective electrophoretic mobilities were scarcely affected by an increasing ACN content. The reduction of effective electrophoretic mobilities was either very low (below 5 %), or the effective electrophoretic mobilities even exhibited a slight increase, as e.g. by 3 % for Phe or 2 % by Asp, compared to the values determined in aqueous BGE.

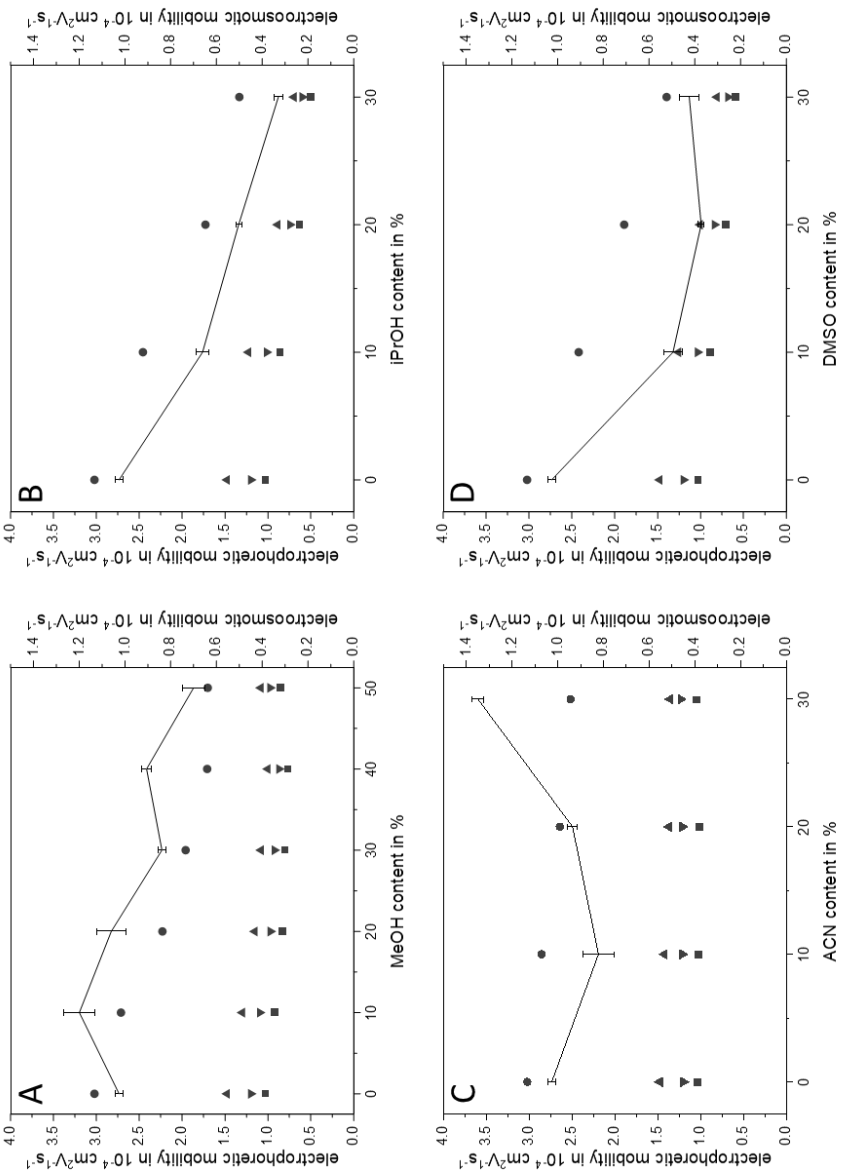

Figure 4.3: Dependence of calculated effective electrophoretic mobilities of Arg (●), Ser (▲), Phe (▼) and Asp (■) on increasing organic solvent content (v/v) in the BGE. Relative standard deviations were below 4 %, in most cases below 1 % (n = 3, compare Tables A 6-10 in the appendix), and are not indicated for reasons of clarity. For reference, the respective calculated μ_{EOF} is shown (black line, right y-axis) with standard deviation given as error bars (n = 66). Separation conditions and capillary lengths of measurements with aqueous BGE as stated in Figure 4.2. (A) BGEs with MeOH, capillary lengths: L_{cap} = 50.0 cm, L_{eff} = 34.5 cm (except for 50 % MeOH: L_{cap} = 49.5 cm, L_{eff} = 34.0 cm). (B) BGEs with iPrOH, capillary lengths: L_{cap} = 50.0 cm, L_{eff} = 34.4 cm. (C) BGEs with ACN, capillary lengths: 10 % ACN L_{cap} = 50.0 cm, L_{eff} = 34.4 cm; 20 % ACN L_{cap} = 50.0 cm, L_{eff} = 33.5 cm; 30 % ACN L_{cap} = 49.5 cm, L_{eff} = 34.0 cm. (D) BGEs with DMSO, capillary lengths: 10 % DMSO L_{cap} = 50.0 cm, L_{eff} = 34.4 cm; 20 % DMSO L_{cap} = 50.0 cm, L_{eff} = 33.5 cm; 30 % DMSO L_{cap} = 50.0 cm, L_{eff} = 34.4 cm.

The course of the effective electrophoretic mobilities in Figure 4.3D shows a steady decrease for all analytes with increasing contents of protophilic aprotic DMSO in the BGE. This decrease was more pronounced than in BGEs containing MeOH and comparable to the mobility reduction which was observed in BGEs containing iPrOH. The mobility reduction observed was strongest for basic analytes, μ_{eff} was reduced by 54 % for Arg in a BGE with 30 % DMSO compared to μ_{eff} in aqueous BGE. The effects of increasing DMSO content on the effective electrophoretic mobilities of polar, nonpolar and acidic analytes were comparable. μ_{eff} values of Ser, Phe and Asp were reduced by 45 %, 43 % and 43 %, respectively, compared to the values obtained in measurements with aqueous BGE.

4.6. Discussion

In an attempt to understand the influences of different organic solvents and their varying contents on current, EOF and effective electrophoretic mobilities in CE separations, the following sections discuss the influences of the parameters given in Table 4.1 and their effects in hydroorganic mixtures separately. An explanation for the observed dependencies is approached based on the interaction of the different parameters and their effects. Most work on the influence of hydroorganic BGEs on electrophoretic separations was accomplished for MeOH and ACN among the solvents tested here. In the following sections, the influence of organic solvents on the electric current, EOF and effective electrophoretic mobilities is discussed starting with the amphiprotic solvents. The discussion of the course of the current with increasing organic solvent contents is compiled as it was observed to be comparable for all applied solvents.

4.6.1. Influence of hydroorganic background electrolytes on electric current

The magnitude of the electric current gives first hints on the changes in the physicochemical characteristics of the different hydroorganic BGEs and helps to understand its impact on the EOF as the conductivity is determined by the effective electrophoretic mobility of the ions involved. The BGEs contained only monovalent ions (acetate, H^+ and OH^-). Thus, the current was influenced by viscosity, ionic strength and relative permittivity, just like the zeta-potential of the capillary surface and the EOF, see Equation (4.1). With regard to electrolyte ions, the electric current in CE is influenced mainly by two properties of the BGE with solvent added: viscosity and relative permittivity. In terms of the impact of H^+ and OH^- in the buffer, autoprotolysis of the solvent and the ability to form hydrogen bonds (EZE) have to be considered. Proton transfer via EZE is e.g. not possible in DMSO, as was shown by Kler at al. [34] who deliberately used DMSO as solvent for ITP electrolytes to overcome the EZE. A

decreased current is expected if 1) the relative permittivity is decreased, reducing the degree of dissociation of the electrolyte, 2) the viscosity is increased leading to pronounced hydrodynamic friction, 3) autoprotolysis is reduced and, thus, the number of charge carriers in solution, and/or 4) the EZE is reduced or inhibited due to reduced hydrogen bond formation.

The progression of the current upon increasing organic solvent contents is comparable for all solvents used in this work (see Figure 4.1). Thus, similar effects influenced the current. The course of the parameters relative permittivity, viscosity and autoprotolysis with increasing organic solvent content varies for the different solvents used, therefore, these parameters seem to have less correlation with the current course. Instead, the main effect on current probably was a result of the dilution of water by organic solvent, reducing the high conductivity of H^+ and OH^- by suppressing the formation of hydrogen bonds and the EZE. Additionally, the aqueous buffer in this work was made of 2.3 mol/L HAc with pH 2.2. At this high concentration, HAc is not completely dissociated in aqueous media as it is a weak acid. Upon addition of organic solvents, the degree of dissociation will be reduced further due to the changing pK_a of HAc, as it is increased by approx. 1 unit in hydroorganic mixtures with 50 % MeOH [183-184] or 30 % ACN [179] and by approx. 0.5 units in hydroorganic mixtures with 30 % DMSO [164]. As a result, the number of charge carriers in the BGE was reduced and the current decreased. The current course observed in this work goes well along with the reduction of HAc conductance under addition of MeOH which was observed by Shedlovsky and Kay [183].

4.6.2. Influence of methanol in the background electrolyte

4.6.2.1. Electroosmotic flow

An increase of the EOF was observed in BGE with 10 % of MeOH compared to a completely aqueous BGE, followed by a decrease upon addition of higher amounts of MeOH (Figure 4.2). The relative permittivity of binary mixtures of water and MeOH decreases with an increasing amount of organic solvent [8, 150, 183, 185]. Although the dynamic viscosity of pure MeOH is clearly lower than that of water, the viscosities of MeOH/water mixtures increase until reaching a maximum between 40 % and 50 % MeOH content [8, 150-151, 183, 186]. According to Equation (4.1), both a reduced relative permittivity and an increased viscosity will lead to a decrease of the EOF as observed in this study (see Figure 4.2) at higher percentages (> 10 %).

According to Brønsted's theory, MeOH can be categorized as an amphiprotic solvent with high basicity and acidity [28]. Furthermore, MeOH exhibits medium stabilization of anions and very high stabilization of cations [173] and has a slightly higher autoprotolysis

constant than water (compare Table 4.1). Determinations of the autoprotolysis constants in MeOH/water mixtures showed only small changes in the autoprotolysis which was comparable to water up to MeOH contents of 50-60 %, including the range studied here [167, 187]. Thus, this parameter is expected not to induce changes of the EOF. As an amphiprotic solvent, MeOH is able to form hydrogen bonds. The addition of MeOH to water was observed to strengthen the hydrogen bonding network in water [188], supporting the stabilization of ions and keeping the high mobility of H^+ and OH^- in CE. In order to explain the increase in EOF observed when adding 10 % MeOH to the aqueous BGE, pH and pK_a changes of HAc and silanol groups at the capillary surface have to be discussed.

In this study, the aqueous HAc BGE had a pH of 2.2, thus, the dissociation of silanol groups was very low, resulting in a low EOF (see Figure 4.2). As described in the introduction, organic solvents change the thermodynamic pK_a values. This holds true for analytes, electrolytes and the capillary's silanol surface. We presume that the effect on the silanol surface groups was rather small with silanol being a strong acid and with the low EOF in our study. The addition of MeOH to the BGE slightly increased the pK_a of HAc used in the BGE (its pK_a is increased by 1 unit upon addition of 50 % MeOH [183-184]) resulting in slightly increased thermodynamic pH values in MeOH-containing BGEs. The higher thermodynamic pH probably shifted the dissociation constants of the surface silanol groups towards a higher charge resulting in a higher EOF, as observed in this study (Figure 4.2).

The course of the dependence of current and EOF on the MeOH content observed in this study is different (see Figure 4.1 and Figure 4.2). This observation is not consistent with the measured current, thus, some factors influenced the EOF without influencing the current, e.g. the behavior of silanol groups. At low MeOH contents, strong deviations from the behavior of ideal mixtures, e.g. concerning the partial molar volume (compare [189-190]) were observed. The water structure is reinforced upon adding organic solvent up to 10 %, which augments some of water's intrinsic properties such as its inter-molecular orientation based on hydrogen bonding [191]. EOF increasing parameters such as a slightly increased thermodynamic pH and reinforced hydrogen bonding are assumed to cause the increase of EOF observed at low MeOH concentrations, whereas the changes of viscosity and relative permittivity are still low and their influence seems negligible. At higher MeOH contents, however, the EOF pronouncing effects are counteracted by decreased relative permittivity and increased dynamic viscosity of the BGE, causing a reduction of EOF with increasing solvent content (as visible in Figure 4.2).

Contrary to our results, other studies on EOF in hydroorganic BGEs showed a steady decrease of EOF upon MeOH addition, however, at high pH values of the BGE (between 9 and 12) [8, 151]. Without additional ionic species, MeOH/water mixtures have a minimum of μ_{EOF} at approx. 40 % MeOH [150]. At high pH, silanol groups are fully dissociated, resulting in a relatively high EOF. The impact of the organic solvent on the electrical double layer at the capillary surface becomes more pronounced, most likely also due to the influence of the ionic strength on the zeta-potential. The absolute increase of EOF we observed at low MeOH concentrations in the BGE is rather small compared to e.g. the increase of EOF with increasing pH of the BGE (compare e.g. [192], showing an increase of nearly factor 10 at pH 7-8 compared to pH 2). Furthermore, it is probably difficult to obtain stable EOF and/or zeta-potential behavior at the low pH of BGE used in our work, which has to be considered when discussing the small EOF increase observed.

4.6.2.2. Amino acids

Contrary to the EOF values determined here, the effective electrophoretic mobilities of all amino acids decreased with increasing MeOH contents compared to the aqueous BGE (as visible in Figure 4.3A). The decrease of μ_{eff} values of basic analytes upon increasing MeOH content in the BGE was stronger than for nonpolar, polar and acidic analytes (which have the lowest μ_{eff} under cationic separation conditions due to a lower degree of protonation). This might be caused by changes of the thermodynamic pH of the BGE upon increasing MeOH contents: the degree of protonation is reduced as the thermodynamic pH of the BGE rises. This effect is more pronounced for basic analytes which are expected to be completely protonated at pH 2.2 in purely aqueous BGE. Figure 4.3A depicts the dependence of μ_{eff} of the chosen analytes on the MeOH content in the BGE. The effective electrophoretic mobilities showed strong changes upon MeOH contents of 10-40 %, as expected from combined effects of decreasing relative permittivity, increasing pK_a values (affecting both HAc and analytes) and increasing viscosity. The small changes of μ_{eff} observed at 40-50 % MeOH may reveal a minimum due to the viscosity maximum observed in MeOH/water mixtures at around 40-50 % MeOH [8, 151, 183, 186]. This could probably counteract the effect of decreasing relative permittivity and explain the observed plateau in μ_{eff} at 40 % and 50 % MeOH. At higher MeOH contents, the decreasing viscosity could possibly induce an increase in μ_{eff}. The calculated effective electrophoretic mobilities portend no changes in the migration order of the amino acids and, thus, no major selectivity changes, indicating that the overall separation mechanism was not changed throughout increasing MeOH contents in the BGE.

4.6.3. Influence of isopropanol in the background electrolyte

4.6.3.1. Electroosmotic flow

iPrOH is the second amphiprotic solvent which was investigated here. Due to its low ε/η ratio (Table 4.1), iPrOH is used less often than the other solvents as organic modifier in CE applications (e.g. [193-195]) and data on iPrOH/water mixtures is limited. Of all applied solvents, pure iPrOH has the highest dynamic viscosity and the lowest relative permittivity. Its autoprotolysis constant is relatively high (see Table 4.1). In mixtures with water, the relative permittivity decreases steadily with increasing iPrOH content, comparably to addition of MeOH [8, 170, 185], while the viscosity is strongly increased to a maximum at 50-60 % iPrOH [8, 151, 169]. The increase in viscosity is stronger than for addition of MeOH. From both parameters, a reduction of the EOF was expected and observed in our measurements, as visible in Figure 4.2. Furthermore, autoprotolysis of iPrOH is less than of water or MeOH resulting in lower amounts of charge carriers in the BGE. The autoprotolysis decreases almost linearly with increasing iPrOH contents [167, 187] and was an additional cause for the reduction of the EOF observed in Figure 4.2. In contrast to MeOH, the dependencies of both current and EOF on increasing iPrOH contents in the BGE corresponded well to each other. Overall, the decrease of the electric current with increasing amounts of iPrOH and reduction in EOF were stronger than upon addition of MeOH (compare Figure 4.1 and Figure 4.2), which can probably be assigned to the stronger increase of viscosity, stronger decrease of relative permittivity and the reduction of autoprotolysis in iPrOH/water mixtures. Other investigations of the EOF in iPrOH containing BGEs showed the same trend for EOF reduction [8, 151], indicating that in hydroorganic BGEs with iPrOH the parameters relative permittivity, viscosity and autoprotolysis outweigh the changes of thermodynamic pH and the silanol pK_a values.

4.6.3.2. Amino acids

Increasing iPrOH contents resulted in a remarkable reduction of μ_{eff} for all categories of analytes compared to MeOH (see Figure 4.3B). At 30 % iPrOH content, the calculated mobilities were 50-60 % lower compared to the mobilities determined in aqueous BGE. Changes of the thermodynamic pH of the BGE due to increasing iPrOH contents are probably more pronounced for arginine, reducing the degree of protonation and inducing a stronger effect on μ_{eff}. The decreasing relative permittivity and increasing viscosity with increasing iPrOH contents seem to act synergistically on the reduction of effective electrophoretic mobilities. In addition, increasing pK_a values of analytes and HAc probably shifted the pI of amino acids towards higher values. Thus, the degree of

protonation is expected to be reduced, resulting in lower μ_{eff}, coinciding with our results. The relative permittivity of iPrOH is well below 30, the value which is considered a threshold value for ion pair formation. In a solvent with a relative permittivity below 30, mainly ion pair formation takes place [156, 191], thus, less free ions are available as charge carriers. Due to the low content of iPrOH in the investigated BGEs, the medium autoprotolysis and the ability to form hydrogen bonds, this ion pair formation effect might not preponderate. Furthermore, the relative permittivity in iPrOH/mixtures is above 30 for low iPrOH contents: in mixtures with 20 % iPrOH, the relative permittivity is approx. 67, in mixtures with 30 % iPrOH, the value is still above 55 and the relative permittivity comes below the threshold value of 30 in mixtures with iPrOH contents above 70 % [170]. Therefore, ion pair formation was not expected to cause the reductions of μ_{eff} observed in our measurements. As for MeOH-containing BGEs, changes of the migration order with increasing iPrOH amounts were not observed from the calculated effective electrophoretic mobilities.

4.6.4. Influence of acetonitrile in the background electrolyte

4.6.4.1. Electroosmotic flow

Acetonitrile is an aprotic solvent with intermediate relative permittivity but low acidity and basicity [28]. The relative permittivity of pure ACN is comparable to that of MeOH which holds also true for ACN/water mixtures [8, 196]. This would decrease the EOF as observed for low contents of ACN (Figure 4.2). ACN has the lowest dynamic viscosity of all solvents applied. It was shown that the viscosity in ACN/mixtures hardly decreases for concentrations of up to 20 % ACN, then decreases upon higher ACN contents [8, 151]. This explains the increasing EOF observed for the BGE with 30 % ACN content compared to the purely aqueous BGE. Furthermore, ACN has the highest autoprotolysis constant of all applied solvents (compare Table 4.1) which increases linearly in ACN/water mixtures [167, 187, 197]. Its ability to create hydrogen bonds is low and even the addition of small amounts of ACN weakens the hydrogen bonding network of water [188]. Being aprotic, solvation of ions by ACN strongly differs from hydration. Together with its low permittivity, especially the stabilization of anions is decreased, strong changes of the pK_a values of anions were observed: in case of HAc an increase of the pK_a value by 1 unit in ACN/water mixtures with 30 % ACN was determined [179]. The relative permittivity of hydroorganic mixtures with 30 % ACN is around 70 [196], indicating a low probability for ion association and ion pair formation in our measurements. We expect that the solvation shell in ACN/water mixtures is smaller than in pure water, which is justified given the higher selectivity for structural isomers

observed in NACE with ACN/HAc mixtures [178]. The charge of electrolyte ions and the surface charge of the capillary are less effectively shielded, the ionic strength will decrease and the zeta-potential will increase due to a steeper slope of the potential drop in the electrical double layer. This explains the increase of the EOF observed with increasing ACN contents above 10 %.

The EOF course (Figure 4.2) for contents higher than 10 % is contrary to the dependence of the current on the ACN content (Figure 4.1), leading to the assumption that distinct parameters influenced current and EOF to different extents. Interestingly, opposite trends for the EOF were observed in MeOH, see Figure 4.2.

To summarize, at ACN contents of 10-20 % in the BGE, the reduced relative permittivity and reduced hydrogen bond formation caused a decrease of the EOF compared to the purely aqueous BGE. At ACN contents above 20 %, the reduction of viscosity and increased zeta-potential promoted an increased EOF. Furthermore, at these concentrations smaller solvation shells could preponderate for an increased EOF as hydrodynamic and dielectric friction were reduced. Our findings are contrary to EOF investigations in ACN/water mixtures in the literature, where a steady decline of the EOF was observed in ACN/water BGEs, however, with high pH values [8, 151].

4.6.4.2. Amino acids

Upon increasing ACN contents, the mobilities of basic analytes slightly decreased while they remained stable for polar, nonpolar and acidic analytes, as visible in Figure 4.3C. The decreasing viscosity should result in increased mobility due to less hindrance in migration. This is, however, counteracted by the decreasing relative permittivity, which has a mobility reducing effect. Furthermore, cations are not well stabilized in ACN [173]. Ion association and ion pair formation can take place in ACN/water mixtures with ACN contents of at least 35 % [198-199]. This changes the separation conditions of analytes remarkably, as the separation is based both on migration of the free protonated base in equilibrium with an ion pair and on the migration of possible charged heteroconjugates. The ACN contents in the BGEs used were 10-30 % and the relative permittivity in hydroorganic mixtures with 30 % ACN is around 70 [196], thus, a reduction of μ_{eff} based on ion association or ion pair formation was not expected in our measurements.

The decreasing μ_{eff} with increasing ACN contents we observed for basic and polar analytes (see Arg in Figure 4.3C) were probably caused by the decreasing relative permittivity, lower ion stabilization and reduced autoprotolysis. For the other analytes, these mobility reducing effects seemed to be counteracted by the smaller solvation shells we expect in ACN and the decreasing viscosity upon increasing ACN contents. Furthermore, as the amino acids were separated as cations, they can be considered as

basic analytes. In some experiments, pK_a values of basic analytes were affected differently compared to these of neutral and acidic analytes: Espinosa et al. [180] observed decreasing pK_a values of bases with increasing ACN content. This could possibly counteract the concurrent effects from the thermodynamic pH of the BGE and result in only low to no reduction of effective electrophoretic mobilities as observed for polar, nonpolar and acidic analytes in this study. Only minor selectivity changes were visible from the calculated effective electrophoretic mobilities, reinforcing the assumption that ion association and ion pair formation were probably not present at ACN contents of 10-30 %.

4.6.5. Influence of dimethyl sulfoxide in the background electrolyte

4.6.5.1. Electroosmotic flow

Comparable to ACN, DMSO is an aprotic solvent, however, with high relative permittivity but low acidity and basicity [28]. For binary mixtures of DMSO/water, the relative permittivity does not change at contents below 50 % DMSO [8, 168] while the viscosity strongly increases. Consequently, the EOF was expected to decrease [8, 165, 200] which was observed in our experiments conducted at contents up to 30 %. The autoprotolysis constant of pure DMSO is comparable to that of ACN (Table 4.1) and increases linearly with increasing DMSO amounts in hydroorganic mixtures [167, 197]. Low autoprotolysis reduces the ionic strength and, thus, the EOF was expected to decrease. This was observed when switching from purely aqueous BGE to DMSO-containing BGE, as visible in Figure 4.2.

The small dependence of the relative permittivity on the DMSO content in DMSO/water mixtures up to 50 % DMSO will have a negligible influence on the EOF. The zeta-potential of the Stern layer at the capillary surface in DMSO/water mixtures was observed to increase for DMSO contents of up to 20 % [8]. The ability of DMSO to stabilize cations is comparable to MeOH [173], probably promoting the stability of the fluid layer attached to the capillary surface. Possibly, the resulting competition between these effects led to the small changes of the EOF in BGEs containing 10-30 % DMSO, visible in Figure 4.2.

4.6.5.2. Amino acids

For DMSO, a reduction of μ_{eff} was observed for all analyte categories, as depicted in Figure 4.3D. The reduction was stronger than observed in MeOH-containing BGEs and was comparable to that observed in iPrOH-containing buffers. Contrary to MeOH/water and iPrOH/water mixtures, the relative permittivity in DMSO/water mixtures remains constant up to concentrations of 40 % DMSO [8]. Thus, the reduction of the effective electrophoretic mobility observed was largely due to the increasing viscosity.

In contrary to ACN, DMSO can act as proton acceptor in hydrogen bond formation, as it is a protophilic aprotic solvent and it has a strong ability to stabilize cations but the stabilization of anions is low [173]. This could result in remarkable changes of the thermodynamic pH in the BGE, as the stabilization of acetate ions is affected. By this, the degree of protonation of the analytes is reduced and, subsequently, μ_{eff} is reduced as well, coinciding with our results. In addition, pI values of anion acids are lowered, however, only small selectivity changes were observed. At higher pH values than chosen in this study, this effect may induce selectivity changes.

4.7. Conclusion

The influence of increasing contents of methanol, isopropanol, acetonitrile or dimethyl sulfoxide in the background electrolyte on the electroosmotic flow and the effective electrophoretic mobilities of amino acids was investigated. From the data presented here and the discussion based on these data, it is clear that the complex interplay of solvent properties such as relative permittivity, viscosity, ability to form hydrogen bonds, induction of pK_a changes and ion pair formation currently prevents a prediction of solvent effects in capillary electrophoresis using hydroorganic mixtures. Whereas the electric current showed a very similar dependence for all organic solvents applied in this study, this was not the case for the electroosmotic flow, where a different dependence on the content of the organic solvents in the BGE was observed. However, a general trend to a decrease of the EOF was visible except for acetonitrile. Obviously, the complex interplay of the solvent properties on the BGE (including thermodynamic pH, ionic strength, hydrogen bonding network, relative permittivity and viscosity) affect the surface charge of the capillary surface and the electrical double layer attached to it. From our results and physicochemical data of hydroorganic mixtures, we hypothesize that for MeOH, the reinforced hydrogen bonding and increased thermodynamic pH are dominating the dependence at small content, while the decreasing relative permittivity and increasing viscosity counteract these effects at higher contents. For acetonitrile, we hypothesize that mainly the decreasing viscosity at contents above 20 % ACN and the very strong change in pK_a values of HAc are the major factors governing the difference to the other solvents. For iPrOH, the EOF dependence on the organic solvent content seems to be governed mainly by the strongly increasing viscosity and the reduction of autoprotolysis. In DMSO-containing BGEs, the same effects as for iPrOH are present but they are probably strongly counteracted by the increasing zeta-potential at the capillary surface, thus, we observed only small changes of the EOF for 10-30 % DMSO in the BGE.

The effective electrophoretic mobilities of amino acids showed very similar trends for all solvents, except acetonitrile, where the changes were very small. Here, counteracting

effects are likely, with decreasing analyte pK_a values, smaller solvation shells and decreasing viscosity counteracting the decreasing relative permittivity and reduced autoprotolysis. Interestingly, the dependence of μ_{eff} on the solvent content was nearly identical for DMSO and iPrOH, despite the strong difference in physicochemical properties (see Table 1). This demonstrates that it is not possible to use these physicochemical data to predict changes in effective electrophoretic mobilities and, thus, optimize selectivity and resolution or analysis time in hydroorganic systems. Due to the interaction of parameters of both solvents in HOCE, these predictions are even more difficult than in NACE, where some basic principles as e.g. the Walden's rule for limiting conditions can be applied if the solvent parameters are known [142].

The effective electrophoretic and electroosmotic mobilities obtained from the measurements in this work will form the base for the simulation of CE separations in hydroorganic BGEs. Simulations of HOCE separations are a promising tool to enhance the understanding of the influences and interactions of the varying solvent parameters.

5. Comparison of different proteolytic enzymes for peptide analysis via capillary electrophoresis-mass spectrometry

5.1. Abstract

Trypsin is considered the “gold standard” in bottom-up protein analysis although the interest in other enzymes for bottom-up and middle-down approaches is on the rise. Especially in protein analysis by capillary electrophoresis-mass spectrometry, where the separation is based on charge differences between peptides, the application of other proteases could improve resolution and, thus, extend the information obtainable from measurements of protein digests. In this work, bovine serum albumin was digested with three other endoproteases, namely Glu-C, Lys-C and Lys-N. Capillary electrophoresis-mass spectrometry measurements of the peptides from these digests were compared to measurements of tryptic digests with regard to sequence coverage, peptide charge states, missed cleavages and migration time windows. The results show that Lys-C and Glu-C are interesting alternatives to the commonly used trypsin, as they generate a lower number of peptides while differing more strongly in the number of basic side chains.

5.2. Introduction

5.2.1. Motivation

Trypsin is still the most commonly applied endoprotease in bottom-up protein analysis. Nevertheless, other endoproteases are of interest for capillary electrophoresis-mass spectrometry (CE-MS) analysis as the peptides from these digests could provide a larger range of effective electrophoretic mobilities due to larger differences in charge numbers. In this work, bovine serum albumin (BSA) as model protein was digested with four different enzymes, i.e. trypsin, Glu-C, Lys-C and Lys-N. The CE-MS measurements of these digests was envisaged to be conducted on two neutrally coated capillaries: an acrylamide based LN-coated capillary prepared in-house and a commercially available polyvinyl alcohol (PVA)-coated capillary. We investigated, if a digestion with enzymes other than trypsin has positive influences on parameters such as separation efficiency, resolution and, thus, peptide identification due to different migration time windows spanned between the fastest and slowest peptide detected. The question is whether CE-MS separations could benefit from the use of other enzymes generating larger peptides with a broader range of charge numbers.

5.2.2. State of the art of CE-MS analysis of enzymatically digested proteins

Proteins can be characterized by two different approaches: top-down with the analysis of intact proteins and bottom-up, the latter focusing on the analysis of peptides after enzymatic or chemical digestion (i.e. peptides of ca. 300-5000 Da). Bottom-up

approaches are more commonly applied and are used to generate peptide mass fingerprints to identify and characterize proteins or for *de novo* sequencing to obtain the amino acid sequence by tandem mass spectrometry (MS/MS) [12, 201]. In the past years, a so-called middle-down approach gained interest, where the generated peptides are larger (2000-20000 Da) than in bottom-up approaches so that advantages of both top-down and bottom-up strategies can be combined [12, 202]. Although liquid chromatography-mass spectrometry (LC-MS) is the most commonly applied separation technique [12, 202], CE-MS is on the rise and protein analysis has always been one of the main interests in CE-MS method developments [203]. It is important to notice that LC-MS and CE-MS are not competitive but rather complementary approaches [12, 203-204].

The interest in CE for peptide analysis is mainly based on the possibility to separate peptides with similar masses due to charge-specific trends. The migration time can be used as an additional information for peptide identification [205]. CE-MS of peptides has three interesting features: 1) the migration time provides information on the charge, 2) peptides strongly differing in polarity or with extreme pI values can be analyzed, which may be difficult to achieve with classical reversed-phase LC and 3) the separation of charge variants such as those coming from deamidation is possible [206].

Erny and Cifuentes [207] introduced a 2D mapping approach of CE-MS data for detection and characterization of proteins based on the connection of electrophoretic parameters obtained from the electropherogram (migration time, peak symmetry and peak variance) with parameters provided by MS (*m/z*, peak area). Peptides from tryptic digests of cytochrome c were grouped according to their charge states. Thus, no high resolution mass analyzer was needed for the analyses due to the additional information from this connection. The 2D maps obtained revealed fingerprint-like data depictions, with enough selectivity to distinguish cytochrome c of different animal species while strongly reducing the amount of data and enhancing their clarity [207]. Impressive results were presented e.g. by Gahoual et al. [83-84], who obtained 100 % sequence coverage for tryptically digested monoclonal antibodies from one single injection using CE with transient isotachophoresis coupled to MS/MS via a sheathless electrospray ionization (ESI) interface. Similarly, CE with a sheathless ESI interface to MS/MS was shown to be useful e.g. for the identification of post-translational modifications and the deamidation of asparagine [208].

However, the most common interface uses a sheath liquid-assisted ESI. It is commercially available and enables easy and robust online coupling of CE and MS. The CE separation in bottom-up protein analyses mainly uses a low pH background

electrolyte (BGE) and, thus, cationic peptide separations. Consequently, the positive ionization mode is most commonly used for MS determination of peptides. Mainly formic acid or acetic acid were applied as BGE electrolytes at low pH [204] as they are MS-compatible and have suitable pK_a values. At low pH, the dissociation of silanol groups is low, thus, the adsorption of peptides to the wall of fused silica capillaries is reduced. Another possibility to prevent peptide adsorption on the capillary walls is the use of neutral or cationic capillary coatings, either covalently bound or statically adsorbed to ensure the compatibility with MS detection. Very often, low pH of BGE and the use of coated capillaries are combined for optimal separation performance [68, 201].

5.2.3. Enzymatic digestion of proteins

Trypsin is the proteolytic enzyme of choice as it cleaves the protein at the basic amino acids lysine and arginine, generating basic residues for protonation on all peptides and, generally, peptides with low charge numbers [201, 203-204, 209]. Thus, peptides from tryptic digests are well-suited for analysis with reversed-phase LC-MS making it the “gold standard” in bottom-up protein analysis [12]. Nevertheless, the interest in other enzymes for digestion of proteins is growing as peptides from these digests could provide other information on the protein sequence than tryptic peptides. Switzar et al. [12] gave an overview on different digestion procedures with enzymes of increasing interest. While trypsin generates peptides of an average length of 14 amino acids with two basic residues on average, other enzymes such as the endoproteinases Lys-C, Lys-N or Glu-C usually generate larger peptides with higher numbers of basic residues possible as they cleave specifically only at one amino acid (i.e. lysine or glutamic acid, respectively) [12, 210]. Digests with these enzymes are sometimes already classified as middle-down approaches as the peptides consist of approx. 20-25 amino acids [202].

All four enzymes used in this work, i.e. trypsin, Glu-C, Lys-C and Lys-N, are endoproteases meaning the cleavage takes place within the protein’s amino acid sequence at specific amino acids. Endoproteases cleave the protein at the peptide bond which is established during protein translation. Thus, by this cleavage, the original amine function and carboxyl function are reestablished. If the amine function of the specific amino acid is reestablished, the cleavage is called N-terminal, while reestablishment of the carboxyl function of the certain amino acid is termed C-terminal cleavage.

Giansanti et al. [210] introduced optimized protocols for enzymatic digestion with different endoproteases with minimal changes to the tryptic digest protocols commonly applied. The digest procedures were optimized for LC-MS analysis and a cumulative sequence coverage of 94 % for BSA from the digests with six different enzymes was obtained. Their work proved that the application of alternative enzymes to trypsin does

not necessarily evoke more laborious digestion procedures but it is even possible to conduct different digests with particular enzymes in parallel. Table 5.1 lists the cleavage sites, the pH ranges in which the respective enzyme is active and the pH values for inactivation as well as the digestion conditions of the four enzymes used in our work. All four endoproteases require the same incubation temperature, similar digestion times and similar ranges of enzyme/protein ratios (w/w). Furthermore, the pH range, in which the four enzymes are active, is comparable.

Trypsin induces cleavage specifically at the C-terminus of Lys and Arg, except when Pro is located C-terminal to Lys or Arg. The cleavage might be missed if an amino acid with an acidic residue (Glu or Asp) is placed next to the susceptible bond. Glu-C cleaves proteins specifically C-terminally to Glu and sometimes Asp. The cleavage at Glu is preferred in ammonium bicarbonate and ammonium acetate buffers, while phosphate buffers induce cleavages at both Glu and Asp. Lys-C cleaves proteins at the C-terminus of Lys, and Lys-N induces specific cleavages at the N-terminus of Lys.

Table 5.1: Digest conditions and specifications as given by the manufacturer of the endoproteases trypsin, Glu-C, Lys-C and Lys-N.

enzyme	**trypsin**	**Glu-C**	**Lys-C**	**Lys-N**
cleavage sites	C-terminal to Lys and Arg	C-terminal to Glu and Asp	C-terminal to Lys	N-terminal to Lys
pH range	7-9	4-9	7-9	7-9
inactivation pH	4, reversible	n.a.	2-3	2-3
protease/substrate ratio (w/w)	1/100-1/20	1/200-1/20	1/100-1/20	1/100-1/20
incubation temperature	37 °C	37 °C	37 °C	37 °C
incubation time	> 1 h	2-18 h	1-18 h	1-18 h

In CE separations, the electrophoretic mobility of analytes is determined by the hydrodynamic radius and the charge of an analyte. The amino acid sequence of a peptide determines the number of possible charges per peptide at a given pH and, thus, influences the electrophoretic mobility: beside charges at the C- or N-terminus, Lys and Arg carry a positive charge under acidic conditions, while Asp and Glu can carry negative charges if the pH is higher than approx. 3. Thus, in most cases low pH separation electrolytes are used to ensure that all peptides have sufficient cationic effective electrophoretic mobilities. As trypsin cleaves at Lys and Arg, peptides from tryptic digestion mainly carry two positive charges at low pH, one at the N-terminus of the

peptide, the other at the side chain of Lys or Arg. Thus, peptides with very similar charge numbers are generated and CE separation will mainly be based on different masses of the peptides. Peptides from digests with Glu-C, Lys-C and Lys-N are likely to show a larger heterogeneity in their charge numbers: peptides from digestion with Glu-C will carry one positive charge at the N-terminus of the peptide plus one positive charge at each Arg and Lys in the sequence. Peptides generated by digestion with Lys-C will carry one positive charge at the side chain of the C-terminal Lys and at the N-terminus. Peptides from Lys-N digestion will carry one positive charge at the N-terminal Lys and, possibly, a second positive charge at the Lys side chain. In both cases, each Arg side chain in the sequence provides additional protonation sites.

Gennaro et al. [211] gave an example for the application of Lys-C for bottom-up protein analysis. The group implemented CE-MS for the identification of signals in CE-UV assays in the Biotech industry. Their method was optimized to reveal mass traces similar to CE-UV profiles which were already in use in industry to show the applicability and advantages of CE-MS measurements for Biotech industry requirements. Brownstein et al. [212] analyzed BSA digested with Lys-N and Lys-C using LC-MS/MS for *de novo* sequencing by collision-induced dissociation fragmentation. As Lys-N and Lys-C cleave proteins specifically at the same position but N- or C-terminally, peptides with similar molecular mass and similar retention times in LC were obtained from the digests. The comparison of measurements of both digest procedures resulted in an improved confidence in peptide identification as similar peptides were detected. Another investigation of Lys-N, Lys-C and Glu-C generated peptides in a *de novo* sequencing application with electron capture dissociation was conducted by Kalli and Håkansson [213], reaching an average sequence coverage of 80-81 % for each digest. The three endoproteases generated medium size proteolytic peptides with multiple charges which proved optimal for *de novo* sequencing. This indicates that these enzymes are better suited for a *de novo* sequencing applications than trypsin. Using CE-MS analysis of glycopeptides and glycoform characterization of recombinant human erythropoietin was facilitated by additional data obtained from digests with Glu-C instead of tryptic digests alone [214].

5.3. Materials and methods

5.3.1. Chemicals

Acetonitrile (LC-MS grade) and isopropanol (LC-MS grade) were purchased from Carl Roth GmbH & Co. KG (Karlsruhe, Germany). Acetic acid (100 % for LC-MS), formic acid (≥ 98-100 %, for LC-MS), methanol (LC-MS grade), water (LC-MS grade) and sodium

hydroxide (30 % aq.) were obtained from Merck (Darmstadt, Germany). Ammonium bicarbonate (≥ 99-101 %), bovine serum albumin and iodoacetamide (≥ 99 %) were acquired from Sigma-Aldrich (Steinheim, Germany). Dithiothreitol (molecular biology grade) was purchased from VWR Chemicals (Fontenay-sous-Bois, France). Glu-C (sequencing grade), Lys-C (sequencing grade), Lys-N (sequencing grade) and modified trypsin (sequencing grade) were obtained from Promega (Mannheim, Germany). Hydrochloric acid (analytical grade) was from Fisher Scientific (Loughborough, UK), RapiGest SF surfactant was acquired from Waters (Milford, MA, USA) and UltraTrol Dynamic Pre-Coat LN® was obtained from Target Discovery (Palo Alto, CA, USA).

5.3.2. Preparation of enzymatic bovine serum albumin digests

Digests were prepared in triplicate for each enzyme solution based on the procedure for tryptic digests used by Pattky and Huhn [215]. All pipetting steps were conducted on ice and mixing was done by vortexing for approx. 2 s. Glu-C, Lys-C and Lys-N were dissolved to a concentration of 10 µg/mL with water. Modified trypsin was dissolved to a final concentration of 10 µg/mL with a 5/14/81 (v/v/v) mixture of 20 mmol/L acetic acid/acetonitrile/water.

8 µL of 10 g/L BSA solution were mixed with 60 µL of 0.1 % RapiGest solution and 5.2 µL of an aqueous dithiothreitol solution (c = 50 mmol/L). The mixture was incubated at 60 °C for 1 h. Then, the reaction tube was covered with aluminum foil, 16 µL of a 50 mmol/L iodoacetamide solution were added and the mixture was incubated at room temperature in darkness for 30 min. 80 µL of the enzyme solution were added and the digest was incubated at 37 °C overnight (18 h). In case of digests with Lys-C and Lys-N 1.7 µL formic acid conc. were added after 18 h to stop the enzymatic reaction. All digests were stored in the freezer at -18 °C until use.

5.3.3. Instrumentation

All measurements were conducted using a 7100 Capillary Electrophoresis from Agilent Technologies (Waldbronn, Germany) coupled to a 6550 iFunnel Q-TOF LC/MS system (Agilent Technologies, Santa Clara, CA, USA) with a 1260 Infinity isocratic pump (Agilent Technologies, Waldbronn, Germany) with 1/100 flow split to deliver a stable sheath liquid flow to the electrospray ion source. A fused silica capillary with 50 µm i.d. for the in-house coating procedure was purchased from Polymicro Technologies (Phoenix, AZ, USA). A PVA-coated capillary with 50 µm i.d. was acquired from Agilent Technologies (Waldbronn, Germany).

5.3.4. Methods

5.3.4.1. Capillary preparation

For peptide analysis, two different neutrally coated capillaries were applied. For the in-house preparation of a neutrally coated capillary, a coating procedure based on [215] was conducted. In brief, a new 60 cm piece of fused silica capillary was flushed at 1 bar with methanol for 10 min, 1 mol/L HCl for 10 min, 1 mol/L NaOH for 25 min and water for 10 min. Then, the capillary was flushed at 1 bar for 30 min with coating solution consisting of 1/5 (v/v) UltraTrol Dynamic Pre-Coat LN/water. The coating solution was left in the capillary overnight. Then, the capillary was flushed with air to remove the coating solution. It was subsequently rinsed by flushing with BGE at 1 bar for at least 10 min. To condition the capillary surface for measurements, a voltage of 30 kV was applied for 10 min, the capillary was rinsed with BGE and a voltage of -30 kV was applied for 10 min. After another 10 min of flushing with BGE at 1 bar, the capillary was ready for use. The outlet end of the capillary was polished to an angle of 45° using sand paper. The commercial PVA-coated capillary was cut to 63 cm length and the capillary outlet was polished to an angle of 45°.

5.3.4.2. CE separation parameters for BSA digest measurements

BSA digests were prepared in triplicate and measurements were conducted in triplicate each (meaning nine measurements per enzyme). A background electrolyte with 0.75 mol/L acetic acid and 0.25 mol/L formic acid (pH 2.0) was prepared in water. For CE separation, the capillary was flushed with BGE for 240 s at 1 bar before each measurement. Samples were injected hydrodynamically at 50 mbar for 5 s, then, the capillary inlet was dipped twice into fresh BGE to avoid carryover. A separation voltage of 30 kV was applied. The temperature was kept at 25 °C inside the instrument to guarantee stable separation conditions.

5.3.4.3. Mass spectrometric parameters

To support electrospray generation in the ion source, a sheath liquid consisting of 50 % (v/v) isopropanol in water with 0.1 % (v/v) formic acid was delivered at 4 µL/min. The electrospray ion source was set to a nebulizer pressure of 4 psig, drying gas temperature was set to 150 °C and drying gas flow was 11 L/min. Fragmentor voltage was 175 V, transfer capillary voltage was 3500 V and octopole voltage was 750 V. Mass spectra were recorded over a range of *m/z* 50-3000 and obtained at a data rate of 0.5 Hz for CE-MS measurements.

5.3.4.4. Data acquisition and processing

Data was acquired with MassHunter B.06 and processed with BioConfirm 10.0, both programs are from Agilent Technologies (Santa Clara, CA, USA). For data processing, the BioConfirm tool for protein digest analysis was applied, parameters were set to: reduced protein, modification by alkylation with iodoacetamide and dithiothreitol, free cysteines allowed, up to 3 missed cleavages allowed, peptide length range for peptide mapping 5-70, and all further settings were left as default. The respective enzyme was selected for data processing (i.e. trypsin, Lys-C or Glu-C) except in case of Lys-N which was not available in the program. Therefore, "nonspecific" enzyme cleavage was chosen and the resulting peptides were manually filtered for peptides resulting from N-terminal cleavage at Lys-sites in the protein. The peak mass lists of assigned peptides generated from data processing were then used for Mascot Server 2.7.0 (Matrix Science, Boston, MA, USA) peptide mass fingerprint search to generate molecular weight search (MOWSE) scores for identification. Settings for the database search were: SwissProt database, the respective enzyme chosen, up to three missed cleavages allowed, all entries for taxonomy, no fixed or variable modifications chosen, peptide tolerance ± 1.2 Da, mass values as $[M+H]^+$ with respective monoisotopic masses. All further settings were left as default.

5.4. Results

5.4.1. CE-MS measurements of BSA digested with trypsin, Glu-C, Lys-C and Lys-N

BSA was digested with trypsin, Glu-C, Lys-C or Lys-N following the same digestion protocol (see Section 5.3.2). Digests were measured via CE-MS on both LN-coated and PVA-coated capillaries. The base peak electropherograms generated from the *m/z* values of all assigned peptides are depicted in Figure 5.1.

For determination of the repeatability, selected peptides were chosen to calculate the relative standard deviations of the migration times. Two peptides were chosen from each digest, following the criteria: 1) high peak intensity, 2) peptide sequence of at least 5 amino acids, 3) preferably high difference in migration time and 4) no missed cleavages. All of the selected peptides were detected as $[M+2H]^{2+}$ ions, probably due to the decision to take only peptides consisting of more than 5 amino acids into account. Relative standard deviations of migration times were between 0.4 % and 5.6 % using the LN-coated capillary and between 0.2 % and 2.1 % using the PVA-coated capillary (see Table 5.2). Although the PVA-capillary seemed to be superior regarding repeatability,

relative standard deviations were lower for digests from Glu-C and Lys-C measured on the LN-coated capillary.

Table 5.2: Average (n = 9) migration times t_m and relative standard deviations thereof of selected peptides from CE-MS measurements of BSA digested with trypsin, Glu-C, Lys-C or Lys-N on LN- and PVA-coated capillaries.

enzyme	**LN**		**PVA**	
peptide sequence	**t_m in min**	**RSD t_m**	**t_m in min**	**RSD t_m**
trypsin				
LCVLHEK	4.38	3.8 %	6.16	0.4 %
LVNELTEFAK	6.09	5.6 %	9.80	0.2 %
Glu-C				
HVKLVNE	4.24	0.4 %	5.96	0.7 %
GPKLVVSTQTALA	6.16	0.5 %	10.13	1.1 %
Lys-C				
SEIAHRFK	3.62	0.7 %	4.92	1.2 %
SLHTLFGDELCK	4.75	0.9 %	7.11	2.1 %
Lys-N				
KIETMRE	4.08	2.3 %	5.81	0.9 %
KSLHTLFGDELC	4.70	2.5 %	7.06	1.1 %

5.4.2. Migration time window

The migration time window is defined here as the time span during which the analytes pass the detector, i.e. between the detection time of the first and the last analyte. The migration time windows obtained for separations of peptides from enzymatic BSA digests were considerably smaller for LN-coated than for PVA-coated capillaries (see Table 5.3 and compare to Figure 5.1). This may be due to a residual electroosmotic flow (EOF) due to an inhomogeneous or incomplete LN surface coating which leads to an additional transport of analytes towards the detector.

Table 5.3: Average (n = 9) migration time windows $t_{m,win}$ of assigned peptides and relative standard deviations thereof from BSA digests separated on LN-coated and PVA-coated capillaries.

	LN		**PVA**	
enzyme	**$t_{m,win}$ in min**	**RSD $t_{m,win}$ in %**	**$t_{m,win}$ in min**	**RSD $t_{m,win}$ in %**
trypsin	5.2	10.9	12.3	2.1
Glu-C	3.6	1.5	8.3	1.3
Lys-C	4.5	1.8	13.6	15.2
Lys-N	2.5	4.3	11.2	38.1

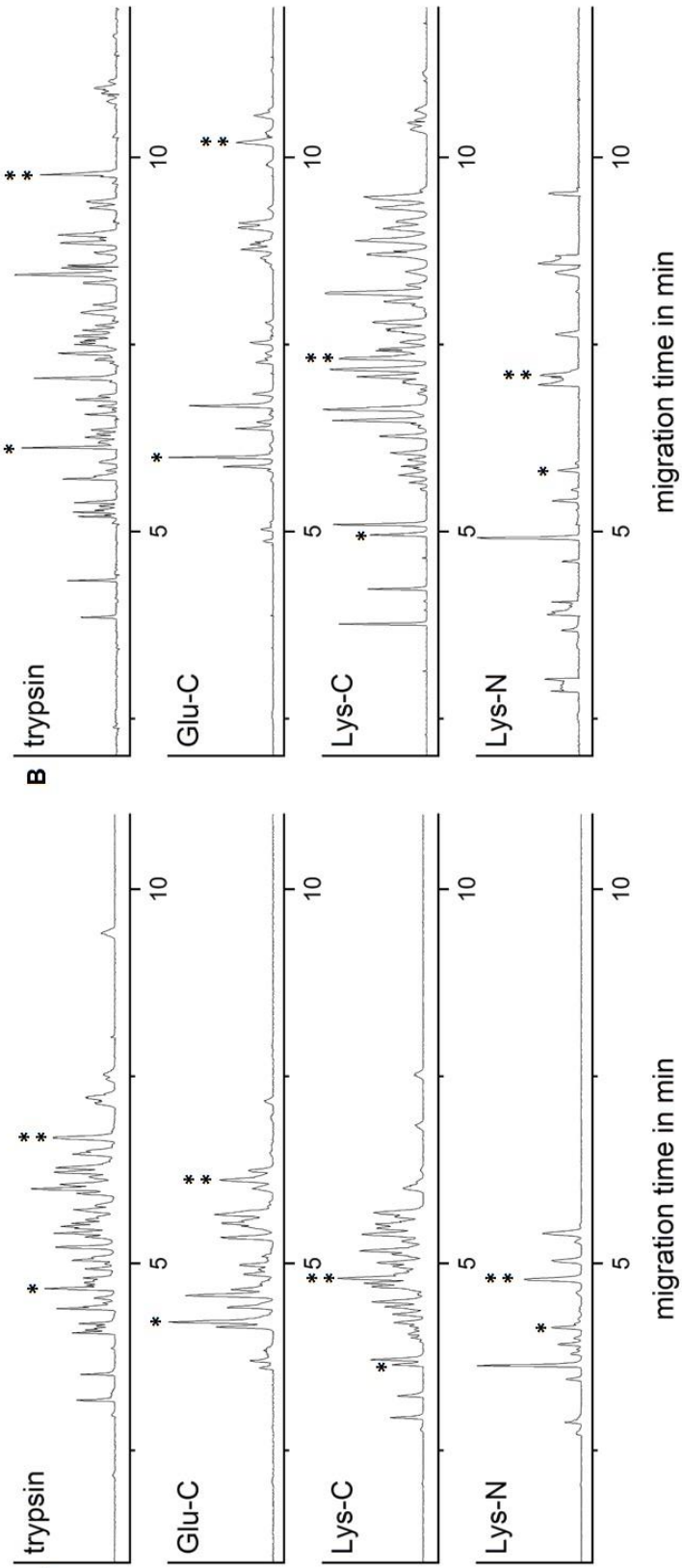

Figure 5.1: Base peak electropherograms of assigned peptides from BSA digests with trypsin, Glu-C, Lys-C or Lys-N. CE-MS measurements on (A) LN-coated capillary, 60 cm length, 50 µm i.d. and (B) PVA-coated capillary, 63 cm length, 50 µm i.d. BGE: 0.75 mol/L acetic acid and 0.25 mol/L formic acid (pH 2.0), + 30 kV separation voltage, hydrodynamic injection at 50 mbar for 5 s, positive ionization mode, scan range m/z 50-3000. The asterisks mark the two peptides selected for repeatability determination and estimation of μ_{EOF} (respective peptide with lower t_m, ** respective peptide with higher t_m, compare Table 5.2).*

To investigate the differences of the electrophoretic mobilities μ_{EOF} on both capillaries, two peptides were selected from each digest (see Section 5.4.1 and Table 5.2) and their electrophoretic mobility μ_{mes} observed in the electropherogram was calculated following Equation (4.4) in Chapter 4, see Table 5.4. To determine the effective electrophoretic mobilities μ_{eff}, the mobility of the EOF in the PVA-coated capillary, $\mu_{EOF,PVA}$, was assumed to be 0 $cm^2V^{-1}s^{-1}$. Thus, following Equation (4.5) in Chapter 4, μ_{mes} was equal to μ_{eff} for peptides separated on the PVA-coated capillary Table 5.4. Based on the values for μ_{mes} calculated for peptides separated on the LN-coated capillary and μ_{eff} obtained from measurements on the PVA-coated capillary, $\mu_{EOF,LN}$ was calculated by Equation (4.5). The average value for $\mu_{EOF,LN}$ was $0.11 \pm 0.01 \cdot 10^{-4}$ $cm^2V^{-1}s^{-1}$ (n = 8) (see Table 5.4).

Table 5.4: Observed electrophoretic mobilities $\mu_{mes,LN}$, effective electrophoretic mobilities μ_{eff} and electroosmotic mobilities $\mu_{EOF,LN}$ calculated for selected peptides from CE-MS measurements of BSA digested with trypsin, Glu-C, Lys-C or Lys-N on LN-coated capillaries. Average values from 8 measurements.*

	$\mu_{mes,LN}$ in 10^{-4} $cm^2V^{-1}s^{-1}$	$\mu_{mes,PVA} = \mu_{eff}$ in 10^{-4} $cm^2V^{-1}s^{-1}$	$\mu_{EOF,LN}$ in 10^{-4} $cm^2V^{-1}s^{-1}$
trypsin			
LVNELTEFAK	0.33	0.23	0.10
LCVLHEK	0.46	0.36	0.10
Glu-C			
HVKLVNE	0.47	0.37	0.10
GPKLVVSTQTALA	0.33	0.22	0.11
Lys-C			
SEIAHRFK	0.55	0.45	0.11
SLHTLFGDELCK	0.42	0.31	0.11
Lys-N			
KIETMRE	0.49	0.38	0.11
KSLHTLFGDELC	0.43	0.31	0.11

** μ_{eff} values were assumed to be similar to the $\mu_{mes,PVA}$ values of selected peptides in CE-MS measurements with a PVA-coated capillary (assumption $\mu_{EOF,PVA} = 0$)*

5.4.3. Sequence coverage and number of assigned peptides

The sequence coverage and numbers of assigned peptides were determined for BSA digests with trypsin, Glu-C, Lys-C and Lys-N. The average sequence coverage and number of assigned peptides obtained from measurements with an LN-coated and a PVA-coated capillary, as well as relative standard deviations of both values are given in Table 5.5. In addition, the number of peptides theoretically detectable from complete digestion is given. Thus, a higher number of different peptides could be obtained from

the measurements if parts of the sample were not digested completely and peptides with missed cleavages were present.

The sequence coverage obtained for BSA digests was comparable for both capillaries. A slightly higher number of peptides could be assigned for separations on the PVA-coated capillary (see Table 5.5). The highest sequence coverage was obtained for digests with trypsin and Lys-C. The sequence coverage was above 80 % which is the threshold value in BioConfirm for confirmed protein identification. Thus, these enzymes seem to be suitable for protein identification by CE-MS. For measurements of digests with Glu-C, sequence coverages were higher than 60 %, which is the threshold value for partially confirmed protein identification in BioConfirm. The measurements of digests with Lys-N resulted in both very low sequence coverages (23-25 %) and low numbers of assigned peptides (maximum of 25 peptides assigned).

Table 5.5: Average (n = 9) sequence coverages (SC) with relative standard deviations thereof and average (n = 9) numbers of assigned peptides (including peptides with missed cleavages, the number of assigned peptides without missed cleavages is stated in brackets) with relative standard deviations thereof obtained for BSA digests separated on LN-coated and PVA-coated capillaries. The theoretical number of peptides generated by complete digests with the respective enzyme is given as well.

enzyme	**average SC in %**		**RSD SC in %**		**average no. of assigned peptides[1]**		**RSD assigned peptides in %**		**no. of theoretical peptides[2]**
	LN	**PVA**	**LN**	**PVA**	**LN**	**PVA**	**LN**	**PVA**	
trypsin	92.5	91.8	2.0	2.3	81(63)	89(71)	4.2	3.1	82
Glu-C	62.2	63.3	5.9	4.2	41(30)	42(35)	7.9	7.5	60
Lys-C	85.7	87.4	3.0	2.1	56(49)	69(62)	1.4	10.7	61
Lys-N	23.6	25.2	10.5	7.9	17(17)	25(25)	11.3	26.5	61

[1] the average numbers (n = 9) of assigned peptides without missed cleavages is stated in brackets
[2] number of peptides which are theoretically obtained from a complete digest with respective enzyme, i.e. no cleavage is missed during digestion

The peak mass lists of assigned peptides obtained from data processing with BioConfirm were then used to generate molecular weight search (MOWSE) scores via Mascot's peptide mass fingerprint database search tool. It combines the molecular weight search algorithm with probability to obtain statistically significant scores. For the given analyses, a Mascot score around 70 was considered significant at a significance level of 0.05 employed by Mascot. The average Mascot scores obtained for peptide mass fingerprint search of all different measurement series are given in Table 5.6.

Table 5.6: Average (n = 9) Mascot scores obtained via Mascot peptide mass fingerprint database search and relative standard deviations of the scores.

	LN		PVA	
enzyme	**Mascot score**	**RSD Mascot score in %**	**Mascot score**	**RSD Mascot score in %**
trypsin	169	5.9	167	5.9
Glu-C	71	9.4	90	10.2
Lys-C	191	3.0	186	3.3
Lys-N	72	11.4	66	11.3

Highest scores were obtained for digests with trypsin or Lys-C on both capillaries, being above 160 for tryptic digests and around 190 for Lys-C digests. Mascot scores obtained for Glu-C digests were above 70 and Lys-N digests resulted in Mascot scores around 70, with the only score below the significance threshold for measurements on the PVA-coated capillary. Relative standard deviations of the Mascot scores were slightly higher than of the sequence coverages obtained from BioConfirm data processing (compare Table 5.5 and Table 5.6).

5.4.4. Missed cleavages

For data analysis, up to three missed cleavages were accepted for peptide assignment. Average numbers of assigned peptides without missed cleavages and with one, two or three missed cleavages are shown in Figure 5.2 for each enzyme and different capillary coatings. Furthermore, the percentage of peptides with missed cleavages relative to the total number of assigned peptides is stated.

Generally, a lower number of peptides with missed cleavages indicates a more comprehensive protein digestion and shows that the digestion conditions were well suited, as the enzyme was able to cleave the protein at most of the specific sites. Similar results were obtained from measurements on both LN-coated and PVA-coated capillaries, although a slightly higher number of assigned peptides without missed cleavages was observed for measurements on the PVA-coated capillaries. These small differences between LN-coated and PVA-coated capillaries were due to changes in separation efficiency and ionization, as will be discussed in Section 5.5.

Regardless of the enzyme applied for BSA digestion, not more than 1/4 of all peptides assigned had missed cleavages and among those, single missed cleavages dominated (see Figure 5.2). The lowest percentage of peptides without missed cleavages was determined in digests with Glu-C measured on an LN-coated capillary (73 % of assigned peptides were without missed cleavages). Peptides with more than 1 missed cleavage

accounted for less than 5 % (< 3 peptides) of all peptides assigned in digests with trypsin, Glu-C and Lys-C. For Lys-N, no missed cleavages were observed, but for the sequence coverage was low, partly due to the manual data processing.

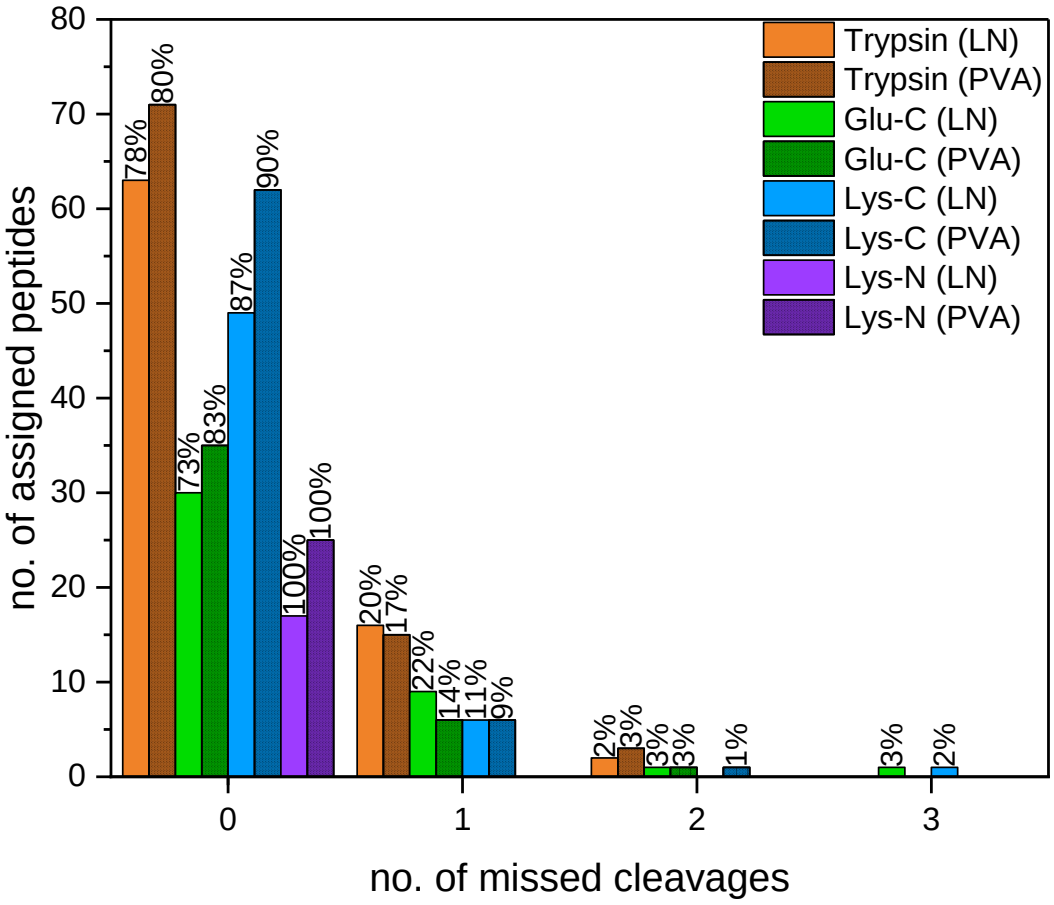

Figure 5.2: Average (n = 9) numbers of assigned peptides with zero, one, two or three missed cleavages in BSA digests separated on LN-coated and PVA-coated capillaries. Values at the column ends indicate the percentage in regard to the total number of assigned peptides.

5.4.5. Charge states of peptides

Besides singly charged peptides by simple protonation ($[M+H]^+$), also higher charge states ($[M+2H]^{2+}$ and $[M+3H]^{3+}$ and even higher) were detected by ESI-MS, see Figure 5.3. The distribution of average numbers of peptides which were detected in each of these different charge states as well as the percentage share in regard to the total number of detected peptides is shown in Figure 5.3 for measurements conducted on LN-coated and PVA-coated capillaries. In our experiments, peptides were not observed to have more than two different charge states as summarized in Table 5.7 (see also comparison to the total number of peptides).

The majority of peptides was detected as $[M+2H]^{2+}$ (between 43 % and 58 %, depending on the enzyme used for digestion and the capillary, see Figure 5.3). $[M+H]^{+}$ accounted for 39 % of all peptides, $[M+3H]^{3+}$ for 14-28 % and other for less than 15 %.

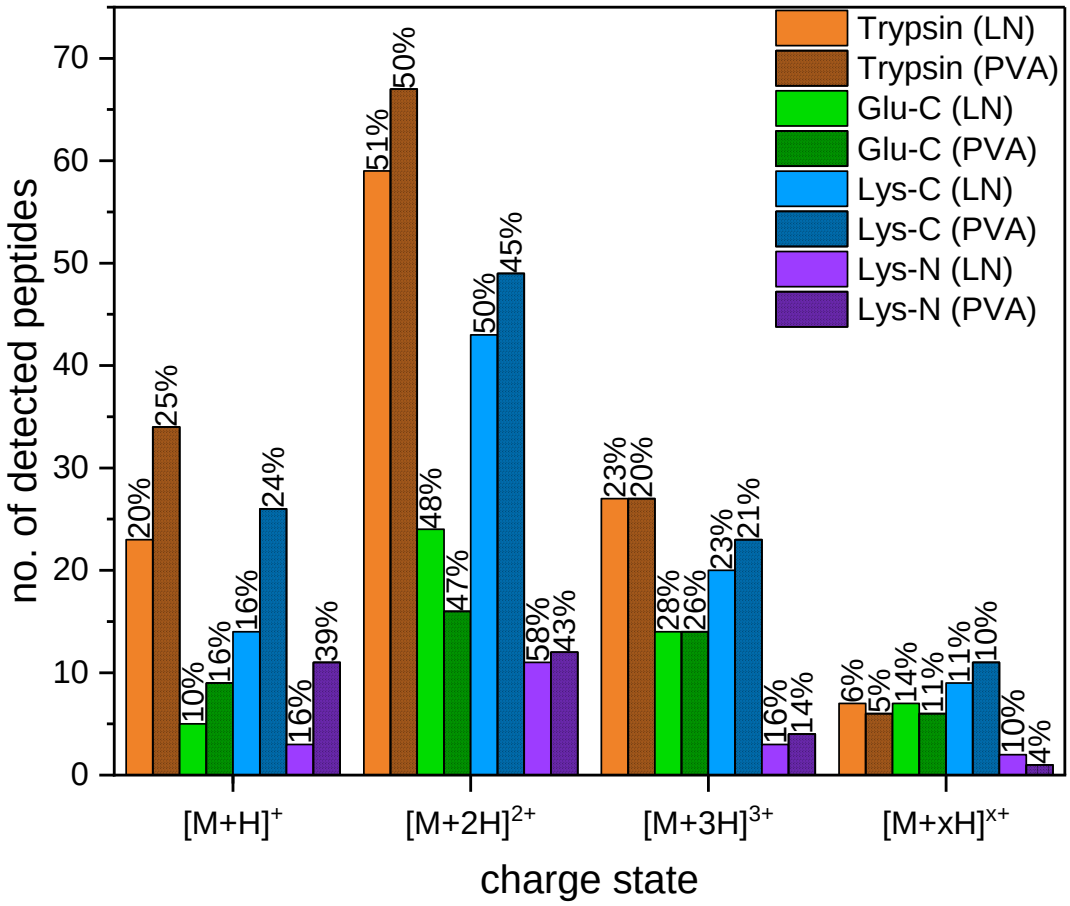

Figure 5.3: Average (n = 9) numbers of assigned peptides' charge states observed in BSA digests separated on LN-coated and PVA-coated capillaries. Values at the column ends indicate the percentage relative to the sum of all detected peptides.

Table 5.7: Average (n = 9) numbers of assigned peptides detected in only one or two different charge states and the percentage relative to the total number of assigned peptides found in BSA digests separated on LN-coated and PVA-coated capillaries.

	LN				PVA			
enzyme	**peptides detected in one charge state**		**peptides detected in two charge states**		**peptides detected in one charge state**		**peptides detected in two charge states**	
trypsin	47	58 %	34	42 %	44	49 %	45	51 %
Glu-C	31	76 %	10	24 %	29	69 %	13	31 %
Lys-C	28	50 %	28	50 %	30	43 %	39	57 %
Lys-N	15	88 %	2	12 %	21	84 %	4	16 %

In tryptic digests, approx. half of the assigned peptides were detected in only one charge state, while the other half was detectable in two different charge states (compare Table 3). Digests with Lys-C resulted in similar distributions. Digests with Glu-C and Lys-N resulted in an increased number of assigned peptides which were detectable only in one charge state, which is reasonable given the lower absolute number of assigned peptides here. From these results, we conclude that a higher reliability of peptide assignment can be obtained from digests with trypsin and Lys-C.

5.5. Discussion and outlook

The influence of different digestion enzymes on CE-MS peptide analysis was studied using the enzymes trypsin, Glu-C, Lys-C and Lys-N and evaluated using the following criteria: 1) the migration time window in which peptides were detected, 2) the sequence coverage and the number of assigned peptides in comparison to the number of theoretically available peptides, 3) the number of peptides with missed cleavages and 4) the peptides' charge states. All these parameters were available from data processing with BioConfirm for digestion with trypsin, Glu-C and Lys-C. In contrast, Lys-N was not included in the database. Thus, data obtained from digests with Lys-N were first analyzed for peptides from nonspecific cleavages. Then, peptides with N-terminal Lys were searched manually from the results using the amino acid sequence of the peptides provided after data processing. The peptide mass lists of assigned peptides were further evaluated against Mascot's peptide mass fingerprint database search algorithm to obtain MOWSE scores for the reliability of the identification.

In samples with a high number of analytes, a broad migration time window in combination with an even distribution of analytes along the migration time window is favored to obtain high separation efficiency and minimized comigration to avoid ion suppression. Taking the migration time window of the tryptic digests as reference, separations of digests with Glu-C exhibited migration time windows reduced by approx. one third on either type of capillary coating (see Table 5.3). Given the lower theoretical number of peptides expected and the lower number of assigned peptides obtained, the narrowed migration time window is not expected to reduce separation quality or increase ion suppression based on comigration, but no benefit is gained in turn. The migration time windows obtained for separations of digests with Lys-C were comparable to the separations of tryptic digests on both capillaries. The peptide distribution among the migration time windows was comparable for separations in PVA-coated capillaries for both digests. Approximately 60 % of peptides were detected at a migration time between 5 and 8 min. On LN-coated capillaries, peptides from digests with Lys-C were slightly less distributed among the migration time window than peptides from digests with trypsin: 75 % of tryptic

peptides and 84 % of peptides from Lys-C digests were detected at migration times between 5 and 6 min. As both, the number of peptides expected theoretically and the number of assigned peptides in our work is lower than for tryptic digests, the comparable size of the migration time window indicates that there is an advantage with regard to lower risk for ion suppression due to comigration as well as improved resolution. Our results for migration time windows of separations of digests with Lys-N were ambivalent for the capillaries used: while the migration time windows were comparable to separations of tryptic digests if the separations were conducted on a PVA-coated capillary, they were considerably smaller if separations were carried out on an LN-coated capillary. Again, this could be a result from the manual data processing. Furthermore, the relative standard deviation of the migration time windows determined for separations on the PVA-coated capillary was high (38 %, see Table 5.3) indicating additional effects on electrophoretic and electroosmotic mobilities and, thus, selectivity.

Migration time windows obtained for the separation of the different digests varied from one capillary coating to the other. The migration time windows obtained using an LN-coated capillary were considerably smaller than those obtained on a PVA-coated capillary. We assume, that the coating procedure was not completely successful, although all other investigated parameters were comparable for both capillaries. For the calculation of $\mu_{EOF,LN}$ (see Table 5.4), $\mu_{EOF,PVA}$ was assumed to be 0 $cm^2V^{-1}s^{-1}$ as the commercial capillary was expected to have an intact coating. $\mu_{EOF,LN}$ was approx. ten times lower than the EOF under acidic conditions on an uncoated capillary (compare Chapter 4) - nevertheless, commercial PVA-coated capillaries may still have a small residual EOF. Thus, it can be assumed that the actual $\mu_{EOF,LN}$ was actually higher than calculated. Based on these EOF differences, the large differences in the size of the migration time windows obtained with LN-coated and PVA-coated capillaries can be explained. Albeit the differences in absolute values for the migration time window, the trends observed for the different enzymes were comparable for both capillary coatings.

Sequence coverages of 92 % for BSA digests with trypsin and of 86-87 % for digests with Lys-C were obtained, while the sequence coverage of peptides from digests with Glu-C was 62-63 % (see Table 5.5). In BioConfirm, a sequence coverage of at least 80 % is set as threshold for the confirmation of the protein identity, a sequence coverage of at least 60 % is considered a “partially confirmed” identification. This would be insufficient if protein identification is needed from samples of unknown composition. The sequence coverage obtained is below literature values for BSA digests with Glu-C analyzed by direct MS/MS with electron capture dissociation, e.g. by Kalli and Håkansson [213] who obtained a sequence coverage around 80 %. Sequence coverage

for peptides from Lys-N digest was only 24-25 % (Table 5.5). This was probably due to the manual data evaluation of digests with Lys-N, as this enzyme could not be chosen for automated cleavage assignment. The number of assigned peptides is comparable to the number stated in a brief communication of Taouatas et al. [216] who were able to identify 27 peptides from BSA digests with Lys-N, analyzed by LC-MS. Nevertheless, the sequence coverage obtained in their work was 56 %, which is clearly higher than the sequence coverage we obtained from our experiments.

Mascot scores were above the significance threshold of 70 for all digests except for the Lys-N digest separated on a PVA-coated capillary (Mascot score of 66, compare Table 5.6). The scores generated by Mascot's peptide mass fingerprint database search include the probability of false positive hits at a significance level of 0.05. The significance threshold depends on the protein's molecular weight and the number of database entries [217]. Thus, the probability of a false positive value increases with database size. For more reliable protein identification, Damodaran et al. [218] suggested to combine different parameters (molecular weight, pI, sequence coverage, number of peptides matched and significance scores of protein identification databases) to calculate another score with increased reliability. The group suggested a threshold of 15 as significant for protein identification. According to their score, BSA could be identified with a score of 14 from digests with trypsin, Glu-C or Lys-C and a score of 10 from digests with Lys-N in our work, without taking the protein molecular mass and pI into account. This probably indicates a high suitability of the enzymes Glu-C and Lys-C to be applicable as alternatives to trypsin even in protein mixtures when protein identification is envisaged. Of course, the use of MS/MS for the identification of the peptide amino acid sequence will further aid in protein identification and significantly increase scores.

All different digests generated at least 73 % of assigned peptides without missed cleavages (see Figure 5.2), indicating the applicability of the protocol originally optimized for tryptic digestion also for the other endoproteases used here, but further optimization especially for Lys-N is required. Regarding the peptide charge states, comparable numbers of singly, doubly and triply charged peptides were obtained from digests with trypsin, Lys-C and Lys-N. A slightly increased tendency towards peptides with more than three charges was observed for Lys-C and Glu-C. Digests with Glu-C produced fewer singly charged peptides and revealed a trend towards triply charged peptides (Figure 5.3). In tryptic digests, approx. half of the assigned peptides were detected in two different charge states and comparable results were obtained for digests with Lys-C. Peptides from digests with Glu-C and Lys-N were detected mainly in one charge state (see Table 5.7).

Compared to the tryptic digests, Glu-C, Lys-C and Lys-N were expected to result in lower numbers of assigned peptides but with higher mass due the lower number of cleavage sites in the protein. Table 5.5 shows that the average numbers of assigned peptides obtained from measurements of BSA digests with trypsin and Lys-C on a PVA-coated capillary are higher than the theoretical number of peptides. The higher number of assigned peptides indicated that peptides with missed cleavages were present in the sample. Altogether, the low percentage of peptides with missed cleavages (see Figure 5.2) indicated that the transfer of the digest method from trypsin to the other enzymes was successful. The results show that it is possible to digest BSA with different enzymes in parallel under conditions similar to the standard procedure, as was already described by Giansanti et al. [210].

For the larger peptides generated by Glu-C, Lys-C and Lys-N we expected a higher possibility for peptides in higher charge states. As visible from Figure 5.3, this seems to be the case when comparing the charge states of peptides from digests with Glu-C and Lys-C to tryptic peptides, although doubly charged peptides were still the most commonly detected. Nevertheless, a slight trend towards higher charge states could be observed, especially for digests with Glu-C and Lys-C. A clear correlation of migration times and peptide charge states was not observed. Peptides from digests with Lys-N measured on a PVA-coated capillary were an exception, as a clearly higher amount of singly charged peptides was determined. However, these results have to be treated with caution due to very low number of assigned peptides.

From our results, we can deduce that Lys-C provides an interesting alternative or complement to digest proteins as comparable results to trypsin were obtained concerning sequence coverage and migration time windows. The comparison of the segments of the BSA sequence detected in measurements of digests with trypsin or Lys-C (Figure 5.4A) shows that the sequence coverage obtained was largely comparable and only few peptides were not detected in both digests. The medium peptide mass determined was 1276.6 Da with the LN-coated capillary and 1214.4 with the PVA-coated capillary (versus 1141.1 Da and 1099.5 Da medium peptide mass of tryptic digests on the LN-coated and PVA-coated capillaries, respectively). Thus, a slight trend towards higher peptide masses was observed. Due to the slightly lower number of peptides generated and the comparable migration window, comigration could be reduced and, thus, MS detection might profit from reduced ion suppression and quenching effects. Furthermore, less comigration can be advantageous for MS/MS as it allows higher precursor ion sampling and dissociation times

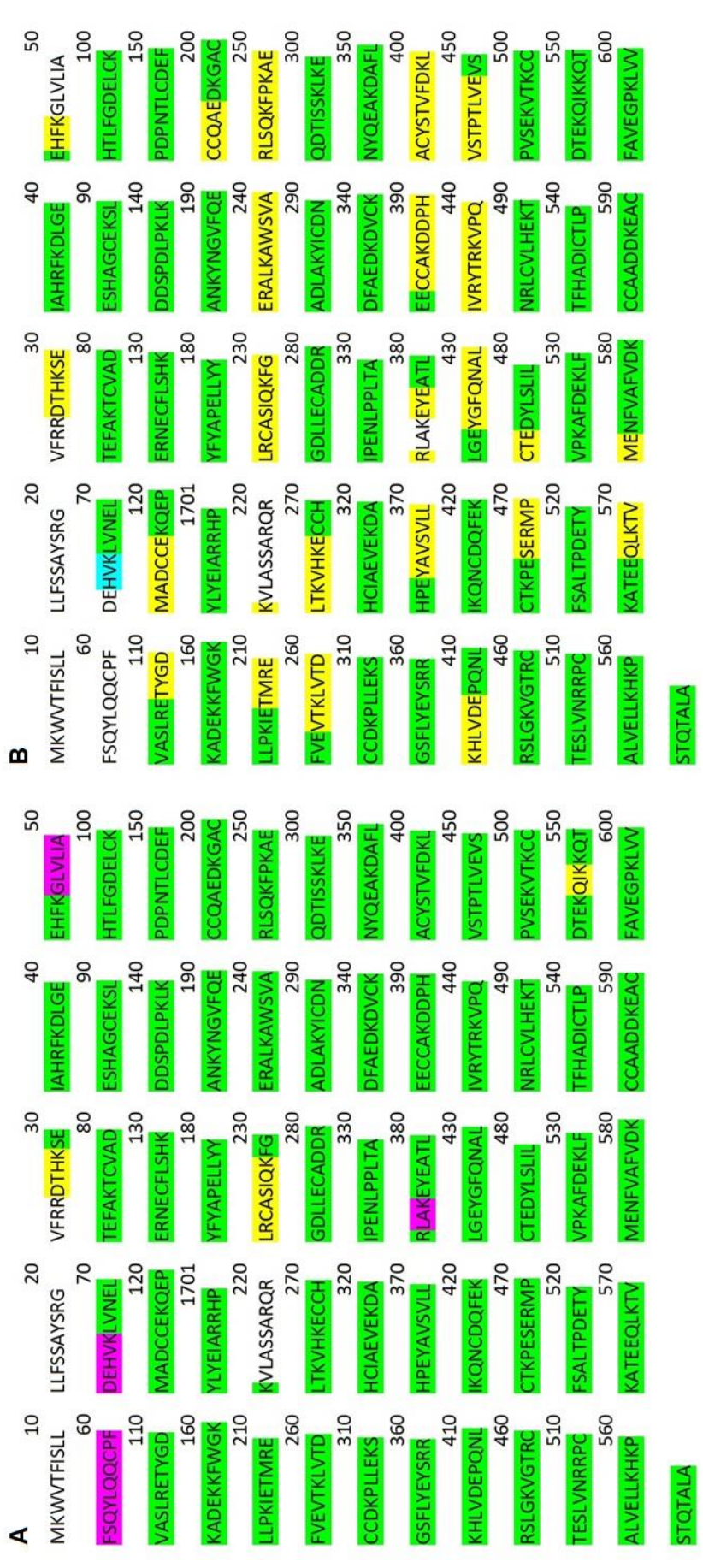

Figure 5.4: Comparison of identified sequence segments of BSA. (A) Sequence segments of digests with trypsin or Lys-C. The parts of the sequence detected only in measurements of tryptic peptides are highlighted in yellow, sequence parts detected only in measurements of digests with Lys-C are highlighted in pink and sequence parts detected in measurements of both digests are highlighted in green. (B) Sequence segments of digests with trypsin or Glu-C. The parts of the sequence detected only in measurements of tryptic peptides are highlighted in yellow, sequence parts detected only in measurements of digests with Glu-C are highlighted in teal and sequence parts detected in measurements of both digests are highlighted in green.

Glu-C may provide additional information to those obtained by tryptic digests, as the comparatively large peptides generated might differ more strongly in their effective electrophoretic mobility so that higher resolution can be expected. The lower number of peptides reduces data load and, thus, simplifies data processing. Nevertheless, in our work, the sequence coverage obtained for digests with Glu-C was only partially satisfying. No additional information on the sequence could be obtained from digests with Glu-C in comparison to digests with trypsin as visible in Figure 5.4B. Further optimization of the digestion protocol is required, although identification via Mascot's peptide mass fingerprint database search could be considered sufficient.

Furthermore, as larger peptides are generated (medium peptide masses of 1386.6 Da and 1289.0 Da on LN-coated and PVA-coated capillaries, respectively), it is also possible that the charge distribution in terms of size-to-charge remains small, so that no gain in the peak capacity is obtained. In contrary to our expectations, a trend of lysine- and arginine-containing peptides towards lower migration times could not be observed. It will be interesting to compare the digestion enzymes when using BGEs of different (elevated) pH in the future as differences in effective electrophoretic mobilities may become more pronounced.

The results we obtained for digests with Lys-N were probably not reliable enough to deduce the usefulness of Lys-N for peptide generation for CE-MS analysis. The automated data processing used in this work was not completely possible for Lys-N as it was for the other endoproteases because Lys-N was not available to be chosen as specific enzyme in the algorithm. An algorithm for nonspecific enzymatic cleavage was chosen as alternative and peptides with N-terminal Lys were picked manually. Thus, only a low number of peptides was assigned, resulting in sequence coverages well below 30 %, which is by far not sufficient for protein identification. Mascot scores were very close to the significance threshold, strengthening the assumption of insufficient digestion. Furthermore, inconsistent results were obtained with the two capillaries in comparison to other digests, especially regarding migration time windows and medium peptide masses (1023.9 Da and 901.6 Da on LN-coated and PVA-coated capillaries, respectively).

In conclusion, it can be stated that other enzymes than trypsin offer interesting features for CE-MS analysis by generation of larger peptides with possibly higher variation in peptide charges. While evenly charged peptides as generated by tryptic digestion are favorable for LC-MS analyses, CE-MS could benefit from a higher variation of peptide charges as this might broaden the window of effective electrophoretic mobilities. Thus, peak capacity might be increased using proteases other than trypsin. Furthermore, highly

polar peptides might not be accessible for reversed-phase LC separations as they elute with or very close to the void volume. Due to the limited polarity window of LC stationary phases, it might be problematic, if both very hydrophilic and very hydrophobic peptides are present simultaneously in the digests. By CE, both types of peptides can be separated within the same measurement as long as they are charged in the given BGE (see Section 5.2.2). Thus, CE-MS can provide a helpful alternative for peptides with a wide polarity range.

Although our results indicate that the transfer of the protocol designed for tryptic digestion towards Glu-C and Lys-C was successful, the optimization of the digestion protocol for these enzymes with regard to enzyme/substrate ratios or incubation times could further increase sequence coverage. The use of alternative endoproteases seems to be promising for CE-MS analysis and could extend the CE-MS proteomic toolbox.

6. Conclusive discussion

The combination of isotachophoresis (ITP) with capillary electrophoresis-mass spectrometry (CE-MS) is expected to improve concentration detection limits significantly and, thus, widen the applicability of CE-MS separations for investigation of environmentally relevant substances at low concentrations. Two already existing ITP electrolyte systems for preconcentration of all proteinogenic amino acids in one isotachophoretic zone were further optimized to increase their tolerance to aqueous sample and for higher MS-compatibility in direct ITP-MS coupling. The hydroorganic electrolytes used dimethyl sulfoxide/water as solvent mixture, imidazole as leading ion and H^+ as terminating ion. Either oxalic acid or trifluoroacetic acid were used as counterions. While the MS-compatibility of electrolyte systems with oxalic acid was low and contamination of the ion source occurred, the electrolyte system with trifluoroacetic acid showed low tolerance for aqueous samples, which led to current breakdowns. Thus, two new electrolytes for ITP-MS and ITP/CE-MS were developed in this work. The new ITP electrolyte systems evoked very similar electrophoretic migration behavior and pK_a values of 1.47 or 1.00, using either trimethylpyruvic acid or difluoroacetic acid, respectively, as counterion. The preconcentration of all proteinogenic amino acids within one isotachophoretic zone was possible with increased MS-compatibility and higher tolerance for aqueous samples, making this new electrolyte system highly suitable for direct ITP-MS analyses and ITP/CE-MS hyphenation. Furthermore, a hydroorganic background electrolyte (BGE) applicable after ITP preconcentration was developed, using acetic acid in isopropanol/water. CE-MS measurements with this BGE resulted in sufficient resolution of the amino acids for qualitative analysis, although suction effects from the ion source clearly reduced the migration time window in CE-MS measurements compared to CE-conductivity measurements. In future approaches, coated capillaries and optimized electrospray conditions could broaden the migration time window and increase the resolution by reducing comigration.

Within the scope of this work, the capillary coupling setup, which is considered the most flexible but also more sophisticated 2D hyphenation approach, remained highly challenging. It was shown that it is only possible when intermediate detection at the common intersection is used. A conductivity detector integrated in the microfluidic glass chip interface employed in the 2D setups is currently under investigation and will strongly increase the applicability of this setup. It is envisaged to improve concentration detection limits in the analysis of underivatized glyphosate in environmental samples.

The second approach of ITP/CE-MS hyphenation in this work, a single capillary setup, was successfully established. To our knowledge, this is the first approach of single

capillary ITP/CE-MS which does not use the sheath liquid for counterflow generation. This setup is easily applicable with regard to sample transfer to the second dimension. The risk of sample loss is low, although it was shown that proper sample transfer is needed for successful analyses. The introduction of a side capillary for counterflow generation expanded the useable modes from L-S-L only to all three ITP/CE modes, namely L-S-L, T-S-T and BGE-S-BGE. The superiority of the BGE-S-BGE mode was shown as it provided higher separation efficiency and better detection limits. This setup is very promising for ITP/CE-MS approaches as a compromise is reached between performance and instrumental complexity compared to capillary coupling ITP/CE-MS: the setup is simpler, since it does not need a second high voltage source but uses only a glass chip T-piece as interface and a third pressurized vial as additional equipment. The full enrichment capabilities of single capillary ITP/CE-MS are to be investigated regarding loadability and detection limits, but the results of this thesis demonstrate the high potential of this approach. Especially the capillary length ratios of the capillaries from the CE to the interface and from the interface to the MS are interesting parameters for further optimization, as the separation path length is shortened with increased injection plug lengths.

A major task in ITP/CE is the compatibility of electrolytes in the two dimensions to minimize band broadening by destacking or unsuitable tITP conditions. Adaptation of electroosmotic and electrophoretic properties is possible by using hydroorganic solvents. To gain a better understanding of underlying mechanisms, the influences of hydroorganic BGEs on the electroosmotic mobility and on the effective electrophoretic mobilities of amino acids were investigated. Background electrolytes containing 10-30 % (v/v) of acetonitrile, dimethyl sulfoxide or isopropanol or 10-50 % (v/v) methanol were chosen for a systematic investigation. Results show that there is a complex interplay of the parameters influencing the electroosmotic flow and the electrophoretic mobilities of analytes and, thus, changes are not easily predicted based solely on parameters such as relative permittivity, autoprotolysis or viscosity. The comprehensive data obtained from these measurements will be used to generate databases for simulations of CE measurements in hydroorganic BGEs in the future.

For future ITP/CE-MS applications, the utility of endoproteases Glu-C, Lys-C and Lys-N as alternatives to trypsin in CE-MS based peptide analyses was investigated. It was expected that the other endoproteases improve the migration time window and, thus, the separation of peptides as they produce peptides with more variability in chain length and especially charge number, when proteins are not cut at both basic amino acids lysine and arginine. However, the migration time windows of Lys-C digests were comparable

to tryptic digests, while even inferior results were obtained for digests with Glu-C and Lys-N. Likewise, the number or assigned peptides and sequence coverage were lowered. Nevertheless, a trend slight towards longer peptides with higher charge states could be observed. Further optimization of the digestion protocol for these alternative endoproteases and different pH values for CE separation are expected improve their applicability for CE-MS separations.

7. References

[1] Melzer, T., Wimmer, B., Bock, S., Posch, T. N., Huhn, C., *Electrophoresis* 2020, *41*, 1045-1059.

[2] Kler, P. A., Huhn, C., *Anal. Bioanal. Chem.* 2014, *406*, 7163-7174.

[3] Sydes, D., Kler, P. A., Hermans, M., Huhn, C., *Electrophoresis* 2016, *37*, 3020-3024.

[4] Graf, H. G. *Entwicklung einer on-Chip-Detektionsmethode auf Basis von axialer kontaktloser Leitfähigkeitsdetektion.* Master thesis, Eberhard Karls Universität, Tübingen, 2018.

[5] Haake, A. *Untersuchung des Einflusses verschiedener Lösemittel auf die elektrophoretische Mobilität in nicht-wässrigen kapillarelektrophoretischen Trennungen.* Bachelor thesis, Eberhard Karls Universität, Tübingen, 2019.

[6] Schmitt-Kopplin, P., *Capillary Electrophoresis: Methods and Protocols,* Springer, New York, NY 2016.

[7] Kawai, T., *Chromatography* 2017, *38*, 1-8.

[8] Schwer, C., Kenndler, E., *Anal. Chem.* 1991, *63*, 1801-1807.

[9] Kenndler, E., Jenner, P., *J. Chromatogr. A* 1987, *390*, 169-183.

[10] Kenndler, E., Jenner, P., *J. Chromatogr. A* 1987, *390*, 185-197.

[11] Kenndler, E., Schwer, C., Jenner, P., *J. Chromatogr. A* 1989, *470*, 57-68.

[12] Switzar, L., Giera, M., Niessen, W. M. A., *J. Proteome Res.* 2013, *12*, 1067-1077.

[13] Kendall, J., Crittenden, E. D., *Proc. Natl. Acad. Sci. U.S.A.* 1923, *9*, 75-78.

[14] Malá, Z., Gebauer, P., *Electrophoresis* 2019, *40*, 55-64.

[15] Malá, Z., Gebauer, P., Boček, P., *Electrophoresis* 2017, *38*, 9-19.

[16] Malá, Z., Gebauer, P., Boček, P., *Electrophoresis* 2015, *36*, 2-14.

[17] Malá, Z., Gebauer, P., Boček, P., *Electrophoresis* 2013, *34*, 19-28.

[18] Gebauer, P., Malá, Z., Boček, P., *Electrophoresis* 2011, *32*, 83-89.

[19] Gebauer, P., Malá, Z., Boček, P., *Electrophoresis* 2009, *30*, 29-35.

[20] Gebauer, P., Malá, Z., Boček, P., *Electrophoresis* 2007, *28*, 26-32.

[21] Gebauer, P., Boček, P., *Electrophoresis* 2002, *23*, 3858-3864.

[22] Gebauer, P., Boček, P., *Electrophoresis* 2000, *21*, 3898-3904.

[23] Gebauer, P., Boček, P., *Electrophoresis* 1997, *18*, 2154-2161.

[24] Everaerts, F. M., Verheggen, T. P. E. M., Reijenga, J. C., *Trends Anal. Chem.* 1983, *2*, 188-192.

[25] Pantůčková, P., Gebauer, P., Boček, P., Křivánková, L., *Electrophoresis* 2009, *30*, 203-214.

[26] Stolz, A., Jooß, K., Höcker, O., Römer, J., Schlecht, J., Neusüß, C., *Electrophoresis* 2018.

[27] Boček, P., Deml, M., Gebauer, P., Dolník, V., *Analytical Isotachophoresis,* Wiley-VCH, Weinheim 1988.

[28] Everaerts, F. M., Becker, J. L., Verheggen, T. P. E. M., *Isotachophoresis: Theory, Instrumentation, and Applications,* Elsevier, Amsterdam 1976.

[29] Jooß, K., Hühner, J., Kiessig, S., Moritz, B., Neusüß, C., *Anal. Bioanal. Chem.* 2017, *409*, 6057-6067.

[30] Foret, F., Thompson, T. J., Vouros, P., Karger, B. L., Gebauer, P., Boček, P., *Anal. Chem.* 1994, *66*, 4450-4458.

[31] Bock, S. *Methodenoptimierung für die Trennung von Glyphosat, dessen Abbauprodukte und Analoga.* Bachelor thesis, Eberhard Karls Universität, Tübingen, 2018.

[32] Gebauer, P., Malá, Z., Boček, P., *Electrophoresis* 2013, *34*, 3245-3251.

[33] Malá, Z., Gebauer, P., *J. Chromatogr. A* 2017, *1518*, 97-103.

[34] Malá, Z., Pantůčková, P., Gebauer, P., Boček, P., *Electrophoresis* 2013, *34*, 777-784.

[35] Smith, R. D., Loo, J. A., Barinaga, C. J., Edmonds, C. D., Udseth, H. R., *J. Chromatogr. A* 1989, *480*, 211-232.

[36] Udseth, H. R., Loo, J. A., Smith, R. D., *Anal. Chem.* 1989, *61*, 228-232.

[37] Malá, Z., Gebauer, P., Boček, P., *Electrophoresis* 2013, *34*, 3072-3078.

[38] Gebauer, P., Malá, Z., Boček, P., *Electrophoresis* 2014, *35*, 746-754.

[39] Malá, Z., Gebauer, P., *Anal. Chim. Acta* 2018, *998*, 67-74.

[40] Malá, Z., Gebauer, P., *J. Chromatogr. A* 2020, 460907.

[41] Malá, Z., Gebauer, P., Boček, P., *Anal. Chim. Acta* 2016, *907*, 1-6.

[42] Zhao, Z., Wahl, J. H., Udseth, H. R., Hofstadler, S. A., Fuciarelli, A. F., Smith, R. D., *Electrophoresis* 1995, *16*, 389-395.

[43] Zhao, Z., Udseth, H. R., Smith, R. D., *J. Mass Spectrom.* 1996, *31*, 193-198.

[44] de Lassichère, C. C., Mai, T. D., Taverna, M., *J. Chromatogr. A* 2019, *1601*, 350-356.

[45] Khurana, T. K., Santiago, J. G., *Anal. Chem.* 2008, *80*, 6300-6307.

[46] Rubin, S., Schwartz, O., Bercovici, M., *Phys. Fluids* 2014, *26*, 012001.

[47] Posch, T. N. *Implementation of capillary electromigrative separation techniques coupled to mass spectrometry in forensic and biological science.* Dissertation, Westfälische Wilhelms-Universität, Münster, 2014.

[48] Kenndler, E., Haidl, E., *Fresenius Z. Anal. Chem.* 1985, *322*, 391-396.

[49] Marák, J., Staňová, A., Gajdoštínová, S., Škultéty, L., Kaniansky, D., *Electrophoresis* 2011, *32*, 1273-1281.

[50] Smith, R. D., Fields, S. M., Loo, J. A., Barinaga, C. J., Udseth, H. R., Edmonts, C. G., *Electrophoresis* 1990, *11*, 709-717.

[51] Peterson, Z. D., Bowerbank, C. R., Collins, D. C., Graves, S. W., Lee, M. L., *J. Chromatogr. A* 2003, *992*, 169-179.

[52] Kler, P. A., Posch, T. N., Pattky, M., Tiggelaar, R. M., Huhn, C., *J. Chromatogr. A* 2013, *1297*, 204-212.

[53] Tomáš, R., Koval, M., Foret, F., *J. Chromatogr. A* 2010, *1217*, 4144-4149.

[54] Park, J. K., Campos, C. D. M., Neuzil, P., Abelmann, L., Guijt, R. M., Manz, A., *Lab Chip* 2015, *15*, 3495-3502.

[55] Vio, L., Cretier, G., Chartier, F., Geertsen, V., Gourgiotis, A., Isnard, H., Morin, P., Rocca, J.-L., *J. Anal. At. Spectrom.* 2012, *27*, 850-856.

[56] Vio, L., Crétier, G., Chartier, F., Geertsen, V., Gourgiotis, A., Isnard, H., Rocca, J.-L., *Talanta* 2012, *99*, 586-593.

[57] Harris, D. C., *Quantitative Chemical Analysis,* W. H. Freeman and Company, New York, NY 2007.

[58] Timerbaev, A. R., Hirokawa, T., *Electrophoresis* 2006, *27*, 323-340.

[59] Tomáš, R., Klepárník, K., Foret, F., *J. Sep. Sci.* 2008, *31*, 1964-1979.

[60] Kler, P. A., Sydes, D., Huhn, C., *Anal. Bioanal. Chem.* 2015, *407*, 119-138.

[61] Grochocki, W., Markuszewski, M. J., Quirino, J. P., *Electrophoresis* 2015, *36*, 135-143.

[62] Grochocki, W., Markuszewski, M. J., Quirino, J. P., in, *Encyclopedia of Analytical Chemistry*, John Wiley & Sons, Hoboken, NJ 2016, pp. 1-17.

[63] Chen, L., Prest, J. E., Fielden, P. R., Goddard, N. J., Manz, A., Day, P. J. R., *Lab Chip* 2006, *6*, 474-487.

[64] Gebauer, P., Thormann, W., Boček, P., *Electrophoresis* 1995, *16*, 2039-2050.

[65] Gebauer, P., Křivánková, L., Pantůčková, P., Boček, P., Thormann, W., *Electrophoresis* 2000, *21*, 2797-2808.

[66] Guo, X., Fillmore, T. L., Gao, Y., Tang, K., *Anal. Chem.* 2016, *88*, 4418-4425.

[67] Heemskerk, A. A., Busnel, J.-M., Schoenmaker, B., Derks, R. J., Klychnikov, O., Hensbergen, P. J., Deelder, A. M., Mayboroda, O. A., *Anal. Chem.* 2012, *84*, 4552-4559.

[68] Pattky, M., Barkovits, K., Marcus, K., Weiergräber, O. H., Huhn, C., in: Schmitt-Kopplin, P. (Ed.), *Capillary Electrophoresis: Methods and Protocols*, Springer, New York, NY 2016, pp. 53-75.

[69] Thompson, T. J., Foret, F., Vouros, P., Karger, B. L., *Anal. Chem.* 1993, *65*, 900-906.

[70] Foret, F., Szoko, E., Karger, B. L., *J. Chromatogr. A* 1992, *608*, 3-12.

[71] Stock, L. G., Wildner, S., Regl, C., Gadermaier, G., Huber, C. G., Stutz, H., *Anal. Chem.* 2018, *90*, 11933-11940.

[72] Gysler, J., Helk, B., Dambacher, S., Tjaden, U. R., van der Greef, J., *Pharm. Res.* 1999, *16*, 695-701.

[73] Xia, S., Zhang, L., Qiu, B., Lu, M., Chi, Y., Chen, G., *Rapid Commun. Mass Spectrom.* 2008, *22*, 3719-3726.

[74] Medina-Casanellas, S., Benavente, F., Barbosa, J., Sanz-Nebot, V., *Electrophoresis* 2011, *32*, 1750-1759.

[75] An, Y., Cooper, J. W., Balgley, B. M., Lee, C. S., *Electrophoresis* 2006, *27*, 3599-3608.

[76] Larsson, M., Lutz, E. S. M., *Electrophoresis* 2000, *21*, 2859-2865.

[77] Gao, J., Xu, J., Locascio, L. E., Lee, C. S., *Anal. Chem.* 2001, *73*, 2648-2655.

[78] Wang, Y., Fonslow, B. R., Wong, C. C., Nakorchevsky, A., Yates III, J. R., *Anal. Chem.* 2012, *84*, 8505-8513.

[79] Busnel, J.-M., Schoenmaker, B., Ramautar, R., Carrasco-Pancorbo, A., Ratnayake, C., Feitelson, J. S., Chapman, J. D., Deelder, A. M., Mayboroda, O. A., *Anal. Chem.* 2010, *82*, 9476-9483.

[80] Wang, C., Lee, C. S., Smith, R. D., Tang, K., *Anal. Chem.* 2012, *84*, 10395-10403.

[81] Wang, C., Lee, C. S., Smith, R. D., Tang, K., *Anal. Chem.* 2013, *85*, 7308-7315.

[82] Heemskerk, A. A. M., Wuhrer, M., Busnel, J.-M., Koeleman, C. A. M., Selman, M. H. J., Vidarsson, G., Kapur, R., Schoenmaker, B., Derks, R. J. E., Deelder, A. M., Mayboroda, O. A., *Electrophoresis* 2013, *34*, 383-387.

[83] Gahoual, R., Busnel, J.-M., Beck, A., François, Y.-N., Leize-Wagner, E., *Anal. Chem.* 2014, *86*, 9074-9081.

[84] Gahoual, R., Biacchi, M., Chicher, J., Kuhn, L., Hammann, P., Beck, A., Leize-Wagner, E., François, Y. N., *mAbs* 2014, *6*, 1464-1473.

[85] Ramautar, R., Busnel, J.-M., Deelder, A. M., Mayboroda, O. A., *Anal. Chem.* 2011, *84*, 885-892.

[86] Auriola, S., Thibault, P., Sadovskaya, I., Altman, E., *Electrophoresis* 1998, *19*, 2665-2676.

[87] Lagarrigue, M., Bossée, A., Bégos, A., Delaunay, N., Varenne, A., Gareil, P., Bellier, B., *Electrophoresis* 2009, *30*, 1522-1530.

[88] Křivánková, L., Gebauer, P., Thormann, W., Mosher, R. A., Boček, P., *J. Chromatogr.* 1993, *638*, 119-135.

[89] Křivánková, L., Gebauer, P., Boček, P., *J. Chromatogr. A* 1995, *716*, 35-48.

[90] Beckers, J. L., Boček, P., *Electrophoresis* 2000, *21*, 2747-2767.

[91] Křivánková, L., Boček, P., *J. Chromatogr. B* 1997, *689*, 13-34.

[92] Piešťanský, J., Maráková, K., Veizerová, L., Galba, J., Mikuš, P., *Anal. Chim. Acta* 2014, *826*, 84-93.

[93] Piešťanský, J., Maráková, K., Kovaľ, M., Mikuš, P., *J. Chromatogr. A* 2014, *1358*, 285-292.

[94] Piešťanský, J., Maráková, K., Kovaľ, M., Havránek, E., Mikuš, P., *Electrophoresis* 2015, *36*, 3069-3079.

[95] Piešťanský, J., Maráková, K., Galba, J., Kováč, A., Mikuš, P., *J. Sep. Sci.* 2017, *40*, 2292-2303.

[96] Gysler, J., Mazereeuw, M., Helk, B., Heitzmann, M., Jaehde, U., Schunack, W., Tjaden, U. R., van der Greef, J., *J. Chromatogr. A* 1999, *841*, 63-73.

[97] Bowerbank, C. R., Lee, M. L., *J. Microcolumn Sep.* 2001, *13*, 361-370.

[98] Barmé, I., Bruin, G. J., Paulus, A., Ehrat, M., *Electrophoresis* 1998, *19*, 1445-1451.

[99] Bergmann, J., Jaehde, U., Mazereeuw, M., Tjaden, U. R., Schunack, W., *J. Chromatogr. A* 1996, *734*, 381-389.

[100] Reinhoud, N. J., Tjaden, U. R., van der Greef, J., *J. Chromatogr. A* 1993, *641*, 155-162.

[101] Tia, S., Herr, A. E., *Lab Chip* 2009, *9*, 2524-2536.

[102] Mazereeuw, M., Tjaden, U. R., Reinhoud, N. J., *J. Chromatogr. Sci.* 1995, *33*, 686-697.

[103] Reinhoud, N. J., Tjaden, U. R., van der Greef, J., *J. Chromatogr. A* 1993, *653*, 303-312.

[104] Hernández, M., Aguilar, C., Borrull, F., Calull, M., *J. Chromatogr. B* 2002, *772*, 163-172.

[105] Lamoree, M. H., Reinhoud, N. J., Tjaden, U. R., Niessen, W. M. A., van der Greef, J., *Biol. Mass Spectrom.* 1994, *23*, 339-345.

[106] van der Vlis, E., Mazereeuw, M., Tjaden, U. R., Irth, H., van der Greef, J., *J. Chromatogr. A* 1995, *712*, 227-234.

[107] Ölvecká, E., Kaniansky, D., Pollák, B., Stanislawski, B., *Electrophoresis* 2004, *25*, 3865-3874.

[108] Reinhoud, N. J., Tinke, A. P., Tjaden, U. R., Niessen, W. M. A., van der Greef, J., *J. Chromatogr. A* 1992, *627*, 263-271.

[109] Holloway, C. J., Pingoud, V., *Electrophoresis* 1981, *2*, 127-134.

[110] Kopwillem, A., Merriman, W., Cuddeback, R., Smolka, A., Bier, M., *J. Chromatogr. A* 1976, *118*, 35-46.

[111] Procházková, B., Glovinová, E., Pospíchal, J., *Electrophoresis* 2007, *28*, 2168-2173.

[112] Hirokawa, T., Gojo, T., Kiso, Y., *J. Chromatogr. A* 1986, *369*, 59-81.

[113] Mamunooru, M., Jenkins, R. J., Davis, N. I., Shackman, J. G., *J. Chromatogr. A* 2008, *1202*, 203-211.

[114] Vyas, C. A., Mamunooru, M., Shackman, J. G., *Chromatographia* 2009, *70*, 151-156.

[115] Kaniansky, D., Zelenský, I., *J. Chromatogr. A* 1993, *638*, 225-229.

[116] Kaniansky, D., Madajová, V., Marák, J., Šimuničová, E., Zelenský, I., Zelenská, V., *J. Chromatogr. A* 1987, *390*, 51-60.

[117] Smith, J. T., *Electrophoresis* 1997, *18*, 2377-2392.

[118] Smith, J. T., *Electrophoresis* 1999, *20*, 3078-3083.

[119] Prata, C., Bonnafous, P., Fraysse, N., Treilhou, M., Poinsot, V., Couderc, F., *Electrophoresis* 2001, *22*, 4129-4138.

[120] Poinsot, V., Bayle, C., Couderc, F., *Electrophoresis* 2003, *24*, 4047-4062.

[121] Poinsot, V., Lacroix, M., Maury, D., Chataigne, G., Feurer, B., Couderc, F., *Electrophoresis* 2006, *27*, 176-194.

[122] Poinsot, V., Rodat, A., Gavard, P., Feurer, B., Couderc, F., *Electrophoresis* 2008, *29*, 207-223.

[123] Poinsot, V., Gavard, P., Feurer, B., Couderc, F., *Electrophoresis* 2010, *31*, 105-121.

[124] Poinsot, V., Carpéné, M.-A., Bouajila, J., Gavard, P., Feurer, B., Couderc, F., *Electrophoresis* 2012, *33*, 14-35.

[125] Poinsot, V., Ong-Meang, V., Gavard, P., Couderc, F., *Electrophoresis* 2014, *35*, 50-68.

[126] Poinsot, V., Ong-Meang, V., Gavard, P., Couderc, F., *Electrophoresis* 2016, *37*, 142-161.

[127] Poinsot, V., Ong-Meang, V., Ric, A., Gavard, P., Perquis, L., Couderc, F., *Electrophoresis* 2018, *39*, 190-208.

[128] Stolz, A., Jooß, K., Höcker, O., Römer, J., Schlecht, J., Neusüß, C., *Electrophoresis* 2019, *40*, 79-112.

[129] Martin-Girardeau, A., Renou-Gonnord, M.-F., *J. Chromatogr. B* 2000, *742*, 163-171.

[130] Soga, T., Heiger, D. N., *Anal. Chem.* 2000, *72*, 1236-1241.

[131] Soga, T., Kakazu, Y., Robert, M., Tomita, M., Nishioka, T., *Electrophoresis* 2004, *25*, 1964-1972.

[132] Klampfl, C. W., Ahrer, W., *Electrophoresis* 2001, *22*, 1579-1584.

[133] Rodrigues, K. T., Mekahli, D., Tavares, M. F. M., van Schepdael, A., *Electrophoresis* 2016, *37*, 1039-1047.

[134] Hattori, T., Fukushi, K., *Electrophoresis* 2016, *37*, 267-273.

[135] Okamoto, H., Timerbaev, A. R., Hirokawa, T., *J. Sep. Sci.* 2005, *28*, 522-528.

[136] Davis, N. I., Mamunooru, M., Vyas, C. A., Shackman, J. G., *Anal. Chem.* 2009, *81*, 5452-5459.

[137] Gaš, B., Jaroš, M., Hruška, V., Zusková, I., Štědrý, M., *Lc Gc Europe* 2005, *18*, 282-+.

[138] DIN 32645:2008-11, Chemische Analytik - Nachweis-, Erfassungs- und Bestimmungsgrenze unter Wiederholbedingungen - Begriffe, Verfahren, Auswertung.

[139] Coufal, P., Zuska, J., van de Goor, T., Smith, V., Gaš, B., *Electrophoresis* 2003, *24*, 671-677.

[140] van der Vlis, E., Mazereeuw, M., Tjaden, U. R., Irth, H., van der Greef, J., *J. Chromatogr. A* 1994, *687*, 333-341.

[141] Bellini, M. S., Deyl, Z., Mikšík, I., *Forensic Sci. Int.* 1998, *92*, 185-199.

[142] Kenndler, E., *J. Chromatogr. A* 2014, *1335*, 16-30.

[143] Kenndler, E., *J. Chromatogr. A* 2014, *1335*, 31-41.

[144] Steiner, F., Hassel, M., *Electrophoresis* 2000, *21*, 3994-4016.

[145] Weinberger, R., *Am. Lab.* 2006, *38*, 49-50.

[146] Geiser, L., Veuthey, J. L., *Electrophoresis* 2009, *30*, 36-49.

[147] Kenndler, E., *Electrophoresis* 2009, *30*, S101-S111.

[148] Porras, S. P., Kenndler, E., *J. Chromatogr. A* 2004, *1037*, 455-465.

[149] Sarmini, K., Kenndler, E., *J. Chromatogr. A* 1999, *833*, 245-259.

[150] Valkó, I. E., Sirén, H., Riekkola, M. L., *J. Microcolumn Sep.* 1999, *11*, 199-208.

[151] Masselter, S. M., Zemann, A. J., *Anal. Chem.* 1995, *67*, 1047-1053.

[152] Roy, K. I., Lucy, C. A., *J. Chromatogr. A* 2002, *964*, 213-225.

[153] Sarmini, K., Kenndler, E., *J. Chromatogr. A* 1998, *818*, 209-215.

[154] Sarmini, K., Kenndler, E., *J. Chromatogr. A* 1998, *811*, 201-209.

[155] Sarmini, K., Kenndler, E., *J. Chromatogr. A* 1998, *806*, 325-335.

[156] Cantu, M. D., Hillebrand, S., Carrilho, E., *J. Chromatogr. A* 2005, *1068*, 99-105.

[157] Grob, M., Steiner, F., *Electrophoresis* 2002, *23*, 1853-1861.

[158] Anurukvorakun, O., Suntornsuk, W., Suntornsuk, L., *J. Chromatogr. A* 2006, *1134*, 326-332.

[159] Barthe, L., Ribet, J.-P., Pélissou, M., Degude, M.-J., Fahy, J., Duflos, A., *J. Chromatogr. A* 2002, *968*, 241-250.

[160] Peri-Okonny, U. L., Kenndler, E., Stubbs, R. J., Guzman, N. A., *Electrophoresis* 2003, *24*, 139-150.

[161] Cherkaoui, S., Varesio, E., Christen, P., Veuthey, J. L., *Electrophoresis* 1998, *19*, 2900-2906.

[162] Ahrer, W., Buchberger, W., *Monatsh. Chem.* 2001, *132*, 329-337.

[163] Dong, Y., Chen, X., Hu, Z., *Microchim. Acta* 2006, *154*, 281-286.

[164] Ballash, N., Robertson, E., Sokolowski, M., *Trans. Faraday Soc.* 1970, *66*, 2622-2628.

[165] LeBel, R., Goring, D., *J. Chem. Eng. Data* 1962, *7*, 100-101.

[166] Krishnamoorthy, A. N., Zeman, J., Holm, C., Smiatek, J., *Phys. Chem. Chem. Phys.* 2016, *18*, 31312-31322.

[167] Roses, M., Rafols, C., Bosch, E., *Anal. Chem.* 1993, *65*, 2294-2299.

[168] Yang, L.-J., Yang, X.-Q., Huang, K.-M., Jia, G.-Z., Shang, H., *Int. J. Mol. Sci.* 2009, *10*, 1261-1270.

[169] Pang, F.-M., Seng, C.-E., Teng, T.-T., Ibrahim, M., *J. Mol. Liq.* 2007, *136*, 71-78.

[170] Sato, T., Buchner, R., *J. Chem. Phys.* 2003, *118*, 4606-4613.

[171] Schmitt-Kopplin, P., Fekete, A., in: Schmitt-Kopplin, P. (Ed.), *Capillary Electrophoresis: Methods and Protocols*, Springer, New York, NY 2016, pp. 3-19.

[172] Barthel, J., Gores, H.-J., Schmeer, G., Wachter, R., in: Boschke, F. L. (Ed.), *Physical and Inorganic Chemistry. Topics in Current Chemistry, vol. 111*, Springer, Berlin, Heidelberg 1983, pp. 33-144.

[173] Sarmini, K., Kenndler, E., *J. Biochem. Biophys. Methods* 1999, *38*, 123-137.

[174] Marcus, Y., *The Properties of Solvents,* John Wiley & Sons, Chichester 1998.

[175] Hojo, M., *Pure Appl. Chem.* 2008, *80*, 1539-1560.

[176] Miller, J. L., Shea, D., Khaledi, M. G., *J. Chromatogr. A* 2000, *888*, 251-266.

[177] Kolthoff, I. M., *Pure Appl. Chem.* 1971, *25*, 305-326.

[178] Posch, T. N., Martin, N., Pütz, M., Huhn, C., *Electrophoresis* 2012, *33*, 1557-1566.

[179] Bosch, E., Espinosa, S., Rosés, M., *J. Chromatogr. A* 1998, *824*, 137-146.

[180] Espinosa, S., Bosch, E., Rosés, M., *Anal. Chim. Acta* 2002, *454*, 157-166.

[181] Giesecke, M., Mériguet, G., Hallberg, F., Fang, Y., Stilbs, P., Furó, I., *Phys. Chem. Chem. Phys.* 2015, *17*, 3402-3408.

[182] Porras, S. P., Riekkola, M. L., Kenndler, E., *Electrophoresis* 2003, *24*, 1485-1498.

[183] Shedlovsky, T., Kay, R. L., *J. Phys. Chem.* 1956, *60*, 151-155.

[184] Bacarella, A., Grunwald, E., Marshall, H., Purlee, E. L., *J. Org. Chem.* 1955, *20*, 747-762.

[185] Åkerlöf, G., *J. Am. Chem. Soc.* 1932, *54*, 4125-4139.

[186] Mikhail, S., Kimel, W., *J. Chem. Eng. Data* 1961, *6*, 533-537.

[187] Kiliç, E., Aslan, N., *Microchim. Acta* 2005, *151*, 89-92.

[188] Stehle, S., Braeuer, A. S., *J. Phys. Chem. B* 2019, *123*, 4425-4433.

[189] Moučka, F., Nezbeda, I., *Collect. Czech. Chem. Commun.* 2009, *74*, 559-563.

[190] Soetens, J.-C., Bopp, P. A., *J. Phys. Chem. B* 2015, *119*, 8593-8599.

[191] Popovych, O., Tomkins, R. P. T., *Nonaqueous Solution Chemistry,* John Wiley & Sons, New York, NY 1981.

[192] Lambert, W. J., Middleton, D. L., *Anal. Chem.* 1990, *62*, 1585-1587.

[193] Thredgold, L. D., Ellis, A. V., Lenehan, C. E., *Anal. Methods* 2015, *7*, 1802-1808.

[194] Haunschmidt, M., Buchberger, W., Klampfl, C. W., *J. Chromatogr. A* 2008, *1213*, 88-92.

[195] Haselberg, R., Ratnayake, C. K., de Jong, G. J., Somsen, G. W., *J. Chromatogr. A* 2010, *1217*, 7605-7611.

[196] Gagliardi, L. G., Castells, C. B., Rafols, C., Rosés, M., Bosch, E., *J. Chem. Eng. Data* 2007, *52*, 1103-1107.

[197] Bosch, E., Fonrodona, G., Ràfols, C., Rosés, M., *Anal. Chim. Acta* 1997, *349*, 367-376.

[198] El-Hammamy, N. H., Kawana, A. I., El-Araby, H. A., *J. Chem. Pharm. Res.* 2016, *8*, 693-703.

[199] Raju, K., Manaiah, V., Sethuram, B., Rao, T. N., *Phys. Chem. Liquids* 1990, *22*, 163-167.

[200] Wong, D. B., Sokolowsky, K. P., El-Barghouthi, M. I., Fenn, E. E., Giammanco, C. H., Sturlaugson, A. L., Fayer, M. D., *J. Phys. Chem. B* 2012, *116*, 5479-5490.

[201] Mikšík, I., *J. Sep. Sci.* 2019, *42*, 385-397.

[202] Campbell, J. L., Le Blanc, J. Y., *Bioanalysis* 2011, *3*, 645-657.

[203] Týčová, A., Ledvina, V., Klepárník, K., *Electrophoresis* 2017, *38*, 115-134.

[204] Ramautar, R., Heemskerk, A. A., Hensbergen, P. J., Deelder, A. M., Busnel, J.-M., Mayboroda, O. A., *J. Proteomics* 2012, *75*, 3814-3828.

[205] Williams, B. J., Russell, W. K., Russell, D. H., *Anal. Chem.* 2007, *79*, 3850-3855.

[206] Pattky, M., Nicolardi, S., Santiago-Schübel, B., Sydes, D., van der Burgt, Y. E. M., Klein, A. N., Jiang, N., Mohrlüder, J., Hänel, K., Kutzsche, J., Funke, S. A., Willbold, D., Willbold, S., Huhn, C., *Anal. Bioanal. Chem.* 2015, *407*, 6637-6655.

[207] Erny, G. L., Cifuentes, A., *Electrophoresis* 2007, *28*, 1335-1344.

[208] Faserl, K., Sarg, B., Maurer, V., Lindner, H. H., *J. Chromatogr. A* 2017, *1498*, 215-223.

[209] Heemskerk, A. A. M., Deelder, A. M., Mayboroda, O. A., *Mass Spectrom. Rev.* 2016, *35*, 259-271.

[210] Giansanti, P., Tsiatsiani, L., Low, T. Y., Heck, A. J. R., *Nat. Protoc.* 2016, *11*, 993-1006.

[211] Gennaro, L. A., Salas-Solano, O., Ma, S., *Anal. Biochem.* 2006, *355*, 249-258.

[212] Brownstein, N. C., Guan, X., Mao, Y., Zhang, Q., DiMaggio, P. A., Xia, Q., Zhang, L., Marshall, A. G., Young, N. L., *Rapid Commun. Mass Spectrom.* 2015, *29*, 659-666.

[213] Kalli, A., Håkansson, K., *Mol. Biosyst.* 2010, *6*, 1668-1681.

[214] Giménez, E., Ramos-Hernan, R., Benavente, F., Barbosa, J., Sanz-Nebot, V., *Anal. Chim. Acta* 2012, *709*, 81-90.

[215] Pattky, M., Huhn, C., *Anal. Bioanal. Chem.* 2013, *405*, 225-237.

[216] Taouatas, N., Drugan, M. M., Heck, A. J., Mohammed, S., *Nat. Methods* 2008, *5*, 405-407.

[217] Perkins, D. N., Pappin, D. J., Creasy, D. M., Cottrell, J. S., *Electrophoresis* 1999, *20*, 3551-3567.

[218] Damodaran, S., Wood, T. D., Nagarajan, P., Rabin, R. A., *Geno. Prot. Bioinfo.* 2007, *5*, 152-157.

[219] Fang, X., Wang, W., Yang, L., Chandrasekaran, K., Kristian, T., Balgley, B. M., Lee, C. S., *Electrophoresis* 2008, *29*, 2215-2223.

Abbreviations

ACN	acetonitrile
Ala	alanine
Arg	arginine
Asn	asparagine
Asp	aspartic acid
BGE	background electrolyte
BSA	bovine serum albumin
C^4D	capacitively-coupled contactless conductivity detection
cc-ITP/CE-MS	capillary coupling ITP/CE-MS
CDC	capacitance-to-digital converter detector
CE	capillary electrophoresis
Cys	cysteine
Cys-Cys	cystine
DFA	difluoroacetic acid
DMSO	dimethyl sulfoxide
EOF	electroosmotic flow
ESI	electrospray ionization
EZE	Eigen-Zundel-Eigen flipping mechanism
FA	formic acid
Gln	glutamine
Glu	glutamic acid
Gly	glycine
HAc	acetic acid
His	histidine
HOCE	hydroorganic capillary electrophoresis
i.d.	inner diameter
ICP	inductively-coupled plasma
IEF	isoelectric focusing
Ile	isoleucine
iPrOH	isopropanol
ITP	isotachophoresis
LC	liquid chromatography
LE	leading electrolyte
Leu	leucine
LIF	laser-induced fluorescence

LOD	limit of detection
LOQ	limit of quantification
Lys	lysine
MeOH	methanol
Met	methionine
MOWSE	molecular weight search
MS	mass spectrometry
MS/MS	tandem mass spectrometry
NACE	non-aqueous capillary electrophoresis
NAITP	non-aqueous isotachophoresis
OA	oxalic acid
Phe	phenylalanine
Pro	proline
PVA	polyvinyl alcohol
RSD	relative standard deviation
sc-ITP/CE-MS	single capillary ITP/CE-MS
Ser	serine
SL	sheath liquid
SPE	solid phase extraction
SPME	solid phase microextraction
TE	terminating electrolyte
TFA	trifluoroacetic acid
Thr	threonine
tITP	transient isotachophoresis
TMPA	trimethylpyruvic acid
Trp	tryptophan
Tyr	tyrosine
Val	valine

Appendix

Table A1: Review articles considered.

reference	comments
[14]	review on analytical isotachophoresis 2016-2018
[26]	review on CE-MS coupling, overview on instrumentation, methodology and applications, limited number of MS-compatible CE buffers becomes visible
[7]	review on online sample preconcentration methods for CE-MS, with one chapter dedicated to tITP/ITP
[15]	review on analytical isotachophoresis 2014-2016
[62]	overview on multidimensional capillary electrophoresis, comprehensive 2D, heart-cut 2D, microfluidic 2D approaches
[60]	overview on column coupling techniques in electromigrative separation techniques (also with chromatography)
[61]	overview on multidimensional capillary electrophoresis, description of interface types, comprehensive and heart-cut interfaces, microchips, 3D-CE
[16]	review on analytical isotachophoresis 2012-2014
[17]	review on analytical isotachophoresis 2010-2012
[18]	review on analytical isotachophoresis 2008-2010
[19]	review on analytical isotachophoresis 2006-2008
[59]	review on multidimensional liquid phase separations, theoretical discussion (orthogonality, peak capacity etc.), chapter on ITP/CE
[20]	review on analytical isotachophoresis 2002-2006
[58]	review on tITP/CE in the analysis of small ions from high conductivity matrices
[63]	review on miniaturized isotachophoresis, instrumentation, applications, ITP/CE and tITP
[21]	review on analytical isotachophoresis 2000-2002
[22]	review on analytical isotachophoresis 1997-1999
[23]	review on analytical isotachophoresis 1993-1996

Table A1: cont.

reference	comments
[91]	theoretical discussion of transition from ITP to CE, gradual zone destacking
[64]	theoretical discussion on sample self-stacking as transient ITP, nonselective stacking and sample stacking depending on stacker concentration and concentration differences of sample and BGE
[89]	theoretical discussion on different ITP/CE combinations, practical aspects, basics of destacking from tITP and related zone dispersion
[102]	review on hyphenation of ITP/CE in a single capillary: electrokinetic sample introduction, transient ITP, field amplified focusing in water, counterflow ITP/CE, on capillary reaction ITP/CE, electroextraction ITP/CE
[24]	overview on isotachophoresis equipment development, detection systems and advent of microchip processors

Table A2: Articles on the direct coupling of ITP-MS.

reference	[37]	[32]	[38]
analytes	diclofenac, ibuprofen	salicylic acid, diclofenac, ibuprofen	ibuprofen, diclofenac, salicylic acid, benzoic acid, p-hydroxybenzoic acid
method	ITP-MS	ITP-MS	ITP-MS
capillary	85 cm, 100 µm i.d., fused silica	85 cm, 100 µm i.d., fused silica	85 cm or 105 cm, 100 µm i.d. , fused silica
LE and TE /BGE	LE: 10 mM FA[1], TE: 10 mM propionic acid	(1) LE: 10 mM FA, TE: 10 mM propionic acid, (2) LE: 10 mM FA, 5 mM NH_4^+, TE: 6 mM FA, 4 mM propionic acid, (3) LE: 10 mM FA, 8 mM NH_4^+, TE: 10 mM propionic acid, (4) LE: 10 mM FA, 8 mM NH_4^+, TE: 6 mM FA, 4 mM propionic acid	(1) LE: 8 mM FA, 2 mM propionic acid, 6 mM NH_4^+, TE: 10 mM propionic acid, analytes in 5 mM lactic acid and 8 mM NH_4^+, (2) LE: 9.5 mM FA, 0.5 mM propionic acid, 8 mM NH_4^+, TE: 6 mM propionic acid, 4 mM FA, analytes in 2 mM HAc and 3 mM NH_4^+, (3) LE: 10 mM FA, 8 mM NH_4^+, TE: 7 mM propionic acid, 3 mM FA, analytes in 5 mM lactic acid and 8 mM NH_4^+, (4) LE: 11 mM lactic acid, 11 mM FA, 11 mM NH_4^+, TE:12 mM lactic acid, 8 mM propionic acid, analytes in 2 mM propionic acid, (5) LE: same as (4), TE: 10 mM lactic acid, 10 mM propionic acid, analytes in 2 mM propionic acid
coating	-	-	-
injection	50 mbar·s (15000 mbar·s for real samples)	50 mbar·s	20 or 40 mbar·s
separation conditions	-20 kV	-20 kV	-20 kV
LOD/LOQ	10^{-11} M/10^{-10} M	-	-
linear range	-	-	-
precision	intraday variability of detection times <2 %	intraday variability of detection times <2 %	intraday variability of detection times <2 %
matrix	drinking water, river water	-	-
comments	theoretical discussion on stacking window using FA, lactic acid, propionic acid or HAc[2] as LE or TE, influence of ammonium, comparison with simulations	moving-boundary ITP system with two co-ions, theoretical discussion in stacking windows based on different concentrations of propionic acid, FA and ammonium as counter-ion, comparison with simulations	theoretical discussion of spacer technique in moving-boundary ITP with two co-ions and moving-boundary configuration with two independent ITP systems, comparison with simulations

[1] FA - formic acid, [2] HAc - acetic acid

Table A2: cont.

reference	[34]	[33]	[41]
analytes	tris(hydroxymethyl)aminomethane, histidine, hexamethylene tetramine, ε-aminocaproic acid, thiabendazole	2-hydroxyatrazine, 2-hydroxyterbutylazine	diclofenac, ibuprofen
method	ITP-MS	ITP-MS	ITP-MS
capillary	85 cm, 100 µm i.d., fused silica	100 cm, 100 µm i.d., fused silica	100 cm, 100 µm i.d., fused silica
LE and TE /BGE	(1) LE: 10 mM NH_4^+, 20 mM HAc, TE: 1 mM NH_4^+, 23.54 mM HAc, (2) LE: 10 mM NH_4^+, 10 mM HAc, TE: 2 mM NH_4^+, 13.15 mM HAc, (3) LE: 10 mM NH_4^+, 12 mM HAc, TE: 2 mM NH_4^+, 15.15 mM HAc, (4) LE: 10 mM NH_4^+, 20 mM HAc, TE: 2.5 mM NH_4^+, 22.95 mM HAc, (5) LE: 4 mM NH_4^+, 28 mM HAc, TE: 2.05 mM NH_4^+, 28.77 mM HAc, (6) LE: 4 mM NH_4^+, 20 mM HAc, TE: 0.2 mM NH_4^+, 21.50 mM HAc, (7) LE: 0.8 mM NH_4^+, 0.8 mM HAc, TE: 0.5 mM NH_4^+, 0.92 mM HAc, (8) LE: 10 mM NH_4^+, 20 mM HAc, TE: 20 mM HAc, 0/0.5/1.5 mM NH_4^+, analytes in 5 mM HAc	LE: 10 mM ammonium acetate, TE: 10 mM HAc, 2 mM NH_4^+	LE: 10 mM FA , TE: 10 mM propionic acid
coating	-	-	-
injection	300 mbar·s	10000 mbar·s	15000 mbar·s
separation conditions	+15 kV	+20 kV	-25 kV
LOD/LOQ	10^{-10} M/-	$5 \cdot 10^{-10}$ M/-	$2 \cdot 10^{-12}$ M/$5 \cdot 10^{-12}$ M
linear range	10^{-10}-10^{-6} M	5-200·10^{-10} M	3-25·10^{-10} M 6-50·10^{-12} M (with SPE)
precision	-	detection time RSD 1-3 % peak height RSD 0.4-2.3 % peak area RSD 0.6-3.1 %	migration time RSD 1-2 % peak height RSD 0.4-4 % peak area RSD 0.5-5 %
matrix	orange juice	drinking water, river water	drinking water, river water
comments	leading ion addition to TE to modify stacking window and enhance selectivity of ITP system by concentration adjustment, moving-boundary ITP	addition of leading ion to TE to enhance sensitivity, moving-boundary ITP	offline SPE, free-acid ITP

Table A2: cont.

reference	[35]	[36]	[53]
analytes	angiotensin I, bradykinin, cytochrome c, myoglobin	quaternary phosphonium salts, quaternary ammonium salts, dopamine, epinephrine, lysine, arginine	vitamins, tryptic peptides, thiamine
method	ITP-MS	ITP-MS	ITP/ITP-MS
capillary	100 cm, 50 µm i.d./2,5 m, 100 µm i.d., fused silica	0.6-2.5 m, 100 µm i.d., fused silica	9 cm, 800 µm (preseparation) and 9 cm, 300 µm i.d. (separation), polytetrafluoroethylene
LE and TE /BGE	LE: 10 mM ammonium acetate, pH 4.9, TE: 10 mM alanine, pH 7.1 with BaOH	(1) LE: 1 mM ammonium acetate, TE: 1 mM tetraoctylammonium bromide, (2) LE: 1 mM ammonium acetate, pH 4.8 with hydrochloric acid, TE: as (1)	LE: 10 mM ammonium acetate, pH 7.8, TE: 20 mM HAc, pH 3.5
coating	uncoated/DB-17 bonded and cross-linked	-	-
injection	pressure to 10 cm plug length/64 cm plug length	electrokinetic, +23 kV for 5 min/+35 kV for 30-90 s	syringe, 0.5-10 µL
separation conditions	+32 kV, no pressure/+52 kV, 3 psi	+23 kV/+35 kV	constant current 300 µA (preseparation), 60 µA (separation)
LOD/LOQ	-	approx. 10^{-11} M/-	10^{-10} M
linear range	-	-	-
precision	-	-	migration time and zone length RSD <1 %
matrix	-	-	whole blood
comments	also CE-MS of proteins and polypeptides	first ITP-MS coupling, 50 nL to 10 µL sample volume recommended, process of band separation is shown	large bore capillaries, commercial ITP/ITP instrument connected to MS

Table A2: cont.

reference	[50]	[42]	[43]
analytes	tryptic digest of glucagon	nucleotides	unstable intermediate products from nicotinamide adenine dinucleotide degradation
method	ITP-MS	ITP-MS	ITP-MS
capillary	200 cm, 100 µm i.d., fused silica	80 cm, 50 µm i.d., fused silica	80 cm, 50 µm i.d., fused silica
LE and TE /BGE	LE: 10 mM ammonium acetate, pH 4.9, TE: 10 mM HAc, pH 3.3	LE: 7 mM HCl, 13 mM β-alanine, pH 3.9, TE: 10 mM caproic acid, pH 3.4	LE. 7 mM HCl, 13 mM β-alanine, pH 3.9, TE: 10 mM caproic acid, pH 3.4
coating	DB-17 bonded and cross-linked	-	-
injection	electromigration or hydrodynamic injection by raising inlet 4 cm for 30 s	12000 mbar·s/1200 mbar·s	7830 mbar·s
separation conditions	anionic separation	constant current 1 µA, 20-100 mbar	constant current 1 µA, 150 mbar
LOD/LOQ	-	-	-
linear range	-	-	-
precision	-	-	-
matrix	-	-	-
comments	experiments on uncoated capillaries did not obtain useful results, approx. 25 % of capillary filled with sample, MS/MS experiments were facilitated by stable period of analyte elution from ITP	reversed anionic separation, analyte transport to detector by EOF and pressure, positive ionization for MS, MS/MS for additional structural information	reversed anionic separation, analyte transport to detector by EOF and pressure, positive ionization for MS, monitoring of enzymatic reaction of nicotinamide adenine nucleotide in presence of hydrogen peroxide, MS/MS experiments for additional structural information

Table A2: cont.

reference	[39]	[44]	[40]
analytes	sulfamethazine, sulfamethoxazole, 2,4-dichlorophenol, salicylic acid, inbuprofen	amyloid beta peptides	atenolol, metoprolol, propranolol, sotalol
method	ITP-MS	ITP-MS	ITP-MS
capillary	100 cm, 100 µm i.d., fused silica	100 cm, 100 µm i.d., fused silica	100 cm, 100 µm i.d., fused silica
LE and TE /BGE	(1) LE: 10 mM ammonium acetate, pH 7.00, TE: 10 mM ammonium hydroxide, 2 mM HAc, pH 9.83, (1a) LE and TE with 0.2 mM Carb[3], pH 6.58 and 9.77, (2) LE: 10 mM HAc, 10 mM triethylamine, pH 7.77 , TE: 10 mM triethylamine, 2/4/6 mM HAc, pH 11.20/10.92/10.61, (2a) LE and TE with 0.2 mM Carb, pH 6.63 and 11.16/10.88/10.56, (3) LE: 10 mM HAc, 8 mM ethanolamine, pH 5.36, TE: 10 mM ethanolamine, 4 mM HAc, pH 9.67, (3a) LE and TE with 0.2 mM Carb, pH 5.35 and 9.62	LE: 80 mM acetic acid, 200 mM ammonium hydroxide, pH 9.55, TE: 0.175 % ammonium hydroxide, samples prepared in TE	LE: 10 mM triethylamine, 6 mM HAc, pH 10.6, TE: 10 mM triethanolamine, 10 mM HAc
coating	-	-	-
injection	hydrodynamic, 200 mbar·s or 5000·s mbar	hydrodynamic, 10000 mbar·s	hydrodynamic, 625/800 mbar·s, 400 mbar·s (samples in matrix)
separation conditions	constant voltage, -20 kV	constant current 12 µA (10 µA real samples)	+20 kV
LOD/LOQ	LOQ approx. $7 \cdot 10^{-10}$ M	LOD 0.04 nM	LOQ below 10^{-9} M
linear range	-	0.06-25 nM	10^{-9}-10^{-7} M sotalol in matrix
precision	migration time RSD 1-3 %	migration time RSD 3.6 % (intra-day), 4.7% (inter-day), peak height RSD 4.3-5.3% (intra-day), 5.3-6.3 % (inter-day)	sotalol in matrix: migration time RSD 1-3 %, peak hight RSD 0.4-3 %, peak area RSD 0.5-4 %
matrix	drinking and river water spiked with analytes	cerebrospinal fluid	dried blood spots (for sotalol analysis)
comments	reversed anionic separation, analyte transport to MS by EOF and ESI suction, negative ionization in ESI, OH^- as terminating ion, moving boundary ITP, comparison of simulation and experimental data	35 % of capillary volume filled with sample, reversed anionic ITP, positive ionization in ESI, OH^- as terminating ion, analytes transported to MS by EOF and suction of ESI	cationic ITP at medium alkaline pH for analysis of medium strong bases, simulation of stacking windows and separations, direct injection of dried blood spot extracts, determination of sotalol in matrix in 7 min

[3] *Carb - carbonic acid*

Table A3: Articles on transient ITP/CE-MS with details, tTE = transient terminating electrolyte, tLE = transient leading electrolyte.

reference	[219]	[81]	[75]
analytes	protein/peptide mixtures from synaptic mitochondria	bradykinin, angiotensin I, neurotensin, fibrinopeptide, substance P, kemptide, leu-enkephalin, angiotensin II, melittin, renin	cytochrome c, ovalbumin
method	tITP/CE fractionation for nano-RPLC-MS/MS	tITP/CE-MS	tITP/CE-MS
capillary	80 cm, 100 µm i.d. and 50 µm i.d., fused silica	95 cm, 100 µm i.d./95 cm, 30 µm i.d. fused silica	60 cm, 100 µm i.d., fused silica
LE and TE /BGE	tLE: 2 % pharmalyte in sample, tTE: H^+, BGE: 0.1 M HAc, pH 2.8	LE: 25 mM ammonium acetate, pH 4, samples diluted in LE, BGE: 0.1 M HAc in H_2O/MeOH[4] 9/1	tLE: 30 mM ammonium acetate in sample, BGE: 10 mM HAc, pH 3.0
coating	hydroxypropyl cellulose	hydroxypropyl cellulose	hydroxypropyl cellulose
injection	hydrodynamic	hydrodynamic, 15 psi, different injection times	hydrodynamic, 40 cm sample plug
separation conditions	+24 kV	+30 kV, 1-3 psi	+21 kV
LOD/LOQ	-	-/1-50·10^{-11} M	0.1 M/-
linear range	-	0.01-500·10^{-9} M	-
precision	-	variation coefficient peak area <22 %, variation coefficient migration time <10 %	-
matrix	mouse brain synaptic mitochondria	-	-
comments	sampling of 20 enriched peptide fractions for nano-RPLC-MS/MS, coupling via microtiter plate	sheathless interface to MS, quantification by transition in triple quadrupole-MS	MS/MS, tryptic digest of proteins, mixtures of ovalbumin peptides and cytochrome c peptides in ratios 1/1. to 1/500000, low-abundance ovalbumin peptides detectable

[4] *MeOH - methanol*

Table A3: cont.

reference	[86]	[79]	[83]
analytes	oligosaccharides	tryptic peptides from BSA and *Escherichia coli*	tryptic peptides from monoclonal antibodies
method	tITP/CE-MS	tITP/CE-MS	tITP/CE-MS
capillary	90 cm, 50 µm i.d., fused silica	88.5 cm, 30 µm i.d., fused silica	100 cm, 30 µm i.d., fused silica
LE and TE /BGE	tLE: 50 mM trimethylamine formate, pH 4.5, tTE: 50 mM MES, pH 4.5, BGE: 50 mM triethylamine formate, pH 4.5, samples dissolved in LE	tLE: 10 % ammonium acetate, sample diluted in LE, BGE: 10 % HAc	tLE: 50 mM ammonium acetate, pH 4.4, sample diluted in LE, BGE: 10 % HAc, pH 2.2
coating	-	-	polyacrylamide
injection	up to 10 µL (50 % of capillary) sample plug	hydrodynamic, 15 psi for 90 s	hydrodynamic, 24600 mbar·s
separation conditions	-30 kV separation, -26 kV and 50 mbar during focusing process	+30 kV, 2 psi during stacking process	+20 kV
LOD/LOQ	-	$<10^{-9}$ M/-	-
linear range	-	-	-
precision	-	-	-
matrix	Pseudomonas aeruginosa	Escherichia coli	-
comments	method development for possible structural characterization of lipopolysaccharides, 10- to 50-fold sensitivity improvement by tITP	sheathless MS interface, tITP improves LOD 10- to 86-fold, but decreases peak capacity of separation	sheathless MS interface, determination of amino acid sequences, identification of posttranslational modifications

Table A3: cont.

reference	[84]	[77]	[82]
analytes	tryptic peptides from monoclonal antibodies	tryptic peptides of cytochrome c	IgG
method	tITP/CE-MS	tITP/CE-MS	tITP/CE-MS
capillary	100 cm, 30 µm i.d., fused silica	25 cm/50 cm, 50 µm i.d., fused silica	100 cm, 30 µm i.d., fused silica (?)
LE and TE /BGE	tLE: 50 mM ammonium acetate, pH 4.4, sample diluted in LE, BGE: 10 % HAc, pH 2.2	tLE: 5 mM ammonium acetate in sample, BGE: 0.1 M HAc, pH 3	tLE: 100 mM ammonium acetate, pH 4, sample diluted in LE, BGE: 10 % HAc
coating	polyacrylamide	-	polyacrylamide
injection	hydrodynamic, 24600 mbar·s	syringe pump, 0.1 µL/min, 300 nL sample plug	hydrodynamic, 37 % of capillary
separation conditions	+20 kV	+15 kV	+25 kV, 1 psi
LOD/LOQ	-	-	$8 \cdot 10^{-11}$ M/-
linear range	-	-	4-4000 ng/mL
precision	-	-	interday RSD of intensity1.64-43.13 %
matrix	-	-	human plasma
comments	sheathless MS interface, same methods as in [83] but focus on biological aspects	online tryptic protein digest	glycosylation profiling of IgG tryptic digest, 40-fold increase in sensitivity by tITP, sheathless interface to MS

Table A3: cont.

reference	[87]	[76]	[74]
analytes	alkyl methylphosphonic acids	tryptic peptides of cytochrome c, melagatran, substance P, calcitonin gene-related peptide	opioid peptides
method	tITP/CE-MS	tITP/CE-MS	SPE-tITP/CE-MS
capillary	90 cm, 50 µm i.d., fused silica	85/100 cm, 50 µm i.d., 65 cm, 75 µm i.d., fused silica	72 cm, 75 µm i.d., fused silica
LE and TE /BGE	tTE: 200 mM glycine, pH 10 with ammonium hydroxide in 35:65 MeOH/H_2O, BGE: 30/50 mM HAc, pH 8.8 with ammonium hydroxide, served as tLE	tLE: 10 mM ammonium acetate added to samples, (1) BGE: 150 mM HAc, 55 mM FA, (2) BGE: 20 mM ε-aminocaproic acid/HAc, pH 4	tLE: 0.1 % ammonia, tTE: 0.1 % HAc, BGE: 50 mM HAc, 50 mM FA, pH 3.5 with ammonia
coating	-	polyacrylamide	-
injection	hydrodynamic, 12500 mbar·s TE, 10000 mbar·s sample	hydrodynamic, 24000 mbar·s (tryptic digest), 30000 mbar·s (melagatran), 4500 mbar·s (other peptides)	hydrodynamic, approx. 60 µL into SPE cartridge
separation conditions	+20 kV	+26 kV, then 500 mbar	+17 kV
LOD/LOQ	$4\text{-}70 \cdot 10^{-6}$ M (soil) $4.5\text{-}75 \cdot 10^{-6}$ M (urine)/	$6 \cdot 10^{-6}$ M	5-50 ng/mL (0.01-0.1 ng/mL with SPE)/
linear range	-	-	0.01-1 ng/mL/0.1-10 ng/mL
precision	migration time RSD 1.90-2.09 % (soil)/ 1.79-1.87 % (urine)	coefficients of variation 2-12 %	RSD migration times 0.4-1 % (7-10 % with SPE), RSD peak area 3-12 % (11-13 % with SPE)
matrix	soil samples, rat urine	rat brain tissue	human plasma
comments	40-fold sensitivity enhancement by tITP, counter-EOF separation (TE injected before sample injection)	also quantification	online SPE, LODs 5000-fold better than in CE-MS

Table A3: cont.

reference	[73]	[69]	[72]
analytes	peptide hormones	proteins	human interleukin-6
method	tITP/CE-MS	tITP/CE-MS	tITP/CE-MS
capillary	104 cm, 50 µm i.d., fused silica	50 cm, 75 µm i.d., fused silica	80 cm, 75 µm i.d., fused silica
LE and TE /BGE	tLE: 50 mM ammonium acetate, pH 4.8, BGE: 50 mM HAc, pH 3.1, served as tTE, sample in 0.95 mM HAc	tLE: 10 mM ammonium acetate, pH 5, tTE: 1 mM HAc, BGE: 10 mM 6-aminohexanoic acid, pH 4.4 with glacial HAc, samples diluted in tLE	LE: 20 mM ammonium acetate, pH 4.2, TE: 10 mM HAc, sample dissolved in TE, LE used as BGE (L-S-L)
coating	-	polyacrylamide	polyacrylamide
injection	hydrodynamic 3000 mbar·s (LE), electrokinetic 28 kV, 40-300 s (sample)	siphon injection, inlet vial elevation 20 cm for 10-150 s (50-750 nL)	hydrodynamic, 500 nL
separation conditions	+25 kV	6 µA during tITP focusing, +18 kV during separation	+7 kV, 20 min for ITP, +30 kV for separation
LOD/LOQ	$10\text{-}50 \cdot 10^{-9}$ M	approx. 10^{-7} M/-	$7 \cdot 10^{-13}$ mol absolute LOD/-
linear range	depending on analyte 0.025/0.75-1.0 µmol/L	-	-
precision	intraday: RSD migration times 0.46-0.95 %, RSD peak heights 3.4-4.8 %, interday: RSD migration times 3.0-3.3 %, RSD peak heights 8.7-10.7 %	-	-
matrix	rat hypothalamus tissue	-	-
comments	maximal sensitivity enhancement 230-fold, peptide detection in submicromolar concentration range	concentration detection limits decreased 100-fold compared to CE-MS	nine different artifacts of interleukin-6 resolved, orthogonal separation principle to RPLC-MS

Table A3: cont.

reference	[66]	[78]	[67]
analytes	peptides	tryptically digested proteins	phosphopeptides
method	tITP/CE-MS	SPME[4]-tITP/CE-MS	tITP/CE-MS
capillary	100 cm, 30 µm i.d., fused silica	90 cm, 30 µm i.d., fused silica	100 cm, 30 µm i.d., fused silica
LE and TE /BGE	tLE: 25 mM ammonium acetate, pH 4, BGE: 0.1 M HAc in 9/1 (v/v) water/MeOH, sample dissolved in tLE	tLE: 50 mM ammonium acetate, different amounts MeOH and iPrOH (SPME[5] elution buffer), BGE: 95 mM HAc, 5 % MeOH, pH 3.1	tLE: 25-100 mM ammonium acetate pH 4, BGE: 10 % HAc
coating	-	polyethyleneimine	uncoated for model analytes; polyacrylamide for samples
injection	hydrodynamic, 5 psi, 28.4-227.2 nL	hydrodynamic, 75 psi pressure, injection onto SPME column	hydrodynamic, 250 nL injection volume (37 % of capillary volume)
separation conditions	+30 kV, 1 to 3 psi pressure	-30 kV	+25 kV, 0.8 psi pressure
LOD/LOQ	LOQ ca. 0.025 nM (Kemptide)	-	-
linear range	four orders of magnitude	-	-
precision	kemptide: RSD migration time 0.2-1.8 %, RSD peak area 5-25 %	-	-
matrix	tryptic BSA digest	*Pyrococcus furiosus* tryptic digest	dry bovine milk powder tryptic digest
comments	new sheathless MS interface for tITP/CE-MS, pressure needed during separation for nanoESI spray generation	direct comparison with nLC-MS, online SPME, transient ITP induced by SPME elution buffer, improved S/N in comparison to CE-MS and nLC-MS, MS/MS	comparison with nLC-MS

[5] *SPME - solid phase microextraction*

Table A3: cont.

reference	[85]	[80]	[70]
analytes	urinary metabolites	peptides	proteins
method	tITP/CE-MS	tITP/CE-MS	tITP/CE
capillary	100 cm, 30 µm i.d. (sheathless interface), 100 cm, 50 µm i.d. (sheath liquid interface), both fused silica	88 cm, 75 µm i.d.	27 cm/47 cm, 75 µm i.d., fused silica
LE and TE /BGE	tLE: 90 mM ammonium acetate, pH 4, BGE: 10 % HAc, pH 2.2, samples dissolved in tLE	tLE: 25 mM ammonium acetate, pH 4, BGE: 0.1 M HAc/MeOH (9/1)	tTE: 10 mM HAc, BGE: 20 mM triethylamine pH 4.4 with HAc
coating	-	hydroxypropyl cellulose	linear polyacrylamide
injection	hydrodynamic, injection volume approx. 100 nL	hydrodynamic, approx. 1 µL injection volume	pressure, up to 1 µL
separation conditions	+30 kV, DMSO as EOF marker	+27 kV	22 µA (+8.2 kV)
LOD/LOQ	LOD 0.6-24 nM	LOQs below 50 pM,	nanomolar
linear range	-	4 orders of magnitude, 50 pM to 500 nM (angiotensin II), 50 pM to 100 nM (kemptide)	-
precision	RSD migration times < 2 %, RSD peak areas < 15 %	RSD migration times < 5 %, CV peak areas < 24 %	RSD migration times better than 0.5 %
matrix	human urine	BSA tryptic digest	-
comments	tITP improves sensitivity by up to two orders of magnitude, comparison sheathless vs. sheath liquid ESI interface, improved sensitivity with sheathless interface, tITP improves LODs and increases number of detected metabolite features in urine	sheathless interface for tITP/CE-MS, tITP increases analyte sensitivity 4-fold while peak width remains the same, ion focusing time increases with length of sample plug, LOQs approx. 30 times lower with tITP	30-fold higher volume injected, focusing of proteins in tITP as perfect starting condition for CE, ITP focusing time does not significantly increase measurement time, also possible with ammonium as transient leader, column-coupling ITP/CE presented as well

Table A3: cont.

reference	[65]	[71]
analytes	small ions	recombinant pollen allergen of mugwort
method	tITP/CE	
capillary	37 cm, 100 µm i.d., fused silica or 47 cm, 100 µm i.d., coated fused silica	
LE and TE /BGE	varying	tLE: 125 mM ammonium formate, BGE: 1 M FA, pH 1.80, sample diluted in tLE
coating	linear polyacrylamide	-
injection	hydrodynamic	hydrodynamic, 17250 mbar·s
separation conditions	varying	+25 kV
LOD/LOQ	-	-
linear range	-	-
precision	-	-
matrix	-	-
comments	theoretical discussion on transient ITP in samples containing multiple major coionic components, macrocomponent faster than analyte acts as stacker, macrocomponent slower than analyte but faster than BGE can have destacking effects, critical value of concentration ratio of both bulk components decides if stacking happens	monitoring molecular processes of recombinant protein under thermal stress via tITP/CE-MS, virtual zero EOF due to low BGE pH, increased injection volume enabled by tITP/CE of factor 5 compared to CE, preconcentration of low-abundant species

Table A4: Articles on two-dimensional coupling of ITP and CE-MS, either in a single capillary or a capillary coupling format.

reference	[105]	[106]	[51]
analytes	clenbuterol and analogues, β-antagonists	clenbuterol, salbutamol, terbutaline, fenoterol	angiotensin peptides
method	single capillary ITP/CE-MS	single capillary EE-ITP/CE-MS	ITP/CE-MS
capillary	74 cm, 100 µm i.d., fused silica	70 cm, 100 µm i.d., fused silica	ITP: 20 cm (15 cm L_{eff}), 200 µm i.d., CE: 20 cm, 50 µm i.d., both fused silica
LE and TE /BGE	LE: 50 mM ammonium acetate, pH 4.8, MeOH (1/4 v/v), TE: 50 mM β-alanine, pH 4.8 with HAc, MeOH (1/4 v/v) BGE: same as LE (L-S-L), samples dissolved in LE	LE: 50 mM ammonium acetate, pH 5, with HAc solution - MeOH (20/80 v/v), TE: 12 mM β-alanine, pH 5 with HAc solution - MeOH (85/15 v/v), BGE: same as LE (L-S-L)	LE: 10 mM triethylamine, TE: 10 mM HAc, BGE: same as LE (L-S-L)
coating	-	-	both dimensions: polyvinyl alcohol
injection	hydrodynamic	extraction from 300 µL sample by EE	hydrodynamic from 10 µL sample loop four-port valve
separation conditions	+5 kV for 600 s and backpressure by height difference during ITP to keep sample zone fixed, +20 kV for separation	EE and ITP at +9-15 kV, counterflow 8-50 mbar pressure, +21 kV for separation	LE counterflow, +24 kV for initial ITP focusing (30 min), then +10 kV for subsequent steps
LOD/LOQ	10^{-7} M/-	$2\text{-}5 \cdot 10^{-9}$ M/-	approx. 10^{-7} M
linear range	-	-	-
precision	-	-	-
matrix	calf urine	-	-
comments	real samples need clean up to remove salts which considerably increases focusing time	online liquid-liquid electroextraction, ITP performed simultaneously with EE, low recoveries (4-6 %), 200-fold sensitivity enhancement compared to CE-MS	quartz tee as bifurcation point, transition of last two zones to CE peaks probably not complete, detection limit improvement approx. two orders of magnitude

Table A4: cont.

reference	[92]	[93]	[94]
analytes	varenicline and 2-hydroxy-varenicline	pheniramine, phenylephrine, paracetamol	pheniramine
method	ITP/CE-MS	ITP/CE-MS	ITP/chiral-CE-MS
capillary	ITP: 9 cm, 800 µm i.d., CE: 16 cm, 300 µm i.d., both polytetrafluoroethylene	ITP: 9 cm, 800 µm i.d., CE: 16 cm, 300 µm i.d., both polytetrafluoroethylene	ITP: 9 cm, 800 µm i.d., CE: 16 cm, 300 µm i.d., both polytetrafluoroethylene
LE and TE /BGE	LE: 10 mM ammonium acetate, pH 4.5, TE: 10 mM HAc, pH 3.1, BGE: same as TE (T-S-T)	LE: 10 mM ammonium acetate, pH 4.5, TE: 10 mM HAc, pH 3.1 BGE: same as TE (T-S-T)	LE: 10 mM ammonium acetate, pH 4.75, TE: 5 mM ε-aminocaproic acid, 5 mM HAc, pH 4.5 BGE: 25 mM ε-aminocaproic acid, 25 mM HAc, pH 4.5, 5 mg/mL carboxyethyl-β-cyclodextrin
coating	-	-	dynamic coating in BGE for CE dimension: 0.05 % methyl-hydroxyethyl cellulose (w/v)
injection	syringe injection, 1-10 µL	syringe injection, 10 µL	syringe injection, 1-10 µL
separation conditions	constant current, 300 µA for ITP, 40 µA for CE	constant current, 300 µA for ITP, 40 µA for CE	constant current, 300 µA for ITP, 60 µA for CE
LOD/LOQ	44.12-51,72 pg/mL / 144.2-154.6 pg/mL	57.1-181.3 pg/mL / 190.3-604.4 pg/mL	52.8-85.2 pg/mL / 0.10-0.15 ng/mL
linear range	-	-	-
precision	RSD migration times 0.89-1.57 %, RSD peak areas 5.37-6.29 %	RSD migration times 0.63-1.46 %, RSD peak areas 3.51-7.76 %	intraday RSD 6.37-7.68 %, interday RSD 10.01-14.20 %
matrix	human urine	human urine	human urine
comments	MS/MS, higher injection volume seems to increase repeatability, excellent selectivity of method, better than ITP/ITP as BGE is more compatible with ESI	MS/MS, paracetamol was not detectable in hydrodynamically closed setup, elimination of major urine matrix components	non-volatile buffer constituents can be used in CE-MS, but additional demands for MS maintenance, chiral separation after ITP preconcentration, heart cutting

Table A4: cont.

reference	[2]	[52]	[108]
analytes	proteinogenic amino acids	human angiotensin peptides	anthracyclines
method	(1) ITP/CE-MS, (2) ITP-MS	(1) ITP/CE-MS, (2) ITP-MS	ITP/CE-MS
capillary	(1) ITP: 70 cm, 100 µm i.d., CE: 70 cm, 50 µm i.d., both fused silica, bifurcation point at 35 cm each, (2) 60 cm, 100 µm i.d., fused silica	ITP: 20 cm, 100 µm i.d., CE: 30 cm, 50 µm i.d., side channel: 40 cm, 50 µm i.d., all fused silica	ITP: 15 cm, 320 µm i.d., PTFE, CE: 70 cm, 40 µm i.d., fused silica
LE and TE /BGE	(1) LE: 10 mM imidazole, 25 mM oxalic acid, 80 % DMSO, TE: 10 mM taurine, 15 mM oxalic acid, 80 % DMSO, BGE: 20 mM oxalic acid, 20 % iPrOH, (2) LE: 10 mM imidazole, 35 mM TFA, 100 % DMSO, TE: 10 mM taurine, 20 mM TFA, 100 % DMSO / LE(1), TE(1)	LE: 10 mM ammonium acetate, pH 4.5, TE: 10 mM HAc, BGE: same as LE (L-S-L)	LE: 10 mM sodium phosphate pH 7.2 in 60 % MeOH, TE: 10 mM histidine pH 7.2 in 60 % MeOH, BGE: same as LE (L-S-L)
coating	-	both dimensions and glass chip interface: LN coating	-
injection	(1) hydrodynamic, 700 mbar·s, (2) hydrodynamic, 250 mbar·s	hydrodynamic, 250 mbar·s	ITP: syringe injection, 5 µL, CE: electrokinetic transfer 6 kV for 6 s
separation conditions	(1) +30 kV for ITP, +15 kV for CE, (2) +30 kV	+14 kV	ITP: constant current, 60 µA, CE: constant voltage, 20 kV
LOD/LOQ	-	-	-
linear range	-	-	-
precision	-	-	-
matrix	-	-	-
comments	non-aqueous ITP, coupling directly to MS or to CE-MS, microfluidic glass chip interface, overall analysis time approx. 24 min, CE-MS separation not complete	comparison of polyether ether ketone t-junction and microfluidic glass chip interface for column coupling, hybrid approach between microfluidic chips and commercial equipment	intermediate absorbance detection, CE capillary inserted into ITP capillary, part of ITP zone electrokinetically transferred into CE capillary, then flushing of ITP capillary during CE-MS analysis, improvement in LODs at least by a factor of 200

Table A5: Compositions of all BGEs used in this work, the electric current measured in blank measurements, calculated electroosmotic flow values μ_{EOF} and relative standard deviations (RSD, n = 66) of μ_{EOF}.

organic solvent	solvent content in V-%	$V_{solvent}$ in mL	V_{H2O} in mL	V_{HAc} in mL	current in µA	μ_{EOF} in 10^{-4} $cm^2V^{-1}s^{-1}$	$RSD_{\mu EOF}$ in %
-	0	0	8.68	1.32	26.1	1.03	1.8
MeOH	10	1.0	7.68	1.32	19.7	1.20	5.7
	20	2.0	6.68		13.6	1.06	6.1
	30	3.0	5.68		9.0	0.84	2.2
	40	4.0	4.68		6.1	0.91	2.4
	50	5.0	3.68		3.8	0.70	6.9
iPrOH	10	1.0	7.68	1.32	17.2	0.66	4.1
	20	2.0	6.68		11.3	0.50	2.5
	30	3.0	5.68		7.1	0.33	5.6
ACN	10	1.0	7.68	1.32	17.6	0.82	8.3
	20	2.0	6.68		11.5	0.94	2.3
	30	3.0	5.68		7.6	1.35	1.8
DMSO	10	1.0	7.68	1.32	17.4	0.50	7.9
	20	2.0	6.68		10.8	0.37	3.4
	30	3.0	5.68		5.8	0.42	10.1

Table A6: Categorization, isoelectric points pI, calculated effective electrophoretic mobilities μ_{eff} in purely aqueous BGE and relative standard deviations (RSD, n = 3) of μ_{eff} of all analytes used in this study.

analyte	abbreviation	category	isoelectric point pI	μ_{eff} in 10^{-4} $cm^2V^{-1}s^{-1}$	RSD in %
aspartic acid	Asp	acidic	2.85	1.03	0.49
glutamic acid	Glu	acidic	3.22	1.25	0.31
cysteine	Cys	polar	5.05	1.08	0.11
cystine	Cys-Cys	polar	5.24	1.08	0.60
asparagine	Asn	polar	5.41	1.31	0.10
threonine	Thr	polar	5.60	1.34	0.06
tryptophan	Trp	nonpolar	5.64	1.24	1.44
glutamine	Gln	polar	5.65	1.28	0.37
tyrosine	Tyr	polar	5.66	1.17	0.08
serine	Ser	polar	5.68	1.48	0.12
methionine	Met	nonpolar	5.74	1.31	0.23
phenylalanine	Phe	nonpolar	5.84	1.20	0.22
isoleucine	Ile	nonpolar	5.94	1.57	0.06
valine	Val	nonpolar	5.96	1.59	0.38
glycine	Gly	polar	5.97	2.12	0.44
leucine	Leu	nonpolar	5.98	1.53	0.11
alanine	Ala	nonpolar	6.10	1.91	0.15
proline	Pro	nonpolar	6.30	1.18	0.57
histidine	His	basic	7.47	2.94	0.25
lysine	Lys	basic	9.59	3.17	0.13
arginine	Arg	basic	11.76	3.02	0.11

Table A7: Calculated effective electrophoretic mobilities μ_{eff} of all analytes and relative standard deviations (RSD, n = 3) of μ_{eff} in MeOH-containing BGEs. For BGE compositions, compare Table A5, for further information on analytes, compare Table A6.

	10 % MeOH		**20 % MeOH**		**30 % MeOH**		**40 % MeOH**		**50 % MeOH**	
	μ_{eff} in 10^{-4} $cm^2 \cdot V^{-1}s^{-1}$	**RSD in %**	**μ_{eff} in 10^{-4} $cm^2 \cdot V^{-1}s^{-1}$**	**RSD in %**	**μ_{eff} in 10^{-4} $cm^2 \cdot V^{-1}s^{-1}$**	**RSD in %**	**μ_{eff} in 10^{-4} $cm^2 \cdot V^{-1}s^{-1}$**	**RSD in %**	**μ_{eff} in10^{-4} $cm^2 \cdot V^{-1}s^{-1}$**	**RSD in %**
Asp	0.92	0.11	0.83	0.18	0.80	0.30	0.77	0.08	0.85	3.84
Glu	1.11	0.30	0.98	0.20	0.91	1.22	0.86	0.24	0.96	0.12
Cys	0.93	0.32	0.85	0.47	0.81	0.16	0.78	0.35	0.88	3.86
Cys-Cys	0.92	0.20	0.79	0.13	0.73	0.34	0.68	0.68	0.74	0.93
Asn	1.15	0.57	1.02	0.48	0.97	0.03	0.89	0.40	0.96	0.04
Thr	1.19	0.93	1.06	0.10	1.01	0.15	0.94	0.22	1.03	0.60
Trp	1.15	0.26	1.00	0.10	0.95	0.11	0.89	0.33	0.97	0.55
Gln	1.12	0.60	0.98	0.33	0.93	0.27	0.86	0.26	0.93	0.18
Tyr	1.03	0.18	0.92	0.39	0.86	0.21	0.80	0.13	0.89	1.70
Ser	1.30	0.32	1.15	0.83	1.08	0.03	1.00	0.33	1.08	0.60
Met	1.17	0.82	1.06	0.48	1.00	0.14	0.94	0.14	1.06	2.51
Phe	1.09	0.25	0.97	0.39	0.92	0.21	0.87	0.42	0.98	1.80
Ile	1.44	0.88	1.28	0.23	1.23	0.06	1.15	0.38	1.24	0.29
Val	1.45	0.34	1.29	0.43	1.23	0.11	1.15	0.32	1.24	0.13
Gly	1.84	0.64	1.61	0.84	1.47	0.42	1.35	0.66	1.41	2.03
Leu	1.37	0.84	1.24	0.08	1.19	0.12	1.11	0.12	1.20	0.07
Ala	1.68	0.14	1.50	0.61	1.39	0.04	1.29	0.34	1.38	0.47
Pro	1.03	0.19	0.93	0.69	0.88	0.09	0.83	0.23	0.91	0.62
His	2.71	0.56	2.25	0.87	1.95	0.24	1.68	0.34	1.67	1.67
Lys	2.87	0.31	2.36	0.22	2.08	0.41	1.82	0.29	1.83	0.14
Arg	2.71	0.22	2.23	0.21	1.96	0.29	1.71	0.09	1.70	0.07

Table A8: Calculated effective electrophoretic mobilities μ_{eff} of all analytes and relative standard deviations (RSD, n = 3) of μ_{eff} in iPrOH-containing BGEs. For BGE compositions, compare Table A5, for further information on analytes, compare Table A6.

	10 % iPrOH		**20 % iPrOH**		**30 % iPrOH**	
	μ_{eff} in 10^{-4} $cm^2V^{-1}s^{-1}$	**RSD in %**	**μ_{eff} in 10^{-4} $cm^2V^{-1}s^{-1}$**	**RSD in %**	**μ_{eff} in 10^{-4} $cm^2V^{-1}s^{-1}$**	**RSD in %**
Asp	0.86	0.14	0.63	0.16	0.50	0.60
Glu	1.03	0.20	0.73	0.10	0.59	0.32
Cys	0.88	0.18	0.62	0.12	0.48	0.46
Cys-Cys	0.88	0.22	0.62	0.22	0.48	1.07
Asn	1.10	0.21	0.79	0.08	0.62	0.40
Thr	1.12	0.15	0.81	0.12	0.64	0.39
Trp	0.85	0.42	0.75	0.18	0.51	1.31
Gln	1.05	0.13	0.76	0.15	0.60	1.43
Tyr	0.96	0.21	0.69	0.08	0.56	0.39
Ser	1.23	0.06	0.89	0.22	0.70	0.19
Met	1.10	0.15	0.81	0.12	0.65	0.29
Phe	1.02	0.13	0.74	0.25	0.60	0.27
Ile	1.32	0.10	0.98	0.49	0.80	0.31
Val	1.34	0.15	0.99	0.32	0.81	0.77
Gly	1.76	0.02	1.26	0.13	0.99	0.48
Leu	1.28	0.53	0.95	0.15	0.78	0.27
Ala	1.59	0.27	1.17	0.33	0.93	0.28
Pro	0.95	0.00	0.70	0.25	0.56	0.51
His	2.39	0.26	1.70	0.40	1.31	0.33
Lys	2.61	0.08	1.84	0.37	1.42	0.21
Arg	2.46	0.29	1.73	0.21	1.33	0.21

Table A9: Calculated effective electrophoretic mobilities μ_{eff} of all analytes and relative standard deviations (RSD, n = 3) of μ_{eff} in ACN-containing BGEs. For BGE compositions, compare Table A5, for further information on analytes, compare Table A6.

	10 % ACN		**20 % ACN**		**30 % ACN**	
	μ_{eff} in 10^{-4} $cm^2V^{-1}s^{-1}$	**RSD in %**	**μ_{eff} in 10^{-4} $cm^2V^{-1}s^{-1}$**	**RSD in %**	**μ_{eff} in 10^{-4} $cm^2V^{-1}s^{-1}$**	**RSD in %**
Asp	1.02	0.01	1.01	0.15	1.04	0.11
Glu	1.21	0.16	1.20	0.22	1.23	0.50
Cys	1.04	0.28	0.99	0.19	0.96	0.60
Cys-Cys	1.04	0.24	0.98	0.31	0.92	1.14
Asn	1.27	0.32	1.23	0.36	1.20	0.46
Thr	1.31	0.14	1.27	0.43	1.26	0.61
Trp	1.27	0.61	1.24	0.51	1.26	0.30
Gln	1.23	0.03	1.20	0.36	1.18	0.90
Tyr	1.15	0.32	1.14	0.44	1.13	0.74
Ser	1.42	0.22	1.37	0.49	1.35	0.51
Met	1.30	0.46	1.29	0.30	1.30	0.16
Phe	1.21	0.44	1.21	0.35	1.23	1.15
Ile	1.57	0.23	1.55	0.45	1.63	0.93
Val	1.58	0.06	1.56	0.60	1.63	0.61
Gly	2.03	0.05	1.93	0.36	1.88	0.17
Leu	1.52	0.21	1.50	0.14	1.57	0.10
Ala	1.86	0.15	1.79	0.23	1.80	0.32
Pro	1.17	0.71	1.14	0.30	1.18	1.00
His	2.75	0.18	2.53	0.25	2.44	0.60
Lys	2.99	0.17	2.78	0.03	2.66	0.59
Arg	2.85	0.10	2.64	0.31	2.52	0.33

Table A10: Calculated effective electrophoretic mobilities μ_{eff} of all analytes and relative standard deviations (RSD, n = 3) of μ_{eff} in DMSO-containing BGEs. For BGE compositions, compare Table A5, for further information on analytes, compare Table A6.

	10 % DMSO		20 % DMSO		30 % DMSO	
	μ_{eff} in 10^{-4} $cm^2V^{-1}s^{-1}$	**RSD in %**	**μ_{eff} in 10^{-4} $cm^2V^{-1}s^{-1}$**	**RSD in %**	**μ_{eff} in 10^{-4} $cm^2V^{-1}s^{-1}$**	**RSD in %**
Asp	0.89	0.53	0.71	0.19	0.59	0.10
Glu	1.05	0.43	0.84	0.06	0.67	0.17
Cys	0.92	1.37	0.73	0.20	0.59	0.13
Cys-Cys	0.91	1.12	0.72	0.27	0.58	0.27
Asn	1.12	0.68	0.90	0.08	0.72	0.10
Thr	1.17	1.36	0.93	0.19	0.76	0.26
Trp	0.89	2.24	0.84	0.79	0.67	0.45
Gln	1.07	0.55	0.85	0.07	0.68	0.11
Tyr	0.98	0.39	0.78	0.16	0.62	0.04
Ser	1.26	0.21	1.00	0.06	0.81	0.10
Met	1.12	0.87	0.91	0.15	0.73	0.04
Phe	1.03	0.58	0.84	0.11	0.68	0.08
Ile	1.34	0.33	1.07	0.23	0.85	0.24
Val	1.35	0.46	1.09	0.04	0.87	0.09
Gly	1.78	1.23	1.40	0.07	1.09	0.22
Leu	1.29	0.70	1.03	0.18	0.83	0.07
Ala	1.60	0.66	1.27	0.14	1.00	0.13
Pro	1.00	0.32	0.81	0.20	0.67	0.05
His	2.35	0.45	1.80	0.16	1.33	0.54
Lys	2.58	0.60	2.01	0.33	1.50	0.10
Arg	2.42	0.40	1.89	0.17	1.40	0.09

List of scientific contributions

Publications

G. Gauglitz, B. Wimmer, T. Melzer, C. Huhn, “Glyphosate analysis using sensors and electromigration separation techniques as alternatives to gas or liquid chromatography”, *Anal. Bioanal. Chem.* 2018, *410*, 725-746.

T. Melzer, B. Wimmer, S. Bock, T.N. Posch, C. Huhn, “Challenges and applications of isotachophoresis coupled to mass spectrometry: A review”, *Electrophoresis* 2020, *41*, 1045-1059.

Oral presentations

M. Pattky, B. Wimmer, T. Melzer, C. Huhn, “Comparison of CE-MS-qToF and CE-MS-QQQ glyphosate analysis”
8. CE-Forum, Universität Regensburg

T. Melzer, C. Huhn, “How to improve detection limits in capillary electrophoresis? From enrichment techniques to multiple dimensions”
1st International Conference on Ion Analysis, Technische Universität Berlin

Poster presentations

T. Melzer, P. Rath, D. Sydes, P.A. Kler, M. Hermans, C. Huhn, “Preconcentration and separation of all proteinogenic amino acids by hyphenation of isotachophoresis and capillary electrophoresis-mass spectrometry”
31st International Symposium on Chromatography, University College Cork, Irland (rewarded with Shimadzu Best Poster Award) and *8. CE-Forum, Universität Regensburg*

T. Melzer, A.J. Wicht, G. Weber, C. Huhn, “Comparison of electromigrative enrichment possibilities: Capillary isotachophoresis, capillary electrophoresis and free-flow electrophoresis”
31st International Symposium on Chromatography, University College Cork, Irland and *21. Jahrestagung der the Society of Environmental Toxicology and Chemistry – Europe, German Language Branch e.V., Eberhard Karls Universität Tübingen*

T. Melzer, D. Sydes, P.A. Kler, M. Hermans, C. Huhn, “Hyphenation of isotachophoresis and capillary electrophoresis-mass spectrometry for two-dimensional separation of amino acids”
ANAKON 2017, Eberhard Karls Universität Tübingen

T. Melzer, C. Huhn, “Preconcentration and separation of amino acids by online-coupling of isotachophoresis and capillary electrophoresis-mass spectrometry”
24th International Symposium on Electro- and Liquid Phase-Separation Techniques, Sheraton Hotel Sopot, Polen and *1. Forum für elektromigrative Trennverfahren - Kapillarelektrophorese (CE) und Free-Flow Elektrophorese (FFE), Fraunhofer ICT Karlsruhe-Berghausen*

T. Melzer, C. Huhn, “ITP/CE-MS hyphenation in a single capillary setup for preconcentration and separation of amino acids“
ANAKON 2019, Westfälische Wilhelms-Universität Münster